Rui Américo
Ferreira da Costa

Fenómenos Críticos Atípicos em Processos De Optimização em Redes

Novel Critical Phenomena in Optimization Driven Processes on Networks

Rui Américo Ferreira da Costa

Fenómenos Críticos Atípicos em Processos De Optimização em Redes

Novel Critical Phenomena in Optimization Driven Processes on Networks

Tese apresentada à Universidade de Aveiro para cumprimento dos requisitos necessários à obtenção do grau de Doutor em Física (conferido em conjunto pelas Universidades do Minho, Aveiro e Porto), realizada sob a orientação científica de José Fernando Ferreira Mendes, Professor Catedrático do Departamento de Física da Universidade de Aveiro, e Doutor Sergey Dorogovtsev, Investigador Coordenador do Departamento de Física da Universidade de Aveiro.

Thesis presented to University of Aveiro for fulfillment of the necessary requirements to the attainment of the degree of Doctor in Physics (conferred jointly by Universities of Minho, Aveiro and Porto), carried through the scientific orientation of Doctor José Fernando Ferreira Mendes, Full Professor at the Physics Department of University of Aveiro, and Doctor Sergey Dorogovtsev, Research Coordinator at the Physics Department of University of Aveiro.

Apoio financeiro da FCT e do FSE no âmbito do III Quadro Comunitário de Apoio (SFRH/BD/45628/2008).

Financial Support from FCT and from FSE under the III Community Support Framework (SFRH/BD/45628/2008).

Este trabalho é dedicado à Joana, minha companheira, e ao Joaquim, nosso querido filho.

This work is dedicated to Joana, my partner, and to Joaquim, our beloved son

o júri / the jury

presidente / president	**Prof. Doutor António Carlos Matias Correia** Professor Catedrático do Departamento de Biologia da Universidade de Aveiro (por delegação do Reitor da Universidade de Aveiro)
orientadores / advisors	**Prof. Doutor José Fernando Ferreira Mendes** Professor Catedrático do Departamento de Física da Universidade de Aveiro
	Prof. Doutor Sergey Dorogovtsev Investigador Coordenador do Departamento de Física da Universidade de Aveiro
vogais / examiners committee	**Prof. Doutora Ana Maria Ribeiro Ferreira Nunes** Professora Associada com Agregação da Faculdade de Ciências da Universidade de Lisboa
	Prof. Doutora Maria do Céu Almeida de Morais Marques Professora Associada da Faculdade de Ciências da Universidade do Porto
	Prof. Doutor António Luís Campos de Sousa Ferreira Professor Associado do Departamento de Física da Universidade de Aveiro
	Prof. Doutor João Gama Oliveira Professor Auxiliar Convidado da Faculdade de Engenharia da Universidade do Porto

agradecimentos

Agradeço, em primeiro lugar, aos meus orientadores, Prof. Mendes e Prof. Dorogovtsev, pelos seu valioso tempo, ideias, direcção e apoio. Este trabalho não seria possível sem a sua excelente orientação. Além disso, quero agradecer-lhes aqui pelo privilégio de me terem acolhido no seu grupo de trabalho, e por todos os inestimáveis ensinos e estímulos, que permitiram expandir amplamente o meu conhecimento do campo científico.

Agradeço também a António Luís Ferreira, Fernão Abreu, Massimo Ostilli, Gareth Baxter, João Gama Oliveira, Alexander Samukhin, Sooyeon Yoon, KyoungEun Lee, Detlef Holstein, Olivier Bertoncini, Fabricio Forgerini, Patrícia Silva, Nahid Tafreshi, Marinho Lopes, Orahcio de Sousa, Marta Daniela Santos, e em especial a Alexander Goltsev (co-autor das publicações sobre percolação explosiva), com quem tive o prazer de trabalhar ao longo dos últimos anos. Agradeço ainda a Manuel Barroso por toda a paciência concedida às minhas desmedidas necessidades computacionais.

Agradeço também aos funcionários do Departamento de Física da UA, Francisco Reis, Fátima Bola, Afonso de Carvalho, Gonçalo Ramalho, Cristina Rei e Emília Fonseca pela sua continuada ajuda, competência e solicitude.

Por fim, quero agradecer a toda a minha família e amigos pelo apoio e afecto incondicionais que generosamente me proporcionam, mesmo quando esses são manifestamente imerecidos (como, certamente, aconteceu nos últimos meses, durante a redacção desta tese); especialmente à minha companheira Joana e ao nosso filho, que, diariamente, estiveram sujeitos à convivência doméstica comigo, e a quem devo não só os maiores agradecimentos mas também muitas desculpas.

A todos, um grande e sentido Obrigado.

acknowledgements

First, I thank to my advisors, Prof. Mendes and Prof. Dorogovtsev for their valuable time, ideas, guidance and support. This work would not be possible without their excellent orientation. Additionally, I wish to thank them here for the privilege of integrating their work group, and for all the precious teachings and stimuli, which enabled me to widely expand the knowledge of the scientific field.

Thanks also to António Luís Ferreira, Fernão Abreu, Gareth Baxter, Massimo Ostilli, João Gama Oliveira, Alexander Samukhin, Sooyeon Yoon, KyoungEun Lee, Detlef Holstein, Olivier Bertoncini, Fabricio Forgerini, Patrícia Silva, Nahid Tafreshi, Marinho Lopes, Orahcio de Sousa, Marta Daniela Santos, and especially to Alexander Goltsev (co-author of the paper on explosive percolation), with whom was a great pleasure to work over the last years. I thank to Manuel Barroso as well, for all his patience with my endless computational needs.

From the Physics Department of UA, I thank to Francisco Reis, Fátima Bola, Afonso de Carvalho, Gonçalo Ramalho, Cristina Rei and Emília Fonseca for all of their help, competence and availableness.

At last, I wish to thank to my whole family and friends for their unconditional support and affection that they generously grant me, even when I am notoriously unworthy of it (as certainly I was in the last months, during the composition of this thesis); especially to my partner Joana and to our son, which were daily exposed to my tempers, and to whom I own not only the greatest thanks but also deep apologies.

Many and sincere thanks to all.

palavras-chave

física estatística, transições de fase, processos de optimização, fenómenos críticos, redes complexas, percolação explosiva, fluxo em redes

resumo

O trabalho apresentado nesta tese foi desenvolvido no contexto da teoria de redes complexas, na perspectiva da física estatística. So analisados dois problemas distintos neste campo de investigação, dando especial importância às respectivas propriedades críticas. Em ambos os casos, o estado crítico é produzido por mecanismos de optimização local. Em primeiro lugar, estudamos uma classe de modelos de percolação recentemente proposta, que atraiu uma quantidade significativa da atenção da comunidade científica, e foi prontamente acompanhada por uma abundância de outros trabalhos. As transições de percolação julgavam-se continuas, até recentemente ter sido relatado, em [93], um problema de percolação 'explosiva' ,que possui uma transição de fase descontínua. A evolução do sistema é impelida por um algoritmo do tipo metropolis, o que aparentemente produz um salto no tamanho do componente gigante. Esta noção foi subsequentemente apoiada por vários outros estudos experimentais [96, 97, 98, 99, 100, 101]. Contudo, em [1] nós provámos que a transição de percolação explosiva é, na verdade, contínua. A descontinuidade observada na evolução do tamanho relativo do componente gigante é explicada pela invulgar pequenez do expoente crítico correspondente, combinada com o carácter finito dos sistemas considerados nas experiências. Assim, o salto desaparece quando o tamanho do sistema vai para infinito. Adicionalmente, fornecemos a descrição teórica completa das propriedades críticas de um modelo [2] que generalizada o problema da percolação explosiva, assim como, um método [3] que permite o cálculo preciso dessas propriedades a partir de dados numéricos (útil na ausência de resultados exactos). Em segundo lugar, estudamos um modelo de optimização de fluxo em redes, onde a dinâmica consiste em consecutivas junções e divisões das correntes. A condição de conservação de corrente não impõe qualquer critério em particular para a divisão da corrente pelos canais de saída dos nodos, o que permite introduzir uma regra assimétrica, observada em vários sistemas reais. Resolvemos analiticamente as equações dinâmicas que descrevem estes sistemas para os regimes de altas e baixas correntes. As soluções encontradas são comparadas com resultados numéricos, em ambos os regimes, e mostram uma excelente concordância. Surpreendentemente, no regime de baixas corrente, este modelo exibe alguns dos atributos geralmente associados a transições de fase contínuas.

keywords statistical physics, phase transitions, optimization processes, critical phenomena, complex networks, explosive percolation, network flow.

abstract The work presented in this Ph.D thesis was developed in the context of complex network theory, from a statistical physics standpoint. We examine two distinct problems in this research field, taking a special interest in their respective critical properties. In both cases, the emergence of criticality is driven by a local optimization dynamics. Firstly, a recently introduced class of percolation problems that attracted a significant amount of attention from the scientific community, and was quickly followed up by an abundance of other works. Percolation transitions were believed to be continuous, until, recently, an 'explosive' percolation problem was reported to undergo a discontinuous transition, in [93]. The system's evolution is driven by a metropolis-like algorithm, apparently producing a discontinuous jump on the giant component's size at the percolation threshold. This finding was subsequently supported by number of other experimental studies [96, 97, 98, 99, 100, 101]. However, in [1] we have proved that the explosive percolation transition is actually continuous. The discontinuity which was observed in the evolution of the giant component's relative size is explained by the unusual smallness of the corresponding critical exponent, combined with the finiteness of the systems considered in experiments. Therefore, the size of the jump vanishes as the system's size goes to infinity. Additionally, we provide the complete theoretical description of the critical properties for a generalized version of the explosive percolation model [2], as well as a method [3] for a precise calculation of percolation's critical properties from numerical data (useful when exact results are not available). Secondly, we study a network flow optimization model, where the dynamics consists of consecutive mergings and splittings of currents flowing in the network. The current conservation constraint does not impose any particular criterion for the split of current among channels outgoing nodes, allowing us to introduce an asymmetrical rule, observed in several real systems. We solved analytically the dynamic equations describing this model in the high and low current regimes. The solutions found are compared with numerical results, for the two regimes, showing an excellent agreement. Surprisingly, in the low current regime, this model exhibits some features usually associated with continuous phase transitions.

Contents

List of Figures

List of Tables

Chapter 1

Introduction

Numerous real-world systems can be represented as networks – sets of nodes or vertices joined in pairs by links or edges. Examples include the Internet and the World Wide Web, metabolic networks, protein networks, neural networks, communication and distribution networks, and social networks. The study of networked systems has a history stretching back several centuries, but it has experienced a particular surge of interest in the last one and a half decades, especially in the mathematical sciences, partly as a result of the increasing availability of large-scale accurate data describing the topology of 'natural' networks. Statistical analysis of this data has revealed some unexpected structural features, such as the "small-world" effect and high network transitivity [4], power-law degree distributions [5], and the existence of repeated local motifs [6]; see [7, 8, 9] for reviews. The physicists community has in recent years devoted considerable attention to the study of networks, including social networks, communication networks, biological networks, and others. Some of these networks also have long histories of study on other research fields.

The analysis of large complex networks can be seen as a topic of its own within the field of statistical physics, which strives to describe macroscopic observables in large systems of interacting units from microscopic first principles. If the interaction is sufficiently random, then classical mean-field theory can describe the macroscopic behavior and fluctuations in large systems perfectly well, however, the structure of real-world networks is not completely random. Different rules for the design and evolution of networks can lead to very different structures which, in turn, lead to different macroscopic behaviors.

1.1 Historical Overview

The foundations of graph theory date back to the historical swiss mathematician Leonhard Euler. On his paper, of 1736, he proved that a successful solution of the popular Königsberg bridges problem is, in fact, impossible. At the time there were seven bridges over the Pregel River in Königsberg, connecting two islands to both margins and to each other, as seen in Figure 1.1. The problem consists in finding a *route*, or geometrical path, that crosses all of the bridges once and once only.

In order to address this problem Euler first noted that the specific path inside each land mass is without importance, the only relevant aspect of the path is the sequence of crossed bridges. The implications of this seemingly trivial consideration allowed him to reduce the problem to a list of the land masses and the bridges connecting them. The mathematical

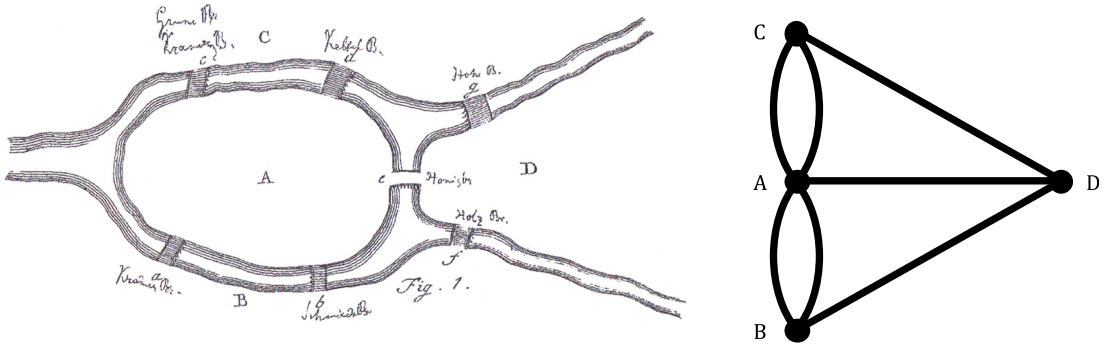

Figure 1.1: Left: Depiction of the Königsberg seven bridges problem included by Euler in his paper from 1736, *Solutio problematis ad geometriam situs pertinentis*. Right: Graph of the Königsberg problem structure. Each land masses of the left-hand side drawing, labeled A, B, C and D, corresponds to the node with the same label on the right-hand side graph, the bridges are represented edges.

---

object resultant from this simplified view (consisting only on the information of how a number of nodes is connected among them) became known as a graph. In Figure 1.1 can be seen the graph corresponding to the Königsberg bridge problem.

It is easily observed that, with the exception of the starting and ending nodes, every time a path enters a node it must leave the node too. If each edge must be used only once, each passage through a node uses two of the edges connected to it. From which follows the conclusion that, in a path that crosses all edges exactly once, the non-terminal nodes must be connected to an even number of edges. In the case of the Königsberg bridges all four nodes have an odd number of connections, thus such a path does not exist. In this way, Euler connected the possibility of a path having the desired property, with the number of connections of the nodes, henceforth referred to as *degree* of the nodes. Almost three centuries old, this relation between the existence of such a path and the degree distribution of the graph nodes was the first theorem of graph theory, and is considered its moment of birth.

Despite numerous advances in the field since Euler's Königsberg problem, it was not until the introduction of the Erdős-Rényi random graph model, in the 1950's [10, 11, 12, 13], that modern graph theory started to develop, and really became able to analyze very large graphs. The innovation of the Erdős-Rényi model (ER model) is in the treatment of the graph not has a deterministic object, but has a statistical ensemble of graphs, where each particular realization has associated a certain probability. In particular, the model is constructed as follows: (i) start from a number N of labeled nodes without connections among them; (ii) add M edges, of the $N(N-1)/2$ possible ones, uniformly at random among the N nodes. In this way, all edges are present with the same probability $2M/(N(N-1))$. Furthermore, all the $\binom{N(N-1)/2}{M}$ different graph realizations with N nodes and M edges have equal probability to be produced by this random process.

The probabilistic approach makes it possible to rigorously define what it means for a property to hold for almost all graphs, and to prove the existence of various properties on the set of graphs belonging to a given ensemble. Often the size of the system considered tends to infinity, the expression *almost all graphs* actually means that the probability of a property being present, on a random realization of the graph, tends to 1 or 0, when N tends to infinity;

in this limit results become independent of N. In physics terms, the condition $N \to \infty$ is called the *thermodynamic limit*.

The ER model, also designated as the classical random graph, will come up several times throughout the present manuscript, on account of its relevance to the field of graph theory, and its relation with percolation, one of the main subjects of this thesis. To avoid awkward redundancies, the proper discussion of this classical model's specific properties will take place in other sections, where it is more pertinent.

1.2 Network Topological Structure

The average shortest path length of a graph is closely related to its diameter, it represents the extension, in length units, of the structure. The smallness of this measure, when compared with the total size of the network, has motivated many studies verifying the abundance of the so-called small-world property on real-world networks, and constructing theoretical support to help understand how it appears. (The mathematical definition of small-world, used in network science, is given in section 1.2.2, along with a discussion on some of its more relevant aspects.)

Furthermore, the scientific community's interest on the field of complex networks was largely amplified by the discovery that many of these natural structures share another important property; power-law degree distributions. The topology of those non-equilibrium systems largely differs from the classical random graph, which has a Poisson degree distribution, indicating that new tools are necessary to address this newly discovered class of objects. The World Wide Web, the network of citations of scientific papers and some biological networks are among the many examples of systems where power-law degree distributions were observed [7].

1.2.1 Scale-free Networks

The numerous appearances, in real-world networks, of power-law degree distributions, $P(k) \propto k^{-\gamma}$, where k is the degree of a randomly chosen node and $\gamma > 2$ is some constant, called scale-free behavior in the language of network analysis, are usually explained by the combination of growth and preferential attachment [5, 14]. If new connections in a growing network appear between vertices chosen without any preference, e.g., between new vertices and old ones chosen uniformly at random, the degree distribution is exponentially decreasing [7]. Yet, in real networks, linking is very often preferential. For example, when someone makes a new reference in their own webpage, the probability that they refer to a popular Web document is certainly higher than the probability that this reference is to some poorly known document that nobody referred to before them. Therefore, popular vertices with high number of links are more attractive for new connections than vertices with fewer links, or, on other words, popularity is attractive.

The simplest model expressing the idea of preferential linking is perhaps the Barabási-Albert model (BA model) [5]. In this model networks are constructed iteratively, in each time step a new vertex is added to the network and connects to one of the pre-existing ones, chosen with probability proportional to its degree. The linking process is done preferentially. It should be noticed that this is only a particular form of a preference function. Nevertheless, this particular case yields a structure characterized by a power-law degree distribution with an exponent $\gamma = 3$ which marks the transition between two different regimes. When $\gamma > 3$, the

degree distribution variance and mean are bounded. If $2 < \gamma < 3$ the variance of the degree distribution becomes unbounded while the mean remains bounded. In the later regime the corresponding networks may show a number of particularly interesting properties, desirable for many applications, such as an almost-constant diameter [15], extreme resilience to random deletions of nodes and edges [7] and search efficiency [16] among others.

A significant number of models were developed to reproduce this effect. In particular, other forms of preference can lead to different degree distributions, including a power law with tunable exponent $\gamma \in]2, \infty[$ [7]. As a simple example, consider a growing network where the new node arriving at each time step connects n times to previous ones, and each connection is made to a node of degree k with probability $p_k \propto k + A$, where the additional fitness $A > -n$ is some constant. It was shown in [17] that these microscopic dynamical rules, in the large system size limit, allow the emergence of a scale-free structure characterized by an exponent $\gamma = 3 + A/n$. Notice that the case $A = 0$ corresponds to the Barabási-Albert preference, returning $\gamma = 3$ as before.

It should be mentioned that the degree distribution may not be sufficient to describe all relevant features of the network structure. In fact, the degree distribution provides complete structural information only for equilibrium uncorrelated networks. However, most real-world networks exhibit intricate topological correlations that may include spatial correlations, degree-degree correlations, clustering, community structure, etc; and are direct consequence of the mechanisms in action. Similarly, many models developed to generate networks with certain desired properties, including the BA model and its variants, introduce these kinds of heterogeneity.

1.2.2 Small-world Networks

The notion of small-world networks is essentially tied with the distance of the shortest paths between nodes on a connected network. The shortest path between two nodes, say i and j, is the shortest sequence of connected nodes that begins with i and ends with j, and its length, l_{ij}, is measured in network steps, i.e., the number of edges the path contains. In undirected graphs every path can be walked in both directions, since the edges are symmetric, so $l_{ij} = l_{ji}$. If the edges are directed, the shortest paths from i to j is distinct form the shortest path from j to i, since directed edges only allow communication in one direction, and in general $l_{ij} \neq l_{ji}$. The diameter of a network, $\bar{l}$, is calculated by taking the average of l_{ij} over all pairs of nodes, $\bar{l} = N^{-2} \sum_{i,j=1}^{N} l_{ij}$, where N is the size of the network. For simplicity l_{ii} can be set to 0 by definition (the distance between a node and itself is zero). If some nodes, or groups of nodes, are isolated, in the sense that there are no edges between any of these nodes to the rest of the system, the network is called disconnected, in consideration of certain pairs of nodes having no paths connecting them. For this reason the discussion of the small-world effect is usually restricted to the class of connected graphs.

While on a d-dimensional lattice the diameter grows with the system size N as $\bar{l} \propto N^{1/d}$ and there is a high density of short loops, on most models of random networks, including the ER and the BA models, there are no finite loops at all, in the thermodynamic limit, and the diameter grows slower than any power of N, usually for random networks $\bar{l} \propto \log N$. For scale-free networks with exponent $2 < \gamma < 3$ the diameter can grow as slowly as $\bar{l} \propto \log \log N$ [15]. The term small-world is intended to reflect such a slow (logarithmic) increase of the diameter with the size of the network.

The Watts-Strogatz model (WS model) stands as a simple instructive model to help

explain the prevalence of the small-world property in real networks, even when they are strongly locally correlated. With their approach, Watts and Strogatz [4] incorporated in a single network model a high density of local clustering and small-world behavior of the diameter. The model starts with N nodes labeled from 1 to N, and connects any pair of nodes whose absolute difference between their labels is smaller or equal to $k/2 \geq 2$, with periodic boundary conditions. In the resulting ringlike regular structure all the nodes have k nearest neighbors, and all connections are established with basis on a purely deterministic geometrical criteria of a single coordinate, producing an abundance of short loops. The topology of this 1-dimensional system has the characteristic of being locally clustered like many real networks, however it lacks the small-world property, and the diameter actually grows linearly with the system size, $\bar{l} \sim N/2k$. A stochastic component is added by rewiring each edge uniformly at random, with probability p, introducing a number of long-range connections, or shortcuts. When $p = 0$ the original network is preserved, and when $p = 1$ the WS model is equivalent to the ER-model. In the thermodynamic limit, even vanishingly small p can trigger the small world effect.

Apart from the existence of a few long-range edges, this simplistic model does not account for any of the other heterogeneous features of real networks, such as scale free degree distributions. Nevertheless, it provides a useful insight into the importance of long-range links, and explains how the small-world property can emerge on any network, even on locally lattice-like networks, if only a vanishingly small amount of randomness is allowed.

1.2.3 Other Topological Features

Apart from the scale-free and small-world properties there are many other non-trivial topological aspects of complex networks. For instance, an essential question to ask is: How much damage can a network take before it breaks down into small pieces, and fails to have a spanning connected component? The answer can be anything between none to almost total, depending on the specific structure of the network, and is determined by its percolation properties. Another attention worthy issue is the finding of the so-called community structure of the network, a feature of many real networks, initially noted and investigated in a sociological context [18]. The existence of communities, groups of nodes that are more densely connected with each other than with other nodes, who belong to other densely connected groups [19], is natural and evident in social networks. Communities reflect social clustering due to family, geographical location, religious beliefs, occupation, personal tastes, etc. In this section some of these non-trivial aspects of the topology of complex networks are briefly discussed.

Percolation

When introducing the concept of percolation, authors frequently prefer to start by describing the process on the square lattice, in virtue of the simplicity of the algorithm and the ability to straightforwardly represent and visualize the state of the system, with figures like Figure 1.2. Also here these advantages will be helpful. A computer experiment can be implemented easily: first build an $L \times L$ matrix of uniformly distributed pseudorandom numbers $0 \leq x_{ij} < 1$. Then build another matrix, representing the state of the system, where each element s_{ij} is set to 1 if $x_{ij} < p$ or to 0 otherwise, and p is the control parameter. The square lattice is represented by a matrix of $L \times L$ unit squares in a 2-dimensional euclidean space, the squares, or sites, can be connected at most to four neighbors (the sites immediately to

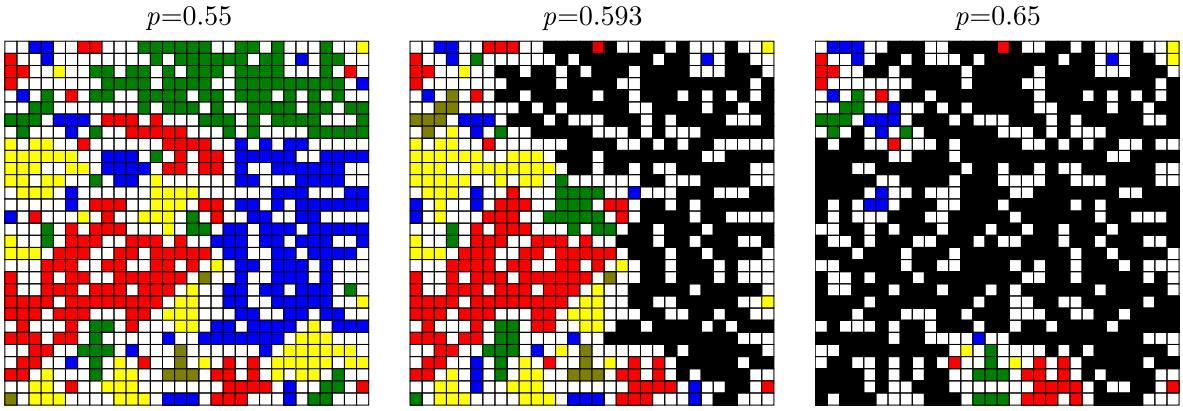

Figure 1.2: Three different concentrations p of active sites on a square lattice with $L = 30$. Inactive sites are white and active sites are shown in color (to help the visualization, all sites belonging to the same cluster have the same color, and black is reserved for the percolating cluster). The site $\{i, j\}$ becomes active when p exceeds the random value of x_{ij}, otherwise it stays inactive. In the left-most panel the system exhibits some relatively large connected components, but not a percolating cluster, that is a cluster touching both top and bottom or right and left borders. What is consistent with the value of $p = 0.55$, smaller than p_c (on the infinite lattice $p_c = 0.5927...$). The central panel, where $p = 0.593$, shows the state of the system when a cluster spanning the system from top to bottom first appears, for the particular realization of the matrix of x_{ij} used in this example. Note that, as expected, the value of p for which the percolating cluster emerges is very close to p_c; in fact, the deviation from p_c is of the order of the resolution on a square lattice of side $L = 30$, $|p - p_c| \sim 1/L^2$. The right-most panel shows the system in the percolating phase. The percolating cluster is now larger than before, and has expanded to incorporate most of the previously existing clusters. From this sequence of "snapshots" of the state of the system, one can see that it evolves from a state without a dominant component to a state in which most of the active sites are condensed in a single component, only with the activation of a small extra portion of sites.

---

the left, to the right, above and below). The site in the position $\{i, j\}$ is active if $s_{i,j} = 1$ and inactive otherwise, hence the number of active sites is on average equal to pL^2, since sites are active independently with probability p. If two neighboring sites are active than they are considered connected and belong to the same connected component, or *cluster*. It is quite obvious that the size of the clusters should grow with the concentration of active sites p. The concern of percolation is how the cluster size distribution depends on p.

In both limiting regimes the system shows trivial behavior; when $p \to 0^+$ the active nodes are isolated and there are pL^2 clusters of size 1, when $p \to 1^-$ the whole system is connected in a single giant cluster, with $(1 - p) L^2$ "holes" of size 1. If p slowly increases from 0 some clusters of size larger than 1 will form, but still the size distribution decays exponentially and there is not a cluster that crosses the entire system [20] (this would be a cluster with at least one site at each of two opposite boundaries of the $L \times L$ matrix). Given that for $p = 1$ the system is condensed in a single cluster, if p continues to increase there must be a point, the percolation threshold $p_c < 1$, when a giant cluster emerges, spanning across the total length of the system. Above that point the giant cluster grows with p until it has absorbed all other clusters at $p = 1$. Figure 1.2 shows this process on a lattice with $L = 30$.

The term percolation alludes to the existence of such a cluster, often called giant connected component or percolating cluster, which has distinct properties from the other clusters. Entertain, for a moment, the following scenario: electrodes are placed on opposite borders of the square lattice, active sites are equipped with electrical conduction properties and inactive site are insulators. When a potential is applied to the electrodes, current can flow through the system if there is a connected path of conductor sites closing the circuit. That path belongs to the percolating cluster, and is inexistent for $p < p_c$. Therefore, the macroscopic electrical properties of the system change dramatically with the concentration of active sites, from insulator to conductor as p crosses p_c from below.

Of course, the exact value of p_c will depend upon L and the particular realization of the matrix of x_{ij}, at least for finite systems. As a matter of fact, since the infinite system can be regarded as an arbitrarily large set of smaller independent infinite blocks and percolation is an extensive property, by the central limit theorem, when $L \to \infty$ the system becomes *self-averaging* and its properties independent of the random realization. Technically, in the thermodynamic limit, the central limit theorem is applicable for all concentrations p except exactly at p_c, where the correlation length diverges and the self-averaging properties are lost [21]. However, since it is applicable for points immediately below and above the threshold, p_c is precisely defined on the infinite system, and for site percolation in the square lattice it is known to be at around 0.5927 [20].

A similar process can be implemented for site and *bond* percolation in any topological structure, and it has been studied for regular lattices in spaces of any dimensionality, random graphs, etc. The previous example is one of site percolation, but it is equally easy to implement a identical procedure for bond percolation. Instead of starting with all edges active, between adjacent sites, and randomly activate a fraction of the sites, for bond percolation start with all sites active and randomly add a fraction p of edges, or bonds, between adjacent sites. The threshold of bond percolation on a square lattice, $p_c = 1/2$, was exactly calculated using renormalization group [22]. In general for percolation, the average size of the largest cluster grows proportionally to $\log N$ for p below p_c (if the system size N is large enough), while above p_c the largest component grows linearly with N. This is the characteristic of the percolating cluster, linear growth with the system size, i.e., the number of nodes on the giant connected component is a non-vanishing fraction of N, when $N \to \infty$ [20].

The existence of this transition has important implications for the integrity of a network. Most functional networks can only operate properly if they are connected, or at least possess a large connected component, of size comparable with the system size. However, real systems often sustain damage: members of a network may lose some connections, or disconnect completely, due to loss of interest, spontaneous failure, external attacks, etc. The structure's percolation properties determine how much damage a network can absorb before the giant connected component dissolves, and the network is reduced to a set of small disconnected clusters. In other words, a network's resilience to random damage is determined by its percolation threshold. E.g, in one extreme of network resilience lies the 1-dimensional lattice, with percolation threshold $p_c = 1$, where the removal of any fraction of nodes or edges results in the global fracture of the system [22]. In the other extreme can be found scale-free networks with degree distribution characterized by an exponent $\gamma \leq 3$, such as the BA network model, where the percolation threshold $p_c \to 0$ with $N \to \infty$. In the thermodynamic limit, these networks maintain a giant connected component if any fraction $p > 0$ of the network survives after random removal of nodes or edges, $p_c = 0$ [23].

1.3 Phase Transition Theory

In an intuitive manner, a phase transition is a sudden alteration in the order of the system. If a thermodynamic system can be found in one of two different states of order, depending on the control parameter, often called *temperature*, e.g. liquid and gaseous, or ferromagnetic and paramagnetic, then by varying the temperature the order of the system can change from one state to the other. More rigorously, the measure of the order, called *order parameter*, on the disordered phase of a phase transition is identically null. If the temperature is varied past the transition temperature, driving the system into the ordered phase, the order parameter becomes non-zero valued. For the liquid-gas transition, a natural order parameter is the density difference between the liquid and the fluid, since the density in the liquid is constant near the transition, the order parameter is zero there, while in the gaseous phase the order parameter becomes non-zero. In ferromagnetic systems the magnetization is regarded as the order parameter.

A question of great relevance is the continuity of the transition. That is, if a continuous variation of the temperature causes the order parameter to jump discontinuously at the transition point, or if, instead, the order parameter varies continuously, and converges to zero from both sides of the transition point. Except at the critical point, the liquid-gas transition is *discontinuous*, or a *first-order* phase transition [24]. There is a latent heat associated to this kind of transition, i.e., an amount of energy the system absorbs or releases, at the transition point, to which there is no corresponding increase or decrease of temperature. At the transition point the system state is not homogeneous and both phases may coexist in equilibrium. Moreover, each phase can exist beyond the transition point, in a metastable state, as a superheated liquid or a supercooled vapor. A well known effect of metastability is the production of hysteretic behavior of the order parameter.

At the *critical point*, the liquid-gas transition is *continuous*, or a *second-order* phase transition, as is the ferromagnetic transition (the transition point of a second-order phase transition is called the critical point). In contrast to discontinuous transitions, the two phases become the same at the transition point. Therefore, during a continuous phase transition the system state is always homogeneous, even at the critical point; and the transition occurs, not due to an abrupt shift of the equilibrium state of some thermodynamic variable, but instead due to a symmetry break. The system symmetry is said to break when the introduction of extra variables is indispensable to fully describe the system's state. In some cases, this can correspond to a change in the actual geometric symmetry, as it does in the case of the continuous crystal-liquid transition, where the symmetry vanishes continuously at the critical point. The liquid phase has maximum symmetry, atoms can move freely and may be found anywhere, while in the crystalline phase the probability distribution for the atoms positions is shaped according to a regular structure, which reduces the symmetry and introduces extra variables to account for the lattice positioning and rotation states. In other cases no geometric symmetries are broken, such as the ferromagnetic transition, where the atoms positions are fixed in both phases, yet in the ordered phase an extra variable is needed to account for the spontaneous magnetization that emerges at the critical point.

Continuous phase transitions show a rich set of properties not present in discontinuous transitions, including diverging susceptibility, infinite correlation length, scaling and universality among others. In the remainder of this section the discussion is restricted to continuous phase transitions, most relevant for the work presented in this thesis.

1.3.1 Landau's Theory

With his phenomenological theory, Lev Landau gave a fundamental contribute to the knowledge of second-order phase transitions [24]. Despite the rather simplistic view over the phenomenon and the neglect of some key aspects, Landau's theory offers a self-consistent qualitative description of the general behavior, near the critical point, of systems with continuous phase transitions. Its greatest accomplishment was to conciliate the singularities observed experimentally near the critical point, a remarkable feature of *critical phenomena*, with the continuity of the thermodynamic variables, namely the order parameter. The theory focus on the properties of a function named *thermodynamic potential*, or *free energy*, which is a scalar function of the system's state. If this potential is known as a function of the thermodynamic variables (such as pressure, temperature, density, magnetization, etc), then all other *thermodynamic quantities* can be calculated by taking its partial derivatives. Thermodynamic quantities are those which describe the macroscopic state of a system. Furthermore, the thermodynamic potential has the very important property of being minimum for the *equilibrium* state of the system, under some given external conditions. The equilibrium, or stable state, corresponds to the macroscopic state to which the system spontaneously evolves, if the control variables are kept constant. Indeed, while the thermodynamic potential remains continuous through the transition, it also has a mathematical singularity at the critical point, and some derivatives of the thermodynamic quantities may diverge there, often as power laws.

A brief, simplified, description of Landau's approach is given in the following, using the ferromagnetic Ising model as an example. The Ising model consists on a structure of magnetic spins σ_i, each of which has one of two possible orientations, $\sigma_i \in \{-1, 1\}$. Each interaction between pairs of neighboring spins contributes to the system energy. For a ferromagnetic interaction the energy increases when the spins are oriented in antiparallel directions, and decreases it when they are parallel. The strength of the interactions is inversely proportional to the temperature T. Two limiting behaviors can easily be identified from the previous statement: when $T \to 0$ all spins are aligned in one direction, and when $T \to \infty$ the interactions no longer matter and each spin is randomly oriented, independently of its neighbors. For any finite temperature the spins are not completely independent, nevertheless, if T is large enough, despite some local coordination, the average of the spins is null, i.e. $m \equiv \sum_{i=1}^{N} \sigma_i / N = 0$. On the other hand, for $T > 0$ small enough most spins still coordinate on the same direction, but some can have the opposite orientation, due to local thermal fluctuations, and $0 < |m| < 1$ (m is often called *spontaneous magnetization*). At some temperature, between these two regimes, there is phase transition. Clearly, the order parameter here is the spontaneous magnetization m, that varies continuously from zero, for all T larger or equal to the critical temperature T_c, to non-zero values at $T < T_c$. The magnitude of the spontaneous magnetization is fixed by the temperature, and its direction can be either of both possible. Yet, for an infinite system at $T < T_c$, the magnetization takes one direction, and cannot spontaneously change it. The sign of the magnetization when $T < T_c$ is actually determined by whatever direction it happened to have at $T = T_c$. This restriction is responsible for the symmetry break associated with the ferromagnetic transition of the Ising model.

Continuous phase transitions are characterized by the fact that the order parameter, m, takes arbitrarily small values near the critical point. Considering the series expansion, in the vicinity if this point, of the thermodynamic potential $\Phi(T, m)$ in powers of m:

$$\Phi(T, m) = \Phi_0(T) + \alpha(T)m + A(T)m^2 + \beta(T)m^3 + B(T)m^4 + \dots \tag{1.1}$$

Note that, in general, the thermodynamic potential Φ is a function of all the system thermodynamic variables, which on the Ising model are temperature and magnetization. Φ_0 is a function of all these variables except m, as are the coefficients α, A, β, B, etc. It should be emphasized that the possibility of such an expansion is a strong assumption. There are no reasons to believe that such an expansion can be continued to terms of arbitrarily high order, or that the coefficients are analytic functions, especially since the critical point is expected to be a singularity of Φ, already mentioned. The stable state of the system at temperature T is given by the condition of minimum of the thermodynamic potential $(\partial\Phi/\partial m)_T = 0$. This property can be used to reveal the dependence of order parameter m as function of the independent parameter T:

$$\alpha(T) + 2A(T)m + 3\beta(T)m^2 + 4B(T)m^3 = 0 \tag{1.2}$$

A number of considerations can be made about the coefficients. Using symmetry arguments, it can be shown that for second-order transitions $\alpha \equiv 0$. In the case of the Ising model, in the absence of external field, if the system is cooled from a temperature $T_1 > T_c$ to a temperature $T_2 < T_c$, the majority of spins, responsible by the spontaneous magnetization, can align in either of the two directions $\{-1, 1\}$, with $1/2$ probability for each. Since the two orientations of the magnetization are equiprobable, $\Phi(T, m)$ should be symmetrical on m, implicating that $\alpha(T < T_c) = 0$. On the other hand, when $T \geq T_c$ the system is in a disordered state, where $m = 0$, so also $\alpha(T \geq T_c)$ must be zero for the condition (1.2) to be observed. In fact, if an external field is applied, a linear term in m will appear. Which is consistent the previous argumentation, since the external field introduces an asymmetry on the potential, by imposing a preferential orientation of the spins.

Coefficient $A(T)$ is easily seen to vanish at the transition point. For $T > T_c$, the thermodynamic potential must have a minimum at $m = 0$, so the coefficient $A(T)$ as to be positive in this range of temperatures. While on the other side, when $T < T_c$, it as to be negative for the potential to have a minimum at $m \neq 0$. Since the potential is expected to vary continuously, close enough to the critical point this coefficient is written as

$$A(T) = a(T - T_c), \tag{1.3}$$

where a is positive and constant with T.

In continuous phase transitions, the critical point itself must correspond to a stable state, as such, at T_c the potential must be minimum for $m = 0$. This means that $\beta(T_c) = 0$ and $B(T_c) > 0$. There are two possibilities concerning β: (i) In the vicinity of isolated critical points, like the ones found at the end of a line of first-order transitions, $\beta(P, T) \not\equiv 0$; this is the case of the liquid-gas transition, where the coefficients of the potential expansion, in addition to T, also depend on the pressure P. In these occasions the condition $A(P, T) = 0$ determines the value of T at which the first-order transition occurs, as a function of P, and vice-versa. The critical point, at the end this line, is given by the additional condition $\beta(P_c, T_c) = 0$. (ii) When $\beta(P, T) \equiv 0$ the only condition left is $A = 0$. If the coefficients depend on two thermodynamic variables, P and T, the condition gives a line of second-order transition points in the PT-plane, similarly to the previous example for first-order transitions. This is the case of the continuous crystal-liquid transition. Also for the Ising model, $\beta(T) \equiv 0$, since the potential must be symmetrical with m in the absence of an external field, as discussed above. But, unlike the previous cases, here is only one variable, and the condition $A(T) = 0$

determines the value of the critical temperature T_c. At this point, the theory follows to consider only the later cases, with $\beta \equiv 0$.

Since $B(T_c) > 0$, close enough to the transition $B(T)$ can be substituted by the value of $B(T_c)$, and for simplicity called B. Then, using equation (1.3), and the fact that $\alpha, \beta \equiv 0$, the thermodynamic potential becomes

$$\Phi(T, m) = \Phi_0(T) + a(T - T_c)m^2 + Bm^4 + \dots, \tag{1.4}$$

with $a, B > 0$. There are now conditions to study the behavior of the potential near the critical point, and calculate the relation between m and T. Differentiating with respect to m, and applying the condition of minimum:

$$m\left(a(T - T_c) + 2Bm^2\right) = 0. \tag{1.5}$$

The solution $m = 0$ corresponds to a minimum of the potential only for $T > T_c$; otherwise, if $T < T_c$, $m = 0$ is actually a local maximum of Φ. The other solution of equation (1.5), $m^2 = a(T_c - T)/2B$, corresponds to the minimum of Φ when $T < T_c$. For the Ising model, when $T < T_c$ and in the absence of external field, the two equivalent minima of Φ correspond to the two possible orientations of the spontaneous magnetization:

$$m = \pm\sqrt{\frac{a(T_c - T)}{2B}}. \tag{1.6}$$

This singularity is characterized by a critical exponent $\beta = 1/2$, since in standard notation the order parameter $m \propto (T_c - T)^\beta$ on the ordered phase.

On the preceding analysis of the changes in the stable state of systems undergoing continuous phase transitions, it became clear that some thermodynamic quantities, such as the order parameter, have singularities at the transition point. Landau's theory of continuous phase transitions can follow to predict an even more interesting kind singularity, conventionally associated with *critical behavior*, the power-law divergence of some derivatives of thermodynamical quantities.

To illustrate this, an uniform external magnetic field is applied to the ferromagnetic Ising model. In this situation, each spin can couple individually with the external field and, when aligned with it, contributes a fixed amount to the decrease of the thermodynamic potential. Thus, a linear term must be included in expansion (1.4), to account for the coupling of individual spins with the uniform external field of magnitude h:

$$\Phi(T, m, h) = \Phi_0(T) - hm + a(T - T_c)m^2 + Bm^4 + \dots. \tag{1.7}$$

Until now, it had not been specified if Φ is the total potential of the system or a potential per volume unit, nor had it been necessary. The potential is an additive property, so the first definition can be transformed into the second merely by dividing by the total volume. Since the solution (1.6) only depends on the ratio a/B, it is not affected by the transformation. In the last expansion, the choice of an external field contribution of the form $-hm$ implies that $\Phi(T, m, h)$ is the thermodynamic potential per volume unit, or simply per spin, otherwise it should be multiplied by the number of spins in the system.

In the presence of an external field, the condition for thermodynamic equilibrium comes

$$\frac{\partial\Phi(T, m, h)}{\partial m} = -h + 2a(T - T_c)m + 4Bm^3 = 0. \tag{1.8}$$

The correct solution of the previous third degree equation is not as straightforward to get as it is in the situation without an external field. To determine the minimum of the thermodynamic potential it is useful to represent the field as a function of the magnetization:

$$h(m) = 2a(T - T_c)m + 4Bm^3. \tag{1.9}$$

The magnetization at $T = T_c$ comes from formula (1.9) $m_c = (h/4B)^{1/3}$, thus defining another critical exponent $\delta = 3$ characteristic of the critical magnetization dependence with the external field, in standard notation $m(T_c) \propto h^{1/\delta}$. Furthermore, the function found by rewriting condition (1.8) with T on the left-hand side,

$$T(m) = T_c + \frac{h - 4Bm^3}{2am},$$

is analytic for $m \neq 0$, and its Taylor expansion centered at m_c is convergent. Thus, also the expansion of the inverse function $m(T)$ is analytic at T_c, and its coefficients can be directly calculated from the coefficients of the expansion of $T(m)$. Then it is clear that the external field cancels the possibility of a continuous phase transition in the Ising model, since $m \neq 0$ for all finite temperatures there is no singularity of the thermodynamic potential. On other words, using the general argument mentioned in the beginning of this section; the external field changes the symmetry of the system, leaving no difference between the symmetries of the phases above and below T_c (the two phases actually become the same), hence, it is impossible for the system to have a phase transition.

The magnetic response function to an external field, or susceptibility, $\chi \equiv (\partial m/\partial h)_{T,h=0}$, can be calculated in the vicinity of the critical point with the help of formula (1.9):

$$\chi \equiv \left(\frac{\partial m}{\partial h}\right)_{T,h=0} = \left(\frac{\partial h}{\partial m}\right)^{-1}_{T,m_0} = \frac{1}{2a(T - T_c) + 12Bm_0^2},$$

where m_0 is the value of the spontaneous magnetization (when $h = 0$). It should be noticed that last derivative is taken in the absence of external field, not interfering with the possibility for a continuous phase transition. Using the solution $m_0 = 0$ for the disordered phase and $m_0 = \pm\sqrt{a(T_c - T)/2B}$ for the ordered phase:

$$\chi = \begin{cases} \frac{1}{4a}(T_c - T)^{-1} & \text{if } T < T_c, \\ \frac{1}{2a}(T - T_c)^{-1} & \text{if } T > T_c. \end{cases} \tag{1.10}$$

The susceptibility χ is well defined in the whole range of temperature except exactly at the critical point, where it diverges. Also this thermodynamic quantity has a mathematical singularity at T_c. On both sides of the transition, when the temperature is close enough to the critical point, the susceptibility behaves as a power law of $|T - T_c|^{-\gamma}$, with exponent $\gamma = 1$, growing to infinity at $T = T_c$. Interestingly, χ shows the same kind of behavior below and above T_c, $\chi \propto |T - T_c|^{-\gamma}$, with different coefficients, or amplitudes. Yet, their ratio is fixed, with the amplitude of the disordered phase being twice the amplitude of the ordered one, as visible in relation (1.10).

The theory laid out in this section neglects terms associated with local fluctuations of the order parameter. It turns out that such fluctuations are not negligible if the system's dimensionality $d \leq d_u$, where d_u is the *upper critical dimension*; $d_u = 4$ for thermodynamic

transitions and $d_u = 6$ for percolation. However quantitatively incorrect the predictions of the theory may be for $d \leq d_u$, it gives a qualitatively correct description of the phenomena, providing a valuable comprehension of the nature the changes occurring at a continuous phase transitions.

The display of this kind of power-law divergences, very common on continuous transitions, is a notable feature of critical behavior. The argument of the power law is a measure of how close the system state is to the critical state, for the examples used above the absolute difference $|T_c - T|$ is a natural measure, since it is given in terms of the independent parameter, and goes to zero when $T \to T_c^{\pm}$. The exponents of such power laws, called *critical exponents*, are always the same above and below the critical point. In fact, the critical exponents and the ratio between amplitudes are often found to be exactly the same for apparently unrelated systems.

1.3.2 Mean-Field Theories

Statistical physics strives to achieve an accurate description of the macroscopic behavior of large systems, from an adequate mathematical treatment of the microscopic interactions from which the system is defined. On a first approximation, it is tempting to reduce the problem to the description of a single particle's behavior, when subjected to an effective field encoding the average interaction with the rest of the system, i.e., a *mean-field*. Such an approximation does not account for the local fluctuations around the mean value of the field, and for this reason is not appropriate when those are relevant to the macroscopic behavior. Intuitively, when the number of interactions per particle is large the mean-field gives a more accurate description of the actual environment of each particle than when this number is small. Namely, a mean-field theory can correctly describe the macroscopic behavior for systems of high dimensionality.

Landau's approach to continuous phase transitions is in fact a mean-field theory, and as such its predictions are quantitatively wrong for dimensionality $d < d_u$. The Ginzburg criterion is a formal expression of how the fluctuations may render mean-field a poor approximation depending on the system's number of spatial dimensions. To account for fluctuations, the order parameter should be written as a function of d spatial coordinates $r \in \mathbb{R}^d$:

$$m(r) = \langle m \rangle + \Delta m(r) \tag{1.11}$$

where $\langle m \rangle = (1/V) \int_V dr\, m(r)$ is the average of the order parameter taken over the whole volume V of the system. The total free energy F is given by a generalization of the form of the potential (1.7), to include local fluctuations of the order parameter, integrated over the system's volume:

$$F = \int_V dr\, \Phi(r) = \int_V dr\, \Phi_0 - h(r)m(r) + a(T - T_c)m^2(r) + Bm^4(r) + g(\nabla m(r))^2 + \dots . \tag{1.12}$$

where the extra term $g(\nabla m)^2$ accounts for the energetic cost of having a non-null spatial gradient of the magnetization. The contribution of the gradient ∇m is subjected to the same arguments of symmetry as m itself (discussed in section 1.3.1), so the lowest power of ∇m in the expansion must be 2.

Evidently, the fluctuations of the order parameter lead to fluctuations of free energy, $F = \langle F \rangle + \Delta F$, which can be expanded in terms of $\Delta m(r)$. Since $\int_V dr\, \Delta m(r) = 0$ such an

expansion cannot have a linear term. So, if $\Delta m(r)$ is small, ΔF is determined by the average square fluctuation of the order parameter:

$$\begin{aligned}\Delta F &\approx \frac{1}{2}\langle (m(r) - \langle m\rangle)^2\rangle \frac{\partial^2 F}{\partial m^2}\bigg|_{m=\langle m\rangle}, \\ &= \frac{1}{2}\langle (\Delta m(r))^2\rangle \frac{\partial^2 F}{\partial m \partial h}\left(\frac{\partial m}{\partial h}\right)^{-1}, \\ &= \frac{V}{2\chi}\langle (\Delta m(r))^2\rangle.\end{aligned}$$

The probability of a free energy fluctuation of magnitude ΔF is given by the Gibbs distribution

$$w \propto e^{-\Delta F/T} = e^{-(V/2T\chi)\langle (\Delta m)^2\rangle}.$$

Such a probability distribution has a mean value of $\langle (\Delta m)^2\rangle$ given by:

$$\begin{aligned}(\delta m)^2 &= \left(\int_0^\infty dx\, e^{-(V/2T\chi)x}\right)^{-1} \int_0^\infty dx\, x e^{-(V/2T\chi)x}, \\ &= \frac{2T\chi}{V}. \end{aligned} \tag{1.13}$$

The difference between $\langle (\Delta m)^2\rangle$ and $(\delta m)^2$ is clear; the first is the square deviation from the mean value $\langle m\rangle$ averaged over the volume, and the second is the expected value of the first average, in a system of volume V. Recalling the expression for χ (equation (1.10), another critical singularity can be seen in last expression. It shows that near the critical point the magnitude of the fluctuations grow with $|T_c - T|^{-1}$.

From statistical mechanics fundamentals the expectation of a quantity x in a thermodynamic system is given by:

$$\langle x\rangle = Z^{-1}\sum_n x_n e^{-E_n/T},$$

where x_n is the value that variable x takes in configuration n, and $Z = \sum_n e^{-E_n/T}$ is the partition function. The interaction with an external field is accounted for in the energy of the configurations E_n as a term $-\sum_{i<N} h_i m_i$ for a discrete system with N particles, or in the continuous version as a integral $-\int_V dr\, h(r)m(r)$ over the system's volume V. Then the expected value $\langle m(r)\rangle$ is given by:

$$\langle m(r)\rangle = T\frac{1}{Z}\frac{\delta Z}{\delta h(r)} = T\frac{\delta \log Z}{\delta h(r)}. \tag{1.14}$$

The generalized susceptibility, defined as the response function of a spin in position r, to a field applied in position r',

$$\chi(r, r') \equiv \frac{\delta\langle m(r)\rangle}{\delta h(r')} \tag{1.15}$$

can be expanded using expectation (1.14):

$$\begin{aligned}\chi(r,r') &= T\frac{\delta^2 \log Z}{\delta h(r)\delta h(r')},\\ &= T\left(\frac{1}{Z}\frac{\delta^2 Z}{\delta h(r)\delta h(r')} - \frac{1}{Z}\frac{\delta Z}{\delta h(r)}\frac{1}{Z}\frac{\delta Z}{\delta h(r')}\right),\\ &= \frac{1}{T}\left(\langle m(r)m(r')\rangle - \langle m(r)\rangle\langle m(r')\rangle\right). \end{aligned} \tag{1.16}$$

The previously defined susceptibility, $\chi \equiv \partial m/\partial h$, where h is a vanishing uniform external field, is expressible in terms of the generalized susceptibility as $\chi = \int_V dr \int_V dr'\, \chi(r,r')/\mathrm{V}$. In other words, the susceptibility is the average, over all spins r in the system, of the sum of the contributions from the local fields $h(r') = h$ to the response of spin r. Then

$$\chi = \frac{1}{VT}\int_V dr \int_V dr'\, \langle m(r)m(r')\rangle - \frac{V}{T}m^2. \tag{1.17}$$

Next step is to find a the correlation length that characterizes the correlation function $G(r,r') = \langle m(r)m(r')\rangle - \langle m(r)\rangle\langle m(r')\rangle$ (note the close relation with the generalized susceptibility given by expression (1.16)). Starting by the condition of minimum of the generalized potential $\Phi(r)$ shown in equation (1.12):

$$-h(r) + 2a(T-T_c)m(r) + 4Bm^3(r) + 2g\nabla^2 m(r) = 0.$$

This condition must be observed by $\langle m(r)\rangle$, so taking the functional derivative in respect to $h(r')$ and substituting by $G(r,r')$ using equality (1.16):

$$\left(2a(T-T_c) + 12B\langle m(r)\rangle^2 - 2g\nabla^2\right) G(r,r') = T\delta(r-r').$$

The function $G(r,r')$ depends only on the distance $|r-r'|$, as is expected and can be seen from last equation. Then, it can be written as $G(|r-r'|)$ or simply $G(r)$. Using the equilibrium values of m in the absence of external field for each phase, calculated in section 1.3.1 ($m=0$ for $T > T_c$ and $m^2 = a(T_c - T)/2B$ for $T < T_c$), the equation for the correlation function comes

$$\left(\frac{1}{\xi^2} - \nabla^2\right) G(r) = \frac{T}{2g}\delta(r). \tag{1.18}$$

with,

$$\xi = \begin{cases} \left(\frac{2a(T_c-T)}{g}\right)^{-1/2} & \text{if } T < T_c,\\ \left(\frac{a(T-T_c)}{g}\right)^{-1/2} & \text{if } T > T_c. \end{cases} \tag{1.19}$$

The $G(r)$ that satisfies equation (1.18) can be obtained by applying a Fourier transformation to the equation to get

$$\hat{G}(k) = \frac{T}{2g}\frac{1}{k^2 + \xi^{-2}}.$$

In d-dimensional space the inverse transform gives

$$G(r) = \frac{T}{8\pi g}\frac{e^{-r/\xi}}{r^{d-2}}. \tag{1.20}$$

This solution comes with a dominant factor $e^{-r/\xi}$, and ξ is identified as the *correlation length*. For continuous phase transitions ξ diverges as a power law, $\xi \propto |T_c - T|^{-\nu}$, with exponent $\nu = 1/2$ in Landau's theory.

The validity of a mean-field approach, as the one presented in section 1.3.1, can be verified by comparing the magnitude of the order parameter's fluctuations with the magnitude of the order parameter itself. In particular, expansion (1.1) is a correct description of the thermodynamic potential density Φ only if the terms depending on the spacial derivatives of m give a negligible contribution. In other words, the integral (1.12) taken over the correlation volume ξ^d should be well approximated by $\xi^d\Phi$. This requirement is the Ginzburg criterion [25], and is equivalent to the condition

$$(\delta m)^2_{\xi^d} \ll \langle m \rangle^2, \tag{1.21}$$

where the subscript ξ^d indicates that the value of the mean square fluctuation $(\delta m)^2$ is calculated for the correlation volume. Near the critical point, the only length scale characteristic of the system's state is ξ. If the integration (1.12) is done on a volume $V \gg \xi^d$ arbitrarily large, then, by relation (1.13) $(\delta m)^2 \to 0$ when $V \to \infty$, and the information about the contribution of the fluctuations is lost. On the other hand, a volume $V \ll \xi$ is not large enough to produce a proper average of the fluctuations magnitude, since these extend over distances of the order of ξ.

Substitution of the expressions (1.13) and (1.6) into the Ginzburg criterion for Landau's mean-field theory yields the dependence of the theory's validity with the spacial dimensionality of the system under consideration [26]:

$$\frac{2T\chi}{\xi^d} \ll \frac{a(T_c - T)}{2B}.$$

Both χ and ξ have power-law critical singularities with exponents -1 and $-1/2$ respectively. Using expressions (1.10) and (1.19) for $T < T_c$. Near T_c the Ginzburg criterion is then reduced to the condition:

$$\left(\frac{2}{g}\right)^{d/2} BT_c \left(a(T_c - T)\right)^{-2+d/2} \ll 1.$$

For systems in a space of dimensionality $d < 4$ the left-hand side of last condition increases when the temperature approaches the critical point and diverges exactly at T_c, violating the condition. At $d < 4$ dimensions Landau's theory can give a correct description of the system's behavior only far away from the critical point; when T is close enough to T_c the Ginzburg criterion is no longer observed and Landau's expansion of the thermodynamic potential is incomplete. For $d > 4$ the left-hand side of the condition vanishes at T_c, rendering the mean-field approximation valid for a range of temperatures around T_c. Landau's mean-field theory is actually self-consistent for $d > 4$, and the critical exponents and amplitude ratios it predicts become exact. For $d = 4$ the theory almost works, renormalization group analysis gives logarithmic corrections to the mean-field behavior. In general the number of dimensions d_u above which the mean-field approximation predicts the right exponents is called *upper critical dimension* (for Landau's theory $d_u = 4$).

It is also found that the correlation function (1.20), decays as $G \propto r^{-d+2-\eta}$ at the critical point, where the critical exponent η is non-zero for $d < d_u$ (in the above is shown that for mean-field behavior $\eta = 0$). Exponent β characterizes the order parameter on the ordered phase only, where $m \propto (T_c - T)^\beta$, for $T > T_c$ the order parameter is identically zero. Exponents

γ and ν characterize, respectively, the susceptibility χ and the correlation length ξ in the region near critical point, for both $T < T_c$ and $T > T_c$. And δ is the characteristic exponent of the critical magnetization m_c for $T = T_c$.

1.3.3 Self-Organized Criticality

Critical points are ubiquitous in nature, as discussed in the section 1.3.1 every continuous phase transition has one. In addition, there are some non-equilibrium dynamical systems that display *self-organized criticality*, a concept introduced by Bak et al. [27] demonstrating how some of the special properties of critical points might arise in real systems. While critical points of continuous phase transitions are only achievable by precisely tuning the independent parameters to their critical values, in the self-organized criticality the critical state is reached spontaneously.

In this kind on dynamics, the source of the critical behavior is on the type of interaction, and is maintained over a wide range of the parameters. The main idea is that large systems self-organize into highly interactive critical states, where minor perturbations may lead to events called *avalanches*, of all sizes. These system exhibit periods of seemingly equilibrium behavior, punctuated by bursts of activity. Since there is a stochastic component of the dynamics, that can be interpreted as noise, the actual events cannot be predicted, however their statistical distribution can [28]. The size of the avalanches is distributed in a heavy tailed power-law fashion, much like the local fluctuations around the equilibrium state of thermodynamic systems near criticality. This suggests that in these complex systems the self-organization induces some kind of critical macroscopic behavior, also characterized by an infinite correlation length. In non-equilibrium *sandpile*-like systems, the self-organized criticality emerges when in-flow and out-flow are present simultaneously, but they are infinitely low.

Examples of dynamical systems exhibiting self-organized criticality exist in many distinct, apparently disconnected, fields; and include fluctuations on stock markets [29], distribution of earthquake sizes [30], avalanches of evolution/extinction in living systems [31, 32] and vehicular traffic flow and jams [33]. The similarities between this class of dynamical complex systems and critical points of thermodynamic phase transition was first made in [27] using a *sandpile* model. In this paradigmatic manifestation of self-organized criticality, model sand is added grain by grain to a model sandpile built upon a d-dimensional lattice. In between additions, sand may fall downhill in response to the growth of the pile's local slope. Each of these events may trigger others, in cascades that form avalanches. The size of the avalanches can be small or can cover the systems entire system many times over. Another interesting feature shared by phase transitions and self-organized criticality is the emergence of fractal or multi-fractal behavior [34]. A direct consequence of the scaling properties conferred, in both cases, by the divergence of the correlation length, expressed by the lack of a cut-off for the size of the fluctuations and avalanches.

1.4 Percolation Transition

The modern understanding of disordered systems in statistical and condensed matter physics is essentially based on the notion of percolation [20]. The elementary process of progressively increase the density of edges or nodes in a network, above some value (the

percolation threshold), leads to the formation of a giant connected component (a percolation cluster), in addition to finite clusters. The number of nodes and connections contained in the percolation cluster represents a non-vanishing fraction of the network, even at the thermodynamic limit.

The introduction to percolation given in section 1.2.3 is rather incomplete and superficial; even the most basic aspects of this random process were omitted, and for that reason its importance could not be properly assed there. In fact, the percolation transition stands in many respects the simplest non-trivial phase transition [20, 21]. The percolation threshold is actually a critical point, and near it, the system's cluster structure shows all the properties of criticality discussed during section 1.3. The symmetry break involved in this phase transition is due to the need of an extra variable to account for the relative size of the giant component above the percolation threshold, which is a measure of the order. Specifically, the fraction of the system contained in the percolation cluster, S, is null when there is no such cluster, below the critical density of nodes or links p_c, and strictly positive for densities p above p_c. In general, for thermodynamic phase transitions, above the critical temperature the system is in a state of disorder, while below the critical temperature the macroscopic state of the system changes qualitatively, which requires the introduction of an order parameter to account for the spontaneous ordering. Contrarily to thermodynamic transitions, for percolation the disordered phase corresponds to values of the independent parameter $p < p_c$ when $S = 0$, and the ordered one to $p > p_c$ and $S > 0$. But this poses no incongruence, and all the essential notions of continuous phase transitions theory, such as divergent correlation length and other critical singularities, scaling and universality, are observed in the percolation transition.

Clearly, the threshold concentration for percolation to occur depends on the network structure. In particular, p_c depends on the dimensionality of the network, on the local details of its underlying structure and also on which one, concentration of active nodes or edges, the density p refers to, i.e., if the process in question is one of site or bond percolation. However, all available evidence strongly suggests that the critical behavior associated with the percolation threshold depends neither on the type of percolation, site or bond, nor on the local details of the network. It is widely believed that the critical exponents and certain ratios depend only on the dimensionality of the network. In two dimensions for instance, the square lattice bond percolation has a threshold $p_c = 1/2$ and the site version has $p_c \approx 0.5927$, while the critical concentration on the triangular lattice is $p_c \approx 0.3473$ for bonds and $p_c = 1/2$ for sites. Yet, percolation critical exponents are equal for these systems and all other lattices in two dimensions, a manifestation of the universality feature of phase transition critical points [20]. In addition to numerical evidence, renormalization group theory lends further support to the universality hypothesis: any informations about the local structure are lost on an infinite size rescaling operation, or eventually if enough finite size rescaling operations are made, nonetheless at criticality the system's macroscopic state stays invariant under such transformations. Therefore the critical behavior cannot depend on structural details, i.e., depends only on the number of dimensions of the lattice [21].

There are a few exactly solvable percolation models, which may be used to analytically show how the critical behavior can come by in these random systems. Despite of the absence of an ordered phase, since the critical density $p_c = 1$, some aspects of the solution of one dimensional problem are also present at higher dimensions, as shown in next section 1.4.1. In section 1.4.2 a similar analysis is done for the Bethe lattice, providing the mean-field critical the behavior of the percolation transition. At last section 1.4.4, is given the solution to another model with mean-field properties, the Erdős-Rényi random graph, which is one of

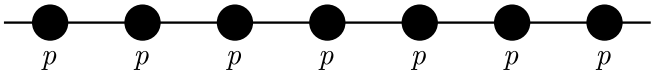

Figure 1.3: One-dimensional percolation on a chain of sites. Each site is occupied uniformly at random, with probability p, independently.

the most fundamental models for percolation, and has a direct relation with the percolation model studied this thesis.

1.4.1 One Dimension

Like many other problems in theoretical physics, such as the Ising model, the percolation problem can be solved exactly in one dimension. Consider a chain of nodes, each connected to two neighbors by an edge, as depicted in Figure 1.3, where each node is occupied with probability p. Obviously, for any concentration of empty sites $1-p>0$ the fraction of nodes and edges in the larger cluster is null, in the thermodynamic limit, and the system does not percolate, hence the threshold $p_c = 1$ in one dimension. Then, the size of the giant component $S = 0$ for any p except exactly at 1, where $S = 1$. This discontinuity is inconsistent with the theory of phase transitions laid out in section 1.3, and is associated with the absence of an ordered phase; since the transition occurs only at the very last moment, when the last empty node is occupied, the region $p > p_c$ is not accessible, making this a somewhat unusual transition. Yet, some general critical properties of the percolation transition can still be seen in this simple model, approaching p_c from below.

Thanks to the universality feature, it is not relevant for the critical behavior whether the random occupation process is defined for sites or for bonds. In the system of Figure 1.3 this is rather evident: each node could be replaced by an edge and each edge by a node, resulting in exactly the same structure, since each node is connected to two edges and, of course, each edge to two nodes. So that, the probability p and all other measures, initially applied to the edges, can be after the transformation applied to the nodes giving exactly the same results. Thus, the equivalence of site and bond percolation in one dimension is easily proven.

Considering the site percolation version, each site is occupied independently at random with probability p, and the probability that n arbitrary sites are occupied is p^n. The probability of each neighbor of a site being empty is $1-p$, also independently. Since every cluster is surrounded by two empty sites, one on each side, the probability that a randomly chosen node is isolated, i.e., is in a cluster of size one, is $(1-p)^2p$, and the probability that it is the leftmost site of a cluster of size two is $(1-p)^2p^2$, and so on. In general, the probability of a randomly chosen node being the leftmost site of a cluster of size s is $(1-p)^2p^s$. To say leftmost site is merely a convention, the same is true for the rightmost site, or any site at another specific position. It is more convenient to simply regard these probabilities as the density of clusters of size s, since for a chain of length L the number of clusters of size s is on average $L(1-p)^2p^s$. Thus, the cluster structure, and with it everything else in the system, is completely described by the *cluster numbers* $n(s,p)$, i.e., the number of clusters of size s per lattice site:

$$n(s,p) = p^s(1-p)^2. \tag{1.22}$$

Alternatively, it is also usual to work with the probability $P(s,p)$, that a randomly chosen

node belongs to a cluster of size s, independently of the position, for this quantity $LP(s,p)$ is the average number of nodes in clusters of size s, in a chain with L nodes. Moreover, to avoid confusion between upper and lower case symbols, and since the percolation model studied later is one that can only be defined as a dynamical process, the occupation probability is hereafter denoted as $t \equiv p$. Both conventions are equally well suited for the analysis purposes, and simply relate to each other, i.e.

$$\begin{aligned} P(s,t) &= sn(s,t) \\ &= st^s(1-t)^2. \end{aligned} \tag{1.23}$$

The sum over all finite sizes s of the probabilities $P(s,t)$ equals the probability that a site belongs to any cluster, i.e., the occupation probability t,

$$\sum_{s=1}^{\infty} P(s,t) = t. \tag{1.24}$$

This equality can be checked directly for $t < 1$ using relation (1.23) and the formula for the geometric series $\sum_s t^s = t/(1-t)$. For $t = 1$ the right-hand side of equation (1.23) is identically zero, and clearly equality (1.24) no longer holds. In general the cluster size distribution $P(s,t)$ does not include the giant connected component, and for the previous condition to hold also in the ordered phase, it needs to explicitly include the probability that the randomly chosen node belongs to the giant connected component, given by $S(t)$:

$$\sum_{s=1}^{\infty} P(s,t) + S(t) = t. \tag{1.25}$$

Which simply states that an occupied node either belongs on a finite cluster on in the infinite one, and is valid for any model at any dimension.

The size distribution of finite clusters $P(s,t)$ (or $n(s,t)$) can be used to calculate any percolation related property of the system. For instance, the total number of clusters per lattice site is simply equal to $\sum_s P(s,t)/s = \sum_s n(s,t) = \sum_s t^s(1-t)^2 = t(1-t)$, with a maximum of $1/4$ at $t = 1/2$. It is also interesting to ask what is the average size of the cluster to which a random node belongs, $\langle s \rangle_P$. The subscript indicates that this is the average of distribution P, but it also intends to imply that only finite clusters are considered. In higher dimensions, when $t_c < 1$ and there is a phase with a percolation cluster, if that cluster is not excluded from the sum, the average $\langle s \rangle_P$ will be divergent for any $t > t_c$, since a fraction of the nodes is in a cluster with infinite size. If a node is targeted uniformly at random, it might belong to a cluster of size s with probability $P(s,t)$, to the giant cluster with probability $S(t)$, or it may be empty with probability $1-t$. Again, from equation (1.23) and the formula for the geometric series:

$$\begin{aligned} \langle s \rangle_P &= \sum_{s=1}^{\infty} sP(s,t) \\ &= (1-t)^2 \sum_{s=1}^{\infty} s^2 t^s \\ &= \frac{t(1+t)}{1-t}, \end{aligned} \tag{1.26}$$

which diverges as $t \to t_c = 1$.

Similar results are obtained for higher dimensions when approaching t_c from either side, as shown later. This divergence is very plausible, if for $t > t_c$ a giant component exists, then for t slightly below t_c some very large, although finite, clusters might be expected. These continue to grow unboundedly with t until it reaches t_c. This kind of behavior is typically associated with critical points, and despite the absence of an ordered phase, the one dimensional case still retains this property of continuous phase transitions.

Another important quantity, worthy of attention, is the correlation function and respective correlation length for this system. Here the correlation function, $G(r,t)$, is defined as the probability that a site at a distance r from an occupied site belongs to the same cluster. For $r = 0$ the two sites are the same and $G(0,t) = 1$, while for $r = 1$ the sites are at neighboring positions and G is just the probability that the site is occupied, $G(1,t) = t$. For two sites, at a distance r from each other, to belong to the same cluster, all sites between them must be occupied without exception, as well as themselves. By definition the site at 0 is always occupied, so this happens with probability:

$$G(r,t) = t^r. \tag{1.27}$$

For $t < 1$, the correlation function goes to zero exponentially as the distance $r \to \infty$, and it can be rewritten as

$$G(r,\xi) = e^{-r/\xi}, \tag{1.28}$$

where

$$\xi(t) = \frac{-1}{\ln t} \simeq (t_c - t)^{-1}. \tag{1.29}$$

The last equality is only valid near the critical point, when t is close enough to $t_c = 1$ the expansion $\ln(1-x) \simeq -x$ can be used. Thus, defining the correlation length for this problem, in an way analogous to what was made for thermal phase transitions in section 1.3.2, but using a much simpler mathematical procedure.

It was seen, from the exact solution in one dimension, that such quantities as $\langle s \rangle_P$ and ξ diverge as t approaches the percolation threshold t_c, and that the divergences follow simple power laws as $(t_c - t)^{-1}$, at least close enough to t_c. The same happens in higher dimensions d, although the exact solution is not known for $d > 1$ finite. Near t_c the behavior is qualitatively the same in all dimensions, and is comparable with the critical behavior of thermal phase transitions (all the relevant quantities have counterparts there [20]). In section 1.3.2 was shown how the correlation length diverges within Landau's theory of continuous phase transitions. Moreover, $\langle s \rangle_P$ can be regarded a response function to an external stimulus, if a number $hL \ll L$ of occupied sites is chosen at random and connected to an external source, the size of the cluster formed by the clusters to which these sites belong is on average $hL\langle s \rangle_P$, on the disordered phase where $S = 0$. In the ordered phase $S > 0$ and a number hLS of the external bonds fall inside the giant connected component, then $(1-S)hL\langle s \rangle_P$ is the number of sites added to the giant component due to the external bonds. The analogy is now complete, with h playing the role of an external field, and $\langle s \rangle_P$ the one of a susceptibility. In this way the derivative of the order parameter $\partial S/\partial h = \langle s \rangle_P$ (for $d > 1$ the transition is continuous, and close enough to the critical point $1 - S \simeq 1$). Furthermore, the behavior of the magnetic susceptibility χ given by expression (1.10) is the same as $\langle s \rangle_P$, a critical power-law divergence at t_c.

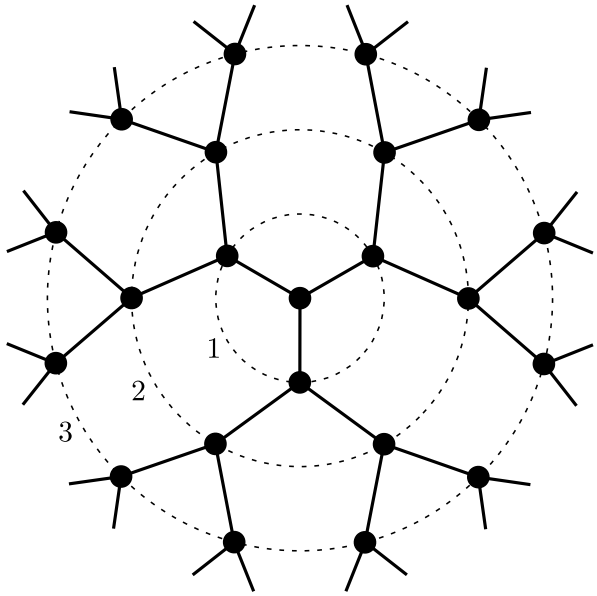

Figure 1.4: Bethe lattice with coordination number $z = 3$. Only a small part of the lattice is shown in this figure, the structure considered in the text extends to infinity. The central node is regarded as the root, and the labeled dashed lines mark the nodes in the n-th generation. In this regular lattice, every node, other than the root, connects once to the previous generation, and $z-1$ times to the next. There are no loops, as such, the z branches formed by the nodes and edges accessible through each neighbor of the root do not overlap.

1.4.2 Bethe Lattice

Besides the one dimensional case, there is another simple percolation model that can be exactly solved, which corresponding dimensionality is infinite. The Bethe lattice is a regular graph, without any loops (a *tree*), which, by its distinctive topological properties, allows for exact calculations. The special structure of the Bethe lattice can be seen in Figure 1.4, for the coordination number $z = 3$. Emanating from a central node, the *root*, there are edges to z neighbors, which constitute the first *generation* . Each node in the first generation has $z-1$ descendants in the second generation, in addition to a connection to the root, hence, its total number of neighbors is also z. Each node in the second generation is also connected to $z-1$ descendants in the third generation, and so on. The z branches emanating from the root are independent, i.e., share no nodes; as such, there are no loops in the graph, the only path connecting two branches is through the root. The number of nodes in the n-th generation is $z(z-1)^{n-1}$, as can be seen in Figure 1.4.

For d-dimensional objects, the volume v grows with its diameter r as $v \propto r^d$, and the surface is $s \propto r^{d-1}$. Therefore,

$$s \propto v^{1-1/d}.$$

The total number of sites in a Bethe lattice composed of n generations is given by the sum $1 + z\sum_{i=0}^{n-1}(z-1)^i = 1 + z\left[(z-1)^n - 1\right]/(z-2)$, of these, $z(z-1)^{n-1}$ belong to the n-th generation, and are at the surface. Both these numbers grow exponentially with n. For the example of $z = 3$ shown in Figure 1.4, the volume and surface, in number of sites, are 3×2^n and $3 \times 2^{n-1}$ respectively. For a generic z the fraction of sites at the surface tends to

$(z-2)/(z-1)$ for large n, which corresponds to an exponent $1/d = 0$ in the surface to volume relation. On other words, a proportional growth of the surface with the volume occurs only when $d \to \infty$, as in the case of the Bethe lattice. For this reason, this is a mean-field model, in the sense that the its dimensionality is surely larger than the upper critical dimension (as is shown in the section 1.4.3 $d_u = 6$ for the percolation transition). The critical exponents of this model should also correctly describe the critical singularities of other models with $d \geq 6$, as previously discussed.

Even in the thermodynamic limit, $n \to \infty$, the surface amounts to a finite fraction of the system. However, for the study of the percolation transition in this model, only the behavior of the bulk needs be considered. On the infinite system the borders are at infinite distance from all the nodes in the bulk, rendering all such nodes topologically equivalent, i.e., since the graph is a tree and all nodes have degree exactly z, the topological structure around any site of the bulk is the same as for the root site. Consequently, any result calculated for the root is also valid for any other site in the bulk of the infinite Bethe lattice.

Thanks to its special topological properties, the percolation threshold can be exactly calculated for this model. Considering the possibility of finding an infinite path of occupied sites starting at the root; is clear that walking along such path, at any new site there are $z-1$ possible sites where to advance next, each of which occupied with probability t independently. Then at each site in the path, the average number of occupied sites to where the path can be continued is $t(z-1)$. If this number is smaller than unit, the average number of paths leading to infinity decreases at each generation by the factor $t(z-1) < 1$ – the probability of finding a path of occupied sites goes to zero exponentially with the path length, if $t < 1/(z-1)$. Thus, the percolation threshold of the Bethe lattice with *coordination number* z is

$$t_c = \frac{1}{z-1}. \tag{1.30}$$

Precisely the same argument can be used for the bond percolation threshold, and the result (1.30) is valid for site and bond percolation on the Bethe lattice. In fact, bond and site percolation in Bethe lattices are equal in all aspects; for each configuration of occupied bonds, in the bond problem, there is a corresponding configuration in the site version, where the occupied sites are positioned at the outermost end of each occupied bond (see figure 1.4). Since to each node corresponds only one such bond (into the previous generation), the two configurations have the same probability, each on its model, and also have exactly the same connectivity properties.

It is clear that when $t < t_c$ the root never has a path to infinity, however a density of occupied sites $t > t_c$ does not ensure the existence of such a path. For instance, for any $t < 1$ there is alway a probability $t(t-1)^z > 0$ that the root site is occupied and all of its z neighbors are empty. Therefore, the probability S that the root or any other bulk site belongs to the infinite cluster must be considered. Evidently, for $t < t_c$ there is no infinite cluster and $S = 0$, the interest is in the behavior of S for $t > t_c$.

As mentioned, the critical properties of models of dimensionality larger than d_u are similar, in particular, they show the same critical exponents. For the sake of simplicity, from here fourth, the simplest case of a Bethe lattice with $z = 3$, depicted in Figure 1.4, will be considered, since the exponents should not depend on this number ($z = 2$ returns a chain corresponding to $d = 1$, while for any $z \geq 3$ the dimensionality d becomes infinite).

Letting R denote the probability that a given edge emanating from a particular site does not lead to a site connected to infinity; which is the same for every edge of every site of the

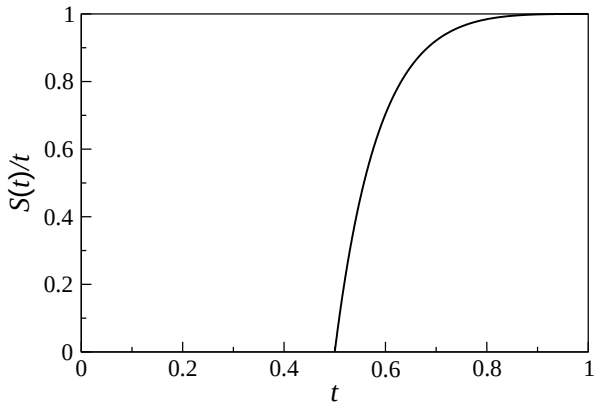

Figure 1.5: Fraction of occupied sites that belong to the percolating component S/t as a function of the density of occupied sites t in the Bethe lattice with $z = 3$. For $z = 3$ expression (1.30) gives $t_c = 1/2$, below this density $S = 0$, and above S is given by expression (1.31).

bulk. The probability that none of two edges, emanating from a site in the first generation into the second, leads to an infinite cluster is simply R^2 (as they are statistically independent). Then, the probability R, that a particular edge emanating from the root does not lead to a site in the first generation connected to infinity, is also equal to the probability of this site being empty, $1 - t$, plus the probability of being occupied and none of the edges into second generation lead to infinity, i.e., $R = 1 - t + tR^2$. This quadratic equation has solutions $R = 1$, which corresponds to the solution of the disordered phase, and $R = (1 - t)/t$ which is larger than unit for $t < t_c = 1/2$ and smaller for $t > 1/2$, corresponding to the solution for the ordered phase. Now, the probability that the root is occupied but does not belong to the infinite cluster, $t - S$, can also be written as $tR^3 = t\,[(1 - t)/t]^3$, yielding the expression for the fraction of sites belonging in the percolation cluster $S(t)$ when $t > t_c$:

$$\frac{S(t)}{t} = 1 - \left(\frac{1-t}{t}\right)^3 . \tag{1.31}$$

If instead, the solution $R = 1$ is used, the size of the giant component S comes identically null, coherently with the expected behavior for $t < t_c$. It should be emphasized that, in the infinite system, the probability of belonging to the giant component is equal for all the sites, and is just the fraction of sites in that component S. Obviously, the number of sites in the percolating component cannot be larger than the number of occupied sites, so it is perhaps more appropriate to speak of the fraction of occupied sites in the infinite cluster S/t, nevertheless close to the critical point both conventions are simply related by a proportionality factor of $1/t_c$. Figure 1.5 shows the dependence of the size S/t with the density t for the infinite Bethe lattice with $z = 3$; that kind of qualitative behavior is a typical manifestation of continuous phase transitions.

In the absence of an infinite cluster, the average cluster size $\langle s \rangle_P$ can be exactly calculated in a recursive fashion, similarly to the procedure used for S. Letting U be the average number of sites connected to a particular site of the first generation, by occupied paths that pass through each edge into the second generation. Since the sites are equivalent, U is also the average number of sites connected to the root by paths passing trough a particular node in the first generation. Then the equation $U = (1 - t)0 + t(2U + 1)$ gives the expression for

U. On the right-hand side of the equality the null contribution corresponds to when the first generation site is empty, and the corresponding edge connects the root to zero sites, which happens with probability $1-t$; with probability t the site is occupied, and each of its two edges into the second generation contribute with an average of U sites, plus 1 to account for the site itself. For $t < t_c$ the solution comes $U = t/(1-2t)$. The average cluster size to which a random occupied site belongs is $1 + 3U$:

$$\langle s \rangle_P = 1 + 3U = \frac{1+t}{1-2t}. \tag{1.32}$$

below the threshold.

So far, the special structure of the Bethe lattice allowed the exact calculation the giant component's size $S(t)$ for $t > t_c$ (equation (1.31)), and of the average finite cluster size $\langle s \rangle_P$ for $t < t_c$ (equation (1.32)). Since at the percolation threshold an infinite cluster appears, the average cluster size would be expected to be very large when approaching $t_c = 1/2$ from below, and indeed, close enough to t_c, relation (1.32) gives

$$\langle s \rangle_P \simeq \frac{3}{4}(t_c - t)^{-\gamma}, \tag{1.33}$$

a typical critical singularity with exponent $\gamma = 1$. An essential aspect of continuous phase transitions is that both phases converge to the same at t_c, as discussed in section 1.3, which is verified by equation (1.31), since when t approaches t_c from above the size of the giant component

$$S \simeq 6(t - t_c)^{\beta} \tag{1.34}$$

with critical exponent $\beta = 1$. Although $S(t)$ is known for both phases (for the $t < t_c$ phase $S \equiv 0$) the average cluster size $\langle s \rangle_P$ for $t > t_c$ was not considered in the previous calculations. However, it is known from phase transition theory, that critical divergences with the same exponent should be expected on both sides of the threshold.

Another simplicity of Bethe lattices becomes apparent when calculating the cluster size distribution $P(s,t)$. There the number of empty sites surrounding a cluster of size s is always $(z-2)s + 2$, and in fact, the cluster size distribution $P(s,t)$ can be exactly found, by calculating the *animal numbers*, g_s [35]. Here, however, a simpler approach is adopted for brevity reasons. The cluster size distribution is given by $P(s,t) = g_s s t^s (1-t)^{(z-2)s+2}$, so, to avoid the calculation of g_s, one can write for $z = 3$:

$$\begin{aligned} \frac{P(s,t)}{P(s,t_c)} &= \left(\frac{1-t}{1-t_c}\right)^2 \left(\frac{t(1-t)}{t_c(1-t_c)}\right)^s, \\ &= \left(\frac{1-t}{1-t_c}\right)^2 \left[1 - 4(t-t_c)^2\right]^s, \\ &\propto e^{-cs}, \end{aligned} \tag{1.35}$$

with

$$c = -\ln(1 - 4(t-t_c)^2) =_{t \to t_c} 4(t-t_c)^{1/\sigma}, \tag{1.36}$$

with $\sigma = 1/2$. This ratio of distributions decays rapidly, as an exponential of the cluster size s. At this point, a description of the behavior of $P(s,t_c)$ is the the only thing missing.

Approaching t_c from below, the behavior of $P(s,t)$ must be consistent with equation (1.33), in particular,

$$\langle s\rangle_P = \sum_s sP(s,t) \tag{1.37}$$

must diverge as $(t_c - t)^{-\gamma}$. However, an exponential decay of $P(s,t)$ in the last expression, leads to an average cluster size that is always finite, and cannot reproduce the divergence of $\langle s\rangle_P$ at t_c. Thus, the critical distribution must decay slower than any exponential. A power-law decay of $P(s,t_c)$ is then more plausible, and a new critical exponent is then defined through the ansatz:

$$P(s,t_c) \propto s^{1-\tau}, \tag{1.38}$$

for large s. The 1 in the exponent is summed to obey the conventional notation, since the exponent τ is usually defined for the cluster numbers $n(s,t) = P(s,t)/s \propto s^{-\tau}$.

The right-hand side of equation (1.37) can now be evaluated using the asymptotics (1.38). The divergence of the average cluster size at the percolation threshold clearly shows that the sum (1.37) is dominated by large s terms near t_c, which is the validity region of expression (1.38). The value of the critical exponent τ, is then given by comparison with equation (1.33). For t close below t_c, the substitution of expressions (1.36), (1.35) and (1.38) into (1.37) gives:

$$\begin{aligned}
\langle s\rangle_P &\propto \sum_s s^{2-\tau} e^{-cs}, \\
&\approx \int ds\, s^{2-\tau} e^{-cs}, \\
&= c^{\tau-3} \int dx\, x^{2-\tau} e^{-x}, \\
&\propto c^{\tau-3}, \\
&\propto |t_c - t|^{(\tau-3)/\sigma},
\end{aligned} \tag{1.39}$$

where the modulus $|t_c - t|$ must be used when substituting $c \propto (t_c - t)^{1/\sigma}$, since the exponent of final expression results from taking the $\tau - 3$ power of an already a squared number ($1/\sigma = 2$). The behavior of expression (1.33) is recovered if the exponent τ is such that $(\tau - 3)/\sigma = -\gamma$. Given that for Bethe lattices $\sigma = 1/2$ and $\gamma = 1$, the exponent characteristic of the critical cluster size distribution is $\tau = 5/2$.

It should be noticed that none of the ingredients, used to derive expression (1.39), involves assumptions about the existence of a giant component, thus it should hold on both sides of the transition. Exact equation (1.33), written for the absence of giant component, predicts a critical divergence of $\langle s\rangle_P$ when approaching t_c from below. Last expression states that a similar behavior with the same exponent is observed approaching the t_c from above, as expected for continuous phase transitions. Yet, in general the proportionality factors may be different on each side of the critical point [36]. On either side of the transition, close to the critical point, equation (1.35) can finally be rewritten in its scaling form, for large s:

$$P(s,t) \propto s^{-3/2} e^{-4(t_c - t)^2 s}. \tag{1.40}$$

Critical exponents were calculated using the Bethe lattice specially simple structure. The infinite dimensionality of these lattices is surely superior to the upper critical dimension for

percolation d_u, and the exponents $\gamma = 1$, $\beta = 1$, $\sigma = 1/2$ and $\tau = 5/2$ correspond to the mean-field critical behavior of the percolation transition.

1.4.3 Scaling Theory of Percolation

It was seen in the previous sections that the finite cluster size distribution follows rather simple laws, and that an exponentially decaying tail is quite frequent (see equations (1.23) and (1.40)). The general theory, for the near critical point behavior, of the percolation transition is discussed in this section. Since in one dimension there is only the non-percolating phase, and for that reason no actual phase transition, such theory needs only to generalize the results obtained for more than one dimension. It turns out, however, that many properties of percolation in higher dimensions are also observed in one dimension.

In general, close enough to the critical point, the asymptotic behavior of the cluster size distribution is given by [36, 37]:

$$P(s,t) = s^{1-\tau} f\left((t-t_c)s^{\sigma}\right), \tag{1.41}$$

where $f(x)$ is the so-called *scaling function*, which contrarily to the critical exponents σ and τ is determined not only by d, but also by the particulars of the model under consideration. This expression configures the central assumption of percolation theory, despite the equal sign holding only for the limits of $t \to t_c$ and $s \to \infty$. The average cluster size, $\langle s \rangle_P$, power-law critical divergence at the percolation point implies that the behavior is dominated by clusters of large sizes s. Which is also consistent with the divergence of the correlation length expected for continuous phase transitions. The scaling assumption (1.41), is very well supported by experimental evidence, and no deviations from this behavior are known so far [20]. Application of renormalization group arguments to percolation lend further support to the scaling assumption, and in addition provides effective methods to calculate the critical exponents [38, 39, 40, 41]. Moreover, the scaling assumption allows to find relations between critical exponents from rather basic considerations (which is done latter in this section), showing that in fact there are only two independent exponents, and the values of all others are determined by those.

It is easily verifiable that both equations (1.23) and (1.40), for one-dimensional chain and infinite-dimensional Bethe lattice respectively, are particular cases of the scaling form (1.41). For the Bethe lattice with coordination number $z = 3$, it is evident from expression (1.40) that $f(x) \propto e^{-4x^2}$. While in one dimension the cluster size distribution (1.23) can be rearranged, in the limit of $t \to t_c = 1$, as follows:

$$\begin{aligned} P(s,t) &= st^s(1-t)^2, \\ &= s(1-(t_c-t))^s(t_c-t)^2, \\ &= s(t_c-t)^2 e^{s\ln[1-(t_c-t)]}, \\ &= s^{-1}\left[(t_c-t)s\right]^2 e^{-(t_c-t)s}. \end{aligned} \tag{1.42}$$

This expression observes assumption (1.41), with exponents $\tau = 2$ and $\sigma = 1$, and scaling function $f(x) = x^2 e^{-x}$. For one dimension, the cluster size distribution near t_c assumes a scaling form for all sizes s and not just for large s.

Another property associated with continuous phase transitions also observed in one-dimensional percolation is the singular behavior of the average cluster size near t_c. Expression (1.26)

shows exactly that. It also shows that the relation between the critical exponents of the cluster size distribution, τ and σ, and the critical exponent for the average cluster size calculated in the end last section for the Bethe Lattice,

$$\gamma = \frac{3-\tau}{\sigma}, \tag{1.43}$$

still holds in one dimension, where $\tau = 2$, $\sigma = 1$ and $\gamma = 1$. In fact, this equality is a direct consequence of the scaling assumption (1.41). It is a so-called *scaling relation*, and holds a fundamental significance to percolation theory, as it is observed for all percolation models in any dimensions. A similar procedure to the one leading relation (1.39) can be employed to check the validity of the scaling relation in general:

$$\begin{aligned}
\langle s \rangle_P &= \sum_{s=1}^{\infty} sP(s,t), \\
&= \sum_{s=1}^{\infty} s^{2-\tau} f\left((t_c - t)s^{\sigma}\right), \\
&\approx \int_1^{\infty} ds\, s^{2-\tau} f\left((t_c - t)s^{\sigma}\right), \\
&= |t_c - t|^{(\tau-3)/\sigma} \sigma^{-1} \int_{|t_c-t|}^{\infty} dx\, x^{(3-\tau)/\sigma - 1} f\left(\mathrm{sgn}(t_c - t)x\right), \\
&\propto |t_c - t|^{(\tau-3)/\sigma}.
\end{aligned} \tag{1.44}$$

As in expression (1.39), here the modulus must be introduced to avoid taking a non-integer power of a negative number, when changing of integration variable. In addition, the argument of function f should take positive values when $t < t_c$, and when $t > t_c$ it should be negative; which is achieved with the function $\mathrm{sgn}(t_c - t)$. The lower limit of the integral, $|t_c - t|$, is put to zero, as t is arbitrarily close to t_c (assuming that the integral is convergent as the lower limit goes to zero, which is true for $\tau < 3$).

It is clear now that, in general, the proportionality of factor in relation (1.44) may be different on below and above the critical point, since it is determined by the shape of $f(x)$, for positive and negative x respectively. When the scaling function is symmetric around the origin, as in the case of the Bethe lattice, this factor is same on both sides; however, as seen in Figure 1.6, for $d < \infty$ dimensions $f(x)$ is not symmetric, which results in different factors on each side of the threshold.

A few aspects of the behavior of the scaling function $f(x)$ may be pointed out. For $d > 1$, the scaling function should be continuous at $x = 0$, and take the value $0 < f(0) < \infty$. The condition that $P(s,t)$ should vary continuously with t imposes that f is actually continuous everywhere else too, but the point $x = 0$ is especially important since it is related to the critical distribution:

$$P(s, t_c) = f(0)s^{1-\tau} \tag{1.45}$$

for large s. Only in one dimension $f(0) = 0$, consistently with the lack of a true phase transition. Furthermore, the asymptotic behavior of $f(x)$ should reproduce an exponential-like decay of $P(s,t)$ for large s, when $t \neq t_c$, observed here for one- and infinite-dimensions

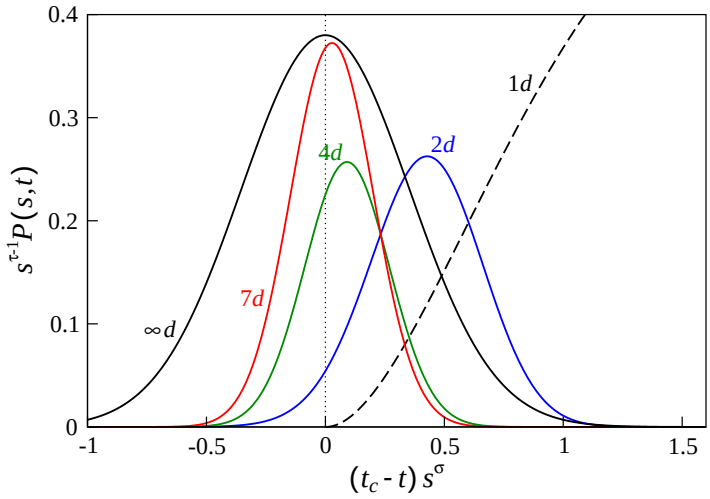

Figure 1.6: Scaling functions $f(x) = s^{\tau-1}P(s,t)$, with $x = (t_c - t)s^{\sigma}$, entering the scaling assumption (1.41), for several different dimensions d. The black curves are the exact functions calculated above, for one dimension, $f(x) = x^2 e^{-x}$ (dashed), and for the infinite dimensionality Bethe lattice with $z = 3$, $f(x) = f(0)e^{-4x^2}$ (solid). The curves for $d = 2, 4$ and 7 are fits, obtained in reference [36] from experimental data. For increasing d, the position of the maximum of f is seen to approach 0, as the function becomes symmetric at infinite dimensions.

(equations (1.23) and (1.40)). The strong decay of $f(x)$ for large $|x|$ is in fact a general characteristic of all percolation models, and it produces a crossover effect between two regimes [20]. For $s \ll \delta^{-1/\sigma}$, with $\delta \equiv |t_c - t|$, the distribution only slightly deviates from the pure power law (1.45). While for $s \gg \delta^{-1/\sigma}$ the behavior of $P(s,t)$ corresponds to far from critical point conditions, showing a much stronger, exponential-like, decay with s.

The crossover effect can be exploited to facilitate further approximate calculations; since probability of finding a cluster of size $s \gg \delta^{-1/\sigma}$ goes to zero very rapidly with s, a cutoff size can be defined as

$$s_\xi \sim \delta^{-1/\sigma} \tag{1.46}$$

below which $P(s,t)$ can be roughly approximated by the power law (1.45), and above which it can be truncated. This approximation to the real distribution conserves the main properties of the transition, such as the singular behavior of the average cluster size:

$$\langle s \rangle_P \approx f(0) \int_1^{s_\xi} ds\, s^{2-\tau} \propto \delta^{(\tau-3)/\sigma}, \tag{1.47}$$

which is the same result of expression (1.44), but found in a much simpler fashion. Another fundamental scaling relation between critical exponents can be easily derived, using the same approximation scheme. The size of the giant connected component surely shows singular behavior at the threshold, since it grows when t increases above t_c, and is zero for all t below

t_c, by definition. Making use of identity (1.25):

$$\begin{aligned} S(t) &= t - \sum_{s=1}^{\infty} P(s,t), \\ &\approx t - f(0) \int_1^{s_\xi} ds\, s^{1-\tau}, \\ &\approx \text{analytic terms} + \frac{f(0)}{\tau - 2} s_\xi^{2-\tau}. \end{aligned}$$

The analytic terms should cancel out each other near t_c, since $S(t)$ is null immediately below the transition point, where $s_\xi^{2-\tau} \to 0$; then main contribution comes from the singular part. Therefore, the giant component's size in the phase with $t > t_c$ obeys:

$$S \propto s_\xi^{2-\tau} \propto \delta^{(\tau-2)/\sigma}. \tag{1.48}$$

This relation fits perfectly in the current theory of percolation transitions; the previous derivation is consistent with $\tau > 2$ and $f(0) > 0$, in which case the S should grow continuously from zero following the power law (1.48) with a positive exponent, as it does for $d > 1$ dimensions, see Figure 1.6 and Table 1.1. On the other hand, in one dimension the cluster size distribution (1.42) is characterized by an exponent $\tau = 2$ and $f(0) = 0$, and clearly last expression does not hold, in agreement with the discontinuous variation of S from 0 to 1 at $t_c = 1$. Another scaling relation is thereby obtained, for the characteristic exponent of the giant component's size:

$$\beta = \frac{\tau - 2}{\sigma}. \tag{1.49}$$

The two scaling relations (1.43) and (1.49) are fundamental results of percolation theory, and imply that only two of the exponents are independent, while the others are determined by these. An important consequence of these relations is the setting of bounds to the values that τ can take; in order for both β and γ to be positive the critical distribution must decay with an exponent $2 < \tau < 3$.

Percolation models exhibit the full set of critical properties associated with continuous phase transitions. There are other quantities, besides $S(t)$ and $\langle s \rangle_P$, that display the same kind of critical power-law behavior. Scaling relations for their characteristic exponents can also be found. As repeatedly argued in several of the preceding sections, an essential aspect of critical points is the divergence of the correlation length ξ; in general it may be expected that

$$\xi \propto |t_c - t|^{-\nu}. \tag{1.50}$$

The exact definition of correlation length is not important to the discussion made here, it only matters that it is some average of the distance between two nodes belonging to the same cluster, and it can be regarded as the typical linear size of non-percolating clusters, for detailed definitions and discussion see [20]. For example in two dimensions $\nu = 4/3$, and for $d = 3$ the correlation length diverges with as exponent $\nu \approx 0.9$, whereas for the Bethe lattice $\nu = 1/2$, analogous to mean-field theories of thermal phase transitions.

Exactly at the critical point the relative size of the largest cluster is still null, which might seem to be incompatible with an infinite correlation length. The reason why, instead, these two aspects are consistent with each other, is that such cluster has fractal structure at t_c. It

d	τ	σ	γ	β	ν	d_f
1	2	1	1	-	1	1
2	187/91	36/91	43/18	5/36	4/3	91/48
3	2.18	0.45	1.80	0.41	0.88	2.53
4	2.31	0.48	1.44	0.64	0.68	3.06
5	2.41	0.49	1.18	0.84	0.57	3.54
≥ 6	5/2	1/2	1	1	1/2	4

Table 1.1: Percolation universal exponents. For $3 \leq d \leq 5$ the values shown are numerical estimates, and can be found for example in [20].

is clear that at $t > t_c$ the largest cluster is not fractal, since the number of sites in it depends on the system size as $L^d S(t)$, where L is the system's length. However, at $t = t_c$ the number sites in the largest cluster depends on L as $\propto L^{d_f}$, where $d_f < d$ is the fractal dimension of the cluster structure at the critical point [42, 43, 44], which is related to the other critical exponents.

The fractal behavior is not an exclusive property of the largest cluster at the critical point. In fact, at t_c the fractal structure is observed on clusters of all large sizes, i.e., the whole structure has fractal properties. Furthermore, finite clusters of size s show fractal structure in the region where $s \ll s_\xi \sim \delta^{-1/\sigma}$. This is related with the aforementioned crossover effect. Smaller clusters have less empty neighbors, as such, are less affected by small variations of the occupation density t, and for this reason are expected to maintain critical properties in a wider range of densities t around t_c. Conversely, larger clusters have a larger number of empty neighbors, and are more likely to be changed by a small variation of t, abandoning the critical regime sooner than smaller clusters. The cutoff s_ξ marks the region of crossover between the two regimes, for small δ. Clusters of size $s \ll \delta^{-1/\sigma}$ are found in the critical regime, while for $s \gg \delta^{-1/\sigma}$ the corresponding clusters become exponentially rare with increasing s, and no longer retain fractal properties [37, 43, 44].

It seems rather obvious that the correlation length ξ and the cutoff s_ξ should be related, as a diameter and a volume. Combining relations (1.50) and (1.46), and considering the fractal properties at length scales smaller than ξ:

$$\begin{aligned} \xi^{d_f} &\sim s_\xi, \\ &\sim \delta^{-1/\sigma}, \\ &\sim \xi^{1/\sigma\nu}, \end{aligned}$$

yields another relation between critical exponents. It relates the two newly introduced exponents ν and d_f, with σ:

$$\frac{1}{d_f} = \sigma\nu. \tag{1.51}$$

Nevertheless, if there are only two independent exponents, then another scaling relation involving the new exponents must exist. Above t_c, for small δ the giant component's relative size is expected to behave as $S \propto \delta^\beta$, and the total number of sites it contains is roughly SL^d, for $L \gg \xi$. On the other hand, in a finite system of linear size $L \ll \xi$ the number of

sites in the largest component is expected to grow as L^{d_f}. If L is of the order of ξ these two expressions should be of the same order, i.e., $SL^d \propto L^{d_f}$ when $L \sim \xi$, then:

$$S\xi^d \propto \xi^{d_f},$$

$$\delta^{\beta - d\nu} \propto \delta^{-d_f \nu},$$

gives the missing relation:

$$d_f \nu = d\nu - \beta. \tag{1.52}$$

The last equality is often called hyper-scaling relation, because they enters with dimensionality d. Combining equations (1.51) and (1.52) together, and with the other scaling relations, gives:

$$\begin{aligned} d\nu &= d_f \nu + \beta, \\ &= \frac{1}{\sigma} + \beta, \\ &= \frac{\tau - 1}{\sigma}. \end{aligned} \tag{1.53}$$

Interestingly, for large dimensionality this expression fails to apply. Taking the exponents of the Bethe lattice $\tau = 5/2$, $\sigma = 1/2$ and $\nu = 1/2$, which correspond to $d \to \infty$, clearly shows that it does not hold in this limit. The only value of d for which it holds with those exponents is 6. Expression (1.53) is also believed to apply for $d < 6$. Thus $d_u = 6$ is identified as the upper critical dimension for percolation. It can be shown that for $d \geq d_u$ the transition is characterized by mean-field critical exponents, but the hyper-scaling relation fails and the fractal dimension retains its value for $d = 6$, i.e., $d_f = 4$ [20, 35].

There is still another relation, involving the system's dimensionality d, that can be found thanks to the crossover effect. Near the critical point the correlation function, i.e., the probability that two nodes separated by a distance r belong in the same finite cluster, behaves as:

$$G(r) \propto r^{-d+2-\eta} e^{-r/\xi}, \tag{1.54}$$

identically to expression (1.20) for thermal phase transitions. The crossover is clear here, for distances $r \ll \xi$ the correlations decay as a power law, while for $r \gg \xi$ the probability that the two nodes belong to the same finite cluster decays exponentially. For $t - t_c > 0$ small, the probability that two nodes separated by $r \ll \xi$ belong in the same finite cluster is larger than the probability of both belonging in the giant component, S^2. On the other hand, the probability that two nodes at a distance $r \gg \xi$ belong in the same finite component is smaller than the probability of both being in the giant component. Then at distances $r \sim \xi$ the two probabilities should be of the same order, i.e., $\xi^{-d+2-\eta} \sim S^2 \propto \delta^{2\beta} \propto \xi^{-2\beta/\nu}$, leading to another hyper-scaling relation [20]

$$d - 2 + \eta = \frac{2\beta}{\nu}. \tag{1.55}$$

Above the upper critical dimension the exponent η should be null, since it measures deviations from the mean-field behavior. Indeed, replacing β and ν by 1 and 1/2, respectively, and putting $\eta = 0$ in relation (1.55) gives again the result $d = 6$ (the upper critical dimension d_u). When $d > d_u$, the system's dimensionality d should be substituted by d_u in the hyper-scaling relations.

1.4.4 Classical Random Graph

Besides the Bethe lattice and the one-dimensional chain there exists another exactly solvable percolation model. This is the already mentioned classical random graph model. Yet, it was not mentioned that there are two versions of this model. Both of them start with a number N of isolated nodes, but in one case M edges are added uniformly at random among nodes (this is the Erdős-Rényi random graph or $G_{N,M}$ model), while in the other each of the $\binom{N}{2}$ pairs of nodes are connected independently with probability p (this is the Gilbert, or Bernoulli, or Binomial or $G_{N,p}$ model). However, the differences between these two versions vanish when $N \to \infty$, and they become equivalent in this limit; that is, if the probability of a random pair being connected by an edge in the second model is set to give an average number of edges equal to the first model, i.e., if $pN(N-1)/2 = M$ [45]. Since percolation, and continuous phase transitions in general, are concerned with the behavior of infinite systems, no distinction between these two versions is made in the following.

The topological structure of the underlying graph, which edges may be occupied with probability p, is quite simple: all nodes are neighbors to each other, i.e., it is the full graph. And the structure resultant of the random occupation of edges on the full graph, i.e., the set of all nodes and the edges occupied independently at random, is also known as the *classical random graph*. When $N \to \infty$ the average degree of the random graph is pN, which is infinite to any finite p. So, it comes without surprise that the minimum p for which there is a giant component is zero, in the infinite system. Furthermore, on the previously discussed models the number of edges, or bonds, of the underlying structure was proportional to the number of nodes, or sites, but in the full graph is grows as N^2. For this reasons, to access the region where the transition takes place, it is conventional to use a different measure of the concentration of edges present in the random graph: the average number of occupied edges per node, also denoted here by t, which is equal to half the average degree of nodes. On the previous models the control parameter t was simply identified with p, however on the Erdős-Rényi model $t = M/N = p(N-1)/2$. Then, the percolation threshold takes the finite value $t_c = 1/2$ (see below), i.e., the system percolates when the average degree exceeds 1.

Clearly, the dimensionality of the full graph is infinite. Therefore, the percolation transition of the random graph is expected to belong to the same universality class of Bethe lattices: mean-field percolation. Actually, both models for percolation are equivalent if the coordination number z of the Bethe lattice tends to infinity, and in this limit not only they have the same critical exponents, but also the same scaling function f of the cluster size distribution (1.41) (for the Bethe lattice, when $z \to \infty$, $f(x) \to (2\pi)^{-1/2} e^{x/2}$ with $x \equiv (1-t/t_c)^2 s$ [46]). As such, the critical behavior of these two systems is either very similar or equal. The reason for the inclusion of a discussion on the Erdős-Rényi model, is its close relation with the model of explosive percolation studied and presented here. For distinction, the class of percolation problems where sites or bonds are occupied independently at random, to which belong all the models described so far (including the classical random graph), is referred to, hereon, by ordinary percolation. In explosive percolation models, edges are occupied at random but not independently, which may cause dramatic changes on the critical behavior.

Ordinary percolation can be viewed as a dynamical process under equilibrium conditions. Identifying t with time, rate equations may be written for the cluster size distribution evolution with t (which motivates the choice of the letter t). Such rate equations are exact, in the thermodynamic limit, and do not contain any unknown factors due to correlations, i.e.,

the equations are written in only terms of the distribution $P(s,t)$. It is possible to do so, because every node is a potential neighbor of all the others, and the number of empty edges between two clusters of sizes s and t is simply $s \times t$. Thus, all the nodes are at the surface of their respective clusters. As such, all the nodes are subjected to the same surrounding environment, and in this sense, those are mean-field equations.

Additionally, in the following treatment of the classical random graph an important transformation will be introduced, that allows to condense the infinite system of rate equations for $P(s,t)$ in a single differential equation for the *generating function*, which encodes the behavior of the whole distribution in its derivatives, as seen below. This powerful technic is also useful in the tackling of the explosive percolation problem.

The occupation of edges in the random graph may be regarded as a dynamical random process with discrete time. Start with N isolated sites, and at each time step T, introduce an new edge chosen uniformly at random, among the ones yet empty. Then, at any point, the total number of edges in the random graph is $M = T$. Rigorously speaking, the model studied in the rest of this section is slitly different from this description. In the dynamical process considered by the following equations, at each step two nodes are chosen independently uniformly at random and an edge is added between them. However, when the number of nodes $N \to \infty$, this is equivalent to the classical random graph.

In finite systems, the later process may select the same pair of nodes to connect more than once (which is forbidden Erdős-Rényi model) and the probability of such repetition depends on N and M as $2M/(N(N-1))$. Hence, the total number of these events at critical point, i.e., for $M = t_c N = N/2$, is on average:

$$\sum_{T=0}^{M-1} \frac{2T}{N(N-1)} = \frac{1}{4} - \frac{1}{4(N-1)}.$$

The number of repetitions stays bounded and is very low (1/4 at t_c, on average), which is irrelevant in large systems. Therefore, in the thermodynamic limit, both processes are equivalent throughout the transition region.

A master equation for the dynamics can be easily set up for a system with N nodes, as follows. The number of clusters of size s at time T is $Nn(s,T)$, and the number of nodes in those clusters is obviously $sNn(s,T)$. The edge introduced at step $T+1$ may merge two clusters that together have s nodes, incrementing the number of clusters of size s by 1 with probability $\sum_{u+v=s} un(u,T)vn(v,T)$. On the other hand, each of the two ends of the new edge may fall in nodes of clusters of size s, independently. The number of clusters is then reduced by 1 with probability $2sn(s,T)(1-sn(s,T))$, and by 2 with probability $sn(s,T)(sn(s,T)-s/N)$ (where the $-s/N$ accounts for the possibility of the two random nodes belonging to the same cluster, which vanishes for finite s when $N \to \infty$, and happens exclusively on the giant component with probability S^2). Therefore, in the thermodynamic limit, the average number of clusters of size s that merge with other clusters is simply $2sn(s,T)$. The master equation, giving the average number of clusters of size s in step $T+1$, as a function of cluster numbers at step T, comes:

$$Nn(s,T+1) = Nn(s,T) + \sum_{u+v=s} un(u,T)vn(v,T) - 2sn(s,T), \tag{1.56}$$

which can be written in terms of the cluster size distribution $P(s,T/N)$ by multiplying s on

both sides,

$$NP(s,t+1/N) = NP(s,t) + s\sum_{u+v=s} P(u,t)P(v,t) - 2sP(s,t).$$

The two terms of last expression with a factor N may be passed to the left-hand side, and give

$$\frac{P(s,t+1/N) - P(s,t)}{1/N} = \frac{\partial P(s,t)}{\partial t},$$

when $N \to \infty$. Then, the dynamics of the infinite system is exactly described by the rate equation:

$$\frac{\partial P(s,t)}{\partial t} = s\sum_{u+v=s} P(u,t)P(v,t) - 2sP(s,t), \tag{1.57}$$

defined for continuous time t. This is the standard Smoluchowski's equation for aggregation processes. Given initial conditions $P(s,0)$, the infinite set of equations (1.57) completely describes the evolution of the finite clusters size distribution, which determines all other quantities of interest. For example, the fraction of nodes in the giant component is given by the condition

$$\sum_{s=1}^{\infty} P(s,t) + S(t) = 1, \tag{1.58}$$

for bond percolation. According to equation (1.57), the derivative of $P(s,t)$ depends on $P(u,t)$ for all $u \leq s$, but not for sizes larger than s. Then, these exact equations may be solved sequentially, either analytically or numerically with arbitrary precision.

There is, nonetheless, a technique that avoids the cumbersome task of solving the infinite set of differential equations (1.57), by transforming it in a single, exactly solvable, equation for the so-called *generating function*. The generation function of the distribution $P(n)$, of the positive integer variable s, is defined as $\rho(z) \equiv \sum_n P(n)z^s$. Such that, the n-th term's coefficient of the series expansion of $\rho(z)$ around $z = 0$ is $P(n)$, i.e., the n-th derivative of the generating function $(\partial^n \rho/\partial z^n)|_{z=0} = n!P(n)$. Now, the set of ordinary differential equations (1.57) can be transformed into a single partial differential equation of this function, by applying $\sum_s z^s$ on both sides of equation (1.57):

$$\begin{aligned}
\frac{\partial \rho}{\partial t} &= \sum_s z^s s \sum_{u+v=s} P(u,t)P(v,t) - 2\sum_s z^s sP(s,t), \\
&= \sum_s \sum_{u+v=s} z^{(u+v)}(u+v)P(u,t)P(v,t) - 2\sum_s z^s sP(s,t), \\
&= 2\sum_u \sum_v z^u uP(u,t)z^v P(v,t) - 2\sum_s z^s sP(s,t), \\
&= 2(\rho - 1)\frac{\partial \rho}{\partial \ln z}.
\end{aligned} \tag{1.59}$$

To reach the final equation, the generating function identity $\sum_s sz^s P(s) = (\partial\rho/\partial \ln z)$ was used. Additionally, the sum $\sum_s \sum_{u+v=s}$ is equivalent to $\sum_u \sum_v$; in both cases all combinations of different sizes u and v are counted twice, except when $u = v$ which are counted only once.

Equation (1.59), is the inviscid Burgers equation, which be transformed into a linear partial differential equation, and solved quite easily [47]. Take $w \equiv \ln z$, to simplify, and consider the total differential $d\rho = (\partial\rho/\partial t)dt + (\partial\rho/\partial w)dw$. At constant ρ, the total derivative (dw/dt) is equal to $(\partial w/\partial t)_\rho$. Then the partial derivatives are related by $(\partial\rho/\partial t) = -(\partial\rho/\partial w)(\partial w/\partial t)_\rho$, allowing to rewrite (1.59) as

$$\left.\frac{\partial w}{\partial t}\right|_\rho = 2(1-\rho).$$

The solution is simply $w = 2t(1-\rho)+f(\rho)$, where $f(\rho)$ is determined by the initial conditions. At $t = 0$ there are no edges present (all nodes are isolated in clusters of size 1), then the initial distribution is quite simple $P(s,0) = \delta_{s,1}$ (where $\delta_{s,1}$ is the Kronecker delta), and $\rho(t=0) = z = e^w$. The function f must reproduce this dependence at $t = 0$. For that $f(\rho) = \ln\rho$, which completes the solution:

$$e^{w-2t} = \rho e^{-2t\rho}. \tag{1.60}$$

The series expansion of ρ is found from last equation with the aid of contour integrals. Putting $y \equiv 2t\rho$ and $x \equiv 2te^{w-2t}$, x may be written as a function of y:

$$x(y) = ye^{-y}. \tag{1.61}$$

The n-th coefficient, A_n, of the power series expansion around the origin of an inverse function $y(x) = \sum_n A_n x^n$ is given by Lagrange inversion formula:

$$A_n = \frac{1}{2\pi i}\oint dx\,\frac{y(x)}{x^{n+1}} = \oint dy\,\frac{dx}{dy}\frac{y}{x(y)^{n+1}} = \oint dy\,x'(y)\frac{y}{x(y)^{n+1}}.$$

Where the integration is over a circle centered at the origin of the complex plane. This inversion method can be regarded as an application of Cauchy's residue theorem. Substituting x from (1.61) and $x' = e^{-y}(1-y)$:

$$\begin{aligned}
A_n &= \frac{1}{2\pi i}\oint dy\,e^{-y}(1-y)\frac{y}{(ye^{-y})^{(n+1)}},\\
&= \frac{1}{2\pi i}\oint dy\,e^{ny}\left(y^{-n} - y^{1-n}\right),\\
&= \frac{1}{2\pi i}\oint dy\sum_{k\geq 0}\frac{n^k}{k!}\left(y^{k-n} - y^{k+1-n}\right).
\end{aligned}$$

The residue theorem ensures that the closed integral of each term in the sum is null, except for terms in y^{-1}. For these, $\oint dy\,y^{-1} = 2\pi i$. Then,

$$A_n = \frac{n^{n-1}}{(n-1)!} - \frac{n^{n-2}}{(n-2)!} = \frac{n^{n-1}}{n!}, \tag{1.62}$$

for $n > 0$.

Now that the problem is solved, is just a matter of returning to the original distribution $P(s,t)$. The generating function ρ is found from y as:

$$\rho = \frac{y}{2t} = \frac{1}{2t}\sum_{n=1}^{\infty} A_n x^n = \frac{1}{2t}\sum_{n=1}^{\infty}\frac{n^{n-1}}{n!}(2tze^{-2t})^n = \sum_{n=1}^{\infty}\frac{(2tn)^{n-1}e^{-2tn}}{n!}z^n. \tag{1.63}$$

Finally, from the very definition of generating function, the coefficients of this power series are identically equal to the cluster size distribution, i.e.,

$$P(s,t) = \frac{(2ts)^{s-1}e^{-2ts}}{s!}, \tag{1.64}$$

as was desired.

It should be emphasized that the last result is exact for every s. However, the scaling behavior discussed in last section, $P(s,t) = s^{1-\tau}f(\delta^{1/\sigma}s)$, is observed near the critical point only for asymptotically large sizes. Using Stirling's approximation of the factorial, $n! = \sqrt{2\pi n}(n/e)^s$ when $n \to \infty$, the asymptotic behavior of the distribution comes:

$$P(s,t) = \frac{(2ts)^{s-1}e^{-2ts}}{\sqrt{2\pi s}(s/e)^s} = \frac{s^{-3/2}e^{(1-2t+\ln 2t)s}}{2t\sqrt{2\pi}}.$$

When t approaches $t_c = 1/2$ the substitution $1 - 2t + \ln 2t = (1-2t)^2/2 = -(1-t/t_c)^2/2$ can be made, and the cluster size distribution scaling form is:

$$P(s,t) = s^{-3/2}f\left((1-t/t_c)^2 s\right), \tag{1.65}$$

where

$$f(x) = \frac{e^{-x/2}}{\sqrt{2\pi}}. \tag{1.66}$$

Notice that no restrictions to the existence, or absence, of a giant component were imposed, at any point of last deduction. Therefore, the scaling function $f(x)$ is symmetric around $x = 0$, as is the cluster size distribution around t_c, and consequently, all other percolation related properties (in a region small enough, around the transition threshold). With exception, of course, for the existence of a percolating component, which relative size can also be calculated using the generating function. Condition (1.58) and the generating function's property $\rho(1) = \sum_s P(s,t)$ imply $\rho(1) = 1-S$; thus, putting $z = 1$ ($w = 0$) in equation (1.60), and substituting ρ by $1 - S$ gives:

$$S = 1 - e^{-2tS}. \tag{1.67}$$

For $t < 1/2$ the only solution of this equation is $S = 0$, but above the critical point a non-trivial solution exists, with $S > 0$. Equation (1.67) is not analytically solvable, yet, the behavior of the solution at $t = t_c + \delta$, for small δ, can be found by taking the series expansion of last equation at $t = 1/2$. Close enough to t_c the size of the giant component is:

$$S = 4(t - t_c). \tag{1.68}$$

A consequence of the scaling function's symmetry is, for example, that the proportionality factor in equation (1.44) for the average cluster size $\langle s\rangle_P$ is the same on both sides of the transition. From the definition of the generating function it is clear that the derivative $(\partial\rho/\partial z)|_{z=1} = \langle s\rangle_P$. The exact expression for $\langle s\rangle_P$ may be found by differentiating equation (1.60) at $z = 1$ ($w = 0$) to get:

$$\langle s\rangle_P = \frac{1}{e^{-2t(\rho(1)-1)} - 2t}.$$

As seen above $\rho(1) = 1 - S$; since $S = 0$ below the transition point t_c, the average cluster size for $t < t_c$ is simply $\langle s\rangle_P = \frac{1}{1-2t}$. Above t_c the behavior of S given by equation (1.68) for t

close to t_c; substituting and expanding the exponential in the denominator gives $\langle s\rangle_P = \frac{1}{2t-1}$ when $t \to t_c$ from above. Therefore, the average cluster size for in the critical region behaves as

$$\langle s\rangle_P = \frac{1}{2|t_c - t|}. \tag{1.69}$$

on both sides of the critical point.

The critical behavior of ordinary percolation in the classic random graph turned out as expected, for mean-field models of ordinary percolation. Expressions (1.65), (1.68) and (1.69) show that $\tau = 5/2$, $\sigma = 1/2$, $\beta = 1$ and $\gamma = 1$; as discussed in section 1.4.3, all other exponents are determined by any two of these, through scaling relations between critical exponents. Here, the critical properties were exactly calculated outside scaling theory's framework. To do so, provided an opportunity to introduce the generating function technique, and show some of its basic properties and uses, resulting in the exact solution of the problem (equation (1.64)), which is in complete agreement with the general theory of percolation previously introduced. Similar methods, also based on generating functions, will be employed in Chapter 2, for the treatment of explosive percolation.

1.5 Network Flow

A wide variety of real systems of many agents support transport processes. A list of examples may include the routing of information packages in communication networks [48, 49, 50], the transport and distribution of consumer products in supply chains [51, 52], the traffic of vehicles on roads [53, 54], the circulation of blood in the cardiovascular network [55, 56], the flow of biomass in food-webs [57, 58] and even the spread of rumors or diseases in social networks [59, 60] among many others. This kind of dynamics can be regarded as a flow through a network. In a broad perspective, the exchanges among agents, nodes, are enabled by the channels, edges, of the underlying graph; two nodes may proceed to exchanges directly with each other only when there is a network connection between them. The particular form of the flow distribution, over the network's edges and nodes, depends on the specific nature of the flow under consideration, as well as on the topology of the underlying network structure.

In some applications it is desired to optimize the network's design, or the flow distribution in a preexistent network, to the performance of certain operation, according to some criteria generally expressible as a cost function of the flow, e.g. in a supply chain the transport over each channel has an associated monetary cost per transported unit [52]. While another line of research focus on the study of spontaneous flows that take place in 'naturally occurring' networks, seeking a basic understanding of the rules that govern the flow's macroscopic properties, preferably from microscopic first principles. In the cases which dynamics is influenceable to a limited extent, some knowledge about the flow patterns formation may be used to increase the network's efficiency, e.g. in highway traffic this can be done by controlling the rate of injection of cars at the on-ramps in order to minimize the travel time of each driver [61], or in urban traffic the same goal can achieved by an adequate implementation of traffic lights systems [62].

The domain of network flow problems lies at an intersection of several disciplines, including applied mathematics, computer science, engineering, management, operations research, etc [63]. And for the last half century or so, these systems have been systematically investigated also by the physicists community, initially with a special interest on vehicular traffic

problems [64, 65]. Expanding later into other contexts, in simultaneous with the development of complex network science (for instance in social networks many different kinds of flow, showing different characteristics, can be identified [66]). The earlier considerations about how the flow gets distributed in such a network-like structure date back to the work of Kirchhoff and other pioneers in electrical engineering and mechanics, who set the foundations of many of the key ideas of network flow theory, and established graphs as useful mathematical objects to represent these systems.

A vast variety of technological, natural and social systems possessing a network structure support relations between nearest neighbors that can be represented as a flow from one node to another. In many of those, the operation of exchanges between the agents is the primary purpose for the very existence of a networked infrastructure; roads are build and interconnected for the single reason of allowing traffic to move across a geographical region, and the cardiovascular system serves the purpose of transporting nutrients, oxygen and others from one region in the organism to the totality of its volume. In fact, because they are the product of an evolutionary optimization process and competition over millions of years, biological systems often sustain high performance designs, and certainly hold the potential to inspire new optimization strategies capable of improving significantly the efficiency of artificial systems, see ref. [67].

The class of network flows occurring in structures designed for that purpose is a wide one. It includes most technological and natural networks designed to perform specific tasks, such as communication networks, roads systems, industrial networks, supply chains, electrical grids, circulatory systems and food-webs. However, other networks flows exist that form spontaneously, within networks which topological structures is not determined by the same kind efficient transport necessities. Social networks are a privileged medium for these spontaneous flow processes to occur, both in networks of personal contacts such as the spread of sexual transmitted diseases [68], and in networks of long distance contacts such as the spread of a certain piece of information through chains of *e-mails* [69].

In some of these systems the normal operation of nodes may depend on a relatively steady supply of some resources, from an external source, which is delivered to the nodes by means of an underlying network, as in an electronic circuit each component uses electrical energy. So that, all the flow enters the circuit from an external common source, is directed to all the nodes in the network. Another example of the same type is biomass flow in food-webs, the source of the flow in this case is one or a few species at the bottom of the web [70]. Nonetheless, in other cases the flow origins from the inside the network, i.e., each node may act as a source of flow, or as a final destination for the flow originated by other nodes, then called a sink. Many real network flows fall in this category, where, depending on the particular conditions, each node may be a source, a sink, both or none; including the flows on communications networks, vehicular traffic systems, social networks, and many others.

Developed by sociology to quantify the importance of the position of each individual on the structure of social networks, the concept of centrality assumes a prominent relevance in the framework of complex network flows. Indeed, the basic idea behind centrality measures inherently refers to some kind of flow [66, 71, 72]. For instance, the centrality betweenness measures the fraction of shortest paths that pass through a given node or edge [18]. Such measure is pertinent only when there is some transport process occurring in the network, which predominantly chooses the shortest paths to travel between the source and sink nodes. An even more explicit example is the eigenvector centrality measure, on which the Google

PageRank algorithm is based [73]. It is equivalent to finding the stationary distribution of a flow process where at each iteration every node receives and sums the popularity scores of his neighbors [74]. An appropriate centrality measure is a quantifier of the importance of a node or a channel for the type of flow process under consideration [66].

The variety of network flows truly is large. In much of the traditional literature dealing with network flows, the flow is regarded as quantity obeying conservation conditions, like a 'material' flow, i.e., the amount of flow entering each channel and node, except sources and sinks, must be equal to the amount exiting that same channel or node, see references [48, 63, 65, 75] and references within. Although not all kinds of network flows have this property, especially in the context of sociology, many real-world applications and important theoretical models are concerned with the transport of such 'material' flows, as is also the case of the model considered in Chapter 3. To stress that the conservation property is verified, the amount of flow crossing a node or edge may be called a *current*, in analogy with electrical current.

A key point is that there are restraints to the amount of flow to be transported by each path. The capacity of the channels or nodes to transport current may be limited, in which case it is natural to ask, for a given source and sink, what is the maximum flow permitted by the network structure of capacities. The solution for this problem, as well as for the generalization with multiple sources and sinks, is given by the important *max-flow min-cut* theorem, briefly discussed in next section 1.5.1, along with some of its implications including Menger's theorem. Alternatively, a cost function associated with the transport of current may be assigned to each channel or node. The question then becomes: for a fixed total amount of flow being transported between sources and sinks, what is the most efficient way to transport it, i.e., the choice of paths starting at the sources and ending at the sinks that minimizes the overall cost. This kind of optimization problems is discussed in section 1.5.2. Other systems, like vehicular traffic networks, are characterized by locally made decisions, i.e., there is no central control of the choices that each particle makes – each driver makes his own decisions based on the local information available. In section 1.5.3 is given a short description of the general behavior of vehicular traffic, and an overview of the modeling methods.

1.5.1 Max-Flow Min-Cut Theorem

One of the most fundamental results on network flow is provided by the *max-flow min-cut* theorem. It is a simple but powerful result that bears a large number of important consequences to network flow theory (including for undirected networks) [75, 45]. In its most simple form this theorem considers a directed graph which edges have finite capacities for transporting flow. In addition, there is one source node s and one sink node t where the conservation of flow is not verified, the source adds current to the network and at the sink it vanishes in equal amount. At every other node and edge the flow is conserved, the quantity of flow entering each channel is equal to the quantity exiting, and the sum of the flows entering a node by the incoming channels is equal to the sum of the flows exiting the node by the outgoing channels. This way, the total amount of current traveling in the network is finite, due to finite capacities of the channels, and does not change in time, since the amount of current entering through s is the same as the one exiting through t.

Evidently, the maximum possible amount of flow traveling through the network from s to t is restricted by the particular topological configuration of the network and distribution of capacities. The ability of node s to send current to t depends not only on their individual

capacities to send and receive current, respectively, but also on the capacity of the network to transport it.

Node i sends current to its neighbor j through a directed edge, characterized by a capacity limiting the maximum current it can transport $c(i,j)$. The information about the network structure enters the theorem under the concept of *cut*. A cut *separating* s from t is a set of edges which removal eliminates all possible paths starting at s and ending at t, so that, in the remaining network, the only possible non-negative value for the total amount of flow traveling from s to t is zero. Then, it is clear that if there is a set of edges, say E, that is a cut separating s from t, the total flow from s to t cannot be larger than the sum of the capacities of the channels in E (since all the current leaving s must cross at least one edge of E to reach t). So, letting f be the maximum possible amount of flow from s to t in such a system, the following inequality always holds,

$$f \leq \sum_{E} c(i,j),$$

for any cut E separating s from t, including the cut $E = E^{min}$ for which the sum $\sum_E c(i,j)$ takes its minimum value. Therefore it can be written in all rigor:

$$f \leq \sum_{E^{min}} c(i,j),$$

Ford and Fulkerson proved in 1956 [76], with the celebrated max-flow min-cut theorem, that the previous trivial inequality is, in fact, an equality, i.e., the maximum of the flow from s to t is determined by the minimum of the capacities of cuts separating s from t. This subtlety of this result may be partially appreciated by the amount and importance of other results that could be deduced from it [75].

An immediate generalization is given by considering the version of the problem with multiple sources and sinks. Here the conservation of flow requires the sum of the currents introduced by the sources to be equal to the sum of the currents removed by the sinks. The theorem can easily be adapted to give the same result if f is the total current, and the cuts considered are such that separate all the sources from all the sinks; so that, in the remaining network no path exists starting at any source and ending at any sink. Then the maximum amount of flow f traveling through the network from the sources to the sinks is equal to the minimum of the cuts' capacities separating sources from sinks.

If some of the channels are allowed to have infinite capacity the total amount of flow f may be finite or infinite (depending of which channels have unlimited capacity), nonetheless the theorem holds in both cases. In particular, if all the cuts separating sources from sinks have at least one channel with unlimited capacity then the capacity of the minimal cut is infinite, and so is the maximal flow. However, if at least one cut has finite capacity, because all the channels in it have finite capacity, then the maximum flow surely smaller or equal to the capacity of such cut, and the theorem holds.

The case of the undirected network is also easily included for analysis in the this framework. In an undirected network the flow on an edge can take any of both directions, depending on the rest of the network. At first sight it may seem like many different networks, with different combinations for the directions of the edges, need to be examined to determine the maximum of the flow. But in fact, only one directed network needs to be considered. The network that has a pair of directed edges in the same positions of the the original undirected

ones, with opposite directions and each holding the same capacity as the corresponding original one. The reason for this to be true is that the total amount of flow exchanged between two neighboring nodes is equal to the difference of the currents (traveling in opposite directions) on the pair of directed channels connecting them. Since each channel of the pair has a limited capacity, equal to the capacity of the corresponding undirected channel in the original network, the maximum amount of current that can be sent between any pair of connected nodes is achieved when one of the two directed channels is empty, and the other is saturated with flow. Moreover, in the presence of sources and sinks, the max-flow min-cut theorem ensures that the total amount of current traveling by the set of channels crossing the cut in the opposite direction is null. So the answer for undirected networks stands the same: the maximum amount of flow traveling from sources to sinks in undirected networks, with limited channel capacities, is equal to the minimum capacity of the cuts separating sources from sinks. For networks, with a mixture of both kind of edges the same line of arguments leads to the same conclusion.

All of these results, derived for limited channel capacities, can easily be adapted to networks where the amount of flow is limited by nodes capacity. The proper definition of cut is slightly different, but the rest of the procedure remains quite the same. In this case channels, by themselves, can transport and unlimited current, and the capacity of any cut of edges, as defined before, is always infinite. On the other hand, a strategical removal of nodes may certainly cause the elimination of all paths starting at s and ending at t, leaving no possibility for a positive amount of flow from s to t. In this case, an appropriate cut is a set of nodes which, upon removal, separates the sources from the sinks. Just like for an *edge-cut* in the case of channel capacities, the capacity of a *node-cut* is limited and equal to the sum of capacities of the nodes in it. To solve this version of the problem, consider the transformation represented in Figure 1.7. For each node i in the network, other than the sources and the sinks, take its capacity $c(i)$, and substitute the i by a set of two nodes, i^+ and i^-, connected by a directed edge from i^+ to i^- with capacity $c(i^+, i^-) \equiv c(i)$. All incoming connections of node i are attached to node i^+ and the outgoing channels are attached to i^-. This can be seen as an expansion of the limited capacity nodes in three sections, an entrance part i^+, an exit part i^-, and an intermediate part, where the current is limited, represented by a directed edge with the capacity of the original node. In the resulting network the only limit to the amount of flow is the capacity of the channels newly introduced, represented in red in Figure 1.7. All channels of the original network as well as all the nodes in the transformed network present no restriction to the passage of current, and the situation is the same as before: a directed network where some channels have limited capacity and others do not. If, in the original network, all paths from any source to any sink pass by at least one node with finite capacity, then the minimal edge-cut of the transformed network must also have finite capacity, and so, it must be a set constituted exclusively by newly added edges. Since to each edge-cut of the new network corresponds a node-cut in the original one with equal capacity, here, the maximal flow is equal to the minimal node-cut separating sources from sinks.

A remarkable accomplishment of the max-flow min-cut theorem is to provide one of the most simple proofs for the Menger's theorem, a fundamental result of graph theory first proved almost three decades before, in 1927 [77, 45]. Menger's theorem was originally formulated for undirected graphs, and states that:
(i) the maximum number of *independent* paths between nodes s and t is equal to the minimum number of nodes that separate s from t. Two paths are independent if they share no nodes,

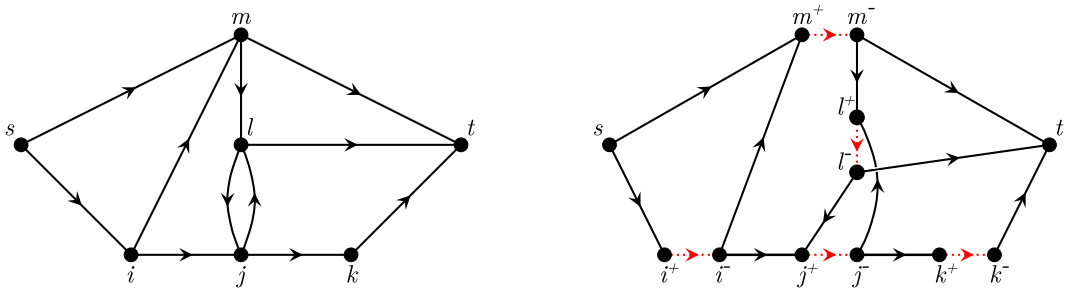

Figure 1.7: Replacing each node with limited capacity of a network flow by an equivalent expansion, constituted an node with the same index marked with $^+$, a node marked with $^-$, and an edge from $^+$ to $^-$ limiting the current to the same amount as in the corresponding node of the original network.

---

and consequently no edges either.
(ii) the maximum number of *edge-disjoint* paths between nodes s and t is equal to the minimum number of edges that separate s from t. Two paths are edge-disjoint if they share no edges. Yet, two such paths may share some nodes of degree equal or larger than four.
The proof is given combining the max-flow min-cut theorem with the integrability theorem. The latter ensures that, if all the capacities are integers then also the maximal flow is integer, and there is a distribution flows corresponding to this maximum value in which all edges and nodes are crossed by an integer amount of current. For the proof of (i) the capacities of all the nodes are set to 1, except for s and t, which are identified as the source and sink of the flow, irrespectively. By the integrability theorem, there is a maximal flow distribution valued 0 or 1 in each channel. Therefore, the maximal amount of flow is equal to the maximum number of independent paths from between s and t. The minimum of the node-cut capacity is clearly equal to the minimum number of nodes that separate s from t. For the proof of (ii) the same procedure is applied to the case with all edge capacities equal to 1.

The list of known implications of the max-flow min-cut theorem is certainly very long, as it stands one of the most fundamental theorems of graph theory and combinatorics in general. The detailed proofs of the results presented in this section can be seen for example in references [45, 75]. Other implications and applications of the max-flow min-cut theorem can be found in [63, 78, 79].

1.5.2 Minimum Cost Problems

In many real-world systems, the restraints to the amount of current transported by each channel, or passing through each node, is not given simply as a limiting capacity that determines the maximum current on that element. In addition to a limited capacity, the passage of some current through a network node or channel has frequently an associated cost, which is a function of the amount of current. In this situation the problem's nature becomes different, and the focus of attention should be shifted from the search for the maximum amount of flow, that can travel in some network from node s to node t, to the search for the minimum of the sum of all individual costs of transporting a fixed amount of current f from s to t. Once again, the directness of the edges and the choice to impose constraints on nodes or edges do not change the answers. An undirected network can be regarded as a special case of the directed kind, where for every edge from i to j there is an edges from j to i, since clearly

the minimum cost condition ensures that, at most, only one of the channels of each such pair is used to transport current. As for the choice of where the restrictions are applied, both possibilities can be regarded as special cases of a general model where each node and edge can have zero or positive costs, as well as finite or infinite capacity.

In maximal flow problems the specific path chosen by the current is not relevant. In last section it was seen that the amount of flow is maximum when the edges and nodes of the minimal cut are fully saturated with current, giving the upper bound for the amount of current traveling in the network. It means that all currents traveling from sources to sinks must pass by one, and only one, of the elements in the minimal cut, and renders the choice of the other sections of the paths an arbitrary one. In this sense, minimal cost problems are much harder. The total cost of transporting an amount of current f from s to t is minimum for a particular realization of the flow distribution in the channels of the network (the current in the nodes is fixed by the current of the incoming channels), and depends on the individual costs of all the nodes and edges of all the paths used to transport current.

Of course, the difficulty of the problem varies greatly with the cost structure. For instance, in an network with constant costs, for nodes and channels, and unlimited capacities, it is clear that the total cost is minimized by using a single shortest path. Or if in the same network the equal costs are linear functions of the current, a cost per current unit, then any distribution of flow that only uses paths with the shortest length gives the minimum total cost. However, if the capacities are finite and the cost structures is heterogeneous, in addition to the existence of a maximum to the total current, the determination of the minimum cost flow becomes less simple. In fact, this general class of problems (that includes also the previous models as specializations) receives a lot of attention from a number of fields of inquiry, from information theory [48] to management [51], especially the version with linear cost functions.

The minimization of the total cost in a network, where each channel and/or edge has associated a cost per unit of transported current, can be formulated as a linear programming optimization problem. Linear programming is a mathematical method for determining the way to achieve the best outcome (such as the minimal cost) in a given model under some list of restrictions expressed as a set of inequalities. An essential aspect of the broad class of problems covered by linear programming is that both the function to be optimized, and the restrictions must be linear with the problem's variables, otherwise the fundaments of linear programming theory fail to apply. For a network flow this means that the individual cost functions are linear with the current, and capacities that do not depend on the flow distribution.

The traditional methods of linear programming should be able to tackle the minimization of cost in these systems without major adaptations, particularly the popular and powerful simplex method, which starts from a feasible arbitrary solution and at each iteration finds a new flow corresponding to an better solution, until no more improvements are possible. However, the efficiency of the algorithm can be significantly improved by exploiting the underlying network structure, conveying a network simplex method [80] that can be used to solve the minimum cost problem in a network more efficiently than the other existing algorithms [81, 82]. For a detailed description of the network simplex method and network flow cost minimization in general, related proofs, specializations and applications see references [63, 83].

1.5.3 Vehicular Traffic Flow

The interest in the dynamics of vehicular traffic arose remarkably early [84]. Already in the 1950's, a significant amount of work on this subject was documented by journals of engineering and operations research [64, 85]. The amount of vehicles traveling in the roads has been increasing ever since, and with it the problem of traffic congestion. It was inevitable for the physicists attention to be caught by these complex systems rich behavior's spectrum. Although a lot of work existed in the field by then, the main activities begun in the early 1990's following a few papers, [53, 86, 87], that triggered an avalanche of publications on various physics journals. The mainstream of these contributions adopted the approach of [53, 86] to vehicular traffic, based on cellular automaton models [88].

Many important empirical notions about traffic flow dynamics were noticed, and introduced in the description of the systems, since the beginning of the activity in this research field. The relation between the average velocity v and density of vehicles circulating ρ has been investigated since the seminal work [84] of 1935. The amount of traffic flow f, i.e., number of vehicles crossing some point in the road per time unit, is given trivially by the product of the velocity with the density of traffic, $f = \rho v$. Nevertheless, due to the nature of the relation of the velocity with the density, it shows a noteworthy behavior.

It is well established that the average velocity is a monotonically decreasing function of the density of vehicles. In the low density limit each driver is free to move at his maximum speed, but when there are other cars in the vicinity the speed can only decrease, because of congestion and for safety reasons, as represented in Figure 1.8(a). In fact, there are some features that appear to be intrinsic to vehicular traffic, as most observations confirm [54]. In multilane roads, the low density regime is characterized by almost constant velocity, and the flow grows linearly with the density with slope $v_{\max}$ (Figure 1.8(b)). In single lane roads, there are no chances to overtake and the velocity decreases substantially with the density, even in this limit. As the density grows, the average velocity decreases monotonically, until it vanishes for some finite value of the density, the *jam density* ρ_{jam}, which corresponds to a state where the total length of the road is occupied by stopped vehicles. Of course, in this situation the flow is null, since it is proportional to the average velocity, and the traffic is said to be jammed. There is a density $\rho_{\max} \in]0, \rho_{\text{jam}}[$ for which the flow takes its maximum value $f_{\max}$. As is seen in Figure 1.8(b), there are two values of the density ρ for each amount of flow $f < f_{\max}$, each of which corresponds to a different average velocity v. The point where the flow is maximum, $\rho_{\max}$, is used to define two branches corresponding to *free-flow* and congested regimes. In the free-flow regime (i.e., for $\rho < \rho_{\max}$) the average velocity is considerably larger than the velocity for the congested regime (i.e., for $\rho > \rho_{\max}$) corresponding to the same f. This qualitative description of the flow's dependence with the density of traffic has been empirically verified since the first traffic studies, so much that its graphical representation, Figure 1.8(b), became known as *fundamental diagram of traffic flow*.

The number of vehicles entering a road per time unit is fixed by external conditions, and with it the total amount of flow f is fixed too. However, this alone, is not sufficient to determine the state of the flow, as there are two regimes, with different characteristic velocity and density, for the same f. An amount of traffic, initially flowing in a free-flow state, may suffer a transition to a congested traffic state, caused by some perturbation, such as a bottleneck, an on-ramp, an accident, etc. This kind of behavior suggests that the dynamics of traffic flow is indeed a non-trivial one. The actual state of traffic flow is determined by an interplay of many variables, that build up to the complex behavior characteristic of these

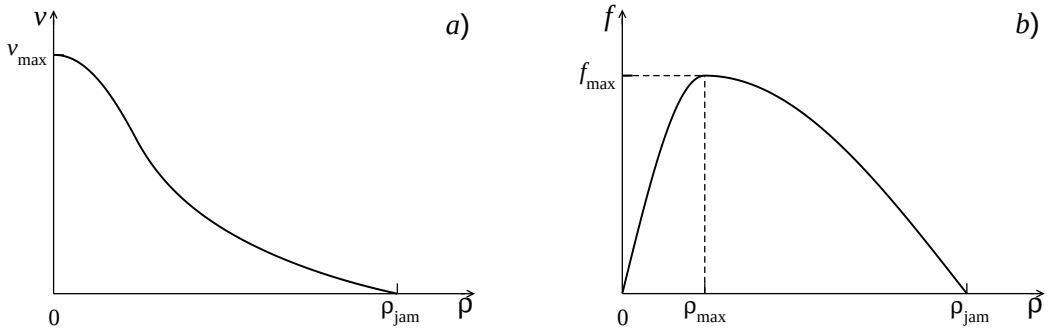

Figure 1.8: Schematic representation of the behavior of traffic. (a) For low densities each driver moves at the speed he desires, and is weakly affected by the other vehicles; in the limit $\rho \to 0$ the velocity $v = v_{\max}$ and the derivative $dv(\rho)/d\rho = 0$ for multilane freeway traffic. With the increase of density the velocity decreases monotonically until eventually it vanishes at $\rho = \rho_{\rm jam}$. (b) The curve given by $f(\rho) = \rho v(\rho)$ is called fundamental diagram of traffic flow. It shows that there is a maximum amount of flow $f_{\max}$, and for each $f < f_{\max}$ there are two distinct states of flow, corresponding to free-flow with $\rho < \rho_{\max}$ and higher velocity, and congested flow with $\rho > \rho_{\max}$ and lower velocity. For low densities the flow grows linearly, $f \approx \rho v_{\max}$.

systems.

In the free-flow phase the average velocity is close to the maximum $v_{\max}$, because interactions are relatively weak and vehicles travel close to their desired speeds. In the congested regime, where interactions are stronger, there is a larger diversity of dynamical states. A number of phases of congested traffic can be identified. In the *synchronized flow* phase the average velocity is the same in all the lanes, because vehicles change lanes to the faster one, until all are synchronized. Another effect of congestion are *wide moving jams*, regions with density $\rho_{\rm jam}$ where the traffic comes to a complete stall. These regions, that may develop and fade spontaneously, move in the direction of incoming traffic and are responsible for such phenomena as stop-and-go waves. *Extended congested traffic* is, however, the most common form of congestion. Here the congestion is not localized as a wide moving jam, but spatially extended and often lasting for several hours. The origin of extended congestion is related to an excess of inflow for the road capacity, frequent at rush hours.

Essentially, there are two different conceptual frameworks for the modeling of traffic dynamics. One employs a macroscopic description of the dynamics, where the vehicles are not considered individually, and traffic is regarded as a compressible fluid characterized by a density function that usually is continuous on space. The other explicitly accounts for the individual behavior of each vehicle, treating it as a particle interacting with its surroundings through some microscopic mechanisms. The choice of the interaction rules reflects the influence that drivers have on each others movements [88].

There are several distinct approaches using different rules for the microscopic interactions. In the so-called *follow-the-leader* models it is assumed that a vehicle's acceleration is determined by the neighboring vehicles, and the dominant contribution comes from the vehicle ahead, the leader. Each driver responds to his environment conditions by accelerating or decelerating the vehicle accordingly. This Newtonian dynamics translates into a deterministic system of as many coupled differential equations as there are vehicles on the road, that must

be solved simultaneously, returning the position of each vehicle as a continuous function only of time and initial conditions.

Contrasting with the simplicity of the models themselves, cellular automaton systems show an exceptional richness of complex behavior, that includes such fascinating phenomena as self-organized criticality [27] or oscillatory and chaotic sequences of states [89]. While the simplicity of the microscopic dynamical rules and the discretization of space and time is attractive in view of an efficient computational implementation, the ability to manifest of a broad range of complex behaviors is desirable for the modeling of traffic flow. Because of this convenient combination, the application of cellular automata to the modeling of traffic dynamics have stimulated a lot of research activity aimed to understand and control the origins of the instabilities that are responsible for stop-and-go traffic and congestion. Despite of the success of this approach in reproducing many real phenomena of traffic, there is no model yet than can account for all aspects of vehicular traffic [88].

The contribution of physics to vehicular traffic theory has been considerably more focused on the dynamics of freeway traffic, i.e., traffic on a single road with multiple lanes and diverse entry and exit points, than in the effects of the road network on the dynamics. Indeed freeway traffic exhibits a number of interesting features, such as the ones described above, and poses enough challenges by themselves. Yet, in cities and urban areas in general the picture may be rather different. While in a freeway all vehicles travel in the one direction, in city traffic each driver has its own origin and destinations. In order to reach the destination he must choose one path, among all the possibilities that the network of roads provides. At intersections there is a confluence of traffic coming from several streets, congestion may arise there and spread to other streets and intersections, above some traffic density [53]. In addition, during the travel the driver may adapt his route when confronted with unpredicted obstacles, such as traffic lights, closed sections of road, jams that can be avoided by taking another path, etc. In order to have an efficient transportation in a high flow regime, the vehicles must coordinate and adjust their own route according to the dynamical changes in his environment [90]. A good understanding of city traffic's flow patterns, can lead to a more efficient planning of the infrastructure itself, as well as to an optimization of the existing one, for instance intervening with traffic lights [62, 91].

A fairly recent review of vehicular traffic flow may be found in reference [54], and in [88] is given a review mainly focused on cellular automaton models.

Chapter 2

Explosive Percolation

In section 1.4, we explained that ordinary percolation in $d > 1$ dimensions has a phase transition of the continuous kind, i.e., $S \propto (t - t_c)^{\beta}$, where the exponent β is related to the other critical exponents by (1.49). In particular, above the upper critical dimension (for $d \geq 6$) the exponent takes the mean-field value $\beta = 1$. Furthermore, the fact that ordinary percolation phase transitions are continuous implies the divergence of the correlation length, which directly leads to a power-law distribution of cluster sizes at the percolation threshold, and to a set of standard scaling properties and relations.

As a matter of fact, the continuity of percolation phase transitions (apart of special problems such as bootstrap percolation and k-cores [92]) was generally accepted until recently. This common understanding was shaken by the work [93], which reported a discontinuous percolation phase transition in models whose evolution was based on ideas from computer science and computational physics [94, 95]. (Recall that numerical studies of cooperative systems and processes widely use the Metropolis algorithm and its variations. In this algorithm, two possible directions of the system evolution are compared at each time step, and the direction minimizing, for example, the energy of the system at the next time step is chosen.)

2.1 Short History of Explosive Percolation

In 2009, Achlioptas *et al.* reported a remarkably different, discontinuous percolation phase transition, in a new so-called "explosive percolation" problem [93]. This work, and the others that followed [96, 97, 98, 99, 100, 101], studied the emergence of the percolation cluster in a system with a Metropolis-like algorithm driven evolution. The model was formulated in the following way. As for the classical random graph percolation model, the evolution starts from a large number N of isolated nodes. At each step, compare two possibilities to add a new bond—to connect a pair of uniformly at random chosen nodes, belonging to clusters with sizes s and s', or to connect a second pair of nodes selected in the same way and belonging to clusters of sizes s'' and s'''. For example, compare the products of the sizes of clusters which these two possible bonds connect, ss' and $s''s'''$, and choose for connection the pair with the smallest product of cluster sizes (the so-called "product-rule"). Other rules, e.g., the "sum-rule"—select for connection the pair with the smallest sum of cluster sizes—lead to similar effects [102, 103].

Clearly these rules favor fusion of small clusters which results in the delayed emergence of the giant cluster compared to ordinary percolation, so the percolation threshold t_c should

exceed 1/2 [104]. Based on a computer experiment for a $512,000$ node system, it was concluded in reference [93] that the percolation transition for this apparently irreversible process (one cannot invent a reverse process to this one) is discontinuous, i.e., $S \to S_0 > 0$ when t approaches t_c from above, and that is why this kind of percolation was termed "explosive percolation". There, was argued that the delay of the transition is responsible for the discontinuity. This conclusion was immediately supported by numerous other simulations of this and similar models [96, 97, 98, 100, 102, 101, 105, 106, 107]. (In the following we discuss only models of this type, where the dynamical rules use only information of the randomly chosen nodes. Other models were proposed, that achieve the desired effect via direct control of the largest component's size [108, 109], which, of course, must use global information, and assume the existence of a central authority with complete knowledge.)

The need for a theoretical description of this exceptional phenomenon, lead to the development of a few new concepts, such as the "powder keg" [99, 110]. According to that idea, the application of the evolution rules generates an accumulation, over time, of large finite clusters in the system, with sizes in a relatively short range, i.e, the "powder keg", which may be triggered by the addition of only a very small number of new links. In fact, most efforts for conceptual descriptions favored the idea that the promotion of small clusters growth, besides delaying the transition point, also provokes a situation with many finite yet large clusters, approaching the threshold from below. And, when those large clusters finally start to merge with each other, the relative size of the largest one, S, suddenly jumps to some S_0 (in a vanishing fraction of time steps), producing a discontinuity [105, 106].

Surprisingly, in addition, the same studies reported the presence of properties typical of continuous transitions. For instance, power-law cluster size distributions at the critical point were observed [100, 101, 102, 105], also the size of the cluster to which a randomly chosen node belongs was seen to diverge approaching t_c from below and above [97, 100, 101], among other scaling features unexpected for discontinuous transitions. This coexistence, of a discontinuous jump in the size of the giant component and critical phenomena, poses a contradiction, which we have removed by showing that the explosive percolation transition is actually continuous [1].

This chapter is organized as follows. Next section presents the work published in [1], where we first shown that the transition is continuous. We did so by analyzing the evolution equation above the critical threshold, where it can be solved using generating functions. In addition, we solved numerically a large number evolution equations (for cluster sizes from 1 to 10^6), and observed the full set of scaling properties expected on continuous transitions, including power-law critical distributions, divergence of the distribution's first moment, scaling functions, etc. In section 2.3 we extend the analysis to a wide set of models, representative for the entire range of these optimization driven processes. We show that the transition is continuous in all models, and write down the scaling relations for these models [2]. Section 2.4 is devoted to the description of a method that allows to calculate critical properties of these models with very high precision, using the numerical solution of a smaller number of evolution equation [3]. In addition we show the precise results obtained with this method for a few models.

The complete solution of this intriguing problem is finally provided in section 2.5. There, we develop a strict scaling theory which supplies the full set of scaling functions and critical exponents (which turn out to be non-universal) with any desired precision. Furthermore, we notice that the relevant order parameter and susceptibility for these models, in fact, differ from ordinary percolation (contrarily to what was generally assumed).

2.2 Explosive Percolation Transition is Actually Continuous

We will show that, contrarily to the conclusions of previous investigations, explosive percolation is a continuous phase transition. So, it is natural to find scaling behavior near the critical point, consistently with the general theory of continuous phase transitions. To show this, we consider representative model displaying this new kind of percolation. Due to its simplicity, our model allows a strict mathematical description of the process (in the form of a set of evolution equations similar to (1.57), for ordinary percolation in the classical random graph), which enabled the possibility of rigorous analytical treatment, for the first time in this class problems, proving the continuity of these transitions.

Our results clash with the conclusions of the preceding works in a key point: the question of the existence of a jump in the giant component's size variation with the independent parameter t. The discontinuity, detected and measured in the simulations performed by those works, is, in fact, an effect of the systems' finiteness, and vanishes in the thermodynamic limit. The application of such an optimization driven microscopic dynamics, as the product-rule, results in a continuous transition characterized by a uniquely small critical exponent β. It is shown below how the smallness of β is responsible for creating the illusion of a discontinuity, even when considering very large, but still finite, systems (as in the aforementioned simulations). The work presented in this section was originally published in [1].

2.2.1 A Simple Model for Explosive Percolation

In addition to the product-rule and sum-rule, several other models that produce a behavior identified as explosive percolation were proposed in the literature. In all of those, the aggregation process is driven by some kind of optimization criterion, which imposes a bias towards the merging of smaller clusters. It was conjectured that if the bias is strong enough, then the transition occurs discontinuously, independently of the selection rule's specific form. This is, the details of the transition, such as the threshold t_c and size of the jump S_0, depend on the selection rule, but, the existence of a jump at t_c is maintained for a wide class of biased rules [99, 105, 106].

In [1] we propose a simple representative model of the explosive percolation class, which is a direct generalization of the classical random graph. Namely, at each step, we sample twice:

(i) choose two nodes uniformly at random and compare the clusters to which these nodes belong; select that one node of the two, which belongs to the smallest cluster;

(ii) choose a second pair of nodes and, again, as in (i), select the node belonging to the smallest of the two clusters;

(iii) add a link between the two selected nodes thus merging the two smallest clusters (Figure 2.1(b)).

Repeat this procedure again and again. Note that in (i) and (ii) a cluster can be selected several times in the same step. This is frequently the case for the percolation cluster. These rules contain the key element of other explosive percolation models, e.g., model [93], namely, for merging, select the minimal clusters from a few possibilities. Importantly, our procedure provides even more stringent selection of small components for merging than model [93] since guarantees that the product of the sizes of two merging clusters is the smallest of the four possibilities (each of the first pair of chosen nodes (i) may connect with any node of the

second pair (ii)) in contrast to selection from only two possibilities in model [93] (see below). Consequently, if we show that the transition in our model is continuous, then model [93] also must have a continuous transition. More generally, in each sampling, one can select at random m nodes thus choosing the minimal cluster from m clusters. Classical percolation corresponds to $m = 1$ (Figure 2.1(a)). In this section we mostly focus on $m = 2$ (Figure 2.1(b)). One should stress that the explosive percolation processes are irreversible in stark contrast to ordinary percolation. In the latter, one can reach any state either adding or removing connections. For explosive percolation, only adding links makes sense, and a reverse process is impossible.

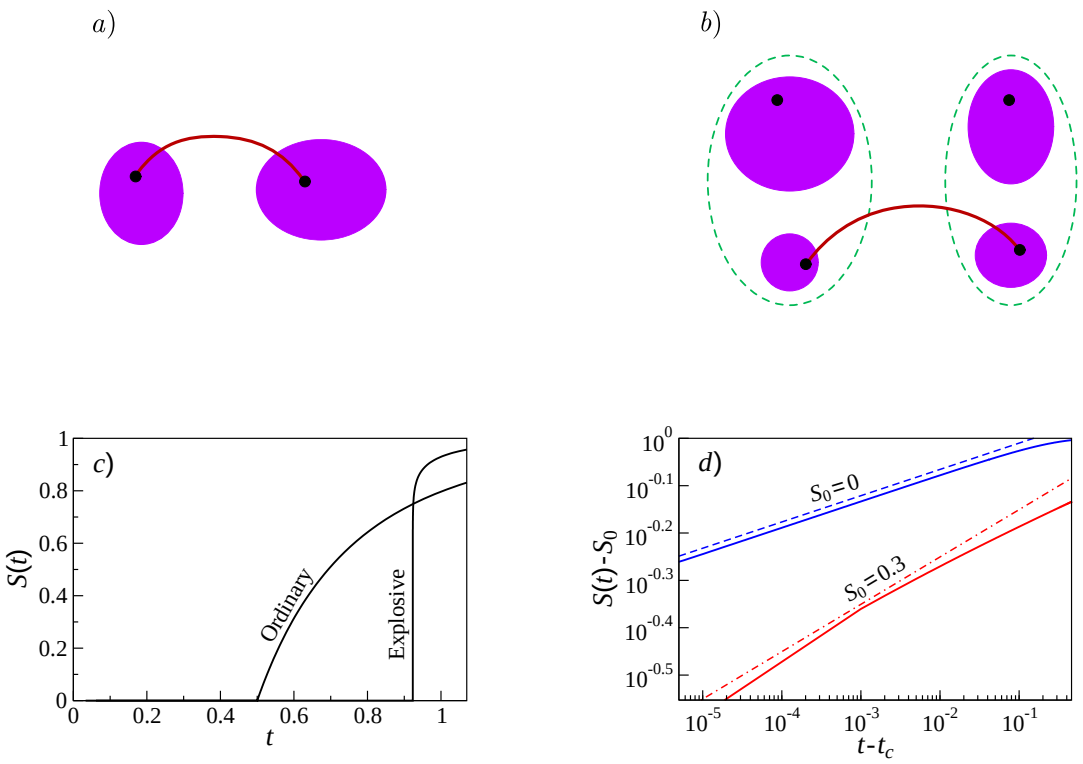

Figure 2.1: Percolation processes. (a) In classical percolation, at each step, two randomly chosen nodes are connected by a new link. If these nodes belong to different clusters, these clusters merge. (b) In the "explosive percolation" model, at each step, two pairs of nodes are chosen at random, and for each of the pairs, the node belonging to the minimal cluster is selected. These two nodes (and so their clusters) are connected by a new link. (c) The relative size of the percolation cluster S versus t (the ratio of the number of links L and nodes N) obtained from simulation of our model with $N = 2 \times 10^9$ nodes (1000 runs). The starting configuration is N bare nodes. The corresponding result for ordinary percolation is also shown. (d) Data $S(t)$ of our simulation (solid blue) is better fitted by the law $a(t - t_c)^\beta$ (dashed blue) than by the $S_0 + b(t - t_c)^\beta$ law, with $S_0 = 0.3$ (dash-dotted red). In the latter case, $\ln(S - S_0)$ (solid red) does not follow a linear law.

We simulated this irreversible aggregation process for a large system of $2{\times}10^9$ nodes. When plotted over the full time range, the obtained dependence $S(t)$ shows what seems to be a discontinuity at the critical point t_c (Figure 2.1(c)) similar to previous results, but a

more thorough inspection of the critical region (log-log plot in Figure 2.1(d)) reveals that the obtained data is definitely better fitted by the law $a\delta^{\beta}$, which indicates a continuous transition, than, say, by $0.3 + b\delta^{\beta}$. Fitting the data of our simulation by the law $S_0 + b\delta^{\beta}$, we find that S_0 is at least smaller than 0.05. This shows that for a definite conclusion, even so large a system turns out to be not sufficient, and a discontinuity can be ruled out or validated only by analytical arguments for the infinite size limit.

Both this explosive model and the random graph, discussed on section 1.4.4, use the full graph as the medium for percolation, as such, they are exactly described by mean-field. Moreover, while explosive percolation is an intrinsically dynamical model, the ordinary percolation model can be viewed as a dynamical process under equilibrium conditions. As such, similar approaches may be employed in both cases. In particular, for the thermodynamic limit, one can write exact rate equations for the evolution of the cluster size distribution.

Comparison Between Explosive Percolation Models

Let us show that our model provides more efficient merging of small clusters than the model [93]. So if the explosive percolation transition is continuous in our model, then model [93] also has a continuous transition.

According to the selection rule in our model, at each step, choose two pairs of nodes, i and j, k and l, uniformly at random. Let they belong to clusters of sizes s_i and s_j, s_k, and s_l, respectively. Connect the smallest cluster of the pair s_i and s_j, with the smallest cluster of the pair s_k, and s_l. One can immediately see that this rule is equivalent to the following one. Let $f(s, s')$ be an arbitrary monotonously growing function of its arguments, e.g., $f(s, s') = ss'$. Consider four possibilities to add a new link, ik, il, jk, and jl, and choose that one which provides the smallest value of $f(s_i, s_k)$, $f(s_i, s_l)$, $f(s_j, s_k)$, and $f(s_j, s_l)$, see Figure 2.2(a).

In the model [93], the product selection rule is as follows. At each step choose nodes i and j, k and l uniformly at random, and select from two possibilities; either connect i and k or connect j and l, choosing the pair with the smallest of the products $s_i s_k$ and $s_j s_l$, see Figure 2.2(b).

Then, the only difference between our model and the model [93] is that we select from four possibilities (comparison of $s_i s_k$, $s_i s_l$, $s_j s_k$ and $s_j s_l$) while in the model [93] the selection is from only two possibilities (comparison of $s_i s_k$ and $s_j s_l$). Therefore our choice guarantees merging of clusters with a product of sizes ss' equal or smaller than in the model [93]. So our process should generate discontinuity even more efficiently. Consequently, if our model has a continuous phase transition, then model [93] also must have a continuous transition.

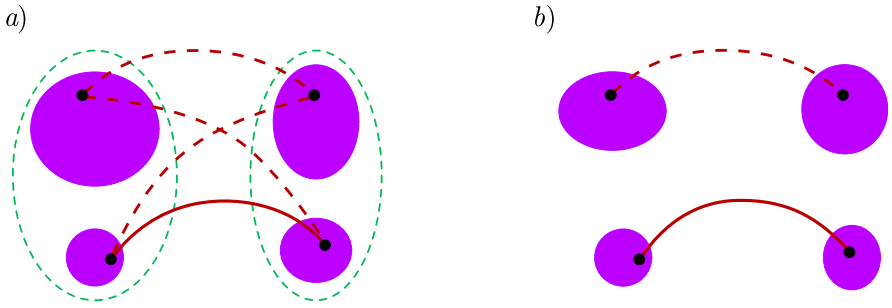

Figure 2.2: Comparison of the linking rules in our model, (a), and in the model [93], (b).

2.2.2 Evolution of the Cluster Size Distribution

We address the explosive percolation problem analytically and numerically by considering the evolution of the cluster size distribution $P(s)$ for a finite cluster of s nodes to which a randomly chosen node belongs. For simplicity, the dependence of the size distribution on time $t \equiv M/N$ is sometimes omitted here, when it causes no confusion (M is the number of links introduced,in a system of N nodes). This distribution satisfies the normalization condition $\sum_s P(s) = 1 - S$. Another important characteristic of this model is the probability, $Q(s)$, that if we choose at random two nodes, the smallest of the two clusters to which these nodes belong is of size s. $Q(s)$ provides us with the size distribution of merging clusters. Here $\sum_s Q(s) = 1 - S^2$. If we introduce the cumulative distributions $P_{\rm cum}(s) \equiv \sum_{u=s}^{\infty} P(u)$ and $Q_{\rm cum}(s) \equiv \sum_{u=s}^{\infty} Q(u)$, then probability theory gives $Q_{\rm cum}(s) + S^2 = [P_{\rm cum}(s) + S]^2$, which simply states that: the probability that the smaller of the two clusters to which two uniformly at random selected nodes belong has size $\geq s$, is equal to the probability that both clusters have size $\geq s$. Consequently

$$\begin{aligned} Q(s) &= Q_{\rm cum}(s) - Q_{\rm cum}(s+1), \\ &= [P_{\rm cum}(s) + S]^2 - [P_{\rm cum}(s) - P(s) + S]^2, \\ &= P(s)\,[2P(u)_{\rm cum} + 2S - P(s)]\,, \\ &= P(s)\left[2 - 2\sum_{u=1}^{s-1} P(u) - P(s)\right], \end{aligned} \tag{2.1}$$

that is, $Q(s)$ is determined by $P(s')$ with $s' \leq s$. The evolution of these distributions in the infinite system is exactly described by the rate equation:

$$\frac{\partial P(s,t)}{\partial t} = s \sum_{u+v=s} Q(u,t)Q(v,t) - 2sQ(s,t), \tag{2.2}$$

which generalizes the standard Smoluchowski equation (1.57). We derived equation (2.2) only assuming the infinite system size. The only difference from the classical percolation problem of section 1.4.4 is the presence of distribution $Q(s,t)$ instead of $P(s,t)$ on the right-hand side.

Thus we have a chain of coupled equations, which should be solved analytically or numerically. To find a numerical solution, first solve the first equation of the chain, which gives $P(1,t)$. Substitute this result into the second equation and solve it, which gives $P(2,t)$, and so on. In this way we find numerically the distributions $P(s,t)$ and $Q(s,t)$ at any t for infinite N. Solving 10^6 equations gives the evolution of these distributions for $1 \leq s \leq 10^6$ and $S(t) \cong 1 - \sum_{s=1}^{10^6} P(s,t)$. The log-log plot (Figure 2.3(a)) shows that the obtained $S(t)$ dependence is well described by the power law: $S \propto \delta^{\beta}$ with $\delta = t - t_c$, $t_c = 0.923207508(2)$, and small $\beta = 0.0555(1)$ (which is very close to $1/18 = 0.05555...$). Here we find t_c as the point at which $P(s)$ is power-law over the full range of s, see below. To check the correctness and precision of our calculations, we repeated them for ordinary percolation and obtained the classical results with the same precision as for our model. Although the small exponent β makes it difficult to approach the narrow region of small S, fitting this data by the law $S_0 + b\delta^{\beta}$, we find that S_0 is smaller than 0.005. This supports our hypothesis that the transition is continuous, but still does not prove it. Moreover, both our extensive simulations

and numerical solution results clearly demonstrate that the analysis of the $S(t)$ data cannot validate or rule out a discontinuity.

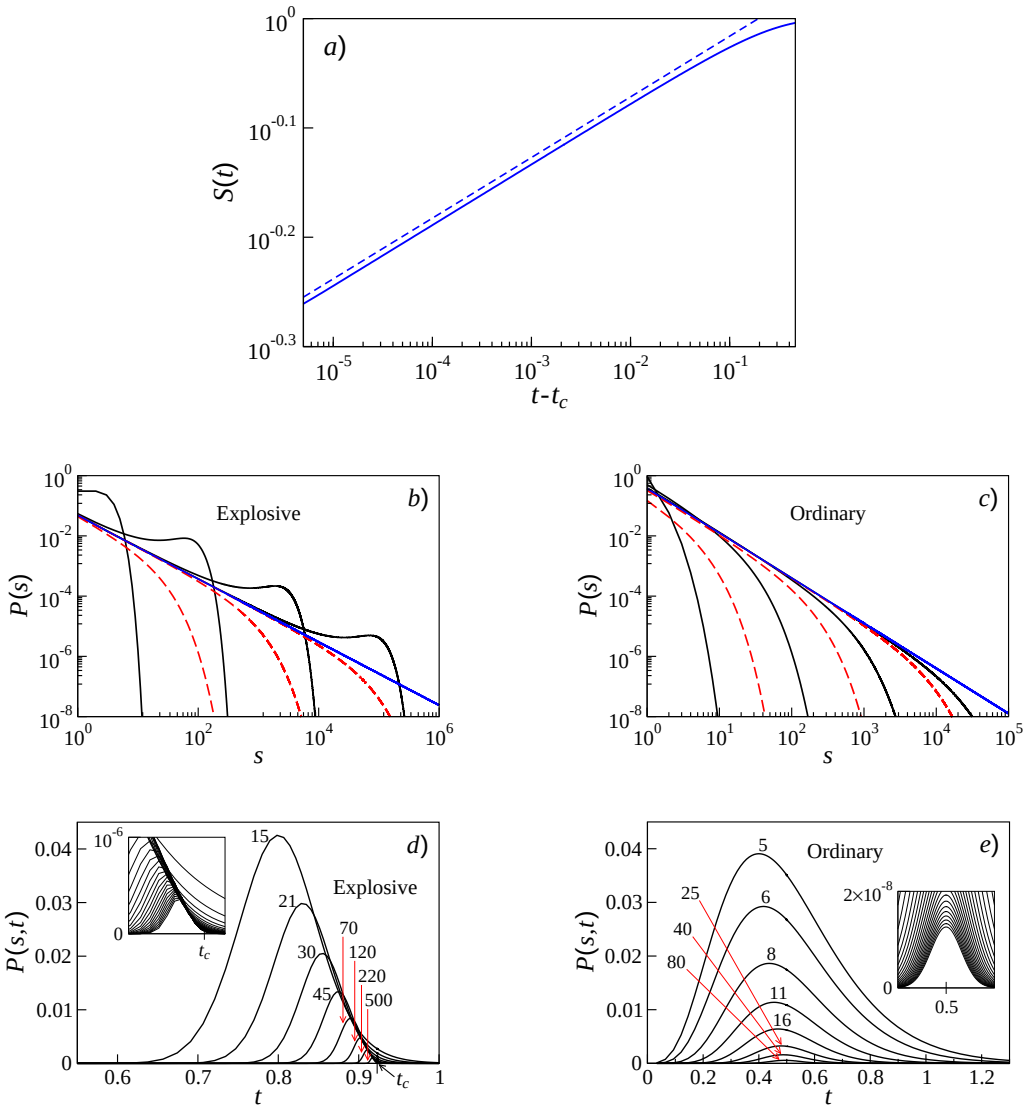

Figure 2.3: Numerical solutions of evolution equations (2.2) for the infinite system. (a) Log-log plot S vs. $t - t_c$. The slope of the dashed line is 0.0555, and $t_c = 923207508$. (b) The evolution of the distribution $P(s)$ below (black lines) and above (red dashed lines) the percolation threshold for explosive percolation. The distribution at the critical point is show by the blue line. (c) The evolution of $P(s)$ for ordinary percolation. (d) Dependence of $P(s,t)$ on t for a set of cluster sizes s for explosive percolation. Numbers on curves indicate s. (e) $P(s,t)$ for normal percolation. The insets show the $P(s,t)$ curves for large values of s.

Figure 2.3(b) shows the evolution of the distribution $P(s,t)$, which we compare with the corresponding evolution for ordinary percolation, Figure 2.3(c). The differences are strong at $t < t_c$, where the distribution for explosive percolation has a bump, but above t_c the behaviors

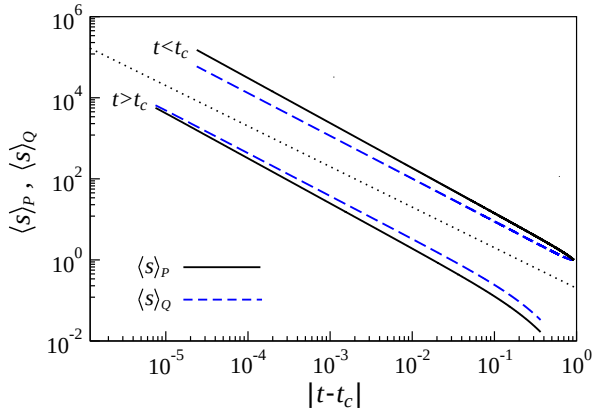

Figure 2.4: In the critical region, the average size of the cluster to which belongs a node chosen uniformly at random, $\langle s\rangle_P = \sum_s sP(s) \propto \delta^{-\gamma_P}$, and a node chosen by the our rule, $\langle s\rangle_Q = \sum_s sQ(s) \propto \delta^{-\gamma_Q}$, show divergent critical singularities, as also happens on ordinary percolation. However, in contrast with ordinary percolation, where $\gamma = 1$, the exponents of these singularities are larger than 1, in particular , $\gamma_P = 1.111(1)$ and $\gamma_Q = 1.0556(5)$ (the dashed line has slope -1).

---

are similar. The distribution function $Q(s,t)$ evolves similarly to $P(s,t)$ in the full time range. At the critical point, we find power laws $P(s) \sim s^{1-\tau}$ and $Q(s) \sim s^{3-2\tau}$ in the full range of s (six orders of magnitude), where $\tau = 2.04762(2)$, which is close to 2, as in [100, 101, 102, 105], in contrast to $\tau = 5/2$ for ordinary percolation. The first moments of these distributions, $\langle s\rangle_P \equiv \sum_s sP(s)$ (the mean size of a finite cluster to which a randomly chosen node belong) and $\langle s\rangle_Q \equiv \sum_s sQ(s)$, demonstrate power-law critical singularities $\langle s\rangle_P \sim \delta^{-\gamma_P}$ and $\langle s\rangle_Q \sim \delta^{-\gamma_Q}$, where $\delta = |t - t_c|$, and exponents $\gamma_P = 1.0111(1)$ and $\gamma_Q = 1.0556(5)$ both below and above the transition, as is shown in Figure 2.4. Note that $\gamma_P > 1$ in contrast to ordinary percolation, where the mean-field value of exponent γ is 1. Figure 2.3(d) shows the set of time dependencies of $P(s,t)$ for fixed cluster sizes (the time dependencies of $Q(s,t)$ are similar). These dependencies strongly differ from those for ordinary percolation (Figure 2.3(e)) in the following respect. The peaks in Figure 2.3(d) for explosive percolation are below t_c, while the peaks in Figure 2.3(e) for ordinary percolation are symmetrical with respect to the critical point at large s.

The inspection of these numerical results in the critical region ($t < t_c$) reveals a scaling behavior typical for continuous phase transitions, $P(s,t) = s^{1-\tau} f(s\delta^{1/\sigma})$ and $Q(s,t) = s^{3-2\tau} g(s\delta^{1/\sigma})$, respectively, where $f(x)$ and $g(x)$ are scaling functions, and $\sigma = (\tau - 2)/\beta$, obeying the standard scaling relation (derived in section 1.4.3). One should stress that these functions are quite unusual. Figure 2.5 shows the resulting scaling functions and, for comparison, the scaling function for ordinary percolation. Remarkably, $f(x)$ and, especially, $g(x)$ are well fitted by Gaussian functions. These functions differ dramatically from the monotonously decaying exact scaling function $e^{-x}/\sqrt{2\pi}$ for ordinary percolation (equation (1.66)). Effective elimination of the smallest clusters in this merging process results in the minima of the scaling functions at x=0. On the other hand, the stunted emergence of large clusters results in the particularly rapid decay of these functions at $x \gg 1$.

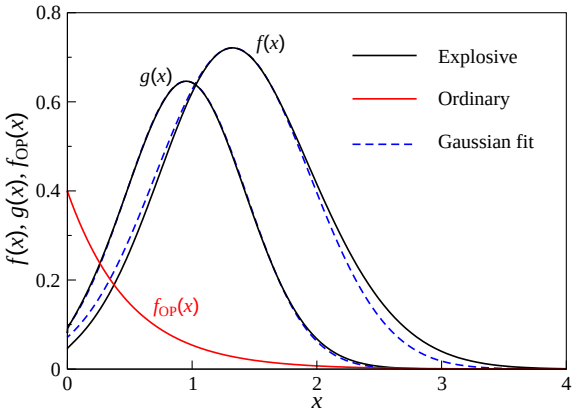

Figure 2.5: Scaling functions $f(x)$ and $g(x)$ for explosive percolation ($t < t_c$) and, for comparison, the exact scaling function $f_{\rm CP}(x) = e^{-2x}/\sqrt{2\pi}$ for ordinary percolation in the random graph, where $x = s(t_c - t)^{-1/\sigma}$. The blue dashed lines show the Gaussian fittings of the explosive percolation scaling functions.

2.2.3 Relations Between Critical Exponents

Here we present a list of relations for critical exponents for the explosive percolation model under consideration ($m = 2$). In the critical region, the distributions $P(s,t)$ and $Q(s,t)$ have a scaling form:

$$P(s,t) = s^{1-\tau} f(s\delta^{1/\sigma})$$
$$Q(s,t) = s^{3-2\tau} g(s\delta^{1/\sigma}), \tag{2.3}$$

where $\delta = |t - t_c|$. Note that the critical exponents below and above the transition are equal, while the scaling functions below t_c differ dramatically from those above the transition. The exponent β of the size of the percolation cluster is expressed in terms of τ and σ, as $\beta = (\tau - 2)/\sigma$ (equation (1.49)). For the first moments of the distributions $P(s)$ and $Q(s)$, critical exponents are γ_P and γ_Q, respectively. Namely, $\langle s \rangle_P \propto |\delta|^{-\gamma_P}$ and $\langle s \rangle_Q \propto |\delta|^{-\gamma_P}$. These exponents are expressed in therms of τ and σ as follows (see derivation (1.44)):

$$\gamma_P = \frac{3-\tau}{\sigma},$$
$$\gamma_Q = \frac{5-2\tau}{\sigma}.$$

Note the relation between γ_P and γ_Q:

$$\gamma_P + 1 = 2\gamma_Q,$$

that can be easily checked by applying $\sum_s s$ on both sides of the master equation (2.2).

Finally, we give the full set of critical exponents, the fractal dimension $d_f = 2/\sigma$ and the

upper critical dimension $d_u = d_f + 2\beta$ in terms of the exponent β:

$$\tau = 2 + \frac{\beta}{1+3\beta},$$
$$\sigma = \frac{1}{1+3\beta},$$
$$\gamma_P = 1 + 2\beta,$$
$$\gamma_Q = 1 + \beta,$$
$$d_f = 2(1+3\beta),$$
$$d_u = 2(1+4\beta).$$

For a detailed discussion on upper critical dimension and fractal dimension see section 2.5.2.

2.2.4 Analysis of the Evolution Equation Above the Percolation Threshold

The key point of our report is the following strict analytical derivation. Let us consider the master equation for our model. Recall the relations (2.1) and (2.2),

$$\frac{\partial P(s,t)}{\partial t} = s \sum_{u+v=s} Q(u,t)Q(v,t) - 2sQ(s,t),$$

where

$$Q(s) = P(s)\left[2 - 2\sum_{u=1}^{s-1} P(u) - P(s)\right].$$

Next, we introduce generating functions for the distributions $P(s)$ and $Q(s)$,

$$\rho(z) \equiv \sum_{s=1}^{\infty} P(s) z^s \tag{2.4}$$

and

$$\sigma(z) \equiv \sum_{s=1}^{\infty} Q(s) z^s. \tag{2.5}$$

Note that $\rho(z=1) = 1 - S$ and $\sigma(z=1) = 1 - S^2$, where S is the relative size of the percolation cluster. Using these generating functions for the distributions we represent the master equation (2.2) in the following form:

$$\frac{\partial}{\partial t}[1 - \rho(z,t)] = -\frac{\partial}{\partial \ln z}[1 - \sigma(z,t)]^2. \tag{2.6}$$

In ordinary percolation, $\sigma(z,t)$ in this equation is substituted by $\rho(z,t)$, namely

$$\frac{\partial \rho(z,t)}{\partial t} = 2[\rho(z,t) - 1]\frac{\partial \rho(z,t)}{\partial \ln z},$$

which corresponds to equation (1.59) of section 1.4.4.

In the critical region above the percolation threshold, identity (2.1) gives

$$Q(s) \cong 2SP(s) \tag{2.7}$$

asymptotically at large s, which leads to a simple relation between the generating functions $\sigma(z)$ and $\rho(z)$ in the range z close to 1. Indeed,

$$1 - S^2 - \sigma(z) = \sum_s Q(s)[1 - z^s] \cong \sum_s 2SP(s)[1 - z^s] = 2S[1 - S - \rho(z)],$$

so

$$1 - \sigma(z) \cong 2S[1 - \rho(z) - S/2] \tag{2.8}$$

if z is close to 1 in the critical region at $t > t_c$. The last summations run over all sizes s, which includes the range of small s where expression (2.7) is not valid. However, when $z \to 1$ the contribution from those sizes becomes negligible as $1 - z^s \to 0$. One can check this relation at $z = 1$:

$$1 - \sigma(1) = S^2 = 2S[1 - \rho(1) - S/2] = 2S(S - S/2) = S^2.$$

Therefore, in the critical region above the percolation threshold, at z close to 1, relation (2.6) takes a convenient form,

$$\frac{\partial \rho(z,t)}{\partial t} = 8S^2(t)[\rho(z,t) - 1 + S(t)/2]\frac{\partial \rho(z,t)}{\partial \ln z}. \tag{2.9}$$

Note that this equation essentially differs from equation (1.59) for ordinary percolation, because of the terms $S(t)$ on the right-hand side. Nonetheless equation (2.9) can be analyzed in a similar fashion to ordinary percolation.

Our numerical solution of equations (2.2) showed convincingly that at the critical point, the distribution $P(s, t_c)$ is power-law, namely, at large s, $P(s, t_c) \cong f(0)s^{1-\tau}$. Here $f(0)$ is the critical amplitude for this distribution. (This is also the value of the scaling function for this distribution, $f(x = 0)$, see below.) We observed these power laws over 6 orders of magnitude, and they were also observed in works [100, 101, 102, 105] for explosive percolation though in less wide range of s. Let us show that, if at the critical point $P(s, t_c) \propto s^{1-\tau}$, then equation (2.9) has a solution with $1 - \rho(z = 1, t) = S(t) \propto (t - t_c)^\beta$ in the critical region, which just means that the transition is continuous. The existence of this solution can be demonstrated in the following way. Let us assume that $P(s, t_c) \cong f(0)s^{1-\tau}$ at large s, and $S \cong B(t - t_c)^\beta$ at small $t - t_c$ and check whether this assumption is correct or not. Here we assume that $f(0)$ and the exponent τ are known (numerical solution gave $f(0) = 0.04618(2)$ and $\tau = 2.04762(2)$), while B and the exponent β are to be found.

We use the power-law asymptotics of the distribution $P(s, t_c) \cong f(0)s^{1-\tau}$ as the initial condition for equation (2.9). This corresponds to the following singularity of the generating function at $z = 1$:

$$\begin{aligned}
1 - \rho(z, t_c) &= 1 - \sum_s \left(P(s, t_c) - f(0)s^{1-\tau}\right) z^s - f(0) \sum_s s^{1-\tau} z^s, \\
&= 1 - \sum_s \left(P(s, t_c) - f(0)s^{1-\tau}\right) z^s - f(0)(-\ln z)^{\tau-1} \sum_s (-s \ln z)^{1-\tau} e^{s \ln z}, \\
&= \text{analytic terms} - f(0)(-\ln z)^{\tau-2} \int dy\, y^{1-\tau} e^{-y}, \\
&= f(0)|\Gamma(2 - \tau)|(1 - z)^{\tau-2},
\end{aligned} \tag{2.10}$$

where Γ is the Gamma function. The substitution of the summation by an integral is possible since we are interested in the behavior of ρ in the limit $\ln z \to 0$ (also $\ln z$ can be substituted by $1 - z$ in this limit).

Introducing $\epsilon \equiv (t - t_c)^{2\beta+1}$ and $x \equiv \ln z$, we transform the partial differential equation (2.9) into the following form:

$$\frac{\partial \rho}{\partial \epsilon} = \frac{8B^2}{1+2\beta}\left(\rho - 1 + \frac{B}{2}\epsilon^{\beta/(1+2\beta)}\right)\frac{\partial \rho}{\partial x}. \tag{2.11}$$

To solve this equation we use the same approach employed in section 1.4.4 to find the implicit solution (1.60), for the classical random graph. We pass from $\rho = \rho(x, \epsilon)$ to $x = x(\rho, \epsilon)$, which leads to a simple linear partial differential equation for $x(\rho, \epsilon)$ and enables us to find the general solution

$$\ln z = \frac{8B^2}{1+2\beta}\left[1 - \rho - \frac{B}{2}\frac{\epsilon^{\beta/(1+2\beta)}}{1+\beta/(1+2\beta)}\right]\epsilon + F(\rho),$$

where the function $F(\rho)$ is obtained from the initial condition (2.10), which gives the solution

$$\ln z = \frac{8B^2}{1+2\beta}\left[1-\rho-\frac{B}{2}\frac{(t-t_c)^{\beta}}{1+\beta/(1+2\beta)}\right](t-t_c)^{1+2\beta} - [f(0)]^{-1/(\tau-2)}|\Gamma(2-\tau)|^{-1/(\tau-2)}[1-\rho]^{1/(\tau-2)}. \tag{2.12}$$

We set $z = 1$, and taking into account $1 - \rho(1) = S = B(t - t_c)^{\beta}$ and comparing resulting powers and coefficients of solution (2.12), we obtain again the same relation between the critical exponents,

$$\tau = 2 + \frac{\beta}{1+3\beta}, \tag{2.13}$$

and express the critical amplitude B for the relative size of the percolation cluster in terms of the critical amplitude $f(0)$ for the distribution $P(s, t_c)$,

$$B = \left[4\frac{(\tau-1)(7-3\tau)}{3-\tau}\right]^{(\tau-2)/(7-3\tau)} [f(0)]^{1/(7-3\tau)}|\Gamma(2-\tau)|^{1/(7-3\tau)}. \tag{2.14}$$

It should be emphasized that relation (2.13), unlike in the previous section, was obtained directly from the fact that the critical size distribution decays as a power law, without further scaling assumptions. The relation (2.13) precisely agrees with our numerical results, $\tau = 2.04762(2)$ and $\beta = 0.0555(1)$. Substituting $f(0) = 0.04618(2)$ (our numerical result) into expression (2.14) gives $B = 1.075$, which agrees with the corresponding value 1.080 obtained by solving the master equation numerically.

Furthermore, the power-law distribution at the critical point can be justified strictly by using an equation for scaling functions. In the normal phase ($t < t_c$), we derived an equation for the scaling functions in this problem. This is a nonlinear integral-differential eigenfunction equation, where eigenfunctions are the scaling functions for $P(s, t)$ and $Q(s, t)$ (as defined by expressions (2.3)), and a critical exponent, say τ, plays the role of an eigenvalue. This equation can be solved numerically, which is, however, a difficult task. We verified that the scaling functions and τ, which we found numerically by solving the system (2.2) for $s \leq 10^6$, satisfy this equation. Hence, showing that the critical distributions are indeed power laws (asymptotically). This point is thoroughly explored is section 2.5.

2.2.5 Relation Between the Critical Time t_c and Exponent τ

We can obtain approximate relations between t_c and τ or between the critical amplitude $f(0)$ and τ by applying the sum rule $\sum_s P(s) = 1$ at the critical point. Two estimates are possible. One can estimate $P(s, t_c)$ by its asymptotics $f(0)s^{1-\tau}$, which gives

$$f(0)\zeta(\tau - 1) \approx 1,$$

where $\zeta(x) = \sum_{s=1}^{\infty} s^{-x}$ is the Riemann zeta function. If τ is close to 2, then $\zeta(\tau - 1) \cong 1/(\tau - 2)$, so we have $\tau - 2 \approx f(0)$. This estimate shows that the small values of $\tau - 2$ and $f(0)$ are interrelated. Recall that we obtained numerically $\tau = 2.04762(2)$ and $f(0) = 0.04618(2)$.

In the second estimate we use the following approximation: $P(s, t_c) \approx P(1, t_c)s^{1-\tau}$. We find $P(1, t)$ explicitly by solving the master equation (2.2), which gives

$$P(1, t) = \frac{2}{1 + e^{4t}},$$

so we have

$$\frac{2}{1 + e^{4t_c}}\zeta(\tau - 1) \approx 1.$$

Using $t_c = 0.923207508(2)$ obtained numerically, we find approximately $\tau - 2 \approx 0.05$. That is, exponent τ is close to 2 when t_c is close to 1.

2.2.6 Summary and Conclusions

The most important point of this work is the analytical derivation of section 2.2.4. We start from the fact that in this problem the cluster size distributions are power-law at the percolation threshold. Then we strictly show that if the critical distribution is power-law, this phase transition is continuous. We use the fact that in the critical region above the percolation threshold, the distributions $Q(s)$ and $P(s)$ at large s are proportional to each other, namely $Q(s) \cong 2SP(s)$. This relation crucially simplifies our problem, since the resulting evolution equation for the asymptotics of the distribution in this region contains only $P(s)$ and the relative size $S(t)$ of the percolation cluster. As a result, equation (2.2) becomes very similar to that for ordinary percolation (the only difference is the presence of $S(t)$ terms on the right-hand side), and so it can be easily analyzed explicitly in the same way as for ordinary percolation. Then, using a power-law critical distribution $P(s) \sim s^{1-\tau}$ as an initial condition for this equation at $t = t_c$, we find that the behavior of the distribution $P(s)$ and $S(t)$ in explosive percolation above the percolation threshold is qualitatively similar to that for ordinary percolation. Specifically, we show that the percolation cluster emerges continuously, and $S \propto \delta^{\beta}$, where $\tau = 2 + \beta/(1 + 3\beta)$ and so $\sigma = 1/(1 + 3\beta)$. The obtained numerical values of exponents τ, β, and σ agree with these two scaling relations and thus also confirm the continuous transition. So the results of this report are self-consistent. (Our results are summarized in Table 2.1.)

Assuming a scaling form for the distributions gives $\gamma_P = 1 + 2\beta$ and $\gamma_Q = 1 + \beta$, which agree with our numerical solution of equation (2.2). Furthermore, applying standard scaling relations [20], we calculate the fractal dimension for this model, $d_f = 2/\sigma = 2(1+3\beta)$, and the upper critical dimension, $d_u = d_f + 2\beta = 2(1 + 4\beta)$ (see Table 2.1). The latter determines the finite size effect: $t_c(\infty) - t_c(N) \propto N^{-2/d_u}$, where $2/d_u = 0.818(1)$. Interestingly, the obtained fractal and upper critical dimensions for explosive percolation are less than 3. They are much

t_c	β	τ	σ	γ_P	γ_Q	d_f	d_u	
Ordinary	1/2	1	5/2	1/2	1	—	4	6
Explosive	0.923207508(2)	0.0555(1)	2.04762(2)	0.857(3)	1.111(1)	1.0556(5)	2.333(1)	2.445(1)

Table 2.1: Threshold values, critical exponents, and fractal and upper critical dimensions for ordinary percolation and explosive one. The estimations shown for the explosive model, were obtained from the numerical solution of the first 10^6 equations (2.2), for all exponents except d_f and d_u, which were obtained using the corresponding scaling relations.

smaller than those for ordinary percolation, which are 4 and 6, respectively. Our model is infinite-dimensional, which is above the upper critical dimension, where mean-field theories must work, which makes the observed smallness of exponent β particularly remarkable. We know no other model with such a small β.

We have shown that the "explosive percolation" transition is actually continuous. It is the smallness of the β exponent for the size of the percolation cluster that makes it virtually impossible to distinguish this phase transition from a discontinuous one even in very large systems. Indeed, suppose that $N = 10^{18}$ and $\beta \approx 1/18$. The addition of one link changes t by $\Delta t = 1/N$, which is the smallest time interval in the problem. Then a single step $\Delta t = 10^{-18}$ from the percolation threshold already gives $S \sim (\Delta t)^{\beta} \sim 0.1$. Other critical exponents and dimensions also differ radically from classical values. Furthermore, we have derived a complete set of scaling relations between the critical exponents for this problem, which were also supported by our numerical results. The real absence of explosion toppled an already established view of explosive percolation. We believe, however, that, thanks to the observed unique properties of this phase transition, our findings make this new class of irreversible systems an even more appealing subject for further extensive exploration. In fact, posteriorly, the continuity of the explosive percolation transition was proved mathematically [111] and was observed in references [103, 112, 113, 114, 115, 116] for other models.

2.3 Scaling Properties of the Explosive Percolation Transition

In this section we introduce a natural generalization of the explosive percolation model formulated above. We consider a set of representative models allowing an elegant description and covering the entire range of processes of this type, with two already known limiting cases, namely (i) standard percolation and (ii) the "most explosive" model, where at each step, the two smallest clusters present in the system are merged together (which is a deterministic process, with a trivial evolution [99]). This generalized model is later used, in section 2.5, as the basis for a complete description of explosive percolation phenomena. Here, we show, in general, that the continuity of the transition along with its corresponding scaling properties, follow from the observed power-law critical distributions. Therefore, excluding the possibility of a discontinuity for any selection rules, regardless of the strength of the bias (these results are an extension of the analysis of last section).

We will find that these phase transitions show non-universal critical behavior, so the models have to be strictly specified. In addition, we extend our analysis to a model that mixes the rules of the explosive percolation and the ordinary percolation models, which will be referred to as *mix model* henceforth. As expected, the properties of the mix model show

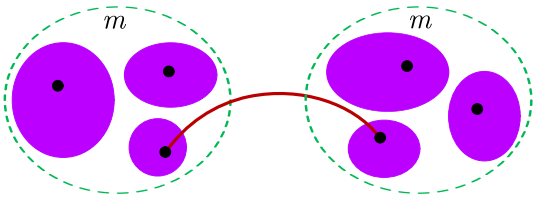

Figure 2.6: Schematic representation of the explosive percolation model rules. At each step, two samples of m nodes are selected uniformly at random. In each of the samples, the node belonging to the smallest (of m) clusters is chosen, and a new link connecting these two nodes is added to the system. In other words, two sets of clusters are chosen with probability proportional to their sizes and two smallest clusters, taken from each of the sets, merge together.

---

qualitative agreement with the general scheme that we develop for explosive percolation, while quantitatively, it presents a critical behavior in-between the ordinary and explosive percolation versions. Most of the results shown in this section may also be found in [2].

2.3.1 The Models

The strength of the optimization-like procedure's bias, used as a selection rule for the merging clusters, determines the model's "explosiveness". If there is no bias, i.e., each node selected to receive a link is chosen uniformly at random, we are left with the ordinary percolation model. The case when we compare the clusters of two nodes chosen uniformly at random was the subject of last section. From hereon, we present all results for the set of infinite-dimensional models of evolving networks, covering the entire range optimization strength, and defined as follows. The number of nodes N in the network does not change during the evolution. At each time step a new link connecting two nodes is added. The evolution rules define how these nodes are selected. Initially the network consists of a given set of finite clusters, in total, of N nodes. For example, these may be N unconnected nodes. At each time step sample two times:

(i) choose $m \geq 1$ nodes uniformly at random and compare the clusters to which these nodes belong; select that node of the m ones, which belongs to the smallest of these clusters;

(ii) similarly choose the second sample of m nodes and, again, as in (i), select the node belonging to the smallest of the m clusters;

(iii) add a link between the two selected clusters thus merging the two smallest clusters (see Figure 2.6).

This model offers a natural continuation of the explosive percolation model introduced in last section, which is accomplished by setting $m = 2$. While $m = 1$ is equivalent to ordinary percolation. On the other hand, if the number m approaches infinity, the pair of the two smallest clusters in the network merge at each step, and so the giant connected component will emerge only after all finite clusters have merged with each other. In fact, the dynamics in this limit is rather trivial. For instance, if $P(s, t = 0) = \delta_{s,1}$, then after $N/2$ connections all nodes are joint in pairs, i.e., $P(s, 1/2) = \delta_{s,2}$, and after $N/4$ more connections $P(s, 3/4) = \delta_{s,4}$, and so forth ($P(s, 1 - 2^{-n}) = \delta_{s,2^n}$ with $n = 0, 1, 2, \ldots$), until a giant cluster emerges, which

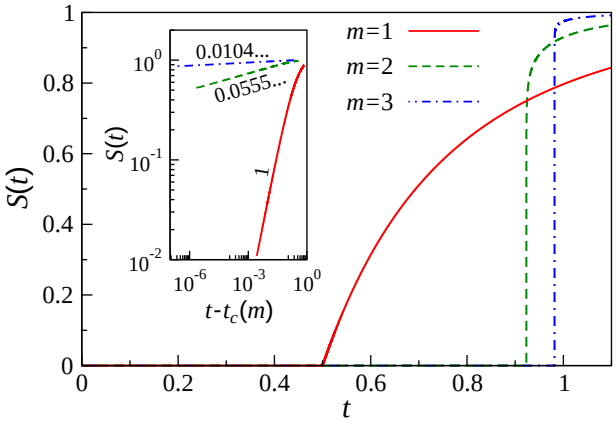

Figure 2.7: Giant component size growth over time, for the explosive percolation models $m = 1, 2, 3$. The curves are obtained by numerically solving 10^5 evolution equations, for the cluster size distributions $P(s)$ and $Q(s)$, corresponding to each model (see below). Here, we used the approximation $S \approx \sum_{s \leq 10^5} P(s)$. It can be seen that as m increases t_c approaches 1 rather rapidly, and the growth of S above t_c becomes more abrupt. Fitting these curves to power laws, i.e., $S \propto (t - t_c)^\beta$, we find that the critical exponent β appears to approach 0, also quite rapidly, with the increase of m (the number next to each line in the inset indicates its slope, which is equal to β).

---

happens at $t_c = 1$, and in this case its relative size is indeed discontinuous at the transition, $S(t_c^-) = 0$ and $S(t_c^+) = 1$ [99]. We will show that this is the only situation with discontinuity. The explosive percolation rules' bias towards small cluster selection is tunable between these two limiting behaviors, with the parameter m. For larger m it takes the system a longer time reaching the critical threshold t_c, which rapidly gets closer to 1. Above that point, the steepness of the giant cluster growth increases dramatically with m (see Figure 2.7).

Note that in our rules, the selected nodes may belong to the same clusters. This happens frequently when a giant connected component is present in the network, however the probability of such event happening in a finite component goes to zero as the system size goes to infinity. Interestingly, if we forbid these events in the model, allowing each cluster to be chosen at random only once per step, then there will be not one but $2m - 1$ giant connected components of the same size.

During the dynamics of the mix model only one of two nodes linked at each step is selected using the sampling procedure (i), the other node is chosen uniformly at random. If we forbid to choose the same cluster more than once at each step, there will be m giant components of the same size.

2.3.2 Evolution Equations

The master equation governing the generalized explosive percolation model looks exactly the same for any m, recalling relation (2.2):

$$\frac{\partial P(s,t)}{\partial t} = s \sum_{u+v=s} Q(u,t)Q(v,t) - 2sQ(s,t). \tag{2.15}$$

The parameter m, governing the selection rule of Figure 2.6, enters only in the next relation, among distributions Q and P. Generalizing equation (2.1) we obtain

$$Q(s) = \left[1 - \sum_{u<s} P(u)\right]^m - \left[1 - \sum_{u\leq s} P(u)\right]^m ,$$

$$= P(s) \sum_{k=0}^{m-1} \binom{m}{k+1} P(s)^k \left[1 - \sum_{u\leq s} P(s)\right]^{m-1-k} , \tag{2.16}$$

where the first term on the right-hand side of first equality accounts for all the cases where all the m randomly chosen clusters have sizes larger or equal to s, and the second term subtracts the cases where all the m clusters have size strictly larger than s This difference is equal to the fraction of cases in which at least one of the clusters has size equal to s and the others have size larger than s, which is equivalent to the probability that a cluster selected by our rule has size s.

Equation (2.15) leads to the following evolution equation for the size of the percolation cluster:

$$\frac{\partial S}{\partial t} = 2S^m \langle s \rangle_Q \tag{2.17}$$

Last equation demonstrates the principal difference of "explosive" percolation from ordinary one. Let us seed a giant component of relative size $h \ll 1$ in the normal phase at some moment $t < t_c$ and consider its evolution. Equation (2.17) shows that the growth rate of this component is proportional to h^m, i.e., it is severely suppressed in the entire normal phase if $m > 1$. This suppression results in the delayed transition compared to $m = 1$.

To check the continuity of the transitions on these models we can use the same approach of last section. Above the percolation threshold t_c, when there is a giant component, the large s asymptotic behavior of expression (2.16) is determined by the first term of the first sum (the lower power of $P(s)$), where the factor $\left(1 - \sum_{u\leq s} P(u)\right)^{m-1}$ can be substituted by S^{m-1}. Instead of simplification (2.7), the relation between asymptotic distributions, above t_c, comes now

$$Q(s) \cong mS^{m-1}P(s).$$

Then for z close to 1, and taking into account $1 - \sum_s Q(s) = S^m$, one can write the relation between scaling functions (2.4) and (2.5) as:

$$1 - S^m - \sigma(z) = \sum_s Q(s)[1 - z^s] \cong \sum_s mS^{m-1}P(s)[1 - z^s] = mS^{m-1}(1 - S - \rho(z)).$$

so

$$1 - \sigma(z) = mS^{m-1} \left[1 - \rho(z) - \frac{m-1}{m} S\right]. \tag{2.18}$$

Substituting the last relation into equation (2.6) one gets the partial differential equation for any m,

$$\frac{\partial \rho(z,t)}{\partial t} = 2m^2 [S(t)]^{2(m-1)} \left[\rho(z,t) - 1 + \frac{m-1}{m} S(t)\right] \frac{\partial \rho(z,t)}{\partial \ln z}, \tag{2.19}$$

which can be tackled in a similar fashion to equation (2.9). To check the continuity of the transition, one again substitutes $S(t) = B(t - t_c)^\beta$ in last equation, and rewrites it in terms of the transformed variables $\epsilon \equiv (t - t_c)^{(m-1)2\beta+1}$ and $x \equiv \ln z$:

$$\frac{\partial \rho}{\partial \epsilon} = \frac{2m^2 B^{2(m-1)}}{1 + (m-1)2\beta} \left(\rho - 1 + \frac{m-1}{m} B \epsilon^{\beta/[1+(m-1)2\beta]} \right) \frac{\partial \rho}{\partial x}. \tag{2.20}$$

The solution of this partial differential equation is obtained with the application of the same technique used above. We take the critical distribution as initial condition (equation (2.10)), thus getting $\rho(t, z \to 1)$ implicitly, for the critical region above t_c (when there is a giant component):

$$\begin{aligned} \ln z =& \frac{2m^2 B^{2(m-1)}}{1 + (m-1)2\beta} \left[1 - \rho - \frac{m-1}{m} B \frac{(t - t_c)^\beta}{1 + \beta/[1 + (m-1)2\beta]} \right] (t - t_c)^{1+(m-1)2\beta} \\ & - [f(0)]^{-1/(\tau-2)} |\Gamma(2-\tau)|^{-1/(\tau-2)} [1 - \rho]^{1/(\tau-2)}. \end{aligned} \tag{2.21}$$

Taking the identity $1 - \rho(t, 1) = S(t)$, inspection of equation (2.21) at $z = 1$ (where it is exact) shows that the assumed continuous variation of giant component size ($S(t) = B(t - t_c)^\beta$) is indeed a solution of the master equation (2.15) under selection rule (2.16). This equation provides us with the relation between critical exponents τ and β:

$$\tau = 2 + \frac{\beta}{1 + (2m-1)\beta}, \tag{2.22}$$

and between critical amplitudes B and $f(0)$:

$$B = \left[f(0) |\Gamma(2-\tau)| \left(2m \frac{[1 - (2m-1)(\tau-2)][1 + (m-1)(\tau-2)]}{3 - \tau} \right)^{\tau-2} \right]^{1/[1-(2m-1)(\tau-2)]}, \tag{2.23}$$

for a generic m. It is clear that the effectiveness of the selection rule's bias is determined by the model parameter m, a larger m leads to a more efficient selection of small clusters. Thus, the previous analysis proves that the explosive percolation transition is always continuous, even for an arbitrarily strong bias, as long as the number of comparisons at each step remains finite (i.e. m is finite). When m is let go to infinity there is indeed a discontinuity at $t_c = 1$, since the dynamics simply merges the two smallest clusters present at each step.

The last analytic procedure is easily adaptable to the mix model. So, it is without surprise that the same kind of solution is obtained, yet with different relations between critical exponents and amplitudes. Since in the mix model, for each new link, we select a node according to the 'smaller of m' rule, and the other is just picked uniformly at random, the master equation comes now slitly different:

$$\frac{\partial P(s,t)}{\partial t} = s \sum_{u+v=s} Q(u,t) P(v,t) - s \left[Q(s,t) + P(s,t) \right]. \tag{2.24}$$

Rewriting it in terms of the generating functions ρ and σ,

$$\frac{\partial}{\partial t} [1 - \rho(z,t)] = - \frac{\partial}{\partial \ln z} [1 - \rho(z,t)][1 - \sigma(z,t)]. \tag{2.25}$$

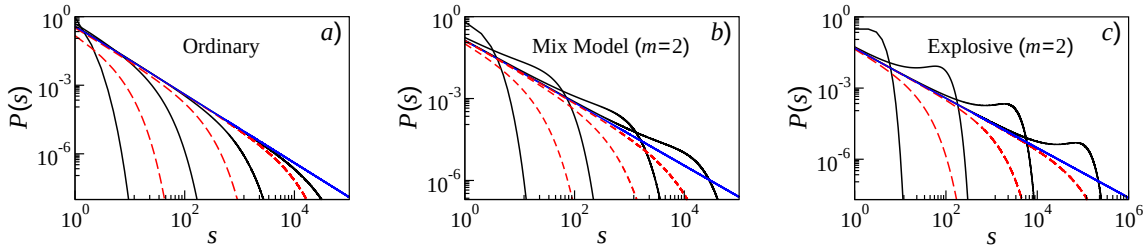

Figure 2.8: Finite cluster size distributions at different times t. The black solid curves correspond to $t < t_c$, the blue dashed curve to $t = t_c$, and the red dot-dashed curves correspond to $t > t_c$. For increasing time, before t_c, the tail of the distribution moves to the right. At t_c the distribution becomes power-law. After t_c it moves to the left. (a) numerical solution of 10^5 master equations (1.57) for the ordinary percolation (also shown in Figure 2.3(c)). (b) numerical solution of 10^5 equations (2.24) with $m = 2$. (c) numerical solution of 10^6 equations (2.15) with $m = 2$ (Figure 2.3(b)).

---

and substituting relation (2.18), and using variables $\epsilon \equiv (t - t_c)^{(m-1)\beta+1}$ and $x \equiv \ln z$, we find:

$$\frac{\partial \rho}{\partial \epsilon} = \frac{mB^{m-1}}{1 + (m-1)\beta} \left(2(\rho - 1) + \frac{m-1}{m} B \epsilon^{\beta/[1+(m-1)\beta]} \right) \frac{\partial \rho}{\partial x}. \tag{2.26}$$

where $S(t)$ was again substituted by $B(t - t_c)^\beta$. Last equation is solvable with the same technique used before, namely in the similar equation (2.20), given the initial condition (2.10). This way we get the implicit solution:

$$\begin{aligned} \ln z = & \frac{mB^{m-1}}{1 + (m-1)\beta} \left[2(1-\rho) - \frac{m-1}{m} B \frac{(t-t_c)^\beta}{1+\beta/[1+(m-1)\beta]} \right] (t-t_c)^{1+(m-1)\beta} \\ & - [f(0)]^{-1/(\tau-2)} |\Gamma(2-\tau)|^{-1/(\tau-2)} [1-\rho]^{1/(\tau-2)}, \end{aligned} \tag{2.27}$$

which is used at $z = 1$ (where $1 - \rho = B(t - t_c)^\beta$) to find the critical relations between exponents

$$\tau = 2 + \frac{\beta}{1 + m\beta}, \tag{2.28}$$

and amplitudes

$$B = \left[f(0) |\Gamma(2-\tau)| \left(\frac{[1 - m(\tau-2)][1 + m + (m-1)(\tau-2)]}{3-\tau} \right)^{\tau-2} \right]^{1/[1-m(\tau-2)]} \tag{2.29}$$

of the mix model.

It was possible to solve numerically the ordinary differential system of equations (2.24) for s between 1 and 10^5 for $m = 2$. Figure 2.8(b) shows $P(s)$ at different times t for the mix model. From that data we estimated the value of critical exponent $\beta = 0.2140(2)$ for the mix model. This value is between what was found for the explosive percolation model (where $\beta \approx 0.0555$), and the value for the ordinary percolation model ($\beta = 1/2$). The estimations of the critical point t_c and the set of critical exponents are shown in Table 2.2.

	t_c	β	τ	σ	γ_P	γ_Q
Ordinary	1/2	1	5/2	1/2	1	–
Mix	0.797(1)	0.2140(2)	2.1499(1)	0.700(5)	1.214(1)	1.000(1)
Explosive	0.923208(1)	0.0555(1)	2.04762(2)	0.857(3)	1.111(1)	1.0556(5)

Table 2.2: Critical points and exponents for ordinary, mix (with $m = 2$) and explosive (with $m = 2$) percolation models. For the mix model, the values were calculated from the numerical solution of 10^5 equations (2.24). Results for the ordinary and explosive models, put here for comparison with the mix model, have already been shown in Table 2.1.

2.3.3 Scaling Relations with m

We observe scaling behavior, near the critical point, for all these continuous phase transitions, consistently with the general theory. As such, for large s, the cluster size distribution P is well described by:

$$P(s,t) = s^{1-\tau} f(s\delta^{1/\sigma}), \tag{2.30}$$

where $\delta = |t - t_c| \ll 1$ and $f(x)$ is a scaling function that depends on the model. The presence of scaling is also observed in Q, as noted in section 2.2.3. For a generic m we find:

$$Q(s,t) = s^{-1-m(\tau-2)} g(s\delta^{1/\sigma}), \tag{2.31}$$

where $g(x)$ is another scaling function. The relation between functions $f(x)$ and $g(x)$ is shown in section 2.5.3.

In this section we shortly derive the set of scaling relations between critical exponents, for generic m, of both the explosive percolation model and the mix model. In fact, only one relation is different between the two models (and some of the others are the same for ordinary percolation). The fundamental relations $\beta = (\tau - 2)/\sigma$ (equation (1.49)) and $\gamma_P = (3 - \tau)/\sigma$ (equation (1.43)) are verified independently of the model. Additionally, a relation for γ_Q may be obtained following the steps of equation (1.44) applied to distribution Q, which gives:

$$\gamma_Q = \frac{1 - m(\tau - 2)}{\sigma}. \tag{2.32}$$

It should be noticed that this scaling relation is valid for both the explosive and the mix model; since $Q(s)$ has the same definition (expression (2.31) holds on both cases).

The difference between the two models is determined by the master equation, which provides the last scaling relation, between exponents γ_P and γ_Q. Below in the normal phase $\sum_s Q(s) = 1$, and the application of $\sum_s s$ on both sides of master equation (2.15) for the

explosive model, gives:

$$\begin{aligned}
\frac{\partial\langle s\rangle_p}{\partial t} &= \sum_s s^2 \sum_{u+v=s} Q(u)Q(v) - 2\sum_s s^2 Q(s), \\
&= \sum_s \sum_{u+v=s} (u+v)^2 Q(u)Q(v) - 2\sum_s s^2 Q(s), \\
&= \sum_u \sum_v \left(u^2+v^2+2uv\right) Q(u)Q(v) - 2\sum_s s^2 Q(s), \\
&= 2\sum_u u^2 Q(u) \sum_v Q(v) + 2\sum_u uQ(u) \sum_v vQ(v) - 2\sum_s s^2 Q(s), \\
&= 2\sum_u uQ(u) \sum_v vQ(v), \\
&= 2\langle s\rangle_Q^2. \qquad (2.33)
\end{aligned}$$

This relation was already used in section 2.2.3, under the form

$$\gamma_P + 1 = 2\gamma_Q. \qquad (2.34)$$

Thus we find four relations between five exponents, which leaves only one independent exponent, i.e., all critical exponents may be expressed in terms of a single unknown exponent, say, for example, β:

$$\tau = 2 + \frac{\beta}{1+(2m-1)\beta}, \qquad (2.35)$$

$$1/\sigma = 1 + (2m-1)\beta, \qquad (2.36)$$

$$\gamma_P = 1 + 2(m-1)\beta, \qquad (2.37)$$

$$\gamma_Q = 1 + (m-1)\beta. \qquad (2.38)$$

Result (2.35) was obtained previously, in section 2.3.2, by the generating functions method (equation (2.22)). The fact that the same relation appears twice, by independent methods, is another manifestation of the consistency of our approach.

The set of scaling relations between exponents for the mix model, is obtained by substituting expression (2.34). Below t_c, the application of $\sum_s s$ to master equation (2.24) for the

mix model yields:

$$\begin{aligned}
\frac{\partial\langle s\rangle_p}{\partial t} =& \sum_s s^2 \sum_{u+v=s} Q(u)P(v) - \sum_s s^2\left[Q(s)+P(s)\right], \\
=& \sum_u \sum_v \left(u^2+v^2+2uv\right) Q(u)P(v) - 2\sum_s s^2\left[Q(s)+P(s)\right], \\
=& \sum_u u^2 Q(u) \sum_v P(v) + \sum_v v^2 P(v) \sum_u Q(u) + 2\sum_u uQ(u) \sum_v vP(v) \\
& - 2\sum_s s^2\left[Q(s)+P(s)\right], \\
=& 2\sum_u uQ(u) \sum_v vP(v), \\
=& 2\langle s\rangle_P \langle s\rangle_Q. \qquad (2.39)
\end{aligned}$$

Interestingly, the scaling relation corresponding to the master equation of the mix model is independent of m, i.e., $\gamma_Q = 1$. Combining this scaling identity with the other three relations we are able to write the set of scaling relations for the mix model:

$$\tau = 2 + \frac{\beta}{1+m\beta}, \qquad (2.40)$$

$$1/\sigma = 1 + m\beta, \qquad (2.41)$$

$$\gamma_P = 1 + (m-1)\beta, \qquad (2.42)$$

$$\gamma_Q = 1. \qquad (2.43)$$

Just as for the explosive model, relation (2.40) agrees with the previous result (2.28).

These scaling relations are verified by the numerical solution's results of the master equations for $m = 2$, shown on Table 2.2. Furthermore, one can notice that the critical exponents characteristic of the distribution in the critical region τ and σ and of the giant cluster size β take intermediate values for the mix model (i.e., between the values for ordinary and explosive models). This apparent trend suggests a monotonous variation of those exponents with the strength of the selection rule's bias towards small clusters. Indeed, it is shown in section 2.5 that this is what happens with increasing m, when the exponents rapidly approach the limits $\beta \downarrow 0$, $\tau \downarrow 2$ and $\sigma \uparrow 1$.

2.3.4 Concluding Remarks

We reduce the explosive percolation problem to a set of infinite-dimensional models, representative of the entire range of this kind of processes. The optimization mechanism's efficiency depends on the parameter $m \geq 1$, i.e., a higher number of random candidate nodes leads to a stronger selection bias towards small clusters. The set of models considered includes the classical random graph, as the particular case with $m = 1$ (on both the explosive and mix models). It can be noticed that the two sets of scaling relations (2.35) to (2.38) and (2.40) to (2.43) become equal for $m = 1$, and are satisfied by the critical exponents of ordinary percolation above the upper critical dimension $d_u = 6$ (Table 2.2). On the other hand, by

letting m diverge in the explosive model, one achieves the extreme case, where at each step both clusters selected to merge have the smallest cluster size present in the system at that time, i.e., the "most explosive" model.

Our method is found to be applicable to both rules variations considered. By examining the evolution equations we were able to find solution (2.21) for the explosive model, and solution (2.27) for the mix version, asserting the continuity of all these transitions for every finite m. Additionally, these solutions provide relations between critical exponents τ and β, which reappear later, independently, in the scaling relations sets of section 2.3.3, thus, backing up the approach used. Those sets allow to express all critical exponents in terms of a single one. Furthermore, the numerically found exponents values shown in Table 2.2, satisfy all such relations, lending further validation to our results.

The differences between the explosive and mix models are merely quantitative. That is shown by the analytical results of this section, and by the numerical solutions of the corresponding master equations (seen in Figure 2.8 and Table 2.2). In the remaining part of this chapter, we abandon the discussion of the mix models, to consider only the explosive models (where both merging clusters are selected using the optimization procedure). By varying the model parameter m, we will be able to cover the entire range of these optimization driven process.

In all our models, the system's dimensionality is infinite, since the process of random occupation of edges takes place in the full graph. As such, each model is surely above its respective upper critical dimension. However, the dependence of the scaling relations upon m, clearly shows that even the mean-field values of the critical exponents depend on the details of the model. Then, it is clear that the critical behavior of these non-equilibrium irreversible processes does not have the usual universal features, in contrast with ordinary percolation.

2.4 Characteristics of the Explosive Percolation Transition

To describe qualitatively the explosive percolation transition, in section 2.2 we reduced the problem to a specific aggregation process and solved numerically 10^6 evolution equations for the cluster size distribution ($s \leq 10^6$). In section 2.3 we have extended the analysis to a generalization of the previous process, which showed that the characteristics of the transition depend on the specific model. Unlike equilibrium phase transitions, the critical properties of explosive percolation do not exhibit universality.

Here we demonstrate how to find characteristics of the explosive percolation transition, even with higher precision, by implementing a more simple method, which does not requires solving a so large array of evolution equations. We develop an efficient method to find the characteristics of a set of explosive percolation models. For each of the models, with high precision, we obtain critical exponents and amplitudes, and the critical point. The description of this method, accompanied by the corresponding results, may also be found in reference [3].

2.4.1 The Method

At the critical point, the cluster size distribution $P(s, t_c)$ has power-law asymptotics. We can solve numerically a finite number of master equations (2.15), say $s_{\max}$, using the sampling rule (2.16). This provides us with $P(s, t)$ for $s \leq s_{\max}$ and any time t. If we knew the value of the critical point t_c, we would readily obtain the exponent τ and the critical amplitude $f(0)$ by sewing together the distribution $P(s \leq s_{\max}, t_c)$ obtained by numerical solution of

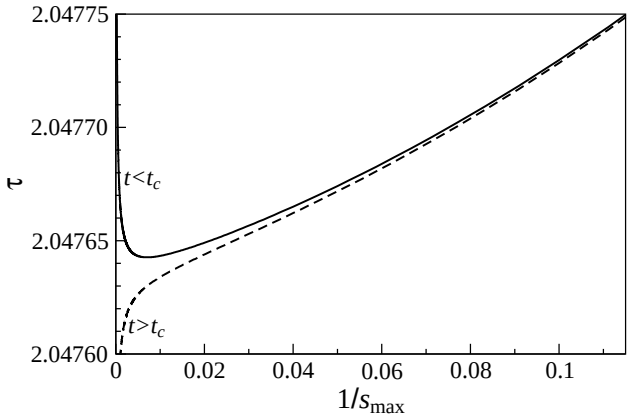

Figure 2.9: Variation of the calculated τ with $1/s_{\max}$, where $s_{\max}$ denotes the maximum cluster size taken into account in the evolution equations, for model $m = 2$. In our calculations, $s_{\max}$ takes a large set of values from 2 to 10^5 The solid and dashed curves correspond to two values of t, namely, $t < t_c$ and $t > t_c$, respectively.

---

the evolution equations and the power-law asymptotics $P(s \geq s_{\max}, t_c) = f(0)s^{1-\tau}$. For that, we should use two conditions: (i) $P(s_{\max}, t_c) = f(0)s_{\max}^{1-\tau}$ and (ii) normalization, namely, $\sum_{s=1}^{\infty} P(s, t_c) = 1$.

The normalization condition can be written to take into account the two parts separately:

$$1 = \sum_{s<s_{\max}} P(s, t_c) + f(0) \sum_{s \geq s_{\max}} s^{1-\tau}.$$

We would like to have an expression with a single unknown variable, which could then be easily calculated. To find such an expression, we now substitute $f(0)$ given by condition (i) in last equation,

$$\begin{aligned} 1 &= \sum_{s\ <s_{\min}} P(s, t_c) + P(s_{\max}, t_c) s_{\max}^{\tau-1} \sum_{s \geq s_{\max}} s^{1-\tau}, \\ &= \sum_{s\ <s_{\min}} P(s, t_c) + P(s_{\max}, t_c) s_{\max}^{\tau-1} \left(\zeta(1-\tau) - \sum_{s<s_{\max}} s^{1-\tau} \right). \end{aligned} \tag{2.44}$$

where $\zeta(x) = \sum_{s=1}^{\infty} s^{-x}$ is the Riemann zeta function. The first sum on the right-hand side of this expression is given by the numerical solution of $s_{\max}$ evolution equations, as well as the multiplicand $P(s_{\max}, t_c)$ of the second term. Therefore, since everything else is known in equation (2.44), we could now solve this equation for the unknown τ. The result would be precise in the limit $s_{\max} \to \infty$.

Although the value of t_c is not known in advance, we can formally perform this procedure at some t, not necessarily equal to t_c. In other words, there is no impediment to the application of last expression to the numerical results for $P(s \leq s_{\max}, t)$ at any t:

$$1 = \sum_{s\ <s_{\min}} P(s, t) + P(s_{\max}, t) s_{\max}^{\tau-1} \left(\zeta(1-\tau) - \sum_{s<s_{\max}} s^{1-\tau} \right). \tag{2.45}$$

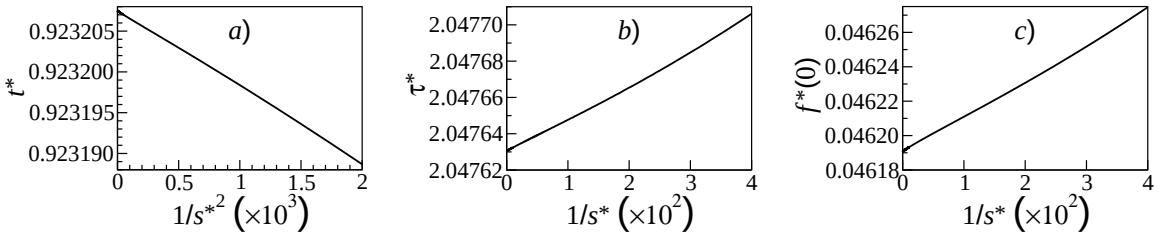

Figure 2.10: Plot of (a) t^*, (b) τ^*, and (c) $f^*(0)$ corresponding to the minima $1/s^*$ of the $\tau(1/s_{\max})$ curves for $t < t_c$, as the one seen in Figure 2.9, in the case of $m = 2$. The precise values of t_c, τ, and $f(0)$, lay at the intersection of these curves with the axis $1/s^* = 0$.

Of course, the correct τ is given by the last equation only for $t = t_c$ (when $s_{\max} \to \infty$). However, we can still use it to find the set of points $\tau(s_{\max})$ corresponding to some time $t \neq t_c$.

The results obtained at two values of t, below and above t_c, are shown in Figure 2.9 for the case of $m = 2$. There, the solid curve shows $\tau(s_{\max})$ at some $t < t_c$ (normal phase), and the dashed curve shows $\tau(s_{\max})$ at some $t > t_c$, which corresponds to a phase with a giant component. The plot shows how the value of the exponent τ, found by using the sewing procedure (equation (2.45)), varies with the inverse maximum cluster size $1/s_{\max}$ taken into account in the equations. With diminishing $1/s_{\max}$, these curves approach infinity and 2 if t is below and above t_c, respectively.

Here, an infinite exponent τ corresponds to a rapidly decreasing cluster size distribution in the normal phase ($t < t_c$). As seen above, except at the critical point, for large enough s, the distribution $P(s,t)$ decays in a exponential-like fashion. The sewing together of such distribution with a power law, leads to an exponent τ reproducing that rapid decay, i.e., for $t < t_c$ the condition (2.45) gives $\tau \to \infty$ when $s_{\max} \to \infty$. On the other hand, the behavior $\tau(s_{\max}) \to 2$, when $s_{\max} \to \infty$, indicates the failure of the normalization condition used in the construction of expression (2.45); $\sum_{s=1}^{\infty} P(s,t) = 1$, which is no longer valid in the phase with a giant component. There, $1 - \sum_{s=1}^{s_{\max}} P(s,t) \to S(t)$ when $s_{\max} \to \infty$. Consequently, the attempt to find an exponent τ, such that $P(s_{\max},t) s_{\max}^{\tau-1} \sum_{s=s_{\max}}^{\infty} s^{1-\tau} = S(t)$, when $s_{\max} \to \infty$, leads $\tau \to 2$ (notice that, for normalization reasons, an exponent $\tau \leq 2$ is impossible).

If we guess t_c properly, the curve would lead to the precise τ as $1/s_{\max} \to 0$. Otherwise, the curves run away from that point, which is precisely the behavior demonstrated by the solid and dashed curves in Fig. 2.9. To find the precise values of t_c, τ, and $f(0)$ we analyzed how the point of the minimum, $1/s^*$, of the solid curve $\tau(1/s_{\max})$ in Fig. 2.9 relates to the values t^*, τ^*, and $f^*(0) \equiv P(s^*,t^*) s^{*\tau-1}$, corresponding to this minimum. Figure 2.10 demonstrates that t^* approaches t_c practically linearly with $1/s^{*2}$, and τ^* and $f(0)^*$ approach τ and, respectively, $f(0)$ practically linearly with $1/s^*$. This enables us to make extrapolations to $s^* \to \infty$ (the maximum $s_{\max}$, that is the maximum number of equations which we used was here 10^5) and find t_c, τ, and $f(0)$ with very high precision.

In principle, one can even avoid extrapolation procedure, which may occur difficult at $m = 4$ and higher. The difficulty is that the curves $\tau(1/s_{\max})$ oscillate (see Fig. 2.11), because the distribution $P(s,t)$ oscillates in the range of low s. The reason for these oscillations is

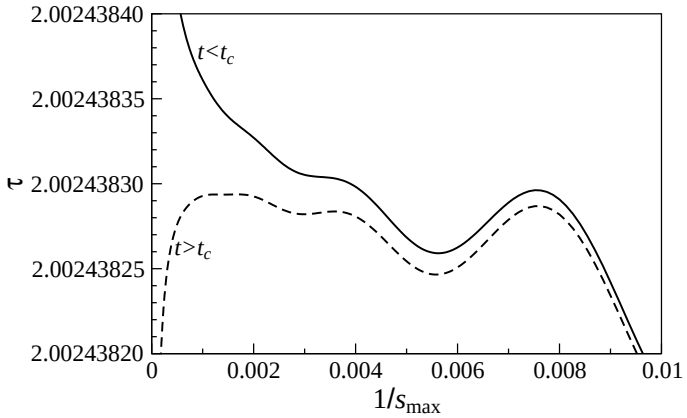

Figure 2.11: Variation of the calculated τ with $1/s_{\max}$ in the case of $m = 4$. The solid and dashed curves correspond to two values of t, namely, $t > t_c$ and $t < t_c$, respectively.

the following. If m tends to infinity, then according to our rules, two smallest clusters in the system should merge at each step. Which is why first single nodes merge into the clusters of size 2, then these clusters merge into the clusters of 4 nodes, and so on. This results in the peaks of the distribution at $s = 2, 4, 8, \ldots$, which are seen already at $m = 4$. In turn, these peaks lead to the oscillations in Fig. 2.11. Fortunately, the amplitude of these oscillations decreases with decreasing $1/s_{\max}$. So one can easily study the run away of the curves from the precise value of τ at small $1/s_{\max}$ and find t_c, with high precision, by adjusting t in such a way that the run away occurs at the smallest value of $1/s_{\max}$. Precise values for τ and $f(0)$ are then obtained by using condition (2.44).

2.4.2 Characteristics of the Transition

The results of the application of this method to the models with $m = 2$, 3, and 4 are shown in Table 2.3. For comparison, in the first column of the table, we show the exact values for the normal percolation problem ($m = 1$). The values of the exponent β are found from τ by using the relation (2.35). In the case of $m = 2$, the values presented in the table agree with our results of section 2.2, although the precision of the numbers obtained with this method is much higher (compare with Table 2.1). It should be noticed that in section 2.2 we solved 10^6 evolution equations, while here, higher precision results are obtained using only the first 10^5 equations (2.15). Furthermore, the results in the table for the models with $2 \leq m \leq 4$ agree with those obtained from equations for scaling functions (we will consider this alternative method in the next section).

The table shows that as expected, when m increases, the difference $1 - t_c$ diminishes, and the exponent β of the giant component size also decreases. Note that the critical amplitude $f(0)$ is close to $P(1, t_c)$, especially when $m \leq 3$. This closeness indicates that the deviations from a power-law asymptotics in these problems are small even at low s. Interestingly, $f(0) > P(1, t_c)$ for classical percolation, while the opposite is true for the explosive percolation transition.

The values of β are remarkably small. In particular, in the case of $m = 4$, β is close to $1/400$. While simulating these systems, the smallest step in t corresponds to the addition of a single link and equals $1/N$, that is the inverse size of a system. Let m be 4. Then the minimum jump at t_c, which one can observe simulating even an unrealistically large system of

m	1	2	3	4
t_c	1/2	0.923207509297(2)	0.9817953173509(2)	0.99497356260563(2)
β	1	0.05557108(1)	0.010428725(1)	0.0024806708
τ	5/2	2.04763045(1)	2.009911883(1)	2.0024383299(1)
$f(0)$	$1/\sqrt{2\pi}\approx 0.3989$	0.04619071(1)	0.009831398(1)	0.0024320386(1)
$P(1,t_c)$	$1/e\approx 0.3678$	0.0485928295546(4)	0.01172146480245(2)	0.003343067143133(1)

Table 2.3: Characteristics of the ordinary percolation ($m = 1$) and explosive percolation ($m = 2, 3, 4$) transitions. These high precision results were obtained by the method developed in this section, using the numerical solutions of 10^5 evolution equations (2.15), for each $m = 2, 3, 4$.

10^{400} nodes, is of the order of $(10^{-400})^{1/400} = 10^{-1}$, which makes observation of a continuous transition in simulations impossible. This suggests that finite size effects in this situation hardly can be investigated. As we noted above, even in the case of $m = 2$, in which β is close to 1/18, simulating a system of 10^{18}, one cannot observe a jump smaller than of the order of 10^{-1} at the critical point.

2.4.3 Concluding Remarks

We have proposed an effective numerical method enabling us to find basic characteristics of explosive percolation transitions with high precision. We obtained the critical points, and the critical exponents and critical amplitudes of scaling functions of these transitions in a set of representative models of explosive percolation. Our results support the conclusion of sections 2.2 and 2.3, that explosive percolation transitions are continuous, namely, the assumption of a critical power-law cluster size distribution. This kind of asymptotic behavior is observed for all the models ($m = 2, 3, 4$).

Our approach provides a useful tool for a quantitative description of a new class of critical phenomena in non-equilibrium systems and irreversible processes. Due to the absence of universality, the critical exponents of these transitions depend on the specific model. Moreover, the applicability of this method may not be limited to explosive percolation models. We notice that, since it relies only on generic scaling properties, this method may be suitable to other continuous transitions characterized by critical asymptotically power-law distributions.

2.5 Solution of the Explosive Percolation Quest

In our works [1, 2], presented in sections 2.2 and 2.3, we have already established that, contrarily to the initial belief, the explosive percolation transition is actually continuous. We obtained this result by analyzing evolution equations for this process in the infinite system size limit. Thanks to the smallness of the critical exponent β, the continuous transition looks so "sharp" that it is virtually impossible to distinguish it from a discontinuous one in computer experiments even for very large systems [113]. Posteriorly, the fact that this transition is continuous was also proven mathematically [111]. Nonetheless, in the physics sense, the quest of the explosive percolation transition actually has not been yet resolved.

The main problem here is actually not the continuity or discontinuity of the transition (in principle, the continuity readily follows from the observed power law at the critical point

and scaling above and below the transition), but rather how to explain its surprising unique features which just led to the original confusion. In general, for a theoretical physicist, the complete description and understanding of a continuous phase transition comprises the following issues: (i) indicating the order parameter and the generalized susceptibility for this transition, (ii) finding the full set of relations between critical exponents, (iii) obtaining the scaling functions and critical exponents entering these relations, and (iv) finding the upper critical dimension d_u for this transition (that is, the dimension, above which, $d > d_u$, mean-field theories are valid; e.g., for ordinary percolation $d_u = 6$, as seen section 1.4.3). In the present work we fulfill this program for infinite systems above the upper critical dimension, and present an exact solution of the explosive percolation transition problem in the evolution of processes driven by Metropolis-like algorithms.

Our results from sections 2.3 and 2.4 show that these phase transitions display non-universal critical behavior, so we have to strictly specify models. We continue to consider the set of representative models introduced in the beginning of section 2.3.1 (depicted in Figure 2.6), which allows an elegant description and covers the entire range of processes of this type. Importantly, we show that the order parameter and susceptibility for phase transitions in these models differ from those for ordinary percolation. Namely, the order parameter here is not the relative size of the percolation cluster, and the susceptibility is not the average size of a finite cluster to which a uniformly randomly chosen node belongs. This already indicates a radical difference from ordinary percolation.

Our approach to the problem is strict. First we assume that the transition is continuous, and then from an infinite set of evolution equations for the infinite systems we derive a single scaling-function equation for each model. This is a nonlinear integral-differential eigenfunction equation whose eigenfunction is a scaling function for the corresponding model and the eigenvalue is one of the critical exponents. We develop a straightforward procedure enabling us to finally obtain the solution of this equation for each model with any desired precision. This shows that our assumption was correct, and the transition is indeed continuous, as already concluded by our previous work. However, here, the conclusion is attained using an alternative method, based on the scaling features near the critical point, while above we have only assumed that the size distribution is asymptotically power-law at the critical point.

In physics terms, finding results with any desired precision just means an exact (though not explicit) solution of a problem, similarly, say, to the solution of a one-dimensional Schrodinger equation with an arbitrary potential. The scaling functions and critical exponents found in this way differ sharply from those for ordinary percolation. We show that these results explain the nature of the transition and, also, the confusing observations in computer experiments.

2.5.1 Susceptibility and Order Parameter

For ordinary percolation, the average size of a finite cluster to which a uniformly randomly chosen node belongs, $\langle s \rangle_P$, and the relative size of the percolation cluster (i.e., the probability that a uniformly randomly chosen node is in the percolation cluster), S, play the role of susceptibility and the order parameter, respectively. So for ordinary percolation, the exponents γ_P and β are the critical exponents of susceptibility and the order parameter. Let us show that susceptibility and the order parameter for explosive percolation have a quite different meaning.

Susceptibility in cooperative models of statistical mechanics is expressed in terms of the average value of the pairwise spin-spin correlator, where averaging is over all pairs of spins

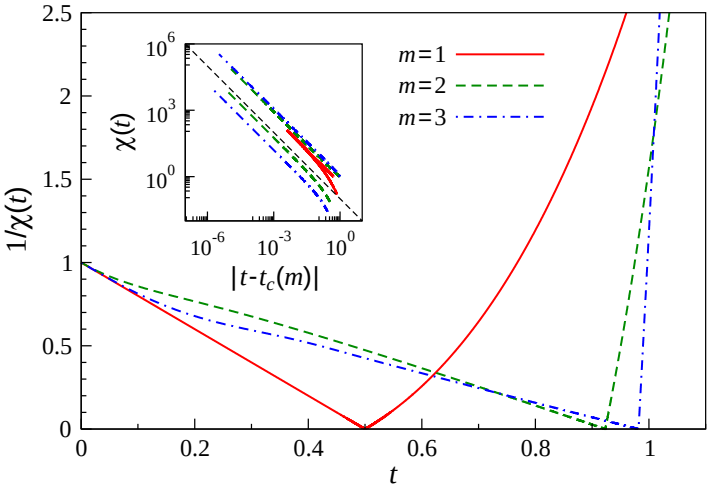

Figure 2.12: True susceptivity of explosive percolation models, as defined by equation (2.47), calculated from the numerical solution of 10^5 evolution equations (2.15) for $m = 1, 2, 3$. On the main plot, the inverse of χ goes to zero at the critical time t_c of each model. The inset shows the two curves (above and below t_c) for each model, plotted in a logarithmic scale as a function of $|t - t_c|$. This produces straight lines, in the region $|t - t_c| \to 0$, with the same slope as the black dashed line, i.e., -1. Which demonstrates that the true susceptibility χ is characterized by a critical exponent -1 in all these models.

---

of a system. For example, on ferromagnetic systems this is given by relation (1.17), where the average spin-spin correlator is $\int_V dr' \int_V dr \, \langle m(r)m(r')\rangle / V^2$. For percolation problems the average correlator is probability p_2, that two nodes chosen using the rules of the corresponding model belong to the same cluster, i.e. the new connection falls within one cluster. This probability provides both the susceptibility χ and order parameter M of the system:

$$p_2 = \chi/N + M^2,$$

where the second summand is the probability that both nodes belong to the percolation cluster. Last expression is the corresponding of equation (1.17) for percolation.

For our models of explosive percolation, the probability that two nodes, selected by using the algorithm from section 2.3.1 (Figure 2.6), belong to the same cluster is

$$p_2 = \sum_s \frac{sQ^2(s)}{P(s)N} + S^{2m}. \tag{2.46}$$

Here the first term on the right-hand side is the probability that two selected nodes belong to the same finite cluster, while the second term is the probability that two selected nodes belong to the giant connected component. The probability that two selected nodes belong to the same finite cluster of size s, is equal to the probability that one of the nodes is in a cluster of size s, $Q(s)$, multiplied by the probability that the other node is in the same cluster, $sQ(s)/(P(s)N)$, which is just $Q(s)$ divided by the number of clusters of size s, $P(s)N/s$.

The first term on the right-hand side of expression (2.46) gives the susceptibility, χ, for the explosive percolation model (divided by N), the second term gives the square of the order

parameter M. In other words, for these transitions

$$\chi \equiv \sum_s \frac{sQ^2(s)}{P(s)} \tag{2.47}$$

and

$$M \equiv S^m, \tag{2.48}$$

that is, the order parameter in these models is S^m and not S as is usually believed. In particular at $m = 1$, equation (2.46) is reduced to the well-known relation $p_2 = \langle s \rangle_P / N + S^2$ for ordinary percolation. Moreover, substituting the scaling forms of the distributions $P(s,t)$ and $Q(s,t)$ near the critical point, equations (2.30) and (2.31), respectively, into equation (2.47), we immediately find that $\chi \sim |\delta|^{-\gamma}$, where the critical exponent of susceptibility is $\gamma = 1$, see Figure 2.12. This is actually the Curie-Weiss law which must be valid for the critical singularity of susceptibility in cooperative systems above an upper critical dimension, where mean-field theories work.

2.5.2 Hyper-scaling

The set of scaling relations in section 2.3.3 between critical exponents for the cluster size distribution, τ and σ, exponents of the critical singularities of the distributions first moments, γ_P and γ_Q, and the exponent for the size of the giant component β (equations (2.35) to (2.38)), was derived for the infinite-dimensional models under consideration in this work (thanks to equation (2.34)). However, these processes can easily be generalized and formulated for systems of arbitrary dimensionality d.

This generalization leads to another set of relations between critical exponents, containing the system's dimension d, the fractal dimension d_f of clusters at the critical point, the correlation length critical exponent ν, and the exponent of the critical correlations η (known as Fisher exponent). These relations, often called hyper-scaling relations, where derived in section 1.4.3 for ordinary percolation (equations (1.51), (1.52) and (1.55)).

For explosive percolation in d-dimensional models one can easily derive the hyper-scaling relations for d below the upper critical dimension d_u in the same way as for ordinary percolation. In fact, relations (1.51) and (1.52) are independent of the underlying process, and relate exponents using only geometrical arguments. Let us rewrite them here:

$$d_f = \frac{1}{\sigma\nu}, \tag{2.49}$$

$$d_f = d - \frac{\beta}{\nu}. \tag{2.50}$$

On the other hand, equation (1.55) relates the critical exponent of the correlation function with the size of the percolation component. In the previous section, we have shown that the correlations should be regarded as the probability that two nodes selected by the model's rules belong in the same cluster. Then, the corresponding hyper-scaling relation for explosive percolation is:

$$d - 2 + \eta = \frac{2\beta_{\text{order parameter}}}{\nu}, \tag{2.51}$$

where the order parameter critical exponent $\beta_{\text{order parameter}} = m\beta$, as we show in last section. These three hyper-scaling relations will hold at $d < d_u$.

To obtain the hyper-scaling relations above the upper critical dimension, one should set in relations (2.49) to (2.51) the exponents ν and η to their mean-field values, 1/2 and 0, respectively, and d to d_u [117] (as is done in section 1.4.3). The resulting relations lead to the following expressions for the fractal and upper critical dimensions, d_f and d_u, in terms of the exponent β:

$$d_f = 2\left[1 + (2m-1)\beta\right], \tag{2.52}$$

$$d_u = 2 + 4m\beta. \tag{2.53}$$

To find these dimensions we need only two of the three hyper-scaling relations (2.49)–(2.51). Indeed, the third relation allows us to check the self-consistency of our argumentation. In particular, the proper definition of the pairwise correlator for these models, which was discussed in last section, and is implicit in equation (2.51).

The upper critical dimension d_u also describes the finite size effect for a continuous phase transition in systems above d_u, namely,

$$t_c(\infty) - t_c(N) \propto N^{-2/d_u},$$

see reference [117]. Here $t_c(\infty)$ is the critical point value in the infinite system (in which the transition is well defined) and $t_c(N)$ is, in particular, the position of the maximum of the susceptibility for the system of N nodes. One can see in Table 2.3 that, for $m \geq 2$, β is small and falls rapidly to zero. Thus, in these models $d_u \approx 2$ is considerably smaller than for ordinary percolation (where $d_u = 6$), and the last difference vanishes nearly as N^{-1} (much faster than for $m = 1$, where $t_c(\infty) - t_c(N) \propto N^{-1/3}$). A visible effect of this attribute is the unusually high precision of the estimates obtained for the critical point and exponents, made from the numerical solution of 10^6 master equations (2.2), for $m = 2$, seen in Table 2.1. (Those results were obtained before the application of the method developed in section 2.4.) As discussed in section 2.4.1, if $t_c(\infty)$ of the continuous phase transition is known with high precision, then we can also calculate critical exponents with high precision.

2.5.3 Equations for Scaling Functions

In our previous works [1, 2], presented in sections 2.2 and 2.3, we have shown that if it is known that the distribution $P(s)$ at the critical point is, asymptotically, power-law with some given critical exponent and amplitude, $P(s, t_c) \cong f(0)s^{1-\tau}$ (as it should be for a continuous percolation transitions), then from equation (2.15) immediately follows the power law $S \cong B\delta^{\beta}$, where $\delta = |t - t_c|$, $\beta = (\tau - 2)/\left[1 - (2m-1)(\tau - 2)\right]$ from relation (2.22) and the coefficient B is expressed in terms of $f(0)$ and τ by relation (2.23). (Here the critical amplitude $f(0)$ is determined by the initial form of the distribution $P(s, t = 0)$, the role of initial conditions is discussed in section 2.5.5 .)

Furthermore, this assumption allows us to find the scaling functions $f(x)$ and $g(x)$ on the upper side of the phase transition, i.e., at $t > t_c$. The form of these functions turn out to be close to exponential, similarly to ordinary percolation above an upper critical dimension. This derivation exploits the convenient simplification of the equations above the critical point, where S differs from zero. In this region, at large s, equation (2.16) is reduced asymptotically to $Q(s) \cong mS^{m-1}P(s)$, and the master equation (2.15) becomes:

$$\frac{\partial P(s,t)}{\partial t} \cong sm^2 S^{2(m-1)}(t) \sum_{u=1}^{s-1} P(u,t)P(s-u,t) - 2smS^{m-1}(t)P(s,t), \tag{2.54}$$

which is similar to that for ordinary percolation (equation (1.57)). The only difference is the appearance of the size of the giant component on the right-hand side of last equation, as a factor in both terms. Nevertheless, in the critical region, the giant component's growth, $S(t) = B\delta^{\beta}$, is completely defined by the critical power-law form of the distribution, with β and B determined by τ and $f(0)$ according to expressions (2.22) and (2.23). Therefore, equation (2.54) is easily solvable with the initial condition $P(s, t_c) \cong f(0)s^{1-\tau}$.

Consequently, our present more difficult task is to find the distribution at the critical point, which we just used in that derivation, its critical exponent (if this distribution will appear to be power-law), and the scaling functions on the normal phase side of the phase transition, i.e. at $t < t_c$. So, simultaneously we verify that the transition is continuous.

First we derive equations for scaling functions (approaching the critical point from the normal-phase side) using equations (2.15) and (2.16). For large s, also in this region, equation (2.16) gets simplified. However, since now there is not a percolation component,

$$Q(s) \cong mP(s) \left(\int_s^{\infty} du\, P(u) \right)^{m-1}, \tag{2.55}$$

from which the relation between scaling functions $f(x)$ and $g(x)$, in the phase $t < t_c$, readily follows. Actually, for the sake of convenience, let us define another pair of scaling functions $\tilde{f}(x)$ and $\tilde{g}(x)$:

$$P(s,t) = s^{1-\tau} f(s\delta^{1/\sigma}) = \delta^{(\tau-1)/\sigma} \tilde{f}(s\delta^{1/\sigma}), \tag{2.56}$$

and

$$Q(s,t) = s^{-1-m(\tau-2)} g(s\delta^{1/\sigma}) = \delta^{[1+m(\tau-2)]/\sigma} \tilde{g}(s\delta^{1/\sigma}), \tag{2.57}$$

where $\tilde{f}(x) \equiv x^{1-\tau} f(x)$ and $\tilde{g}(x) \equiv x^{-1-m(\tau-2)} g(x)$ (the resulting equations will take a more compact form when written in terms of $\tilde{f}(x)$ and $\tilde{g}(x)$).

The direct substitution of these scaling forms into the evolution equation (2.15) is impossible, since these forms are valid at large s, while the contribution from the region of small s to the sum in equation (2.15) is nonzero (actually divergent). Let us rewrite Eq. (2.15) to eliminate this contribution from the sum, and so to remove the non-scaling, low s, parts of the distribution from consideration. We substitute $Q(u) = Q(s) + [Q(u) - Q(s)]$ into the evolution equation, which leads to the following (where, for simplicity, the t dependence of the distributions is omitted):

$$\frac{\partial P(s)}{\partial t} = -s(s-1)Q^2(s) + 2sQ(s) \left[1 - \sum_{u=s}^{\infty} Q(u) \right]$$

$$+s \sum_{u=1}^{s-1} [Q(u) - Q(s)] [Q(s-u) - Q(s)] - 2sQ(s), \tag{2.58}$$

in which we now can safely substitute the sums with the integrals. The resulting equation is

$$\frac{\partial P(s)}{\partial t} \cong -s^2 Q^2(s) - 2sQ(s) \int_s^{\infty} du\, Q(u)$$

$$+s \int_0^s du\, [Q(u) - Q(s)] [Q(s-u) - Q(s)]. \tag{2.59}$$

Substituting the scaling form of the distributions into equations (2.59) and (2.55) we arrive at the following equations for the scaling functions:

$$
\begin{aligned}
&-\frac{\tau-1}{\sigma}\tilde{f}(x)-\frac{1}{\sigma}x\tilde{f}'(x)\\
&=-x^2\tilde{g}^2(x)-2x\tilde{g}(x)\int_x^\infty dy\,\tilde{g}(y)\\
&+x\int_0^x dy\,\left[\tilde{g}(y)-\tilde{g}(x)\right]\left[\tilde{g}(x-y)-\tilde{g}(x)\right] \qquad (2.60)\\
&\tilde{g}(x)=m\tilde{f}(x)\left(\int_x^\infty dy\,\tilde{f}(y)\right)^{m-1}, \qquad (2.61)
\end{aligned}
$$

where $\sigma=1-(2m-1)(\tau-2)=1/[1+(2m-1)\beta]$.

Equation (2.60), with $\tilde{g}(x)$ substituted from equation (2.61) can be treated as a nonlinear integral differential eigenfunction equation for the scaling function $\tilde{f}(x)$, in which a critical exponent, say τ, plays the role of eigenvalue. Note that equations (2.60) and (2.61) inconveniently contain integrals with integration over different intervals, (x,∞) and $(0,x)$. To avoid this inconvenience, we must exclude the integrals over the interval (x,∞). For that, in both equations (2.60) and (2.61) we separate the integrals over (x,∞) then take the derivatives of the both sides of each of resulting equations. The derivation removes the integrals $\int_x^\infty$, but, unfortunately, produces new divergencies within the remaining integrals $\int_0^x$. To avoid these divergencies, it turns out to be sufficient to pass from the integral over the interval $(0,x)$ to integration over $(0,x/2)$ in equation (2.60), namely $\int_0^x dy\,[\tilde{g}(y)-\tilde{g}(x)][\tilde{g}(x-y)-\tilde{g}(x)]=2\int_0^{x/2}dy\,[\tilde{g}(y)-\tilde{g}(x)][\tilde{g}(x-y)-\tilde{g}(x)]$. The resulting system of two equations contains $\tilde{f}''(x)$, $\tilde{f}'(x)$, $\tilde{f}(x)$, $\tilde{g}'(x)$, and $\tilde{g}(x)$. Introducing $\tilde{u}(x)=\tilde{f}'(x)$, we obtain the system of three first order equations for $\tilde{f}(x)$, $\tilde{f}(x)$, and $\tilde{u}(x)$:

$$
\begin{aligned}
&\tilde{f}''(x)=\tilde{u}'(x)=\frac{\tau-1}{x}\left[\frac{\tilde{f}(x)}{x}-\tilde{f}'(x)\right]\\
&+\frac{\tilde{g}'(x)}{\tilde{g}(x)}\left[\frac{(\tau-1)\tilde{f}(x)}{x}+\tilde{f}'(x)\right]-\sigma\tilde{g}^2(x/2)\\
&+\frac{2\sigma}{\tilde{g}(x)}\int_0^{x/2}dy\,\tilde{g}(y)\left[\tilde{g}'(x)\tilde{g}(x-y)-\tilde{g}(x)\tilde{g}'(x-y)\right]\\
&\tilde{g}'(x)=\frac{\tilde{f}'(x)\tilde{g}(x)}{\tilde{f}(x)}-m(m-1)\tilde{f}^2(x)\left(\frac{\tilde{g}(x)}{m\tilde{f}(x)}\right)^{(m-2)/(m-1)}\\
&\tilde{f}'(x)=\tilde{u}(x), \qquad (2.62)
\end{aligned}
$$

where the exponent $\sigma=1-(2m-1)(\tau-2)=1/[1+(2m-1)\beta]$.

One can verify that at small x, the solution of this system has the following expansion:

$$
\begin{aligned}
f(x)&=x^{\tau-1}\tilde{f}(x)=f(0)+a_1x^\sigma+a_2x^{2\sigma}+\ldots,\\
g(x)&=x^{1+m(\tau-2)}\tilde{g}(x)=g(0)+b_1x^\sigma+b_2x^{2\sigma}+\ldots, \qquad (2.63)
\end{aligned}
$$

where $f(0)$ and $g(0)$ are the critical amplitudes of the distributions, $P(s,t_c) \cong f(0)s^{1-\tau}$ and $Q(s,t_c) \cong g(0)s^{-1-m(\tau-2)}$, respectively. One can easily find that $g(0)$ and all other coefficients in these series are expressed in terms of only $f(0)$ and τ. For example, the condition$\sum_{u\geq s} Q(s) = \left(\sum_{u\geq s} P(s)\right)^m$ gives the relation

$$\int_x^\infty dy\, y^{-1-m(\tau-2)} g(y) = \left(\int_x^\infty dy\, y^{1-\tau} f(y)\right)^m, \tag{2.64}$$

from which we immediately obtain

$$g(0) = \frac{m}{(\tau-2)^{m-1}} f^m(0). \tag{2.65}$$

Similarly, we obtain the next coefficients,

$$a_1 = \frac{2f(0)^2 \pi \csc[-m\pi(\tau-2)]\Gamma[1-m\,(\tau-2)]}{\Gamma[1+m\,(\tau-2)]\Gamma[1-2m(\tau-2)]},$$

$$b_1 = g(0)a_1 \left(\frac{1}{f(0)} + \frac{(m-1)\left(\frac{g(0)}{f(0)m}\right)^{1/(1-m)}}{2m(\tau-2)-1} \right),$$

$$a_2 = \frac{a_1 b_1}{2g(0)} + \frac{g(0)b_1 \pi \csc\left[-m\pi(\tau-2)\right]}{\Gamma[1+m(\tau-2)]} \left(\frac{4^{m(\tau-2)}\sqrt{\pi}}{\Gamma[1/2-m(\tau-2)]} - \frac{\Gamma[1-(3m-1)(\tau-2)]}{\Gamma[1-(4m-1)(\tau-2)} \right),$$

$$b_2 = \frac{g(0)[(5m-2)(\tau-2)-2]}{f(0)} \left(\frac{a_1^2(m-1)(\tau-2)}{2f(0)[1-2m(\tau-2)]^2} - \frac{a_2}{\tau-4m(\tau-2)} \right), \tag{2.66}$$

and so on, by substituting the expansions (2.63) into equations (2.60) and (2.64) and comparing the powers of x^σ (where $\Gamma(x)$ is the Gamma function). If we know $f(0)$ and τ, these Taylor series provide the solutions $f(x)$ and $g(x)$ only at sufficiently small x (below the maxima of the scaling functions).

The critical amplitude $f(0)$, as well as the detailed shapes of the scaling functions, is determined by the initial distribution of cluster sizes, $P(s,t=0)$. In contrast to that, the critical exponent values do not depend on initial conditions, if $P(s,t=0)$ decays sufficiently rapidly (see below). So, when searching for the solution of the equation, we can set any convenient value of the critical amplitude $f(0)$. For different values of $f(0)$, the resulting value of the critical exponent τ should be the same, and the scaling functions, while differing from each other, should be qualitatively similar.

For a given critical amplitude $f(0)$, the system (2.62) of first order differential equations can be directly solved numerically. This solution should give the exponent τ together with the scaling functions $f(x)$ and $g(x)$. The unknown critical exponent τ is obtained from the condition that $f(x)$ and $g(x)$ decay rapidly to zero as x approaches infinity. We use the following procedure. For the sake of convenience, set the value of the critical amplitude $f(0)$ such that the maxima $f(x)$ and $g(x)$ are of the order of 1 (with this choice, the numerical solution takes the minimum time). First try some reasonable value of τ. With this pair, $f(0)$ and τ, using truncated series (2.63) with coefficients (2.65), (2.66), and so on as initial

conditions at some small x_0, find the numerical solution of the system of the first order equations (2.62) up to sufficiently large x at which the asymptotic behaviors of the solutions are already clear. Since the value of τ, which we used in this first attempt, of course deviates from the correct one, the obtained solutions will not show a proper rapid decay to zero. Instead, they may decay more slowly than exponentially or even become negative, oscillate, and so on. Then solve the equations numerically with a different value of τ, and repeat this procedure again and again, adjusting progressively the value of τ in such a way that the solutions $f(x)$ and $g(x)$ decay to zero more and more rapidly, staying positive (the proper asymptotic behavior in actually known explicitly, see (2.67)). These calculations converge rapidly giving the final value of τ with any desired precision and the scaling functions $f(x)$ and $g(x)$, see Figure 2.13.

Finally, we find the asymptotic behavior of these scaling functions explicitly. Letting $x \to \infty$, and taking the leading terms on each side of equations (2.60) and (2.61), one can easily check they support the following rapidly decaying forms, at large x:

$$\begin{aligned} \tilde{f}(x) &\cong A x^{\lambda} \exp\left[-C x^{1+\ln m/\ln 2}\right], \\ \tilde{g}(x) &\cong \frac{m A^m x^{m\lambda-(m-1)\ln m/\ln 2}}{\left[C\,(1+\ln m/\ln 2)\right]^{m-1}} \exp\left[-mC x^{1+\ln m/\ln 2}\right] \end{aligned} \tag{2.67}$$

where $\lambda = (1+\ln m/\ln 2)(1+1/(4m-2)) - 2m/(2m-1)$. This procedure also supplies us with a relation between constants A and C,

$$A^{2m-1} = \left(\frac{\ln m}{\pi \ln 2}\right)^{1/2} \frac{(1+\ln m/\ln 2)^{2m-1/2} 2^{\lambda+1+\ln m/\ln 2}}{\sigma m^{3/2}} C^{2m-1/2},$$

however, does not fix them. It turns out that, in fact, their values depend on the initial distribution $P(s, t=0)$, more specifically, on $f(0)$ (when we fix $f(0)$ the functions $f(x)$ and $g(x)$ become completely defined by system (2.62)). The position of the critical point t_c itself, also depends on $P(s,0)$. In the preceding, we solved equation (2.15) for clusters of all sizes $s \gg 1$ without searching for the value of t_c, which is not of great interest for us, since it is dependent on initial conditions.

For the particular case of an initial configuration where all nodes are isolated, the values of t_c and $f(0)$ can be obtained with great precision using the method described in section 2.4.1 (results for $m = 2, 3, 4$ are shown in Table 2.3). This precise $f(0)$ can be used as initial condition of tho ordinary differential equations system (2.62), thus finding the detailed shape of the scaling functions for this specific initial configuration. Nevertheless, using the procedure above we can find τ with any precision without knowledge of $f(0)$ or t_c (since the critical exponents are independent of initial conditions), that is, if $P(s,0)$ decays rapidly enough (see section 2.5.5).

2.5.4 Scaling Functions and Exponents

The resulting scaling functions $f(x)$ and $g(x)$ are shown in Figure 2.13, in the particular case of $m = 2$ (for higher m, the scaling functions are qualitatively similar). The plot shows both the scaling functions for the normal phase, $t < t_c$ (the left-hand side) and for the phase with a giant component, $t > t_c$ (the right-hand side). The normal phase side was obtained from the scaling function equations (2.62) in the way described above. The resulting

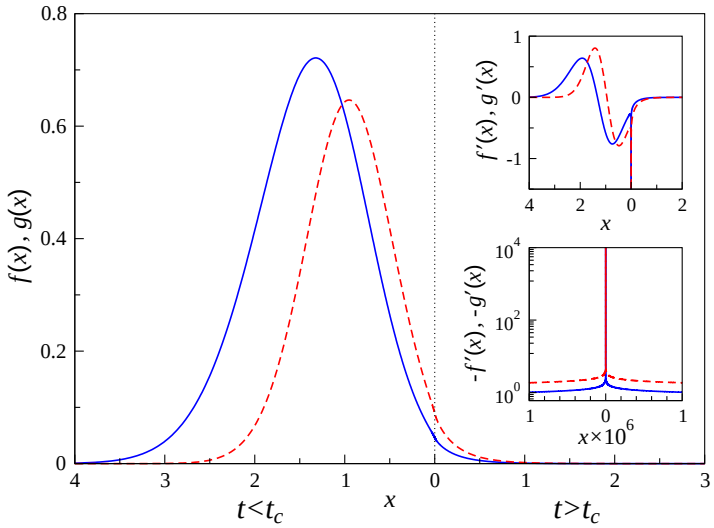

Figure 2.13: Exact scaling functions for $m = 2$. The blue solid line corresponds to scaling function $f(x)$, and the red dashed line to $g(x)$.

---

asymptotics $P(s, t_c) \cong f(0)s^{1-\tau}$ was used as the initial condition for the linearized evolution equations (2.54) in the phase with a giant component. Their solution gave the right-hand side of the plot.

This figure demonstrates a dramatic contrast with the scaling function for ordinary percolation, which is symmetric, namely, both for $t > t_c$ and $t < t_c$. Interestingly, this kind of asymmetry can also be observed at $d < d_u = 6$ dimensions in ordinary percolation [36]. (However, for those equilibrium processes, the asymmetry vanishes for $d > d_u$; see Figure 1.6.) Besides, at low d, the exponent τ of ordinary percolation is also close to 2 (Table 1.1). At $d = 2$ for example, $\tau \simeq 2.139$. In explosive percolation models, the asymmetry of scaling functions persists even in the limit $d \to \infty$.

Insets on Figure 2.13 highlight the behavior of scaling functions near the origin. We find the singularities on $f(x)$ and $g(x)$ at $x = 0$. The top inset shows the derivatives of the curves plotted in the main panel for the same range of x, and the bottom one shows a zoom of the near $x = 0$ region. The derivatives of $f(x)$ and $g(x)$ diverge approaching $x = 0$, from both sides. This singular behavior is correctly predicted by equations (2.63), that were derived for the disordered phase, but, in fact, hold on both sides of the transition. It is clear that $f(0)$ and $g(0)$ should be equal on both phases. Moreover, the series expansion coefficients of the singularities of $f(x)$ and $g(x)$ above t_c, can be found in a similar way that for $t < t_c$, showing that, for the ordered phase, the coefficients $a_1, b_1, a_2, b_2, \ldots$ are simply the inverse of the ones for the disordered phase (i.e, in the percolation phase, $-a_1, -b_1, -a_2, -b_2, \ldots$ are also given expressions (2.66)).

We have solved numerically the exact system of differential equations (2.62), for the scaling functions below the percolation threshold, using expansions (2.63) as initial conditions. With the method developed above we could calculate the value of τ for $m = 2, 3, \ldots, 20$. The ordinary differential equations can be solved with any desired precision, therefore, the corresponding eigenfunction, $\tilde{f}(x)$, and eigenvalue, τ, may be obtained with any precision as well. The scaling functions stay qualitatively similar with increasing $m \geq 2$ (for $m = 2$ they are shown in Figure 2.13). They show a maximum at some $x > 0$ is the region of $t < t_c$,

m	τ
2	2.04763044(2)
3	2.00991188(1)
4	2.002438330(5)
5	2.000625199(1)
6	2.0001601191(4)
7	2.0000404460(1)
8	2.00001006831(5)
9	2.00000247685(5)
10	2.00000060412(2)
11	2.00000014639(1)
12	2.000000035313(5)
13	2.000000008489(2)
14	2.0000000020355(2)
15	2.0000000004870(1)
16	2.00000000011634(4)
17	2.00000000002776(2)
18	2.000000000006617(5)
19	2.000000000001575(2)
20	2.0000000000003746(8)

Table 2.4: Critical exponent τ calculated by our exact method, for each m from 2 to 20.

and decay monotonically in the region of $t > t_c$. The main difference between models is the asymptotic behavior of the functions on the $t < t_c$ phase. For large enough x we find $f(x) \propto \exp\left(-Cx^{1+\ln m/\ln 2}\right)$ and $g(x) \propto \exp\left(-mCx^{1+\ln m/\ln 2}\right)$, where C is some constant (see expressions (2.67)). On the other hand, the value of τ indeed approaches 2 quite rapidly with growing m, as the results of section 2.4 previously suggested. This section's results are summarized in Table 2.4.

The decrease of $\tau - 2$ with m is a very steep one. By plotting the results of Table 2.4 in a semilogarithmic scale we find that the decay of $\tau - 2$ is well described by an exponential law, especially for large m, as is shown by the dashed line in Figure 2.14. It should be emphasized that, as extensively discussed above, in the percolation models under consideration the knowledge of any one of the critical exponents, allows us to immediately calculate all the others, using scaling relations (2.35) to (2.38). Furthermore, it was already clear from the scaling relations that for these irreversible processes, the critical exponents do not take universal values, i.e., depend on the specific details of the model, (particularly, on m). Here, we show how these values actually vary with m.

Such a dependence of critical exponents with a model's parameter (in this case m) is rather unusual. Yet, it is not unprecedented for non-equilibrium phase transitions, even in mean-field models. For instance, this is also the case of the asymmetric reaction-diffusion models considered in [118]. There, when n particles meet, they react with some rate to

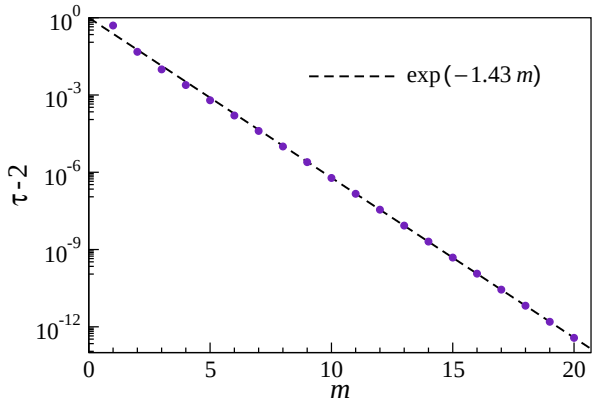

Figure 2.14: Results obtained using our exact method are plotted on a semilogarithmic scale. Each point corresponds to an entry of Table 2.4. The dashed line is obtained by fitting the points to an exponential law. For $m \gg 1$ the critical exponent τ seems to be accurately predicted by the expression $2 + 0.8358e^{-1.4142m}$.

produce new particles, on the other hand, when k particles meet, a fixed number of them are annihilated, with some other rate. If $n < k$, a continuous transition occurs by crossing the threshold separating a phase where the steady state corresponds to a system empty of particles, and another phase where the system remains active in the steady state. The independent parameters here are the rates of reaction and annihilation. Evidently, the order parameter is the density of particles in the steady state, which is characterized by a mean-field critical exponent $\beta = 1/(k-n)$. Notice that, when the difference $k-n$ is increased this exponent diminishes, and approaches the limiting value 0, just as for the explosive percolation models, when m increases. Moreover, similarly to explosive percolation, the upper critical dimension for this non-equilibrium class of reaction-diffusion models was found to be very small $d_u \leq 2$ [119].

2.5.5 Initial Conditions and the Critical Time t_c

If the initial size distribution of clusters decays sufficiently slowly, the transition takes place at the initial moment. Let us assume that $P(s, t=0) \sim s^{1-\tau_0}$, where the exponent τ_0 defines the initial condition. This distribution results in a divergent susceptibility if, according to equation (2.46),

$$\int_{\text{const}}^{\infty} ds\, (s^{(2m-1)-m\tau_0})^2 / s^{-\tau_0} = \infty,$$

that is if

$$\tau_0 \leq 2 + 1/(2m-1). \tag{2.68}$$

The divergent susceptibility indicates the presence of the continuous transition exactly at the point of divergence. So, if condition (2.68) is satisfied, then the transition occurs at the initial instant, and $t_c = 0$. In this case, we have $\tau = \tau_0$, and all other exponents can be found from the scaling relations (2.35) to (2.38), using the known τ. For example,

$$\beta = \frac{\tau_0 - 2}{1 - (2m-1)(\tau_0 - 2)}. \tag{2.69}$$

On the other hand, if $\tau_0 > 2 + 1/(2m-1)$, then we we arrive at the situation described in the previous section, namely, $t_c > 0$, (t_c depends on τ_0) and the critical exponent values (independent of τ_0) presented in Table 2.4.

Our theory provides the critical exponents and scaling functions. As m tends to infinity, τ approaches 2, and, for the particular case of an initial distribution composed solely by isolated nodes, t_c approaches 1 (section 2.3.1). To find t_c, for a given initial cluster size distribution, in principle, one has to solve numerically the set of evolution equations (2.15). This was made in reference [1] (section 2.2) for $m = 2$, and in [3] for $m = 2, 3, 4$ (section 2.4), where the precision of the estimations is posteriorly improved with the method described there. However, if m is not very large, we can estimate t_c for initially isolated nodes, without solving the master equations numerically. The numerical solution of evolution equations for $P(s,t)$ showed that for sufficiently small m, the asymptotic power law at the critical point, $P(s,t_c) \cong f(0)s^{1-\tau}$, is still approximately valid even at small s, and, moreover, $f(0)$ deviates from $P(s=1,t_c)$ only by a small number of the order of $\tau - 2$ if all nodes initially were isolated. In this special case, we can approximate $P(s,t_c)$ in the sum rule $\sum_{s=1}^{\infty} P(s,t_c) = 1$ by $P(s=1,t_c)s^{1-\tau}$ at any $s \geq 1$, which gives

$$P(1,t_c)\zeta(\tau-1) \approx 1, \tag{2.70}$$

where $\zeta(x) \equiv \sum_{s=1}^{\infty} s^{-x}$ is the Riemann zeta function. We find $P(1,t)$ explicitly in the full range of t by solving the master equation (2.15) with the initial condition $P(1,0) = 1$. Let, e.g., $m = 2$. Then the result is

$$P(1,t) = \frac{2}{1+e^{4t}}, \tag{2.71}$$

so we have

$$\frac{2}{1+e^{4t_c}}\zeta(\tau-1) \approx 1, \tag{2.72}$$

and finally

$$t_c \approx \frac{1}{4}\ln[2\zeta(\tau-1)-1]. \tag{2.73}$$

Substituting $\tau = 2.04763044$, which we obtained above at $m = 2$ into this formula, we finally find an estimate for t_c, namely $t_c \approx 0.935$. This estimate is close to a precise value $t_c = 0.923207509297(2)$, which we have found in section 2.4 (Table 2.3)

2.6 Closing Discussion

Throughout this chapter we have addressed a problem that captured a lot of attention since the very first report of this class of phenomenon. We started by showing that, contrarily to what was initially believed, the so-called explosive percolation is in fact continuous [1] (section 2.2). However, the transition in these irreversible processes shows a uniquely small exponent β, which explains the generalized confusion. The only assumption made on our initial proof was a slow decay (power-law) of the critical cluster size distribution. We observed this power law in the numerical solution of 10^6 evolution equations, similarly to the observations in earlier simulations [100, 101, 102, 105]. (Later, the continuity of explosive percolation was also proven mathematically [111].) Furthermore, we verify that all the usual scaling features of continuous percolation transitions are present on these transitions as well.

Our rigorous approach to the problem was possible thanks to the elegant mathematical description allowed by the particular model considered. In section 2.3, we proceed extending

the previous analysis to a set of representative explosive percolation models, which generalizes the one initially considered, and covers the entire range of these optimization-like processes. In particular, we shown that, except the "most explosive" model ($m = \infty$), the transition is always continuous. We also observe the expected scaling behavior of the distributions $P(s,t)$ and $Q(s,t)$, critical singularities of $\langle s \rangle_P$ and $\langle s \rangle_Q$, and derive scaling relations between critical exponents. Moreover, we briefly consider a model mixing the rules from explosive and ordinary percolation, to which we repeat the analysis, with qualitatively similar and quantitatively intermediate results. (These results may also be found in [2].)

In the following section 2.4, we have developed a method that allows to use the numerical solution of a not so large number of evolution equation to obtained the critical exponent τ (recall that there is only one independent exponent), the critical time t_c and amplitude of the critical distribution $f(0)$ [3]. We find that these estimations rapidly converge to the exact values, yielding highly precise results, shown in Table 2.3. We sustain that this method could be successfully applied to the numerical study of other continuous phase transitions, characterized by power-law critical distributions.

Finally, in last section, we presented a complete solution of this intriguing quest. For the wide class of representative models introduced in section 2.3, we developed a strict scaling theory which provides the full set of scaling functions and critical exponents for each of the models with any desired precision. That theory indicates the relevant order parameter and susceptibility for the problem, and explains the continuous nature of this transition and its unusual properties. Furthermore, by exactly solving the problem below the critical point, we prove that the critical distribution is indeed asymptotically power-law.

Chapter 3

A Model for Network Flow Optimization

As discussed in section 1.5, network flow processes are ubiquitous in natural, technological and social networked systems. Within this class of problems, there is a wide variety of fundamentally different dynamics; such as, maximum flow, minimum global cost, minimum individual cost (like in vehicular traffic dynamics), spontaneous diffusion, etc. Additionally, in many real systems the structure of the network itself may be, at some extent, influenced by the transport necessities, increasing the complexity of the problem. According to such variety, investigations on network flows may be centered on the study of a number of different quantities of interest and use different approaches, depending on the nature of the constraints, and the intended applications of a model under consideration.

In this chapter we consider a toy-model for network flow with a locally governed dynamics. Like in urban traffic flow, where each driver makes his own decisions, our model lacks a central authority, and the flow leaving a node is distributed trough its outgoing channels according to some local optimization criterion, applied independently on each node. Many real systems rely on this kind of localized decisions to perform transport operations; from the routing of information on wireless ad-hoc communication networks [120, 121], to the drainage of water in fluvial systems, both in the tributary upstream region (also known as river basin) [122, 123] and in the distributary downstream region (found in river deltas) [124, 125, 126].

The character of tributary and distributary drainage systems are fundamentally different. In tributary systems the water, from rain and snow melting, is conducted by small streams into gradually larger ones, until it reaches the main channel (the river itself). The network structure of river basins is determined by the landscape's topology: the water advances in the surface to positions of lower elevation, driven by gravity, flowing through channels that often meet with each other and join into a single one, which carries sum of the contributions of its tributaries. These natural systems show some remarkable properties, associated with their fractal geometry [123], yet, the directed graph formed the channels (edges) and intersections (nodes) is relatively simple and the network flow dynamics is trivial, since there are no bifurcations, each node has two or more incoming channels and only an outgoing one, in a tree-like structure.

River deltas show a far more interesting network flow dynamics. When entering the ocean or a lake, the water slows down near the river mouth, and the sediments suspended due to turbulence in the upstream deposit at the bottom. Over geological time scales, this process

produces the shallowing of the river mouth, and consequent widening of the discharge area, forming a Δ-like shape [125]. The flow from the river is discharged into the ocean through multiple channels (forming the delta), which arise from consecutive bifurcations of the stream. In deltas with a high density of bifurcations it may be expected a high density of intersections too, and consequent merging of distributary channels. This forms an anastomosed network pattern, which is also observed in braided rivers (where the the effect is due to high slope and/or large sediment load) [127].

There is evidence that, in rivers deltas, the division of flow among channels at the bifurcations is rarely symmetric, see reference [126], in fact, in the same study is shown that asymmetric bifurcations are more stable under perturbations than symmetric ones, explaining their prevalence in nature. Additionally, some channels may be only seasonally active, contributing to the total discharge in the season of higher flow, but standing inactive when the total flow is lower [128]. Pointing in the same direction, another empirical study [129], based on data from 51 river deltas, suggests that the number of active distributary channels, N_d, in a delta grows with the average amount of flow discharged across the delta, f, as a power law $N_c \propto f^{\alpha}$ with exponent α estimated around 0.6.

In vehicular traffic a similar situation may be found when there are alternative roads between two given geographic points. Considering two alternative roads, A and B, with somewhat different distances, travel times or monetary costs, such that, in the absence of other traffic, each driver would always choose the best alternative, say road A. However, if the amount of flow between the two points increases, then the velocity at road A diminishes, and can even become almost null in case of jamming (see section 1.5.3). Therefore, above some amount of flow it becomes advantageous for some drivers to use the alternative road B. In free traffic conditions it would be the worst option, but it becomes comparatively better as the velocity in road A diminishes due to the high density of traffic (this situation is considered in [130, 131]). For this real-world example, as well as for the prior one, the number of used, or active, channels seems to depend on the total amount of flow to be transported. Moreover, in both cases, when there is a split of the flow at bifurcations, it tends to be asymmetric.

In this chapter we propose a model that implements this sort local dynamics on an infinite network. As the system evolves the flow distribution reaches its stationary form, which will be independent of the details of initial conditions. Here, we investigate the properties of the stationary distribution, which are determined by the model's rules and topological structure. We find that the stationary flow distribution strongly depends on the amount of flow initially injected in the system. In fact, the average current per edge (or node) is the only independent parameter of the model.

This chapter is organized as follows. In the next section we define the model's dynamical rules and topological structure. The stochasticity is inserted in the model by randomly assigning some aspects of the structure. In section 3.2 we derive the equations for this model. These equations completely define the model's behavior, and are the basis for the work here presented. In section 3.3 we solve this problem in the high current regime and in section 3.4 in the low current one. Furthermore, these results are compared with numerical iteration of the model's equations in section 3.5.

3.1 The Model

In this section we present a description of the network flow model that we consider. First we identify the mechanisms acting on the currents. Those are responsible for the evolution of the system's state, by imposing deterministic splitting rules at the bifurcations. Later we describe the network where the optimization driven process takes place. It is an infinite directed regular network with two types of edges. Importantly, the pair of edges exiting each node must be composed by one of each type, since that is how the asymmetric splitting is achieved. On the other hand, stochasticity is incorporated in the model by connecting a random pair of edges to the entry of each node, independently of their type.

3.1.1 Flow Optimization

Most models for network flow optimization attribute a fixed cost to the transport of a flow unit, evidently in those case, all the current would flow by the path with lower fixed cost, and for unlimited capacities the solution would be trivial. In our model, the characteristics of the flow splitting dynamics described above, can be regarded from an optimization perspective too. Nonetheless, contrasting with most models, we do not impose limitations to the capacity of nodes or channels, and the non-trivial behavior is achieved with a generalization of the cost function that includes a non-linear dependence with the amount flow transported. Since the flow is conserved at the intersections and bifurcations it is hereby called current, and denoted j.

The simplest form of a non-linear function, $C_i(j_i)$, for the cost of transporting an amount of current j_i in channel i, is $C_i = c_i j_i + j_i^2/2$ (for convenience the arbitrary factor of the quadratic term is set here to 1/2, but the result is qualitatively identical for any choice). When a node, receiving a current j, has two outgoing channels with cost coefficients c_1 and $c_2 \geq c_1$, the total cost to be minimized is $C(j_1, j_2) = C_1(j_1) + C_2(j_2)$, where the currents $j_1 + j_2 = j$, due to the conservation condition (see Figure 3.1(a)). Then, the distribution of flow on the two outgoing channels is simply given by the condition of minimum cost $(dC/dj_1) = c_1 - c_2 + 2j_1 - j = 0$, to which corresponds $j_1 = (j + c_2 - c_1)/2$ and $j_2 = (j + c_1 - c_2)/2$. Yet, for $j < c_2 - c_1$ these expressions give a current $j_2 < 0$, which is not allowed, since the edges of the underlying network are directed all current must be non-negative. So the actual solution of the minimum cost problem under all these constraints is:

$$\begin{cases} j_1 = j \text{ and } j_2 = 0 & \text{if } j \leq j_c, \\ j_1 = \frac{j+j_c}{2} \text{ and } j_2 = \frac{j-j_c}{2} & \text{if } j > j_c, \end{cases} \tag{3.1}$$

where $j_c \equiv c_2 - c_1 > 0$ is a threshold current. So the two parameters, c_1 and c_2, are reduced to a single one, j_c.

Last expression completely defines the splitting mechanism on this model. The key feature of this particular model is that it exhibits two regimes of behavior. If $j \leq j_c$ all the current will exit the node through the link with coefficient c_1, and the other channel, with coefficient c_2, remains unused. If $j > j_c$ both channels are active but the currents flowing through them has a difference of j_c. This effect originates from the quadratic term of C_i.

The concept of cost may be relatively clear in some systems; as for vehicular traffic flow, where most drivers will take into account a number of weighted factors associated to the use of a particular road (duration, safety conditions and monetary cost of the travel, etc).

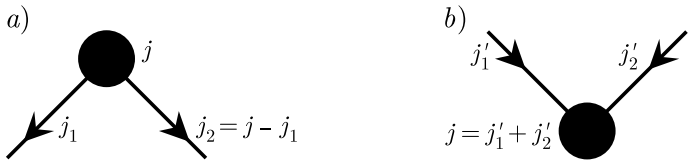

Figure 3.1: The microscopic dynamics obeys current conservation rules. *a*) The splitting mechanism may divide, or not, the total current j passing through a node, according with conditions (3.1). *b*) When two channels meet at the same end node, their currents simply sum up.

However, in other systems, it is not that simple to find an analogous quantity for the cost of a particular channel, as in distributary fluvial systems. It should be emphasized that, our aim here is not to argue for the suitability of non-linear cost functions in general, but to investigate network flow properties in the presence of such a j_c (below which all the current leaves the node by only one of the channels, and above which the smaller part of the current takes another alternative). As such, any considerations about cost functions, including the very the notion of cost, are left out the following discussion, and the desired current splitting behavior is achieved simply by using equations (3.1).

On the other hand, the same conservation condition imposes that two currents, j_1' and j_2', traveling in channels that connect into the same end node, merge together when they meet, and are regarded from then on as a single current $j = j_1' + j_2'$. This complementary part of the microscopic dynamics is also represented in Figure 3.1(*b*).

3.1.2 Network Structure

A microscopic dynamics of successive mergings and splittings, with similar characteristics to the one introduced in last section, was implemented in regular lattices by [130] and [131]. Both works consider a flow in a two-dimensional regular directed network, as depicted in Figure 3.2, where each node is attributed a random value of j_c. The analysis of data from numerical simulations revealed the presence of some scaling-like features, involving the average current and the fraction of used channels, among other quantities. (The fraction of unused channels $B \in [0, 1]$ has a non-trivial behavior, and will be seen to play an important role in the theory of these systems, laid in this chapter). Here, we will be interested in the behavior of the infinite system, when the system extends to infinity both on the left- and right-hand sides.

It should be stressed that, in the network of Figure 3.2, there are two kinds of channels. The pair of channels outgoing from a node to the next layer contains channels of both kinds simultaneously, to ensure the asymmetric splitting properties discussed in last section. However, stochasticity is added to the model, by fixing kinds of the right and left channels (c_1, c_2) or (c_2, c_1), respectively, with equal probability.

We will consider a mean-field version of the model that avoids complications arising from local correlations. For the two-dimensional system, the currents flowing by the two channels into a node in layer t have some correlation between them, since they share one ancestor in the layer $t-2$, two in layer $t-3$ and in general $n-1$ ancestors in layer $t-n$. For that reason, the rigorous mathematical treatment of the model must account for all such correlations, which becomes an unbearable task, in the infinite size limit. Furthermore, in our model the

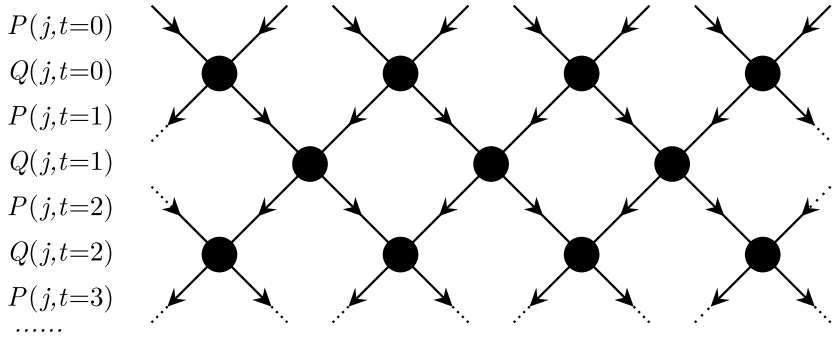

Figure 3.2: In two-dimensional network flow models, as the ones considered in [130] and [131], the flow's circuit consists of a diagonal square lattice. Nodes are organized by layers, labeled $t = 0, 1, 2, \ldots$, and each one is connected to the next layer by two directed channels (one of each of two kinds). The pair of channels outgoing a node is asymmetric, to ensure the splitting rule of expression (3.1), and the asymmetry is assigned at random. In this way, contrarily to the outgoing channels, the two incoming channels of a node are independent. At each step, the current at each node of layer t flows into layer $t+1$ by one or both its outgoing channels. Then, the parameter t is associated with time, i.e., at time step $t = 0$ currents with distribution $P(j, 0)$ are inputed at the top layer, at $t = 1$ the currents have traveled to the next layer taking the distribution $P(j, 1)$, and so on.

---

threshold current j_c is equal for all the nodes (a similar uniform situation was simulated in [131]).

In the mean-field version of the system, nodes are also organized by layers, and each node has two outgoing asymmetric channels. But now, instead of a diagonal square lattice like the one of Figure 3.2 the incoming extremities of the channels exiting a layer are randomly grouped in pairs, and each pair is connected to a random node on the next layer. All local correlations are suppressed by this transformation, which also changes the system's dimensionally from $1 + 1$ to $1 + \infty$. It is then clear that this is a mean-field model in a strict sense.

The local dynamics of this mean-field version is exactly the same as of the two-dimensional case; each node has a random pair of incoming channels, which currents are summed at the node, and a pair of asymmetric outgoing channels, which currents are determined by expression (3.1). For this reason, one might expect the flow properties for these models to be qualitatively similar, as well as for intermediate dimensionality systems. In fact, in reference [130], simulations of a three-dimensional and the mean-field models were also performed . Surprisingly, these results strongly suggest that the flow properties are qualitatively and quantitatively independent of the system's dimensionality.

Evidently, the flow distribution in layer 1 depends on the initial distribution, $P(j, 0)$, which is imposed by some external source; in layer 2 it depends on layer 1, and consequently on the initial distribution as well, and so on for the next layers. In any layer at a finite distance from $t = 0$, the influence of the initial distribution is still felt, and the results will depend of the choice of $P(j, 0)$. Therefore, we will be interested in what happens when $t \to \infty$, and there might be a current distribution that remains unaltered from layer to layer, i.e., a stationary current distribution, which is independent of initial conditions, with exception for the initial average current (since the current is always conserved, and the number of nodes and channels

is the same in all layers, the average value of current, flowing through each node of system, also remains constant throughout the layers of the structure). Then the layer index t can be interpreted as time, as we are looking for the stationary distribution, to which any initial conditions, with the some fixed average current, will eventually converge after an initial period of transience.

Our model's structure is composed by an infinite number of consecutive layers of nodes, through which the current passes only once (i.e., without loops; recall that the edges are directed). For this process, this structure is, in fact, equivalent to a simpler and more familiar structure. Consider the random network with N nodes and $2N$ directed edges (N of each type) where the only restrictions are that every node as one outgoing edge of each type and any two incoming ones. This construction only has one layer of N nodes and $2N$ edges through which the current flows repeatedly. However, from the perspective of our model's dynamics it is equivalent to the multilayer structure. In the multilayer network, at each step t the current exits the nodes at some layer and enters the corresponding channels, leaving that layer's nodes empty of current. It then exits the channels to enter the nodes of the next layer, which were empty before. Since the dynamical rules for the division of current depend only of the amount of current on the node at time t, there is no reason why the current entering the empty nodes of the next layer could not be redirected to the also empty nodes of the same layer. In this sense, the multilayer structure is equivalent to the aforementioned class of random networks.

3.2 Flow Distribution Equations

Given the stochastic nature of the connection procedure, the description of the flow's behavior in our model should be given in terms of its statistical properties. All nodes of a layer occupy equivalent positions, so it is natural to ask what are the flow properties of a node, or channel, chosen uniformly at random. Due to the continuous character of the current j, such properties are described by probability density distributions. For instance, the distribution of current flowing by a random edge into a node in layer t, denoted $P(j,t)$, is defined from the probability of an edge carrying current between j and $j+dj$, which is given by $P(j,t)dj$ when $dj \to 0$. The distribution $P(j,t)$ is then a probability density.

Let us consider the conditions allowing to derive the equations that govern the transformation of the probability density distributions of current on channels and nodes. Above we introduced the distribution $P(j,t)$ for the channels, let us now also introduce $Q(j,t)$, the probability density distribution for the currents on nodes. These two distributions coevolve. They are related to each other in two complementary ways, that correspond to the two parts of the dynamics depicted in Figure 3.1. On one hand, the currents carried by two random channels join at each node; on the other hand, the current at each node is split into two according to expression (3.1).

The following equations are exact in the infinite system size limit, i.e., infinite number of nodes per layer. In terms of probabilities, we can write, for the first stage of the local mechanism (when currents just sum):

$$Q\,(j,t)\,dj = 2B(t)P(j,t)dj + \left(\int_0^j du\,P(u,t)P(j-u,t)\right)dj,$$

when $dj \to 0$. Here, $B(t)$ is the fraction of inactive channels at layer t. On the left-hand

side is the probability that the current in a node is in the interval $[j, j+dj[$. On the right-hand side the first term is the probability that one channel carries no current, $B(t)$, times the probability that the other channel carries some current in the interval $[j, j+dj[$, times 2 because any of both channels can be the one active/inactive. The second term accounts for all the cases in which both channels contribute with some current and their sum is in the interval $[j, j+dj[$.

For the splitting part we can write:

$$P(j,t+1)dj = \begin{cases} \frac{1}{2}Q(j,t)dj + \frac{1}{2}Q(2j+j_c,t)d(2j) & \text{if } j \leq j_c, \\ \frac{1}{2}Q(2j-j_c,t)d(2j) + \frac{1}{2}Q(2j+j_c,t)d(2j) & \text{if } j > j_c, \end{cases}$$

again, when $dj \to 0$. Since the distribution $P(j,t)$ is for a random edge, independently of its cost coefficient, in both equations the factors $1/2$ account for the probability of the channel being assigned with each of the two possible coefficients (this probability is, of course, $1/2$ for each coefficient). On the left-hand side is the probability that the current in a channel is in the interval $[j, j+dj[$. On the right-hand side of the top expression (for $j \leq j_c$), the first term corresponds to the probability of the case when the channel is assigned with the lower coefficient c_1, and the current of the node is in the interval $[j, j+dj[$, below j_c, so that all the current exits the node by only one channel. The second term corresponds to the case when the channel is assigned with the higher coefficient c_2, and the current exiting the node is in the interval $[2j+j_c, 2(j+dj)+j_c[$. The first term of the bottom expression (for $j > j_c$) corresponds to the case when the channel is assigned with the lower coefficient c_1, and the current exiting the node is in the interval $[2j-j_c, 2(j+dj)-j_c[$, above j_c (since $j > j_c$); and the second term is the same as in the above expression.

Dividing by dj we get the equations for the probability density distributions:

$$Q(j,t) = 2B(t)P(j,t) + \int_0^j du\, P(u,t)P(j-u,t). \tag{3.2}$$

$$P(j,t+1) = \begin{cases} \frac{1}{2}Q(j,t) + Q(2j+j_c,t) & \text{if } j \leq j_c, \\ Q(2j-j_c,t) + Q(2j+j_c,t) & \text{if } j > j_c. \end{cases} \tag{3.3}$$

These equations exactly describe the evolution of the current distribution throughout the layers of the infinite system. They can be iterated: start by some arbitrary initial distribution $P(j,0)$, use equation (3.2) to calculate $Q(j,0)$, then, use equation (3.3) to calculate $P(j,1)$, and so on, using equation (3.2) and equation (3.3) alternately. Notice that $P(0,t)$ and $B(t)$ are not the same; while $P(0,t) \in [0,\infty)$ is bounded only from below, because it is a probability density, $B(t) \in [0,1]$ is the fraction of inactive channels, or the probability that a randomly chosen channel is unused. $B(t)$ relates to the distribution $P(j,t)$ as:

$$\int_0^\infty dj\, P(j,t) = 1 - B(t). \tag{3.4}$$

By integrating equation (3.2) and substituting equation (3.4), we obtain the relation between $B(t)$ and the distribution of current on nodes:

$$\int_0^\infty dj\, Q(j,t) = 1 - B^2(t) \tag{3.5}$$

Finally, integrating equation (3.3) and substituting equations (3.4) and (3.5), we get the identity:

$$B^2(t) + \frac{1}{2}\int_0^{j_c} dj\, Q(j,t) = B(t+1) \tag{3.6}$$

Interpreting the index t as time, as argued above, one can speak of a stationary distribution at $t \to \infty$, when $P(j, t+1) = P(j,t) \equiv P(j)$, which is the solution of the following system:

$$Q(j) = 2BP(j) + \int_0^j du\, P(u)P(j-u) \tag{3.7}$$

$$P(j) = \begin{cases} \frac{1}{2}Q(j) + Q(2j + j_c) & \text{if } j \leq j_c, \\ Q(2j - j_c) + Q(2j + j_c) & \text{if } j > j_c, \end{cases} \tag{3.8}$$

$$B = 1 - \int_0^\infty dj\, P(j). \tag{3.9}$$

This system of equations, where the only one scale present is j_c, admits an infinity of solutions. Yet, another restraint is imposed by initial conditions, since equations (3.2) and (3.3) ensure that $\langle j \rangle = \int_0^\infty djjP(j,0)$ is always conserved by iterations. This property provides us another equation, which fixes the particular form of the solution for a given $\langle j \rangle$:

$$\int_0^\infty dj\, jP(j) = \langle j \rangle. \tag{3.10}$$

In fact, the first moment of the distribution $P(j)$, $\langle j \rangle$, is the control parameter of the model, i.e., the solution of the system of four equations (3.7)–(3.10), for the distributions of current, will depend only on $\langle j \rangle$ (which is the only influence of initial conditions on the stationary state).

It can be easily seen that the distributions generated by solving equations (3.7)–(3.10) must scale with parameter j_c, i.e., the currents may be expressed in arbitrary units, and a change of units must not change anything else on the system's behavior. In fact, the most natural way of quantifying current in this model is in units of j_c. Furthermore, the stationary state, corresponding to the solution of equations (3.7)–(3.10) is completely determined by the ratio $\langle j \rangle / j_c$, which is the single independent parameter of our model. On other words, $P(j, \langle j \rangle, j_c) \equiv \frac{1}{j_c} P(j/j_c, \langle j \rangle / j_c)$, $Q(j, \langle j \rangle, j_c) \equiv \frac{1}{j_c} Q(j/j_c, \langle j \rangle / j_c)$ and $B(\langle j \rangle, j_c) \equiv B(\langle j \rangle / j_c)$. Nevertheless, in the next section we will start working with the distributions $P(j, \langle j \rangle, j_c)$ and $Q(j, \langle j \rangle, j_c)$, and allow for these scaling properties to emerge spontaneously, instead of assuming them from the beginning (which clearly we could do).

We find that, because of the bipartite form of equation (3.8), the Laplace transform technique only works on the limit $\langle j \rangle / j_c \to \infty$. Furthermore, as is shown in section 3.4, the failure of this standard method for lower values of average current is, in fact, symptomatic of the unconventional properties of the stationary distributions of this model. The most evident of such peculiarities is the presence of an unusual discontinuity, at j_c, in both $P(j)$ and $Q(j)$. Considering the limit $\Delta P = \lim_{\epsilon \to 0} P(j_c + \epsilon) - P(jc - \epsilon)$, and substituting both branches of

equation (3.8) and equation 3.7, we obtain:

$$\begin{aligned}\Delta P = P\left(j_c^+\right) - P\left(j_c^-\right) &= Q\left(j_c^+\right) + Q\left(3j_c\right) - \left[\frac{1}{2}Q\left(j_c^-\right) + Q\left(3j_c\right)\right] \\ &= 2BP\left(j_c^+\right) - BP\left(j_c^-\right) + \frac{1}{2}\int_0^{j_c} du\, P\left(u\right) P\left(j_c - u\right) \\ &= \frac{1}{1-B}\left[BP\left(j_c^+\right) + \frac{1}{2}\int_0^{j_c} du\, P\left(u\right) P\left(j_c - u\right)\right] \\ &= \frac{Q\left(j_c^+\right)}{2(1-B)} > 0.\end{aligned}$$

Then, there is also a discontinuity on the distribution of current at nodes $\Delta Q = 2B\Delta P > 0$, which follows from equation (3.7).

3.3 High Average Current Regime

Equations (3.7)–(3.10) completely define the model's behavior when $t \to \infty$. So the solution of this problem is reduced to the finding of distributions that satisfy the system of equations (3.7)–(3.10), for given $\langle j \rangle$ and j_c. For that purpose, we start by defining the Laplace transform of the probability density distributions $P(j)$ and $Q(j)$:

$$\Gamma(x) = \int_0^\infty dj\, P(j) e^{-xj},$$

$$\Lambda(x) = \int_0^\infty dj\, Q(j) e^{-xj}.$$

One can easily check that the values of these functions and their first derivatives at $x = 0$ are given by, $\Gamma(0) + B = \Lambda(0) + B^2 = 1$ and $-\Gamma'(0) = -\frac{1}{2}\Lambda'(0) = \langle j \rangle$.

The transformation of equations (3.7) and (3.8) gives, respectively:

$$\Lambda(x) = 2B\Gamma(x) + \Gamma^2(x),$$

and

$$\begin{aligned}\Gamma(x) &= \frac{1}{2}\int_0^{j_c} dj\, Q(j) e^{-xj} + \int_{j_c}^\infty dj\, Q(2j - j_c) e^{-xj} + \int_0^\infty dj\, Q(2j + j_c) e^{-xj}, \\ &= \frac{1}{2}\int_0^{j_c} dj\, Q(j) e^{-xj} + \cosh\left(\frac{xj_c}{2}\right)\int_{j_c}^\infty dj\, Q(j) e^{-xj/2}, \\ &= \cosh\left(\frac{xj_c}{2}\right)\Lambda\left(\frac{x}{2}\right) + \int_0^{j_c} dj\, Q(j)\left[\frac{e^{-xj}}{2} - \cosh\left(\frac{xj_c}{2}\right) e^{-xj/2}\right].\end{aligned}$$

From the expression at the bottom one can see why the standard Laplace transform technic fails to solve this problem in general. The reason is that the transformation of equation (3.8) results in an expression which contains other unknown functions, not expressible in terms of the functions $\Lambda(x)$ and $\Gamma(x)$, as is the case of the integral from 0 to j_c, seen on the right-hand

side of last expression. However, in the $\langle j\rangle/j_c \to \infty$ limit, $B \to 0$ and $\int_0^{j_c} dj\, Q(j) \to 0$, which simplifies the last equations to:

$$\Lambda(x) = \Gamma^2(x), \tag{3.11}$$

$$\Gamma(x) = \cosh\left(\frac{xj_c}{2}\right)\Lambda\left(\frac{x}{2}\right). \tag{3.12}$$

So, in this limit, the stationary distributions that solve the model's equations can be found exactly with the Laplace transform method.

Combining equations (3.11) and (3.12) we get:

$$\Gamma(x) = \cosh\left(\frac{xj_c}{2}\right)\Gamma^2\left(\frac{x}{2}\right), \tag{3.13}$$

which gives $\Gamma(x)$ is a self-recursively, in terms of $\Gamma(x/2)$. Then, one can write $\Gamma(x/2)$ in terms of $\Gamma(x/4)$ and so on. For arbitrary integer number $n \geq 1$, last expression can be rewritten as:

$$\Gamma(x) = \Gamma^{2^n}\left(\frac{x}{2^n}\right)\prod_{k=0}^{n-1}\cosh^{2^k}\left(\frac{xj_c}{2^{k+1}}\right).$$

When $n \to \infty$, $x/2^n \to 0$ and $\Gamma^{2n}\left(x/2^n\right) = \left[\Gamma(0) + \Gamma'(0)x/2^n\right]^{2^n} = e^{-\langle j\rangle x}$. Hence, the solution of equation (3.13) becomes:

$$\Gamma(x) = e^{-\langle j\rangle x}\prod_{k=0}^{\infty}\cosh^{2^k}\left(\frac{xj_c}{2^{k+1}}\right), \tag{3.14}$$

which already is the solution of the problem in the infinite average current limit. The last step is simply to invert back the transformation, from $\Gamma(x)$ to $P(j)$.

Since $\Gamma(x)$ has no poles in the complex plane, the inverse transformation can be calculated by performing the integration along the imaginary axis of the complex plane. Then, to find the inverse transform, we integrate over the real variable x as follows:

$$\begin{aligned}
P(j,\langle j\rangle, j_c) &= \frac{1}{2\pi i}\int_{-i\infty}^{+i\infty} dx\, e^{-(\langle j\rangle - j)x}\prod_{k=0}^{\infty}\cosh^{2^k}\left(\frac{xj_c}{2^{k+1}}\right)\\
&= \frac{1}{\pi}\int_0^{+\infty} dx\, \cosh\left[\left(\langle j\rangle - j\right)ix\right]\prod_{k=0}^{\infty}\cosh^{2^k}\left(\frac{ixj_c}{2^{k+1}}\right)\\
&= \frac{1}{\pi}\int_0^{+\infty} dx\, \cos\left[\left(\langle j\rangle - j\right)x\right]\prod_{k=0}^{\infty}\cos^{2^k}\left(\frac{xj_c}{2^{k+1}}\right)\\
&= \frac{1}{\pi j_c}\int_0^{+\infty} dx\, \cos\left(\frac{\langle j\rangle - j}{j_c}x\right)\prod_{k=0}^{\infty}\cos^{2^k}\left(\frac{x}{2^{k+1}}\right).
\end{aligned} \tag{3.15}$$

We failed to simplify the previous integral. The main difficulty here is the highly oscillatory nature of the integrand, and it is likely that there is no possible simplification. However, solution (3.15) can be found numerically with any desired precision. This gives an exact and complete description of the problem in the limit $\langle j\rangle \to \infty$.

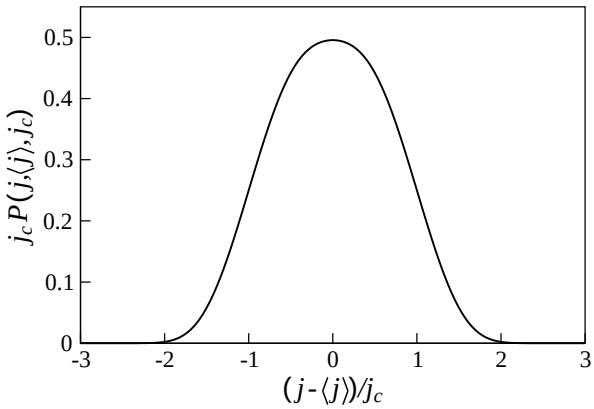

Figure 3.3: Distribution $P(j, \langle j\rangle, j_c)$ in the high current limit (equation 3.15). The area under the curve obeys the normalization condition $\int_o^\infty dj\, P(j, \langle j\rangle, j_c) = 1$.

As discussed above, the currents may be measured in units of j_c, so, in general, the stationary distribution should scale as $P(j, \langle j\rangle, j_c) \equiv \frac{1}{j_c} P(j/j_c, \langle j\rangle/j_c)$. Solution (3.15) is plotted in Figure 3.3 for an arbitrary j_c, demonstrating this property. In the $\langle j\rangle \to \infty$ limit considered in this section, we find an additional reduction of the number of variables necessary to describe the probability density distribution of current. For this particular case, $P(j/j_c, \langle j\rangle/j_c) \equiv P(\delta)$, where $\delta \equiv |j - \langle j\rangle|/j_c$, and solution (3.3) can be written as a function of a single variable:

$$P(\delta) = \frac{1}{\pi} \int_0^\infty dx\, \cos(\delta x) \prod_{k=0}^{\infty} \cos^{2^k}\left(\frac{x}{2^{k+1}}\right), \tag{3.16}$$

where the modulus can be introduced due to the fact that $\cos(x) = \cos(-x)$ is an even function. This expression shows that the current distribution is symmetric around $\langle j\rangle$, and the only relevant variable is the absolute difference between j and $\langle j\rangle$ measured in j_c units. The stationary form of distribution $Q(j)$ is given by putting $B = 0$ in equation (3.7) and inserting the solution for $P(j)$ into the convolution integral.

The expression's (3.16) integral form is rather opaque, in the sense that one can hardly apprehend its behavior just by looking at it. For that reason, in the remainder of this section we search for more explicit expressions corresponding to both the large and small δ limiting behaviors. In the small δ region, this is rather straightforward task. Writing the Taylor series expansion of solution (3.16) around $\delta = 0$, we get:

$$P(\delta) = \sum_{k=0}^{\infty} c_k \delta^{2k}, \tag{3.17}$$

where $c_k = (-1)^k (\pi(2k)!)^{-1} \int_0^\infty dx\, x^{2k} \prod_{n=0}^{\infty} \cos^{2^n}\left(x/2^{n+1}\right)$. Then, the behavior of $P(\delta)$ around its peak is Gaussian-like, and we can write, for $\delta \ll \sqrt{|c_1/c_2|} \approx 0.747$,

$$P(\delta) \cong c_0 \exp\left(c_1/(2c_0)\,\delta^2\right), \tag{3.18}$$

where $c_0 \cong 0.496$ and $c_1 \cong -0.162$.

When $\delta \gg 1$, $P(\delta)$ decays quite rapidly. This is not easy to see from equation (3.16) because the integrand is highly oscillatory for large δ. However, the asymptotic behavior of $P(\delta)$ can be estimated directly from equations (3.7) and (3.8) when $\langle j\rangle/j_c \to \infty$. In this limit $B = 0$, and equation (3.7) assumes the form

$$Q(j) = \int_0^j du\, P(u)P(j-u).$$

This convolution integration, of a function symmetric around $\langle j\rangle$, and rapidly decaying away from this point, has a peak at $2\langle j\rangle$. Furthermore, since $\langle j\rangle \to \infty$, this function is also symmetric around its peak, $2\langle j\rangle$. Similarly to $P(j, \langle j\rangle, j_c)$, the distribution $Q(j, \langle j\rangle, j_c)$ can be written as a function of the absolute difference between j and $2\langle j\rangle$ in j_c units, i.e., for the distribution of current on nodes the deviation δ from the peak is defined as $|j - 2\langle j\rangle|/j_c$. (Recall that in each layer t of the network the number of nodes is half the number of channels, and on average they must carry twice the amount of current.) Then, in the $\langle j\rangle \to \infty$ limit, one can easily show that the distribution $Q(j, \langle j\rangle, j_c)$ can be written in terms of δ using the symmetric properties of $P(\delta)$ as:

$$Q(\delta) = \int_0^\delta du\, P(u)P(\delta-u) + 2\int_0^\infty du\, P(u)P(\delta+u). \tag{3.19}$$

Let us clarify that the notation $P(j)$ ($Q(j)$) is just an abbreviation of $P(j, \langle j\rangle, j_c)$ ($Q(j, \langle j\rangle, j_c)$), and that the distributions $P(j)$ and $P(\delta)$ ($Q(j)$ and $Q(\delta)$) are simply related by $P(\delta) = j_c P(j)$ with $\delta = |j - \langle j\rangle|/j_c$ ($Q(\delta) = j_c Q(j)$ with $\delta = |j - 2\langle j\rangle|/j_c$). Despite the use of the same letter, P (Q), for $P(j)$ and $P(\delta)$ ($Q(j)$ and $Q(\delta)$), they can be easily distinguished from each other by the argument inside brackets, i.e., j or δ.

Furthermore, while investigating the infinite average current limit one should use the form of equation (3.8)

$$P(j) = Q(2j - j_c) + Q(2j + j_c),$$

as long as $j > j_c$. Rewriting this equation for the symmetric scaling form of the distributions:

$$P(\delta) = Q(|2\delta - 1|) + Q(2\delta + 1), \tag{3.20}$$

where the modulus of the argument of the first term is introduced because we have defined $Q(\delta)$ only for $\delta > 0$, which is not a problem since for $Q(j)$ we have $Q(2\langle j\rangle + x) = Q(2\langle j\rangle - x)$.

The function $P(\delta)$ is a rapidly decaying one, consequently, for $\delta \gg 1$, the second integral on the right-hand side of expression (3.19) is subdominant. Additionally, it can be noticed that the terms on the right-hand side of relation (3.20) obey the inequality $Q(|2\delta-1|) > Q(2\delta+1)$, and for large δ we can write:

$$P(\delta) \propto Q(2\delta - 1) \approx \int_0^{2\delta-1} du\, P(u)P(2\delta - 1 - u). \tag{3.21}$$

Since $P(\delta)$ is a rapidly decaying function, the dominant contribution to this integral comes from the region near $\delta - 1/2$, i.e., the center of the integration interval. This expression relates the value of $P(\delta)$ with the behavior of the distribution in the neighborhood of $\delta - 1/2$ for $\delta \gg 1$, which allows us to find its asymptotics.

One can check if equation (3.21) admits an asymptotic solution of the form $P(\delta) \propto \exp\left(-C\delta^k\right)$, where $k \geq 1$ and $C > 0$ are constants, by substituting $P(\delta)$ into both sides, and using the Laplace's method to approximate the integral for large δ:

$$\exp\left(-C\delta^k\right) \propto \exp\left(-2C\left(\delta - 1/2\right)^k\right) \int_{-\delta+1/2}^{\delta-1/2} dx \exp\left(-Ck(k-1)\left(\delta - 1/2\right)^{k-2} x^2\right)$$

$$\approx \frac{\exp\left(-2C\left(\delta - 1/2\right)^k\right)}{\sqrt{Ck(k-1)\left(\delta - 1/2\right)^{k-2}}} = \frac{\exp\left(-2C\sum_{n=0}^{k}\binom{k}{n}\delta^{k-n}\left(-1/2\right)^n\right)}{\sqrt{Ck(k-1)\left(\delta - 1/2\right)^{k-2}}}.$$

If k is kept constant, as we assumed, when $\delta \to \infty$ the argument of the last exponential in this expression, $-2C\sum_{n=0}^{k}\binom{k}{n}\delta^{k-n}\left(-1/2\right)^n = -2C\delta^k + O\left(\delta^{k-1}\right)$, is two times larger than the argument of the first, $-C\delta^k$. So $P(\delta) \propto \exp\left(-C\delta^k\right)$ with k constant is not a solution of equation (3.21). However, if we let $k = a\delta$, where a is some positive constant, the last exponential argument's behavior changes to:

$$-2C\sum_{n=0}^{k}\binom{k}{n}\delta^{k-n}\left(-1/2\right)^n = -2C\sum_{n=0}^{k}\frac{\delta^{k-n}k^n\left(-1/2\right)^n}{n!} + O\left(\delta^{k-1}\right),$$

$$= -2C\delta^k\sum_{n=0}^{a\delta}\frac{\left(a/2\right)^n}{n!} + O\left(\delta^{k-1}\right) =_{\delta\to\infty} -\frac{2C}{\exp\left(a/2\right)}\delta^k + O\left(\delta^{k-1}\right).$$

Setting $a = 2\ln(2)$, the leading order of the argument of the exponential on the right-hand side of equation (3.21) is equal to the argument of the exponential on the left-hand side. Nevertheless, the leading order of the exponent is not sufficient to ensure the proportionality relation of equation (3.21) is respected, moreover, the better agreement achieved using $a\delta$ instead of a constant k as exponent suggests that the exponential's argument might behave as b^δ, where b is some other positive constant.

Let us now show that condition (3.21) admits an asymptotic distribution of the form $P(\delta) = A(\delta)\exp\left(-Cb^\delta\right)$, where $A(\delta)$ is a function that varies much slower than $\exp\left(-Cb^\delta\right)$ and C is some positive constant. Substituting this ansatz into both sides of condition (3.21), and applying the same procedure as above to estimate the integral when $\delta \gg 1$, we have

$$A(\delta)\exp\left(-Cb^\delta\right) \propto A^2(\delta - 1/2)\exp\left(-2Cb^{\delta-1/2}\right)\int_{-\delta+1/2}^{\delta-1/2} dx\, \exp\left(-C\ln^2(b)b^{\delta-1/2}x^2\right)$$

$$\cong A^2(\delta - 1/2)\frac{\exp\left(-2b^{-1/2}Cb^\delta\right)}{\sqrt{C}\ln(b)b^{\delta/2-1/4}}.$$

For $b = 4$ we have $2b^{-1/2} = 1$, and the arguments of both exponentials become exactly equal. Furthermore, for a function $A(\delta) \propto b^{\delta/2}$ we find that $A^2(\delta - 1/2)b^{-\delta/2} \propto b^{\delta/2}$, and the proportionality condition becomes fully verified. This means that, for large δ, equation (3.21) is consistent with a asymptotic behavior of the distribution $P(\delta) \propto \exp\left(\ln(2)\delta - C4^\delta\right)$.

In fact, $Q(\delta)$ approaches 0 so rapidly with δ that $\lim_{\delta\to\infty} Q(2\delta+1)/Q(2\delta-1) \to 0$ (recall that $Q(\delta) \propto P((\delta+1)/2)$), and relation (3.21) can be rewritten as an equality,

$$P(\delta) = Q(2\delta - 1) = \int_0^{2\delta-1} du\, P(u)P(2\delta - 1 - u),$$

in that limit. This yields the complete expression for $A(\delta) = \sqrt{C/\pi} 2ln(2)2^{\delta}$. The approximations above are valid when $2^{2\delta} \gg 1$ and become exact when $\delta \to \infty$, where the distribution $P(\delta)$ takes the form:

$$P(\delta) = \sqrt{\frac{C}{\pi}} 2ln(2)2^{\delta} \exp\left(-C2^{2\delta}\right). \tag{3.22}$$

The only unknown in the above expression is C, everything else is completely defined. Comparing with the numerical solution of equation (3.16) the unknown constant is found to be $C = 0.45(2) \approx \ln(\pi/2) = 0.4516\ldots$. The probability density distribution $P(j)$ of currents approaches zero extremely rapidly, approximately as a double exponential, on both sides of $\langle j \rangle$, for increasing difference $|j - \langle j \rangle| = \delta j_c$. Furthermore, the asymptotics of distribution $Q(\delta)$ can be easily obtained from the previous relation $Q(2\delta - 1) = P(\delta)$, by substituting δ by $(\delta + 1)/2$ in equation (3.22). This asymptotics is quite similar to that of $P(\delta)$.

3.4 Low Average Current Regime

When the average current flowing through the channels is null, the solution is trivial, $B = 1$ and $P(j) = 0$ for all j. When $\langle j \rangle / j_c \to \infty$, the fraction of inactive channels $B \to 0$ and $P(j)$ converges to equation (3.16). Let us now describe the spectrum of solutions of the system of equations (3.7) to (3.10) for finite $\langle j \rangle / j_c$. For a general $\langle j \rangle / j_c$ the scaling properties that allowed to write $P(j, \langle j \rangle, j_c)$ in terms of a single variable do not hold. However, one can still express all currents in any arbitrary units, without changing neither the problem nor its properties. Namely, we can choose to measure all currents in units of j_c, reducing the number of variables to two. The scaling form of the equations for the stationary distributions in terms of the rescaled current $\eta \equiv j/j_c$ and the control parameter $\rho \equiv \langle j \rangle / j_c$ is as follows:

$$Q(\eta, \rho) = 2B(\rho)P(\eta, \rho) + \int_0^{\eta} du\, P(\eta, \rho)P(\eta - u, \rho), \tag{3.23}$$

$$P(\eta, \rho) = \begin{cases} \frac{1}{2}Q(\eta, \rho) + Q(2\eta + 1, \rho) & \text{if } \eta < 1, \\ Q(2\eta - 1, \rho) + Q(2\eta + 1, \rho) & \text{if } \eta > 1, \end{cases} \tag{3.24}$$

$$B(\rho) = 1 - \int_0^{\infty} d\eta\, P(\eta, \rho), \tag{3.25}$$

$$\rho = \int_0^{\infty} d\eta\, \eta P(\eta, \rho), \tag{3.26}$$

where the relations between different forms of the distributions are the same as above, i.e., $P(\eta, \rho) = j_c P(j, \langle j \rangle, j_c)$ and $Q(\eta, \rho) = j_c Q(j, \langle j \rangle, j_c)$.

This is a particularly difficult system to solve for general ρ: differentiation does not simplify the equations nor eliminates the integral in equation (3.23); the unusual bipartite form of equation (3.24) impedes the use of the Laplace transform technique or any other transformation of the distributions that involves integrating along all the domain, as was seen in the beginning of section 3.3. Even a numerical solution was only possible by applying the equations iteratively to an arbitrary initial distribution, characterized by some ρ, a large enough number of times, simulating the evolution of the distribution on the infinite system. Those numerical results are presented is section 3.5. Nonetheless, it turns out that it is possible to extract most interesting features of the stationary distributions without solving

the equations for the whole domain $j \in [0, \infty)$, especially for $\langle j \rangle / j_c \equiv \rho \lesssim 1/4$. This is shown in the following analysis.

As discussed in section 3.2 the stationary distributions $P(\eta)$ and $Q(\eta)$ exhibit a discontinuity at $\eta = 1$, making this an interesting point to initiate our investigation (here, we use $P(\eta)$ and $Q(\eta)$ as abbreviations of the distributions $P(\eta, \rho)$ and $Q(\eta, \rho)$, respectively). From equations (3.23) and (3.24) for $\eta < 1$ we can write:

$$Q(1+2\epsilon) = P(\epsilon) - \frac{Q(\epsilon)}{2} = (1-B)P(\epsilon) - \frac{1}{2}\int_0^{\epsilon} du\, P(u)P(\epsilon - u), \tag{3.27}$$

and from equations (3.23), (3.24) for $\eta > 1$ and (3.27):

$$\begin{aligned} Q(1+2\epsilon) &= 2BP(1+2\epsilon) + \int_0^{1+2\epsilon} du\, P(u)P(1+2\epsilon-u), \\ &= 2B\big[Q(1+4\epsilon) + Q(3+4\epsilon)\big] + \int_0^{1+2\epsilon} du\, P(u)P(1+2\epsilon-u), \\ &= 2B(1-B)P(2\epsilon) - B\int_0^{2\epsilon} du\, P(u)P(2\epsilon-u), \\ &+ 2BQ(3+4\epsilon) + \int_0^{1+2\epsilon} du\, P(u)P(1+2\epsilon-u), \end{aligned} \tag{3.28}$$

where $0 \leq \epsilon < 1/2$. In the limit $\epsilon \to 0$ the substitution of equation (3.27) into (3.28) gives:

$$Q(3+4\epsilon) = \frac{1-B}{2B}P(\epsilon) - (1-B)P(2\epsilon) - \int_0^1 du\, P(u)P(1-u). \tag{3.29}$$

By definition of probability density $Q(\eta) \geq 0$ for all η, so from the right-hand side of the previous equation we have $2BP(2\epsilon) \leq P(\epsilon)$. This inequality reveals that the distribution $P(\eta)$ may be non-convergent at $\eta = 0$, i.e., a distribution for which $\lim_{\epsilon \to 0} P(\epsilon) = P(0)$ with some finite $P(0)$, is not consistent with the model's equations when $B > 1/2$. This means that for $B > 1/2$ there must be a divergence at $\eta = 0$, and also at $\eta = 1$, since both points are related by:

$$P(1+2\epsilon) = \frac{(1-B)}{2B}P(\epsilon) - \frac{1}{2B}\int_0^1 du\, P(u)P(1-u), \tag{3.30}$$

for $\epsilon \to 0$. Notice that, if the distribution $P(\eta)$ diverges at some point $\eta = x$ then also the distribution $Q(\eta)$ must diverge at the same point $\eta = x$, because of the first term on the right-hand side of equation (3.23) ($2BP(\eta)$).

So far, we have shown that in certain conditions there are points where the distributions diverge. As an ansatz we will consider such a divergence, at $\eta = x$, as a singularity that close enough to x is shaped as a power law:

$$P(x+\epsilon) \approx A\epsilon^{-\alpha}, \tag{3.31}$$

for $0 < \epsilon < \epsilon^*$, where ϵ^* is the length of an arbitrary small region immediately above x. Of course, the behavior of any divergence is bounded by the normalization condition $\int_0^{\epsilon^*} d\epsilon\, P(x+\epsilon) < 1$, which is equivalent to the constraint $\alpha < 1$.

With the next proof we show that the stronger divergences, i.e., the divergences with larger exponent α, are located at $\eta = 0$ and $\eta = 1$. If there is a divergence with the larger exponent

α located at $x < 1$, then another divergence with the same exponent α must exist at $1 + 2x$. This is true for the stronger divergences, because in equation (3.23) the contribution from the integral is subdominant near the singularity, diverging at most with exponent $1 - 2\alpha > -\alpha$ for $\alpha < 1$. And then, from equation (3.24) we find that $(1 - B)P(x + \epsilon) \approx 2BP(1 + 2x + 2\epsilon)$, for small ϵ.

Since only the stronger divergences are considered in this proof we will use the following simplification of equation (3.23) for small enough ϵ:

$$Q(x + \epsilon) \approx 2BP(x + \epsilon), \tag{3.32}$$

and search for the possibility of finding a dominant divergence at the point $x = 1 + a$, with $a \geq 0$. It is unnecessary to consider possible dominant divergences at $x < 1$, since, as seen above, for all of those there is always another associated with it at $1 + 2x > 1$. By dominant divergence we mean a power-law divergence, as in equation (3.31), with exponent α equal or larger than the exponents of all the other divergences present in the distribution. Combining iteratively equations (3.32) and (3.24), for $\eta > 1$, one can write:

$$\begin{aligned} P(1 + a + \epsilon) \approx & 2B\big[P(1 + 2a + 2\epsilon) + P(3 + 2a + 2\epsilon)\big], \\ \approx & (2B)^2\big[P(1 + 4a + 4\epsilon)) + P(3 + 4a + 4\epsilon) \\ & + P(5 + 4a + 4\epsilon) + P(7 + 4a + 4\epsilon)\big], \\ \approx & (2B)^n \sum_{i=0}^{2^n - 1} P\left(1 + 2i + 2^n a + 2^n \epsilon\right), \end{aligned} \tag{3.33}$$

for any $n \geq 1$. Let us define

$$P_a^n(\epsilon) \equiv \sum_{i=0}^{2^n - 1} P\left(1 + 2^n a + 2i + \epsilon\right). \tag{3.34}$$

From equations (3.31) and (3.33) we get $P_a^n(\epsilon) \approx \tilde{A}_n \epsilon^{-\alpha}$, for $0 < \epsilon < 2^n \epsilon^*$, with $\tilde{A}_n = A 2^{n(\alpha - 1)} B^{-n}$.

The sum (3.34) runs over 2^n points, each of which is in the neighborhood of a point of the set $\{1 + 2^n a + 2i\}$, with $i = 0, 1, \ldots, 2^n - 1$. If $a > 0$ the position of the first of these points (i.e., $1 + 2^n a$, corresponding to $i = 0$) moves to higher values with increasing n. Furthermore, for all $a > 0$ there is always a finite number n', such that, the last point of the set $\{1 + 2^n a, \ldots, 2^n a + 2^{n+1} - 1\}$, corresponding to the sum of $P_a^n(\epsilon)$, is in a position located below the first point of the set $\{1 + 2^{n+n'} a, \ldots, 2^{n+n'} a + 2^{n+n'+1} - 1\}$ for $P_a^{n+n'}(\epsilon)$. This fact leads to the condition $2^{n+1} - 1 + 2^n a < 1 + 2^{n+n'} a$, which is observed when the intervals between the first and last points of the each set, corresponding to the sums $P_a^n(\epsilon)$ and $P_a^{n+n'}(\epsilon)$, do not overlap. This condition can be rewritten as

$$n' > \frac{\ln\left(\frac{2}{a}(1 - 2^{-n}) + 1\right)}{\ln(2)}.$$

So, we can just set:

$$n'(a) = \left\lceil \frac{\ln(2 + a) - \ln(a)}{\ln(2)} \right\rceil, \tag{3.35}$$

where $\lceil x \rceil$ means the lowest integer larger than x, and ensure that the two intervals corresponding to $P_a^n(\epsilon)$ and $P_a^{n+n'(a)}(\epsilon)$ do not overlap. This way, the singular behaviors of $P_a^n(\epsilon) \approx \tilde{A}_n \epsilon^{-\alpha}$ and $P_a^{n+n'(a)}(\epsilon) \approx \tilde{A}_{n+n'(a)} \epsilon^{-\alpha}$ must come from separate singularities on the distribution.

The above can be interpreted as an infinite propagation of a dominant singularity of the current distribution, initially identified at $x = 1 + a > 1$, towards higher positions in the domain of the distribution. Now we can check for the compatibility of an infinite number of such singularities with the normalization condition. Integrating over singularities of non-overlapping intervals:

$$1 \geq \int_0^\infty d\eta\, P(\eta) > \sum_{n=1}^{\infty} \int_0^{2^{nn'(a)}\epsilon^*} d\epsilon\, P_a^{nn'(a)}(\epsilon) = \sum_{n=1}^{\infty} \int_0^{2^{nn'(a)}\epsilon^*} d\epsilon\, \tilde{A}_{nn'(a)} \epsilon^{-\alpha}$$

$$= \sum_{n=1}^{\infty} \frac{\tilde{A}_{nn'(a)} \left(2^{nn'(a)}\epsilon^*\right)^{1-\alpha}}{1-\alpha} = \frac{A\,(\epsilon^*)^{1-\alpha}}{1-\alpha} \sum_{n=1}^{\infty} B^{-nn'(a)}. \tag{3.36}$$

Since $B < 1$, the right-hand side of last equality is an infinite sum of infinite terms, and is divergent, of course, which poses a contradiction with the normalization condition.

Then, on one hand, equation (3.29) shows that there must be divergences in the distribution when the fraction of inactive channels $B > 1/2$, and on the other, the above shows that the dominant divergences cannot be located at a and $1 + a$ for any $a > 0$. Inevitably, the distribution's stronger divergences must be located at $\eta = 0$ and 1, nowhere else. Notice that, for $a = 0$ the intervals for the points of $P_0^n(\epsilon)$ all overlap, since the first point of the set corresponding to the sum (3.34) is 1 for all n. (This can also be seen from the behavior of $n'(a)$: when $a \to 0$ the number $n'(a) \to \infty$.) For this reason, when $a = 0$, the sum of equation (3.36) cannot be related with normalization, and there is no contradiction at all.

We have established that the dominant divergences (existent for $B > 1/2$) are at $\eta = 0$ and $\eta = 1$. Then the leading order of equation (3.29) gives, for small enough ϵ,

$$P\,(\epsilon) \cong 2BP(2\epsilon). \tag{3.37}$$

This relation confirms that the ansatz (3.31) is indeed correct, since $P(\epsilon) \propto \epsilon^{-\alpha}$ it is the solution of this relation, and furthermore, supplies us with the exponent α characteristic of the dominant divergences at $\eta = 0$ and 1:

$$\alpha = 1 + \frac{\ln(B)}{\ln(2)}. \tag{3.38}$$

Notice that this expression is consistent with the normalization condition, i.e., $\lim_{B \to 1^-} \alpha = 1^-$. Moreover, α decreases monotonically when the fraction of inactive channels B decreases from 1, until $\alpha = 0$ at $B = 1/2$.

Above we showed that for $B > 1/2$ there are divergencies on the distributions $P(\eta)$ and $Q(\eta)$, at least at points $\eta = 0$ and 1, and that the dominant contribution for these divergencies behaves as the power law of equation (3.31) (for $x = \{0, 1\}$) with exponent given in terms of B by equation (3.38). Nonetheless, this result also tells us that for $B < 1/2$ the existence of such divergences is inconsistent with the model's system of equations (3.7)–(3.10). Since

those return an exponent $\alpha < 0$ for the stronger divergences, indicating that the distributions take finite values in all the domain. Actually, for $B < 1/2$, the distributions $P(\eta)$ and $Q(\eta)$ are continuous at all points, except at $\eta = 1$ where there are finite discontinuities ΔP and ΔQ, respectively, as was noted in the end of section 3.2.

When the distribution is finite everywhere (that is, if $B < 1/2$), the values of $P(0)$, $Q(0)$, $P\left(1^+\right)$ and $Q\left(1^+\right)$ are directly related with each other, by the model's equations. Furthermore, the dependence of these particular points upon B can still be examined using equation (3.29) as follows. Setting $\epsilon = 0$ there, we get

$$Q(3) = \frac{1-B}{2B} P\left(0\right)\left(1-2B\right) - \int_0^1 du P(u) P(1-u),$$

and substituting equations (3.23) and (3.24),

$$\begin{aligned} Q(3) &= \frac{1-B}{2B} P\left(0\right)\left(1-2B\right) - \left[Q\left(1^+\right) - 2BP\left(1^+\right)\right], \\ &= \frac{1-B}{2B} P\left(0\right) - \left[P(0) - \frac{Q(0)}{2}\right], \\ &= \frac{1-B}{2B} P(0)\left(1-2B\right). \end{aligned}$$

Finally we find

$$P(0) = \frac{BQ(3)}{1-B}\left(\frac{1}{2} - B\right)^{-1}. \tag{3.39}$$

The other three points, $Q(0)$, $P\left(1^+\right)$ and $Q\left(1^+\right)$, are obtained in terms of B and $P(0)$ using equation (3.23) with $\eta = 0$ and equation (3.24) with $\eta = 0$ and 1^+:

$$\begin{aligned} Q(0) &= 2BP(0), \\ P\left(1^+\right) &= \frac{1-B}{2B} P(0), \\ Q\left(1^+\right) &= (1-B) P(0). \end{aligned}$$

This set of equations is not complete, since we lack the relation between $Q(3)$ and B. However, it is safe to assume that $Q(3)$ is not identically null, and that it tends to some finite value when $B \uparrow 1/2$. Then, in this limit, equation (3.39) yields

$$P(0) \propto \left(1/2 - B\right)^{-1}. \tag{3.40}$$

This form of $P(0)$, valid when B approaches $1/2$ from below, is consistent with the previous result that $P(0) = \infty$ when $B > 1/2$. The value of $P(0)$ increases with B, and when $B \to 1/2^-$ the value of $P(0)$ goes to infinity as a power law with exponent -1. Above $B = 1/2$, $P(0)$ remains divergent, and the strength of the divergence increases with B, i.e., exponent α, in $P(\epsilon) \propto \epsilon^\alpha$, grows with B as $\alpha = 1 + \ln B / \ln 2$.

Strictly speaking, our previous argumentation for a fraction of unused channels $B > 1/2$, as shown that there are power-law divergences at least at points $\eta = \{0, 1\}$, and that these two

divergences have the smallest exponent, $-\alpha$, of all singular divergences that may be present in the distributions. Nevertheless, this does not exclude the possibility of other power-law divergences, characterized by larger exponents, located at points $\eta \neq \{1, 0\}$. Indeed, one can readily see that, if the exponent $-\alpha'$ of a divergence, located at some position x, is smaller than $-1/2$, i.e., if $P(x+\epsilon) \propto \epsilon^{-\alpha'}$ with $\alpha' > 1/2$, then the convolution integral of equation (3.23) will produce a divergence in distribution $Q(\eta)$ at position $2x$ with exponent $1 - 2\alpha' < 0$, i.e., $Q(2x+\epsilon) \propto \epsilon^{1-2\alpha'}$.

The neglect of the convolution integral in equation (3.23) was the only simplification made in the model's equations, in order to prove the impossibility of dominant divergences at points $\eta \neq \{0, 1\}$. Thus, we have shown that any divergences at positions $\eta \neq \{0, 1\}$ must be produced by the convolution integral. For this reason, when $0 < \alpha \leq 1/2$ the distributions of current have divergent singularities only at $\eta = \{0, 1\}$, the next divergences would come with an exponent $1 - 2\alpha$ which is non-negative for $\alpha \leq 1/2$.

The dominant singularities of the distributions are characterized by the same exponent α in the four regions $P(\epsilon)$, $Q(\epsilon)$, $P(1+\epsilon)$ and $Q(1+\epsilon)$. This is easily verified by setting

$$P(\epsilon) \approx A\epsilon^{-\alpha}, \tag{3.41}$$

accordingly to (3.31), where A is some constant and $\alpha = 1 + \ln B / \ln 2$ (in addition, this expression should apply only for $0 < \epsilon < \epsilon^*$, where ϵ^* is some small enough constant). This singularity relates with the other three by equations (3.23) and (3.24). We find not only that all the singularities are proportional to $\epsilon^{-\alpha}$, but also the proportionality factor's ratios :

$$Q(\epsilon) \approx 2BA\epsilon^{-\alpha}, \tag{3.42}$$

$$P(1+\epsilon) \approx (1-B)A\epsilon^{-\alpha}, \tag{3.43}$$

$$Q(1+\epsilon) \approx 2B(1-B)A\epsilon^{-\alpha}, \tag{3.44}$$

with $0 < \epsilon < \epsilon^*$ for the first two expressions and $0 < \epsilon < 2\epsilon^*$ for the third one.

For $\alpha \leq 1/2$ these are the only two divergences present in each of the distributions $P(\eta)$ and $Q(\eta)$. However, when $1/2 < \alpha \leq 2/3$ another set of such points, and associated singular behavior in the corresponding neighborhoods, emerges due to the convolution integral of equation (3.23). The singularities of this set are characterized by an exponent $1 - 2\alpha$. Let us briefly explain how such a set of non-dominant singularities emerges. As mentioned before, the convolution of equation (3.23) gives a divergences at $Q(\eta = 2)$ with exponent $1 - 2\alpha$, due to the integration over the divergence at $\eta = 1$. Substituting the distribution $P(1+\epsilon)$ by its singular form (3.41), we find:

$$Q(2+\epsilon) \approx (1-B)^2 A^2 f_{\alpha,\alpha} \epsilon^{1-2\alpha} \tag{3.45}$$

for $0 < \epsilon < \epsilon^*$, where $f_{x,y} = \int_0^1 dw\, w^{-x}(1-w)^{-y}$ is the Beta function (which usually is denoted by $\mathrm{B}(1-x, 1-y)$; here, we avoid the conventional notation to spare any confusion with the fraction of unused channels B). Similarly, it can be seen that also for the regions near $\eta = \{0, 1\}$ there is a subdominant singular contribution, with exponent $1 - 2\alpha > -\alpha$, given by the convolution integral.

This divergence emerging at $Q(\eta = 2)$, with exponent $1 - 2\alpha < 0$, propagates in the distribution to other lower positions η. Equation (3.24) implies the existence of divergences

with the same exponent at $P(3/2) \approx Q(2)$ and $P(1/2) = Q(1/2)/2 + Q(2)$. These, by equation (3.23), imply divergences $Q(3/2) \approx 2BP(3/2)$ and $Q(1/2) \approx 2BP(1/2)$. The divergence of $Q(1/2)$ does not propagate to anywhere else, however the one in $Q(3/2)$ is related to divergences at $P(5/4) \approx Q(3/2)$ and $P(1/4) = Q(1/4)/2 + Q(3/2)$, and so forth, giving rise to successively more singularities with exponent $1 - 2\alpha < 0$.

Therefore, when $1/2 < \alpha < 2/3$, in addition to divergencies at $\eta = 0$ and $\eta = 1$, we find a divergence at $Q(\eta = 2)$ with exponent $1-2\alpha$, from which follows an infinite set of divergences, on both $P(\eta)$ and $Q(\eta)$, at positions $\eta = 2^{-n}$ and $\eta = 1 + 2^{-n}$, for $n = \{1, 2, \dots\}$. All these singularities are related with the one at $P(\eta = 0)$, since they are sequentially implied from it by the model's equations. Thus, we can write an expression for each them only in terms of the fraction of inactive channels B and amplitude A (as defined by equation (3.41)):

$$\begin{aligned} P(2^{-n} + \epsilon) &\approx \frac{Q(2^{-n} + \epsilon)}{2B} \approx \frac{P(1 + 2^{-n} + \epsilon)}{1 - B} \\ &\approx \frac{Q(1 + 2^{-n} + \epsilon)}{2B(1 - B)} \approx \frac{1 - B}{2B^{1+n}} A^2 f_{\alpha,\alpha} \epsilon^{1-2\alpha} \end{aligned} \tag{3.46}$$

for $0 < \epsilon < 2^{-n}\epsilon^*$. (Recall that $\alpha = 1 + \ln B / \ln 2$.)

When α grows past the threshold $1/2$ the shape of the distributions becomes considerably more complicated, with the emergence of an infinite set of singularities with exponent $1-2\alpha < 0$. Actually, this is a trend that continues as α increases up to 1. For example, when α crosses the next threshold, $2/3$, the convolution of equation (3.23) gives yet more divergences at $Q(2 + 2^{-n})$, for $n = \{1, 2, \dots\}$, with exponent $2 - 3\alpha < 0$. And just like before, each of these will propagate downwards, to $P(2^{-n}(1 + 2^{-m}))$, $P(1+2^{-n}(1 + 2^{-m}))$, $Q(2^{-n}(1 + 2^{-m}))$ and $Q(1 + 2^{-n}(1 + 2^{-m}))$, for $n, m = \{1, 2, \dots\}$, maintaining the exponent $2 - 3\alpha$. Furthermore, expressions for these singularities, in terms of B and A, are:

$$Q(2 + 2^{-n} + \epsilon) \approx \frac{(1 - B)^3}{2B^{1+n}} A^3 f_{\alpha,\alpha} f_{\alpha,1-2\alpha} \epsilon^{2-3\alpha} \tag{3.47}$$

for $0 < \epsilon < 2^{-n}\epsilon^*$, and

$$\begin{aligned} P(2^{-n}\left(1 + 2^{-m}\right) + \epsilon) &\approx \frac{Q(2^{-n}(1 + 2^{-m}) + \epsilon)}{2B} \approx \frac{P(1 + 2^{-n}(1 + 2^{-m}) + \epsilon)}{1 - B} \\ &\approx \frac{Q(1 + 2^{-n}(1 + 2^{-m}) + \epsilon)}{2B(1 - B)} \approx \frac{(1 - B)^2}{4B^{2+2n}} A^3 f_{\alpha,\alpha} f_{\alpha,1-2\alpha} \epsilon^{2-3\alpha} \end{aligned} \tag{3.48}$$

for $0 < \epsilon < 2^{-n-m}\epsilon^*$.

Each time α crosses a threshold $(k - 1)/k$, for $k = \{1, 2, \dots\}$, another set of divergent singularities emerges on the distributions, originating from the convolution integral of equation (3.23), characterized by an exponent $k(1-\alpha)-1$. For simplicity, in the following we refer to the singularities characterized by an exponent $k(1 - \alpha) - 1$, by the k^{th}-order singularities.

The two first-order singularities of each distribution are positioned at the peculiar points $\eta = \{0, 1\}$, which were the starting point of the analysis presented in this section. In the presence of second-order divergent singularities, we found an infinite set of those associated with each of the first-order ones, i.e., there are second-order singularities at $\eta = \{0, 1\} + 2^{-n}$ for $n \geq 1$. Additionally, an infinite set of the third-order singularities was found associated

with each of the second-order ones. Furthermore, the third-order singular points of each of these sets similarly concentrate near the position of the second-order points. That is, when there are third-order singularities, they are found at points $\eta = \{0, 1\} + 2^{-n} + 2^{-m}$, for all $m > n \geq 1$, where $\{0, 1\} + 2^{-n}$ are the positions of second-order singular points. The points at which fourth- and higher order divergent singularities emerge follow the same pattern.

The positions of each set of $k^{\text{th}} + 1$-order singularities extend to infinitely close to the associated k^{th}-order point, and we can find one at each distance 2^{-n} (for sufficiently large n), from the k^{th}-order point. However, the region to the right of each $k^{\text{th}} + 1$-order singular point where a power law is a valid approximation also decreases with the same rate, namely as $2^{-n}\epsilon^*$ (see equations (3.46) and (3.48)). Then, near the k^{th}-order singular point, the total fraction of the domain where the $k^{\text{th}} + 1$-order singularities dominate the distribution is constant, and equal to $\epsilon^* \ll 1$. So, the overall behavior near the k^{th}-order singularities does not change significantly due to the set of $k^{\text{th}} + 1$-order singularities, and the dominant contribution in this region comes from the power law corresponding to the k^{th}-order singularity for a fraction $1 - \epsilon^* \approx 1$ of the domain. (This is shown with detail below, in section 3.5.3, namely in Figures 3.8 to 3.11).

Consequently, for most purposes, namely integrations over large intervals, it gives a good approximation to consider only the two dominant singularities, with exponent $-\alpha$, at $\eta = 0$ and $\eta = 1$. These singularities, which correspond to expressions (3.41)–(3.44), concentrate near their positions almost all the weight of the distributions, even when larger order divergences are present.

So far we have described the problem in terms of the fraction of unused channels B, which was used as a proxy for the control parameter. However, the stationary value of B is fixed (non-trivially) by the system's dynamics after an infinite number of iterations, as everything else. Then also B is determined by the actual control parameter, which is $\rho \equiv \langle j \rangle / j_c$. The value of ρ is determined by initial conditions and remains unchanged as the currents move through the system's layers of nodes and directed channels (recall Figure 3.2). To complete the description of this problem, it is essential to make the connection between B and ρ. For that end, we use the fact that the first moment of the stationary distribution is equal to ρ:

$$\begin{aligned}
\rho &= \int_0^\infty d\eta\, \eta P(\eta, \rho) = \int_0^1 d\eta\, \eta P(\eta, \rho) + \int_1^\infty d\eta\, \eta P(\eta, \rho) \\
&= \int_0^1 d\eta\, \eta P(\eta, \rho) + \int_0^\infty d\eta\, (\eta + 1) P(1 + \eta, \rho) \\
&= \int_0^1 d\eta\, \eta P(\eta, \rho) + \int_0^\infty d\eta\, \eta P(1 + \eta, \rho) + \int_0^\infty d\eta\, P(1 + \eta, \rho).
\end{aligned}$$

For $B > 1/2$ the divergences at $\eta = 0$ and $\eta = 1$ can be related as $P(1 + \epsilon) \approx (1 - B)P(\epsilon)$. Then, the last integral combined with identity (3.25) allows us to write:

$$\begin{aligned}
\rho &\approx \int_0^1 d\eta\, \eta P(\eta, \rho) + (1 - B) \int_0^\infty d\eta\, \eta P(\eta, \rho) + (1 - B) \int_0^\infty d\eta\, P(\eta, \rho) \\
&\approx A(2 - B) \int_0^{\epsilon^*} d\eta\, \eta^{1-\alpha} + (1 - B)^2 \\
&\approx (1 - B)^2,
\end{aligned}$$

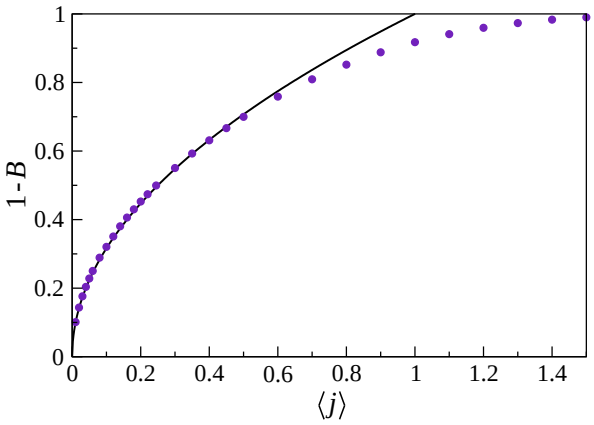

Figure 3.4: Approximation (3.49) (solid line) shows a remarkable agreement with the numerical solution (dots) for the whole region $\rho \lesssim 1/2$ (here $j_c = 1$). Despite it was derived for $B > 1/2$ (which corresponds to $\rho \lesssim 1/4$) this analytical result gives a fair description of the behavior of the fraction of inactive channels for values of ρ up to nearly $1/2$ (to which $B = 0.3002\ldots \approx 1 - \sqrt{1/2} = 0.2929\ldots$ corresponds, i.e., with a $\sim 2\%$ error). As expected, the error of prediction (3.49) diminishes with decreasing ρ, being $\sim 1\%$ for $\rho = 0.24$, $\sim 0.5\%$ for $\rho = 0.1$ and $\sim 0.1\%$ for $\rho = 0.01$.

given that the integration of $\eta^{1-\alpha}$ is surely subdominant. This simple condition finally provides the missing relation between the fraction of inactive channels B and average current ρ:

$$B(\rho) \approx 1 - \sqrt{\rho}. \tag{3.49}$$

The previous calculation uses an approximation valid when $B > 1/2$, and becomes exact when $\rho \to 0$. Remarkably, this kind of power law strikingly resembles the singular behavior of the order parameter near the critical point, typical for continuous phase transitions, see, for example, expression (1.6). In fact, the previous expression can be put in the standard form $1 - B = (\rho - \rho_c)^\beta$, the critical point here is $\rho_c = 0$, and $1 - B$ plays the role of order parameter. Moreover, on this mean-field model exponent β takes the value $1/2$, corresponding to the prediction of Landau's theory, which is exact above the upper critical dimension. Interestingly for a mean-field model, this transition occurs at zero temperature ($\rho_c = 0$), something typically observed in 1-dimensional models.

Furthermore, the amplitude A, of the dominant singular term in the expansion of distribution $P(\epsilon)$ (expression (3.41)), may also be estimated using the normalization condition. (Recall that the amplitude of all other singularities are expressible in terms of A). Approximating the distribution to the truncated form given by equations (3.41) and (3.43), i.e., as power laws in the range $0 < \epsilon < \epsilon^*$, for some small ϵ^* still unknown, and as zero outside this

range, the condition can be written as:

$$1 - B \approx \int_0^{\epsilon^*} d\epsilon\, P(\epsilon) + \int_0^{\epsilon^*} d\epsilon\, P(1+\epsilon),$$

$$\approx A(2-B)\int_0^{\epsilon^*} d\epsilon\, \epsilon^{-\alpha},$$

$$\approx A(2-B)\frac{{\epsilon^*}^{1-\alpha}}{1-\alpha}. \tag{3.50}$$

This expression might appear to be insufficient to find the relation of A with ρ, because it also depends on ϵ^*, of which we know nothing so far. However, let us proceed to write the exponent α in terms of the control parameter, combining relations (3.49) and (3.38):

$$\alpha \approx 1 - \frac{\sqrt{\rho}}{\ln 2}, \tag{3.51}$$

where we used the approximation $\ln(1-\sqrt{\rho}) \approx -\sqrt{\rho}$ for small ρ. Then, we substitute B and α by their dependence upon ρ in expression (3.50):

$$\rho^{1/2} \approx A \ln 2\,(1+\rho^{-1/2}){\epsilon^*}^{\sqrt{\rho}/\ln 2}.$$

This shows that, in fact, the variation of ϵ^* with ρ is not so important. The factor ${\epsilon^*}^{\sqrt{\rho}/\ln 2} \to 1$, when $\rho \to 0$, canceling the expression's dependence on ϵ^*. Then, for small enough currents, the dependence of A on ρ is simply given by:

$$A \approx \frac{\rho}{\ln 2}. \tag{3.52}$$

In this section, we developed a theory concerning the low average current regime of a random network flow. The unusual properties of the stationary current distribution, which determines all other statistical quantities related with the stationary flow, are discovered analytically from the exact equations for the infinite system (3.7) to (3.10). Next, we will compare the results of the preceding sections, with the actual (numerical) solution of the equations, and verify the range of applicability of the approximations employed. A priori, we can expect a quality improvement of our estimations for smaller ρ, moreover, our predictions should maintain a reasonable quality for values of ρ up to $\approx 1/4$ (i.e., the value of ρ below which B becomes larger than $1/2$, according to expression (3.49), and the first divergences appear).

3.5 Numerical Solution of the Model's Equations

To find the stationary distribution of current among nodes and edges, we iterate equations (3.2), (3.3) and (3.4) in this sequence, repeatedly, which is equivalent to simulating the infinite system. Since everything scales with $\langle j\rangle/j_c$, we take $j_c = 1$ without any loss of generality, and start from a uniform initial probability density distribution $P(j,0)$. The average current is conserved, but the shape of the distributions changes at each iteration. When $t \to \infty$, the distributions converge to the stationary solution that corresponds to the value of $\langle j\rangle$ fixed by the initial conditions. Therefore, for each $\langle j\rangle$ the choice of the initial distribution's particular shape does not affect the desired solution, which depends only on the first moment of $P(j,0)$.

3.5.1 Technical Remarks

The implementation of a numerical procedure is not completely straightforward, and deserves a few remarks. First of all, we can only perform a finite number of calculations. Then, the continuous variable j is introduced in our computer program a set of N discreet points, $\{j_{i\leq N}\}$, (close to each other) spread in the interval $[0, j_{\rm m}[$, where $j_{\rm m} \gg \langle j\rangle$ is some point above which the distributions $P(j,t)$ and $Q(j,t)$ are hardly distinguishable from 0. Furthermore, at each time step t we optimize the points' positions. This is achieved by requiring the following integration, over intervals between consecutive points, to give the same value for all such intervals:

$$\begin{aligned}\int_{j_i}^{j_{i+1}} dj\ \left(P(j) - P(j_i) - P'(j_i)(j-j_i)\right)^2 &\approx \int_{j_i}^{j_{i+1}} dj\ \left(P''(j_i)(j-j_i)^2\right)^2,\\ &= P''^2(j_i)\int_0^{j_{i+1}-j_i} dj\, j^4,\\ &= P''^2(j_i)\,(j_{i+1}-j_i)^5\,. \end{aligned} \tag{3.53}$$

On other words, for a fixed N we adjust the distribution of points $\{j_i\}$ on the interval $[0, j_{\rm m}[$ in the following way: the integration over each interval $[j_i, j_{i+1}[$, of the square difference between the actual distribution and the linear part of its series expansion, should be the same for all intervals, say c. Notice that the linear part of the distribution's behavior can be accurately described in a small interval, just by the values of $P(j)$ at the ends of the interval (which we know). Then, errors introduced by the discretization of j are essentially due to the non-linear part of curve's the behavior, for large N. Clearly, the requirement that expression (3.53) gives c for every interval causes the length $j_{i+1}-j_i$ to be smaller in the regions where $P''(j)$ is larger; while conversely, in the regions where $P(j)$ behaves closer to linearly, the length of the intervals increases. Then, we can write for the adjusted distribution of points

$$\begin{aligned} c &= \frac{1}{N}\sum_{i=1}^{N} P''^2(j_i)\,(j_{i+1}-j_i)^5\,,\\ &\cong \frac{1}{N}\int_0^{j_{\rm m}^5} dj\, P''^2(j^{1/5}),\\ &= \frac{5}{N}\int_0^{j_{\rm m}} dj\, j^{4/5} P''^2(j), \end{aligned}$$

and find the value of c. The actual adjusted positions are given by requiring expression (3.53) to be equal to c for every pair of consecutive points. Additionally, we use a cubic spline interpolation to update the distributions $P(j_i,t)$ and $Q(j_i,t)$ for the new positions of $\{j_i\}$; which is followed, of course, by the updating of the spline interpolation itself.

This adjustment ensures a higher density of points in the regions where the curves have stronger curvature, which minimizes the error on any interpolation procedure implemented afterwards. As was shown in the previous section, in some regions the distributions are expected to have a rather abrupt behavior (namely near the singularities). Therefore, the adjustment of the density of points becomes very important to achieve a good description of the distributions in those regions, without increasing the number of points N beyond our

capabilities. The sets of points $\{j_i\}$ corresponding to distributions $P(j_i, t)$ and $Q(j_i, t)$ are considered separately, and any calculations involving points inside the intervals $[j_i, j_{i+1}[$ use the splines mentioned above.

In the end of section 3.2, it was noted that the distributions have discontinuities at j_c, even when the fraction of inactive channels $B < 1/2$, and there is no divergence at j_c. Therefore, one should always consider at least two separate intervals, $[0, j_c[$ and $[j_c, j_\mathrm{m}[$, on the interpolation of the distributions' curves and for numerical integrations. Furthermore, the points of all non-dominant singularities (others than the ones at 0 and j_c) are either divergent (if B large enough) or continuous, then further interval divisions are required only when more divergences emerge. On other words, if B is large enough, the distributions will diverge at certain points, each of which corresponds to the left-most point of a separately considered interval.

Let N_n be the number of points in interval n. The highest point of the discreet set $\{j_{i \leq N_n}\}$, corresponding to each such interval, is set equal to the right-most point of the interval (recall that the singularities are divergent only from above). However, the lowest point of each separate set, j_1, must be larger than the left-most point of the corresponding interval, where the distribution actually diverges. For example, for the interval corresponding to the singularity at $j = 0$, we take some small value j^0 as the first point of the set, i.e., $j_1 = j^0 > 0$, where the distribution is finite, and apply the interpolation to the region above j_1. Any calculation involving points between the singularity at 0 and the first interpolation point j_1 uses the approximation (3.31) that becomes exact in the limit $j^0 \to 0$. We do this also for the divergence at j_c, for which the first point of the set is at $j_c + j_0$, and for all other divergences present in the distribution as well. Furthermore, the proper size of the interval between each singularity and the first point of the corresponding discreet set can be found by identifying j^0 with ϵ^* in equations (3.41) to (3.48). These are also the expressions that describe the stationary distributions in the regions close above the singularities. Additionally, the introduction of a j^0 also prevents us from having to deal with an infinite number of singularities that appear for the first time when B becomes larger than $1/\sqrt{2}$, at positions infinitely close to the other singularities of lower order (as described in previous section).

Not only the exponents and the validity regions of the singular power laws are related to each other by equations (3.41) to (3.48); the amplitudes are related too. It should be noticed, however, that starting from a non-divergent distribution, at $t = 0$, the divergences can only develop after an infinite number of steps, i.e., in the stationary regime. For the numerical iteration of the model's equations, when $B(t)$ becomes larger than $1/2$ we immediately assume the existence of such divergences, with exponents calculated directly from $B(t)$. But, we disregard the relation between power-law amplitudes, and sew each singularity together with the corresponding interpolation part of the interval, by setting the amplitude such that the power law at j_1 is equal to $P(j_1, t)$. Nevertheless, after a large number of iterations the distributions should converge to their stationary forms, and the amplitudes found by the sewing procedure should verify the mentioned relations, if j^0 is sufficiently small.

Finally, let us point out that the low average current regime is expected to require a highest computational effort, since more intervals need to be considered separately. Especially the evaluation of equation's (3.2) convolution integral: for each point of the distribution $Q(j_i, t)$, the integral has to be divided in intervals such that the points where the integral argument's factors ($P(u)$ and $P(j_i - u)$) diverge are at endpoints of the integration intervals. This separation of the integration interval in smaller ones ensures that the numerical integration does not assume continuity at points where the distribution diverge, which might introduce

major errors in the calculations. However, the computational cost of the integral separation increases with the square of the number of divergences. The number of divergences itself, grows exponentially with the maximum order k of divergences present in the distribution. And k grows as $1/(1-\alpha) = -\ln 2/\ln B \propto \langle j\rangle^{-1/2}$. Consequently, the computation time for some fixed j^0 and number of iterations should grow exponentially with $\langle j\rangle^{-1/2}$, for small $\langle j\rangle$.

3.5.2 High Current

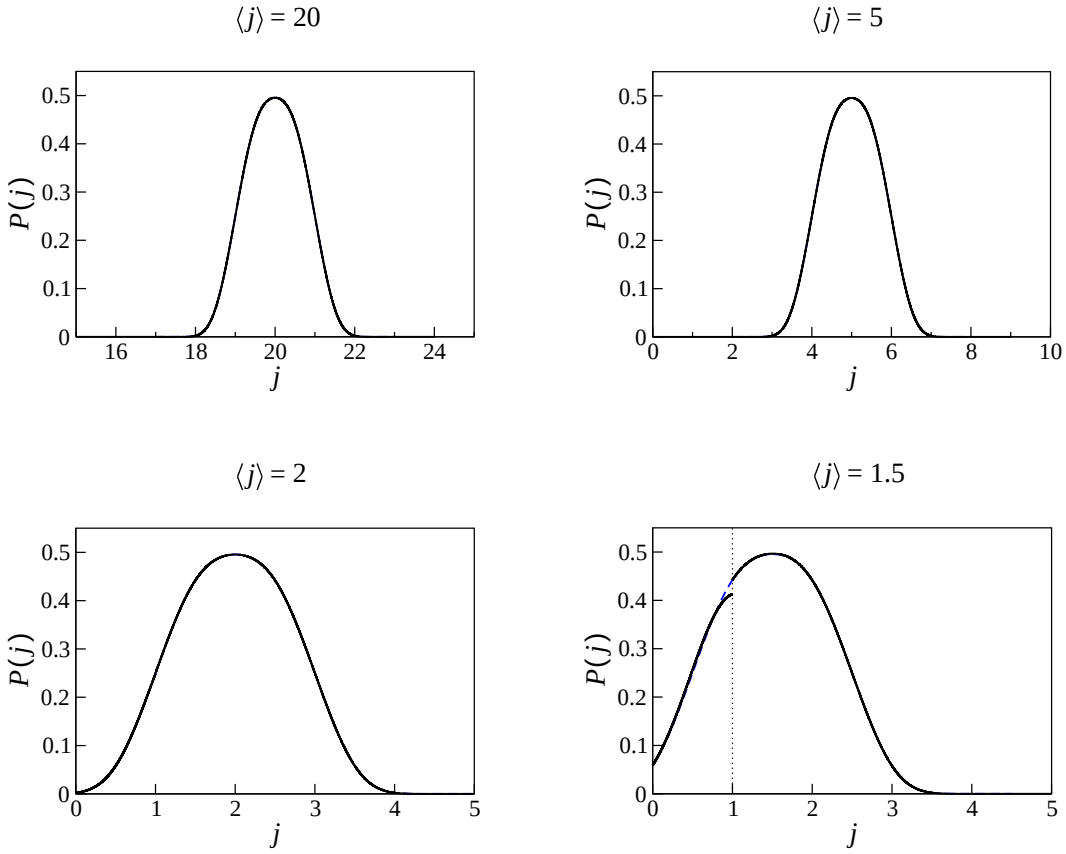

Figure 3.5: Stationary distribution $P(j)$ for different values of the average current (in all cases we used $j_c = 1$). These curves were obtained by iterating 10^4 times the model's equations, for a uniform $P(j, 0)$ with the corresponding $\langle j\rangle$. The solution of the Laplace transform (plotted as a dashed blue line), derived exactly for the infinite $\langle j\rangle$ limit, is indistinguishable of the numerical solution (solid black line) for $\langle j\rangle$ down to around 2. Even for $\langle j\rangle = 1.5$, despite a small discrepancy in the region close below j_c, the analytical solution for the high current regime still gives a good approximation of the actual curve.

The divergences only emerge in the distribution when the fraction of inactive channels $B > 1/2$. So, in the region $\rho \gtrsim 1/4$ there is only one non-divergent discontinuity at j_c in each distribution. Then, for the numerical iteration of equations (3.2) to (3.4) in the high average current regime, we need to consider only two intervals, namely $[0, j_c[$ and $[j_c, j_m[$, and we can

set $j^0 = 0$ ($j_{\rm m}$ and j^0 where defined above, in section 3.5.1).

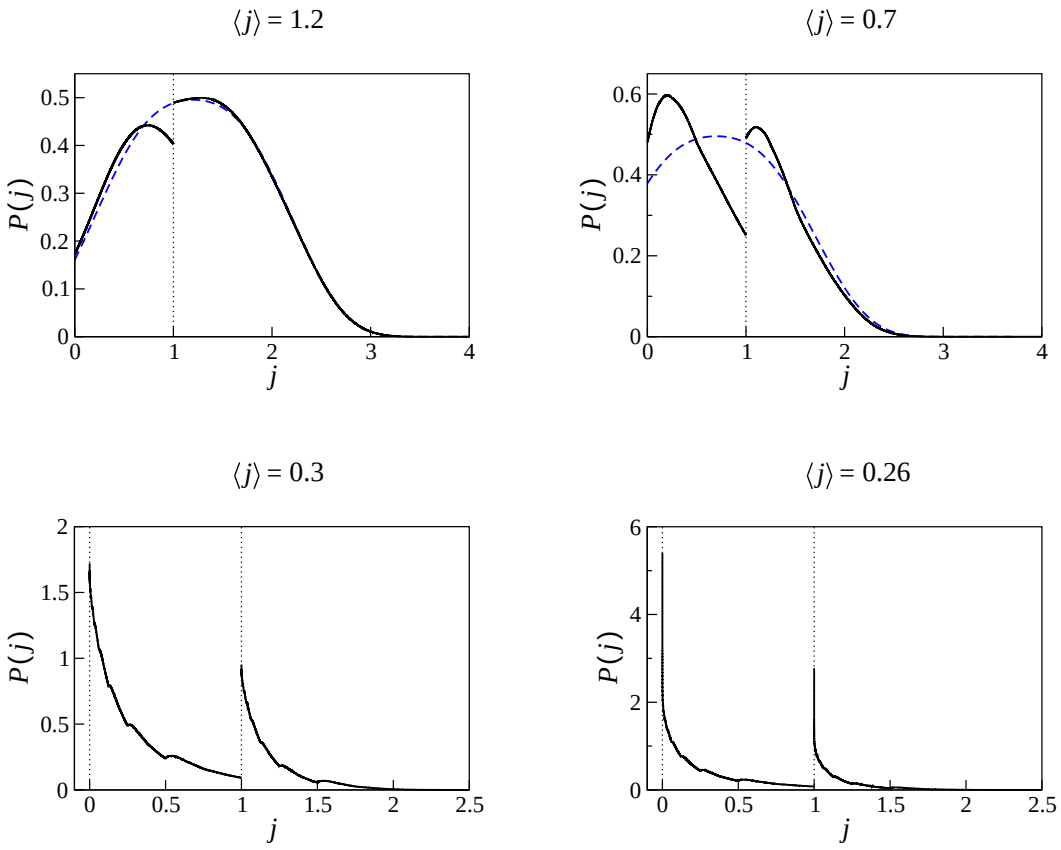

Figure 3.6: Stationary distribution $P(j)$ for several values of $\langle j\rangle$ below 1.5, but above the low current regime ($\langle j\rangle \lesssim 0.25$). Also for these results, the model's equations were iterated 10^4 times for a uniform initial distribution and $j_c = 1$. The high average current solution (dashed blue line) is shown only on the two top panels ($\langle j\rangle = 1.2$ and 0.7), where one can still find some similarities. The bottom panels ($\langle j\rangle = 0.3$ and 0.26) already show a strong concentration of the distribution's weight in the regions above 0 and j_c. Note the sharp increase of $P(0)$ (and $P(1^+)$) from $P(0) \approx 1.7$ for $\langle j\rangle = 0.3$ to $P(0) \approx 5.4$ for $\langle j\rangle = 0.26$.

Numerical results are plotted in Figure 3.5 for different values of $\langle j\rangle$ in the high average current regime, against the exact solution (3.15). (For the purpose of checking the analytic results, it is enough to show curves only for distribution $P(j,t)$). This solution found for the $\langle j\rangle \to \infty$ limit turns out to give an excellent description of the actual curves for finite $\langle j\rangle$ as low as 1.5. When $\langle j\rangle$ decreases below 1.5 the discrepancies (between the numerics and expression (3.15)) begin to increase. Figure 3.6 shows how the distribution $P(j,t)$ gradually concentrates in the regions above 0 and j_c with decreasing $\langle j\rangle$, still larger than 0.25. In the preceding section 3.4 was shown that for $\langle j\rangle \lesssim 0.25$ one should expect divergences to emerge; results for that region (here called the low average current regime) are discussed in detail below.

The main divergent singularities, characteristic for the low average current regime, are

present at 0 and j_c only for $B > 1/2$ (which corresponds to $\langle j \rangle \lesssim 0.25$). On the other hand, expression (3.40) predicts that $P(0)$, as well as $Q(0)$, $P(j_c^+)$ and $Q(j_c^+)$, diverge with $(1/2 - B)^{-1}$ when B approaches $1/2$ from below. In Figure 3.6 it seems that $P(0)$ exhibits this kind of qualitative behavior. However, to check this expression quantitatively (i.e., the exponent), it is perhaps more appropriate to plot $P(0)$ as a function of $(1/2 - B)^{-1}$, as shown in Figure 3.7.

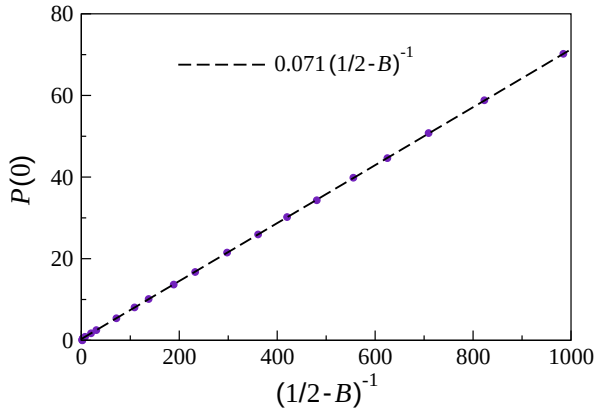

Figure 3.7: The stationary value os $P(0)$ diverges with $(1/2 - B)^{-1}$ as B approaches $1/2$ from below

Indeed, $P(0)$ appears to grow linearly with $(1/2 - B)^{-1}$, when B approaches $1/2$ from below. The value of the control parameter $\langle j \rangle$ for which $B = 1/2$ is predicted by the theory to be nearly 0.25 (since, for $B > 1/2$, we found that $1 - B \approx \sqrt{\langle j \rangle / j_c}$). The numerical work shows that B crosses the threshold $1/2$ approximately when $\langle j \rangle = 0.246$. The accuracy of that result already indicates that the approximations used in section 3.4 for low current introduce only a small error (even when $B \downarrow 1/2$), and one can expect a fair agreement between the numerics and the theory for the whole range $\langle j \rangle < 0.246$.

3.5.3 Low Current

In the end of section 3.4 we show a comparison between the relation $1 - B = \sqrt{\langle j \rangle / j_c}$, for the low average current regime, and numerical results (Figure 3.4). The remarkable agreement between the two, in the region $\langle j \rangle \lesssim 1/4$ (for $j_c = 1$), strongly supports our approach. For values of $\langle j \rangle$ larger than $0.246 \sim 1/4$, up to ~ 0.5, the behavior of B is still well described by the theoretical curve. Given the agreement for $\langle j \rangle \lesssim 1/4$ this is not surprising, since $P(0)$ and $P(j_c)$, while remaining finite, approach large values when $\langle j \rangle$ is close above 0.246. (Recall that it was possible to derive this relation thanks to the existence of divergences on $P(0)$ and $P(j_c)$).

For values of the average current such that $0 < \alpha < 1/2$, the current distributions have divergences only at $j = 0$ and j_c. In Figure 3.8 we show numerical results for $\langle j \rangle = 0.16$. We find that the fraction of inactive channels in this case is $B = 0.5939(1)$, which corresponds to the exponent $\alpha = 0.2483(2)$, according to expression (3.38).

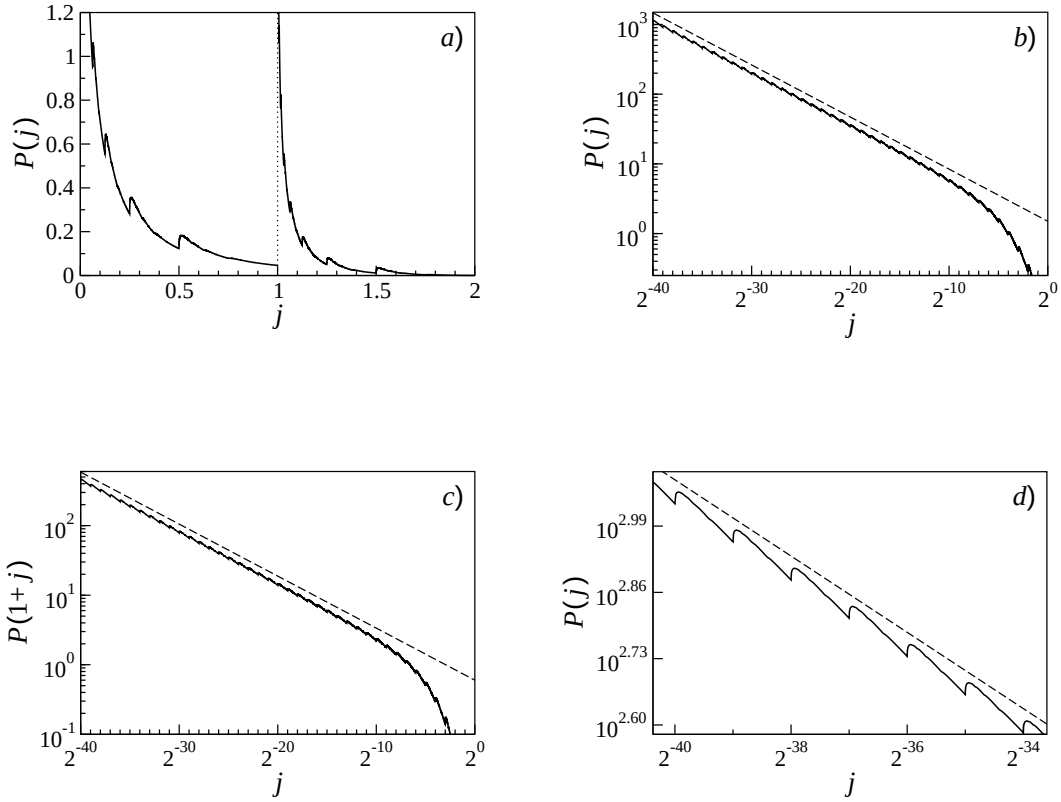

Figure 3.8: Stationary distribution $P(j)$ for $\langle j \rangle = 0.16$ (with $j_c = 1$). The model's equations were iterated 10^4 times. On panel (a) the distribution is represented in a linear scale. Panels (b) and (c) plot the distribution in a logarithmic scale, demonstrating the power-law singularities near 0 and $j_c = 1$, respectively. In each of these plots, the dashed line corresponds to a power law with exponent $-\alpha = -0.2483$. The overall behavior of the distribution near the singularities is correctly predicted by our analytical results, namely by the expression $\alpha = 1 + \ln B / \ln 2$. Panel (d) shows a small top-right portion of the curve (c), notice small periodic oscillations around the overall singular behavior, which are explained in the text.

The distributions obtained numerically verify the existence of these singularities with exponents correctly predicted by the theory (as shown by the dashed lines of Figure 3.8). This figure also shows that the range over which the power laws $P(j) \propto P(1+j) \propto j^{-\alpha}$ are valid approximations of the current distribution (i.e., ϵ^*, as denoted in section 3.4) is of the order of 10^{-3} or 10^{-4}, for $\langle j \rangle = 0.16$. The choice of a logarithmic scale of base 2 in Figure 3.8 is motivated by the fact that second-order singularities in this model (with exponent $1 - 2\alpha$) appear at distances 2^{-n} of the dominant ones, where n is positive integer. The same kind of representation is used on Figures 3.9 and 3.10 for $\langle j \rangle = 0.08$ and 0.04, respectively.

Figure 3.8(d) shows a small region above the dominant singularity at $j = 0$. In this region, small periodic oscillations are visible around the power law of exponent $-\alpha$. The origin of the oscillations is similar to the origin of the non-dominant divergences, which emerge when $\alpha > 0.5$ (explained in the preceding of relations (3.46) for the second-order divergences, in section 3.4). However, here $\alpha = 0.2483 < 0.5$ and the power-law singularities, at positions $j = 2^{-n}$ and $1 + 2^{-n}$ $(n \geq 1)$, are characterized by positive exponents $0 < 1 - 2\alpha < 1$.

Then the distribution remains finite and continuous at the non-dominant singularities, but its derivative diverges at those points, giving rise to these oscillations. In a logarithmic scale the oscillations appear to be periodic, which is also predicted by the set of relations (3.46), between singularities.

If we continue to decrease the average current, exponent α will increase and eventually the second-order singularities start taking negative exponents $(1-2\alpha)$. Then, the distributions will diverge also at those positions. According to our analytical results this will occur when

$$1/2 < \alpha = 1 + \ln B/\ln 2 \approx 1 + \ln\left(1 - \sqrt{\langle j\rangle}\right)/\ln 2,$$

i.e., when $\langle j\rangle \lesssim 3/2 - \sqrt{2} = 0.0858\ldots$. It should be emphasized that in the expression above, the equality relating α and B holds exactly, while the relation between B and $\langle j\rangle$ is an approximation. The quality of the approximation is very high is this regime (as is shown in Figure 3.4), but it is not an exact relation.

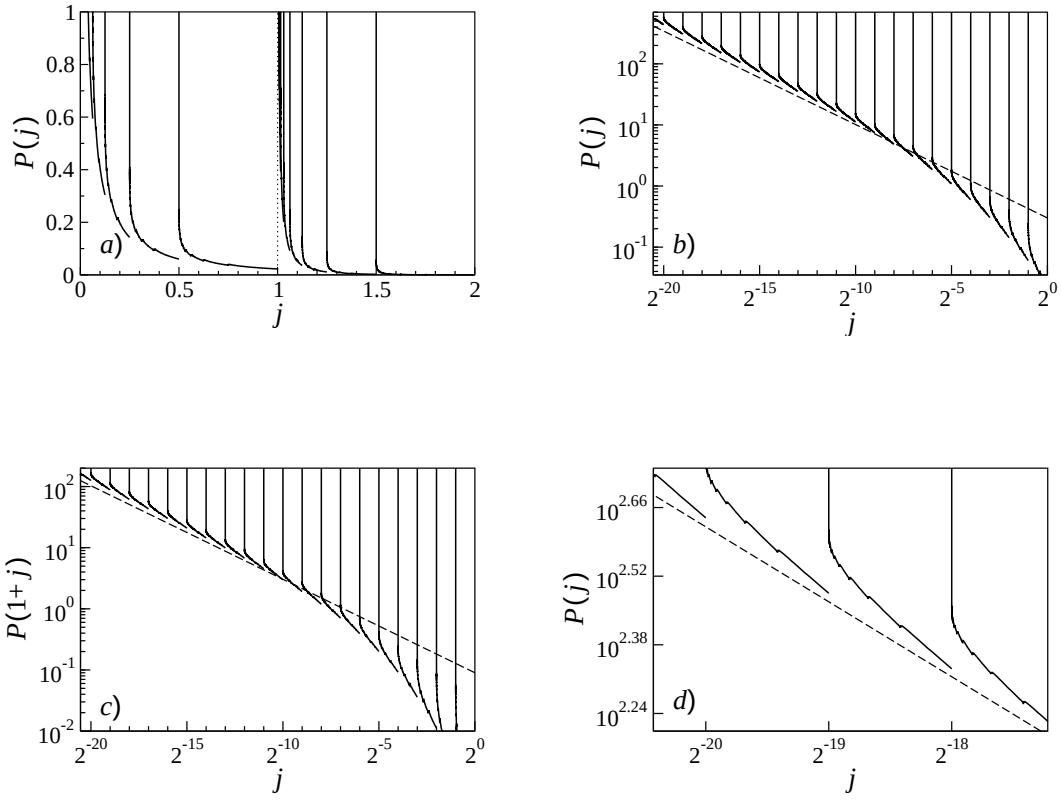

Figure 3.9: Stationary distribution $P(j)$ for $\langle j\rangle = 0.08$ (with $j_c = 1$). The model's equations were iterated 10^4 times. Each panel shows the same aspects of the distribution that the corresponding one of Figure 3.8, for $\langle j\rangle = 0.16$. The dashed lines in panels (b), (c) and (d) represent power laws with exponent $-\alpha = -1 - \ln B/\ln 2 = -0.5080$.

Figure 3.9 shows the numerics for $\langle j\rangle = 0.08$ (in a similar way to Figure 3.8 for $\langle j\rangle = 0.16$). The fraction of inactive channels in this case is $B = 0.7110(1)$, which is very close

to the approximate result $1 - \sqrt{\langle j \rangle} = 0.7171\ldots$. Then, $\alpha = 0.5080(2) > 1/2$ and the second-order singularities, located at positions 2^{-n} and $1 + 2^{-n}$ for $n \geq 1$, will be divergent too. As well as for $\langle j \rangle = 0.16$, the exact relation $\alpha = 1 + \ln B / \ln 2$ is entirely consistent with the numerics for this value of average current. The overall behavior of the curves of Figure 3.9(b) and (c) becomes linear (in logarithmic scale), and parallel to the dashed line on the region of $j < \epsilon^*$. (The dashed line is a power law with exponent $-\alpha$ and amplitude chosen for graphical convenience.) For $\langle j \rangle = 0.08$ the range ϵ^* is not much different than for $\langle j \rangle = 0.16$ ($\epsilon^* \sim 10^{-3}$ or 10^{-4}). In Figure 3.9(d) each curve corresponds to a second-order divergent singularity, at 2^{-n}. Those are seen to be have some irregularities, located at the positions of third-order singularities (which are still non-divergent, since $2 - 3\alpha > 0$). For α above 2/3 these points also are expected to exhibit divergences.

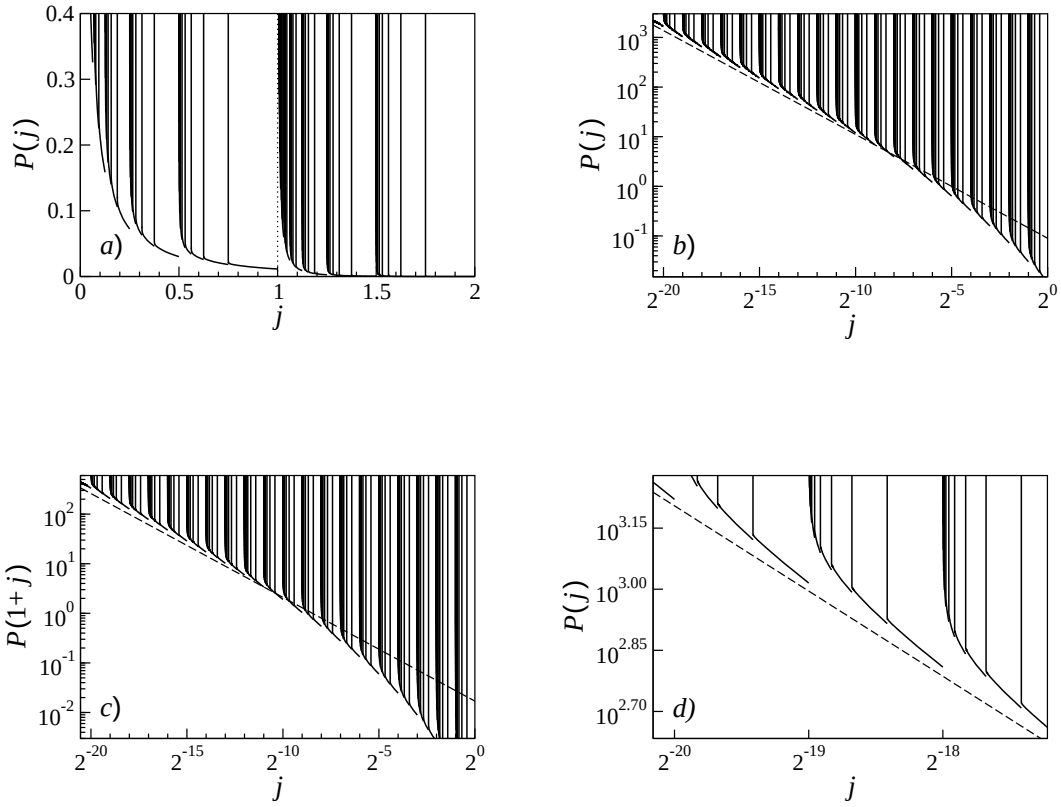

Figure 3.10: Stationary distribution $P(j)$ for $\langle j \rangle = 0.04$ (with $j_c = 1$). The model's equations were iterated 10^4 times. Each panel shows the same aspects of the distribution that the corresponding one of Figures 3.8 and 3.9, for $\langle j \rangle = 0.16$ and 0.08 respectively. The dashed lines represent power laws with exponent $-\alpha = -1 - \ln B / \ln 2 = -0.6697$.

For $\langle j \rangle = 0.04$ the fraction of inactive channels is $B = 0.7954(1)$, and the exponent $\alpha = 0.6697(2)$ becomes larger than 2/3. Figure 3.10 shows several aspects of the stationary current distribution for this values of $\langle j \rangle$, identically to Figures 3.8 and 3.9. The range of validity of the power laws, ϵ^*, for $\langle j \rangle = 0.04$ is again of the order of 10^{-3} to 10^{-4}, similarly

to the larger values of the average current considered above.

Since $\alpha > 2/3$, for $\langle j \rangle = 0.04$, the third-order singularities also exhibit divergent behavior as can be seen in Figure 3.10. Panel (d) shows an enlargement of the left-hand side region of (b), demonstrating that the third-order order singularities are also divergent. (Recall from section 3.4 that the singularities of exponent $2 - 3\alpha$ appear at the points $j = 2^{-n} + 2^{-m}$ and $1 + 2^{-n} + 2^{-m}$, for $m > n \geq 1$.) For a better view of these divergences we plot the distribution around a second-order singularity. Particularly, in Figure 3.11, we plot the distribution $P(2^{-6} + j)$ as a function of j in logarithmic scale.

The numerical results plotted in Figure 3.11 show that the overall behavior near the second-order singularities is consistent with what was found in section 3.4, i.e., a power law with exponent $1 - 2\alpha$, as it should be near every divergent singularity. Also the power law's range of validity for the singularity at 2^{-6}, is correctly predicted by the theory, namely, it is about $2^{-6}\epsilon^*$ in agreement with expression (3.46), (recall that ϵ^* is of the order of 10^{-4} to 10^{-3}).

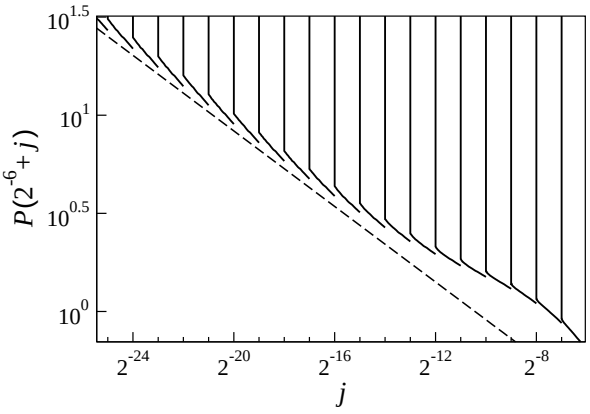

Figure 3.11: Behavior of the stationary distribution $P(j)$ for $\langle j \rangle = 0.04$ (with $j_c = 1$) near the second-order singularity at $j = 2^{-6}$. The dashed line is a power law of exponent $1 - 2\alpha = -0.3395$. Thanks to the logarithmic scale of base 2, it is clear that the positions of the third-order divergences are at the points $j = 2^{-6} + 2^{-m}$, for $m \geq 7$ (for $m = 6$ we get $j = 2^{-5}$ which is actually the point of another second-order singularity).

Furthermore, as mentioned above, the power-law amplitudes relations, given by expression (3.46), were not used in the numerical iteration of the model's equations. Nevertheless, the amplitudes calculated by sewing the distribution with the power laws of exponent $1 - 2\alpha$, verify the analytical relations with errors of at most 1% in our numerics. On the other hand, expression (3.48), for third-order singularities, is also verified by the numerics, but with larger errors (in some cases up to 10%). This happens because the sizes of the regions of validity of the power laws become smaller, and the exponent is actually very low for $\langle j \rangle = 0.04$ $(2 - 3\alpha = 0.0093(5))$, which introduces much larger errors. For smaller $\langle j \rangle$, the exponent $2 - 3\alpha$ becomes higher, which might allow more precise measurements on the numerical data, and to find better quantitative agreement between the expressions for third- and higher order divergences. However, when $2 - 3\alpha$ becomes higher there are more orders of singularities

diverging in the distribution. For instance, when $2 - 3\alpha > 0.5$ there are at least six orders of divergences, which, as discussed above, leads to a dramatic increase of the computation time, forcing us to increase j^0 and reducing the quality of the numerics. Regardless, in the regime $\langle j \rangle \lesssim 1/4$, the numerical results above show an excellent agreement with the analytical results of section 3.4, and fully support them.

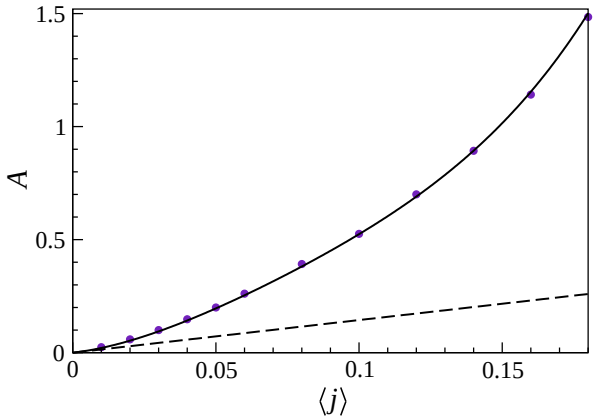

Figure 3.12: Relation between amplitude A and average current. The circles correspond to the numerics of this section. The dashed line is the linear expression (3.52), and the solid one corresponds to the polynomial form $\langle j \rangle / \ln 2 + 70\langle j \rangle^2 - 500\langle j \rangle^3 + 1800\langle j \rangle^4$. The linear expression, derived in section 3.4, is a good approximation only for very small $\langle j \rangle \ll 1/(70 \ln 2) \approx 0.02$.

Finally, in section 3.4 we derived expression (3.52), for the amplitude A of the singularity at $j = 0$ ($P(j) = Aj^{-\alpha}$, for $j \to 0$), in the limit of average current going to zero. Recall that the amplitudes of all other singularities were found in terms of this one. It should be emphasized that this relation is expected to hold in a much smaller range of $\langle j \rangle$, near zero, than all other relations derived in that section (which are valid for $\langle j \rangle \lesssim 1/4$). To derive the very simple expression $A \approx \langle j \rangle / \ln 2$, we have actually assumed that $\langle j \rangle \to 0$ and found only the first term of the corresponding series expansion. In Figure 3.12 we show the value of A obtained numerically for several values of $\langle j \rangle \lesssim 1/4$. The dashed line on the Figure corresponds to the linear law $\langle j \rangle / \ln 2$. The actual value of A deviates substantially from the linear dependence for $\langle j \rangle > 0.01$. However, the dependence can be reasonably well fitted by the polynomial $\langle j \rangle / \ln 2 + 70\langle j \rangle^2 - 500\langle j \rangle^3 + 1800\langle j \rangle^4$, as shown by the solid line.

3.6 Discussion and Conclusions

In the present chapter of this thesis we have proposed a model of network flow, with an optimization driven local dynamics. In particular, we study the stationary distribution of flow in a directed network where each node has two outgoing channels and two incoming

ones. We introduce at random an asymmetric preference for the current to exit the node by one of the two outgoing channels. When, at a node, the current is below a threshold j_c, defined to be equal for every node, it exits the node entirely by the preferred channel, and leaves the other channel inactive. When the current at a node is larger than j_c, it splits into two asymmetrically, according to expression (3.1). This kind of asymmetric optimization at bifurcations of network flows seems to occur naturally in several real systems. At the beginning of this chapter we mentioned the examples of vehicular traffic between two locations connected by two different roads, and the discharge of water from rivers into the ocean, or lakes, through systems of channels geologically formed on the rivers deltas.

Furthermore, as was discussed above, the model with nodes organized in layers, introduced in the end of section 3.1, can also be regarded as a random network, where the only restriction is that every node has one outgoing edge of each type and any two incoming ones. For the purposes of the flow process both structures here considered are equivalent.

The evolution of this network flow model is exactly described by the iterative equations (3.2) to (3.4), in the infinite system size limit, $N \to \infty$. Those equations, which relate the probability density distributions of current on nodes and channels at consecutive times, were derived directly from the microscopic mechanisms acting in the system. It is possible to iterate such equations for any arbitrary initial distribution, and, after a large enough number of iterations, find the form of stationary distributions. According to the model's rules, the amount of current in the system is conserved at all stages of the dynamics. Thus, the value of average current at nodes (and channels) stays constant in time and is determined by the initial distribution. The particular form of the stationary distribution achieved in this way must then correspond to that value, fixed by initial conditions. (The numerical iteration of the model's dynamical equations (3.2)–(3.4), which actually corresponds to the simulation of the infinite system's evolution, is performed for several values of the average current. The numerical solutions obtained in this way are then compared with our theoretical results, in section 3.5).

In our theoretical approach to this problem, we search for stationary distributions of current simply by suppressing the time dependence of model's iterative equations. Then the resulting system of equations (3.7) to (3.9) becomes self-consistent for stationary distributions. However, in doing this, we lose all information about initial conditions, including the average current (which is our control parameter), and these time independent equations admit an infinity of solutions (at least one solution for each possible value of average current). To complete the model's equation system for the stationary distributions, another condition is necessary, one that fixes the average current. Such condition is obtained simply by requiring the first moment of the distribution to be equal to some value fixed by us, which is actually the average current (equation (3.10)). In this manner, the average current naturally arises as the theory's control parameter. Additionally, this choice of control parameter grants the convenience of holding a clear physical interpretation.

In section 3.3 we show that the standard Laplace transform technique succeeds to exactly solve this problem only in the limit of infinite average current. Due to the bipartite form of equation (3.8) (for the asymmetric split of currents at the exit of nodes), the corresponding transformed equation contains non-homogeneous terms, whose contribution vanishes as the average current tends to infinity. Taking this limit, we were able to derive the exact solution (3.15) for the distribution of current among channels, which turns out to be a good approximation for values of average current as low as $\langle j \rangle / j_c \gtrsim 1.5$ as well, see Figure 3.5.

(The solution for the distribution of current on nodes is found simply by putting the solution for the channels into the convolution integral of equation (3.7).)

The breakdown of the Laplace transform method away from that limit, is already a hint for this model's unconventional stationary solutions, in the low current regime. For low average currents, the singular behavior takes over, and the distributions diverge as power laws at certain points. The two dominant singularities can be found at positions $j = 0$ and j_c, in both current distributions (on nodes and channels), and their characteristic exponent, α, varies continuously with the fraction of inactive channels, B, as $\alpha = 1 + \ln B / \ln 2$. Moreover, we find that additional sets of power-law divergences (with subdominant exponents) can develop at other positions of the current distributions, for sufficiently low $\langle j \rangle$. We show how all the singularities are strictly related, and can be expressed in terms of the exponent and amplitude of a single one.

To complete the problem's solution, in the small current regime, we exploit its exotic properties. Assuming that singular behavior in the vicinity of those special points is dominant, we could extract the relation between the control parameter and $1 - B$ (the fraction of active channels), $1 - B \simeq \sqrt{\langle j \rangle / j_c}$. Interestingly, this strongly resembles the relation proposed in [129] for the dependence of the number of active channels present in a river delta on the amount of water flowing through it. There, the authors measured a power law of exponent ~ 0.6 (with low precision), which is rather close to ours, suggesting that they may even be the same, $1/2$. Also the relation between $\langle j \rangle$ and the amplitude of the singularities was found in the limit $\langle j \rangle \to 0$, equation (3.52), however it is a good approximation only for $\rho \ll 0.02$.

Surprisingly, the numerical results, produced by iterating the model's equations and presented in section 3.5, show a remarkable agreement with the theory we developed for this regime, not only for vanishingly small values of the average current, but also up to $\langle j \rangle / j_c \lesssim 1/4$ (and less accurately but still fairly well up to $\langle j \rangle / j_c \lesssim 1/2$, see Figure 3.4). The properties of the distribution in this regime are shown in Figures 3.8 to 3.12. All the numerical data presented in the text and plots results from iterating the equations 10^4 times for every $\langle j \rangle$. We verified that the shapes of distribution after 10^3 and 10^4 iterations are indistinguishable in all considered cases, to ensure that the curves obtained actually correspond to the stationary state.

The curious properties of this dynamical model, found for the low current regime, remarkably resemble the ones characteristic of continuous phase transitions. The divergent power-law singularities of the stationary current distributions already suggest the presence of some kind of "critical-like" behavior. However, the most evident manifestation of critical phenomena is found in the relation between the average current and the fraction of active channels, $1 - B$. It shows a square root singularity, similarly to the order parameter of the continuous thermal phase transitions discussed in section 1.3.1, above the upper critical dimension. In this case, the order parameter $1 - B$ is non-null for all values of the control parameter $\rho = \langle j \rangle / j_c > 0$, then the critical point here is $\rho_c = 0$. Therefore, the model's behavior near ρ_c is typical for continuous phase transitions, with a mean-field exponent, namely $1 - B = (\rho - \rho_c)^{1/2}$, as in the Landau theory, i.e., expression (1.6). The network flow model proposed here appears to undergo a zero temperature phase transition, since the critical point is at $\rho_c = 0$ there is no disordered phase. Only the ordered phase (with order parameter $1 - B > 0$) and the critical point (where $1 - B = 0$) are actually accessible. Interestingly, this kind of transition, typically observed in 1-dimensional models, occurs here under mean-field conditions.

Chapter 4

Conclusions

In chapters 2 and 3 we examined and solved two distinct statistical physics problems. On both cases, the process dynamics is driven by local optimization mechanisms, which lead to the emergence of the discussed critical features. The explosive percolation problem, addressed in chapter 2, possesses a continuous phase transition, in a strict sense, with unique properties. Those result from the application of biased bond occupation rules, according to which the smallest of m random clusters receives the new edge. Surprisingly, the stationary current distribution of the network flow model studied in chapter 3 also revealed several critical-like properties, such as power-law divergences and singular behavior of the order parameter at the critical point, typically observed in continuous phase transitions. In the later case, not all aspects of the transition are completely clear, as they are for the case of explosive percolation. For example, it is not evident what the disordered phase should be, since the critical threshold $\rho_c = 0$ is the only point where the order parameter $1 - B$ vanishes ($1 - B > 0$ for every $\rho > 0$, and the model does not admit negative currents). Moreover, in the analysis of this network flow model, we found no quantity that could be identified as a proper susceptibility, diverging at the phase transition point.

We started chapter 2 by showing that, contrarily to what was initially believed, the so-called explosive percolation is in fact continuous [1], however, this transition shows a uniquely small exponent β. The only assumption made in our initial proof was a power-law decay of the critical cluster size distribution (we observed this power law in the numerical solution of 10^6 evolution equations, similarly to the observations in earlier simulations). Furthermore, we verified the presence of all the usual scaling features of continuous percolation transitions as well. It is now widely accepted that explosive percolation is continuous.

Our rigorous approach to the problem was possible thanks to the elegant mathematical description allowed by the particular model considered. We then proceeded by extending the previous analysis to a set of representative explosive percolation models, which generalizes the one initially considered, and covers the entire range of these optimization-like processes. In particular, we shown that, except the "most explosive" model ($m = \infty$), the transition is always continuous. We also observe the expected scaling behavior of the distributions $P(s,t)$ and $Q(s,t)$, critical singularities of $\langle s \rangle_P$ and $\langle s \rangle_Q$, and derive scaling relations between critical exponents. Moreover, we briefly consider a model mixing the rules from explosive and ordinary percolation, to which we repeat the analysis, with qualitatively similar, and quantitatively intermediate, results. (Those may also be found in reference [2].)

We have also developed a method that enabled us to use the numerical solution of a not so

large number of evolution equations to obtain the critical exponent τ (recall that there is only one independent exponent), the critical time t_c and the amplitude of the critical distribution $f(0)$ [3]. We find that these estimations rapidly converge to the exact values, yielding highly precise results. We suggest that this method could be successfully applied to the numerical study of other continuous phase transitions, characterized by power-law critical distributions.

Finally, we developed a strict scaling theory, which provides the complete solution of this intriguing quest, yielding the full set of scaling functions and critical exponents for each of the models with any desired precision. That theory indicates the relevant order parameter and susceptibility for the problem, and explains the continuous nature of this transition and its unusual properties. Furthermore, by exactly solving the problem below the critical point, we prove that the critical distribution is indeed asymptotically power-law.

In chapter 3 we study the stationary distribution of flow in a directed network, where each node has two outgoing channels and two incoming ones, and there is an asymmetric preference for the current to exit nodes by one of the two outgoing channels. In our theoretical approach to this problem, we search for stationary distributions of current simply by suppressing the time dependence of the model's equations that exactly describe the evolution, in the infinite system size limit. The resulting system of equations becomes self-consistent for stationary distributions, and the current conservation property gives the extra condition that determines the particular form of the its solution. In this manner, the average current naturally arises as the theory's control parameter.

The standard Laplace transform technique succeeds to exactly solve this problem only in the limit of infinite average current. We found that the exact solution in this limit turns out to be a good approximation also for values of average current ρ as low as ~ 1.5. For low average currents the singular behavior takes over, and the distributions diverge as power laws at certain points. The two dominant singularities are located at points $j = 0$ and j_c, and their characteristic exponent, α, varies continuously with the fraction of inactive channels, B, as $\alpha = 1 + \ln B / \ln 2$. Moreover, we find that additional sets of power-law divergences (with subdominant exponents) can develop at other points of the current distributions, for sufficiently low ρ. We show how all the singularities are strictly related, and can be expressed in terms of the exponent and amplitude of a single one.

To complete the description of the small current regime we derive the relation between the control parameter, ρ, and order parameter (i.e., the fraction of active channels), $1 - B \simeq \rho^{1/2}$ (this exponent is similar to what is found in empirical study [129]). The numerical results show a remarkable agreement with the theory developed for values of ρ up to $\sim 1/2$. Also a relation between ρ and the amplitude of the singularities was analytically found for the limit $\rho \to 0$, however it is a good approximation only for $\rho \ll 0.02$. The curious properties of this dynamical model indeed resemble the ones of continuous phase transitions. In particular, the order parameter's critical singularity, i.e, $1 - B \propto (\rho - \rho_c)^{\beta}$, where $\rho_c = 0$, of this zero-temperature transition takes the same mean-field exponent here as it does for the class of thermodynamic phase transitions described in the introductory section 1.3.1, $\beta = 1/2$.

Bibliography

[1] R. A. da Costa, S. N. Dorogovtsev, A. V. Goltsev, J. F. F. Mendes. Explosive percolation transition is actually continuous. *Phys. Rev. Lett.* 105, 255701 (2010).

[2] R. A. da Costa, S. N. Dorogovtsev, A. V. Goltsev and J. F. F. Mendes, Scaling properties of the explosive percolation transition. *Int. J. Comp. Syst. Sci.* 1, 169–173 (2011).

[3] R. A. da Costa, S. N. Dorogovtsev, A. V. Goltsev and J. F. F. Mendes, Characteristics of the explosive percolation transition. *to appear in* Springer Proceedings in Mathematics (PROM) (2013).

[4] D. J. Watts, S. H. Strogatz. Collective dynamics of small-world networks. *Nature* 393, 440–442 (1998).

[5] A.-L. Barabási, R. Albert. Emergence of scaling in random networks. *Science* 286, 509–512 (1999).

[6] R. Milo, S. Shen-Orr, S. Itzkovitz, N. Kashtan, D. Chklovskii, U. Alon. Network motifs: Simple building blocks of complex networks. *Science* 298, 824–827 (2002).

[7] S. N. Dorogovtsev, J. F. F. Mendes. Evolution of networks. *Adv. Phys.* 51, 1079–1187 (2002).

[8] R. Albert, A.-L. Barabási. Statistical mechanics of complex networks. *Rev. Mod. Phys.*,74, 47–97 (2002).

[9] M. E. J. Newman. The structure and function of complex networks. *SIAM Review* 45, 167256 (2003).

[10] A. Rapoport. Cycle distributions in random nets. *Bull. Math. Biophys.* 10, 145–157 (1948).

[11] R. Solomonoff, A. Rapoport. Connectivity of random nets. *Bull. Math. Biophys.* 13, 107–117 (1951).

[12] R. Solomonoff An exact method for the computation of the connectivity of random nets. *Bull. Math. Biophys.* 14, 153–157 (1952).

[13] P. Erdős, A. Rényi. On random graphs. I. *Publicationes Mathematicae* 6, 290–297 (1959).

[14] P. L. Krapivsky, S. Redner, F. Leyvraz. Connectivity of growing random networks. *Phys. Rev. Lett.* 85, 4629–4632 (2000).

[15] R. Cohen, S. Havlin. Scale-free networks are ultrasmall. *Phys. Rev. Lett.* 90, 058701 (2003);

[16] L. Adamic, R. Lukose, A. Puniyani, B. Huberman. Search in power-law networks. *Phys. Rev. E* 64, 046135 (2001).

[17] S. N. Dorogovtsev, J. F. F. Mendes. Scaling properties of scale-free evolving networks: Continuous approach. *Phys. Rev. E* 63, 056125 (2001).

[18] L. C. Freeman. The Development of Social Network Analysis: A Study in the Sociology of Science. *BookSurge Publishing* (2004).

[19] S. Fortunato. Community detection in graphs. *Phys. Rep.* 486, 75-174 (2010); [cond-mat/0906.0612].

[20] D. Stauffer, A. Aharony. Introduction to Percolation Theory. *Taylor and Francis* (1991).

[21] G. Grimmett. Percolation. *Springer* (1999).

[22] P. J. Reynolds, W. Klein, H. E. Stanley. A Real-Space Renormalization Group for Site and Bond Percolation. *J. Phys. C* 10, L167–L172 (1977).

[23] R. Cohen, K. Erez, D. ben-Avraham, S. Havlin. Resilience of the Internet to random breakdowns. *Phys. Rev. Lett.* 85, 4626–4628 (2000); [cond-mat/0007048].

[24] Landau, L. D., and E. M. Lifshitz. Statistical Physics, Vol. 1. *Pergamon* (1980).

[25] V. L. Ginzburg. *Sov. Phys. Solid State*, 2, 1824 (1960).

[26] J. Als-Nielsen, R. J. Birgeneau. Mean field theory, the Ginzburg criterion, and marginal dimensionality of phase transitions. Am. J. of Phys. 45, 554–560 (1977).

[27] P. Bak, C. Tang, K. Wiesenfeld. Self-organized criticality: an explanation of $1/f$ noise. *Phys. Rev. Lett.* 59, 381–384 (1987).

[28] P. Bak, M. Paczuski Complexity, contingency, and criticality *Proc. Natl. Acad. Sci. USA* 92, 6689-6696 (1995).

[29] M. Bartolozzi, D. B. Leinweber, A. W. Thomas. Self-Organized Criticality and Stock Market Dynamics: an Empirical Study. Physica A 350, 451–465 (2005).

[30] Y. Huang, H. Saleur, C. G. Sammis, D. Sornette. Precursors, aftershocks, criticality and self-organized criticality. *Europhys. Lett. 41*, 43–48 (1998).

[31] S. A. Kauffman, S. Johnsen. Coevolution to the edge of chaos: coupled fitness landscapes, poised states, and coevolutionary avalanches. *J. Theor. Biol.* 149, 467–505 (1991).

[32] P. Bak, K. Sneppen. Punctuated equilibrium and criticality in a simple model of evolution. Phys. Rev. Lett 71, 4083–4086 (1993).

[33] K. Nagel, H. J. Herrman Deterministic model for traffic jams. Physica A 199, 254-269 (1993).

[34] L. P. Kadanoff. Scaling and universality in statistical physics. *Physica A* 163, 1-14 (1990).

[35] J. W. Essam. Percolation theory. *Rep. Prog. Phys.* 43, 833–912 (1980).

[36] H. Nakanishi, H. E. Stanley Scaling studies of percolation phenomena in systems of dimensionality two to seven: Cluster numbers. *Phys. Rev. B* 22, 2466–2488 (1980).

[37] D. Stauffer. Scaling theory of percolation clusters. *Phys. Rep.* 54, 1–74 (1979).

[38] P. J. Reynolds, H. E. Stanley, W. Klein. Percolation by position-space renormalisation group with large cells. *J. Phys. A* 11, L199-L207 (1978).

[39] P. J. Reynolds, H. E. Stanley, W. Klein. Large-cell Monte Carlo renormalization group for percolation. *Phys. Rev. B* 21, 1223–1245 (1980).

[40] P. D. Eschbach, D. Stauffer, H. J. Herrmann. Correlation-length exponent in two-dimensional percolation and Potts model. *Phys. Rev. B* 23, 422–425 (1981).

[41] R. M. Ziff. Spanning Probability in 2D Percolation. *Phys. Rev. Lett.* 2670–2673 (1992).

[42] H. E. Stanley. Cluster shapes at the percolation threshold: an effective cluster dimensionality and its connection with critical-point exponents. *J. Phys. A* 10, L211–L220 (1977).

[43] B. B. Mandelbrot. Fractals: Form, Chance and Dimension *Freeman* (1977).

[44] A. Aharony. Percolation, Fractals, and Anomalous Diffusion. *J. Stat. Phys.* 34, 931–939 (1984).

[45] B. Bollobás. Modern graph theory. *Springer* (1998).

[46] M. E. Fisher and J. W. Essam. Some Cluster Size and Percolation Problems. *, J. Math. Phys.* 2, 609–619 (1961).

[47] P. L. Krapivsky, S. Redner, E. Ben-Naim A kinetic view of statistical physics. *Cambridge University Press* (2010).

[48] T. M. Cover, J. A. Thomas. see chapter 15: "Network Information Theory" *in* Elements of information theory, 2nd Ed. *Wiley* (2006).

[49] V. S. Frost, B. Melamed. Traffic modeling for telecommunications networks. *IEEE Commun. Mag.* 32, 3, 70–81 (1994).

[50] R. Ahlswede, N. Cai, S.-Y. R. Li, R. W. Yeung. Network Information Flow. *IEEE Trans. Inf. Theory* 46, 1204–1216 (2000).

[51] D. Bowersox, D. Closs, M. B. Cooper. Supply Chain Logistics Management. *McGraw-Hill* (2002).

[52] C. F. Daganzo. Logistics Systems Analysis. *Springer-Verlag* 4th Ed (2005).

[53] O. Biham, A. A. Middleton, D. Levine. Self-organization and a dynamical transition in traffic-flow models. *Phys. Rev. A* 46, R6124-R6127 (1992).

[54] D. Helbing. Traffic and Related Self-Driven Many-Particle Systems. *Rev. Mod. Phys.* 73, 1067-1141 (2001).

[55] G. B. West, J. H. Brown, B. J. Enquist. A General Model for the Origin of Allometric Scaling Laws in Biology. *Science* 276, 122–126 (1997).

[56] J. R. Banavar, A. Maritan, A Rinaldo. Size and form in efficient transportation networks *Nature* 399, 130–132 (1999).

[57] L.-F. Bersier, C. Banašek-Richter, M.-F. Cattin. Quantitative descriptors of food-wed matrices. *Ecology* 83, 23942407 (2002).

[58] M. Pascual, J. Dunne. Ecological networks: Linking Structure to Dynamics in Food Webs. *Oxford University Press* (2006).

[59] D. Stauffer, M. Sahimi. Discrete simulation of the dynamics of spread of extreme opinions in a society. *Physica A* 364, 537543 (2006).

[60] V. M. Eguíluz, K. Klemm. Epidemic Threshold in Structured Scale-Free Networks. newblock*Phys. Rev. Lett.* 89, 108701 (2002).

[61] B. A. Huberman, D. Helbing. Economics-based optimization of unstable flows. *Europhys. Lett.* 47, 196–202 (1999).

[62] S. Lämmer, D. Helbing Self-control of traffic lights and vehicle flows in urban road networks. *J. Stat. Mech.*, P04019 (2008).

[63] R. K. Ahuja, T. L. Magnanti, J. B. Orlin. Network flows: Theory, Algorithms, and Applications. *Prentice-Hall* (1993).

[64] K. Gardels, R. Herman. Vehicular Traffic Flow. *Sci. Am.* 209, 6, 35-43 (1963)

[65] I. Prigogine, R. Herman. Kinetic theory of vehicular traffic. *Elsevier* (1971).

[66] S. P. Borgatti. Centrality and network flow. *Soc. Networks*, 27, 5571 (2005).

[67] D. Helbing, D. Armbruster, A. S. Mikhailov, E. Lefeber. Information and material flows in complex networks. *Physica A* 363, xi–xvi (2006).

[68] F. Liljeros, C. R. Edling, L. A. N. Amaral, H. E. Stanley, Y. Aberg. The Web of Human Sexual Contacts. *Nature* 411, 907–908 (2001).

[69] F. Wu, B. A. Huberman, L. A. Adamic, J. R. Tyler. Information flow in social groups. *Physica A* 337, 327–335 (2004).

[70] J. A. Dunne, R. J. Williams, N. D. Martinez. Food-web structure and network theory: The role of connectance and size. *Proc. Natl. Acad. Sci. USA* 99, 1291712922 (2002).

[71] P. Holme. Congestion and centrality in traffic flow on complex networks. *Adv. Complex Syst.* 6, 163–176 (2003).

[72] U. Brandes, D. Fleischer. Centrality Measures Based on Current Flow. *STACS* 3404, *Lecture Notes in Computer Science* 533-544 (2005).

[73] S. Brin, L. Page. The anatomy of a large-scale hypertextual Web search engine. *Computer Networks and ISDN Systems* 30, 107–117 (1998); [http://infolab.stanford.edu/pub/papers/google.pdf].

[74] B. Bonacich. Factoring and weighting approaches to status scores and clique identification. *J. Math. Sociol.* 2, 113–120 (1972).

[75] L. R. Ford, Jr., D. R. Fulkerson. Flows in networks. *Princeton University Press* (1962).

[76] L. R. Ford, Jr., and D. R. Fulkerson. Maximal Flow Through A Network. *Canad. J. Math.* 8, 399–404 (1956).

[77] K. Menger. Zur allgemeinen Kurventheorie. *Fund. Math.* 10, 96–115 (1927).

[78] E. Lawler (2001). Combinatorial Optimization: Networks and Matroids. *Dover* (2001).

[79] C. H. Papadimitriou, K. Steiglitz. Combinatorial Optimization: Algorithms and Complexity. *Dover* (1998).

[80] G. B. Dantzig. Application of the simplex method to a transportation problem. In *Activity Analysis and Production and Allocation*, edited by T. C. Koopmans. *Wiley* 359-373 (1951).

[81] V. Srinivasan. G. L. Thompson. Benefit-cost analysis of coding techniques for primal transportation algorithm. *Journal of ACM* 20, 194-213 (1973).

[82] F. Glover, D. Karney, D. Klingman, A. Napier A computational study on start procedures, basis change criteria, and solution algorithms for transportation problem. *Manage. Sci.* 20, 793-813 (1974).

[83] G. B. Dantzig. Linear Programming and Extensions. *Princeton University Press* (1962).

[84] B.D. Greenshields. A study of traffic capacity. *Proc. Highw. Res.* 14, 448–477 (1935).

[85] H. Greenberg. An Analysis of Traffic Flow Oper. Res. 7, 79 (1959).

[86] K. Nagel, M. Schreckenberg. A cellular automaton model for freeway traffic *J. Phys. I France* 2, 2221– 2229(1992).

[87] B. S. Kerner, P. Konhäuser. Cluster effect in initially homogeneous traffic flow. *Phys. Rev. E*, 48, R2335-R2338 (1993).

[88] D. Chowdhury, L. Santen, A. Schadschneider. Statistical physics of vehicular traffic and some related systems. *Phys. Rep.* 329, 199–329 (2000).

[89] M. A. Nowak, R. M. May. Evolutionary games and spatial chaos. *Nature* 359, 826–829 (1992).

[90] D. J. Zawack, G. L. Thompson A dynamic space-time network flow model for city traffic congestion. *Transport. Sci.* 21, 3, 153–162 (1987).

[91] E. Brockfeld, R. Barlovic, A. Schadschneider, M. Schreckenberg. Optimizing traffic lights in a cellular automaton model for city traffic. *Phys. Rev. E* 64, 056132 (2001).

[92] G. J. Baxter, S. N. Dorogovtsev, A.V. Goltsev, J. F. F. Mendes. Heterogeneous-k-core versus bootstrap percolation on complex networks. *Phys. Rev. E* 83, 051134 (2011).

[93] D. Achlioptas, R. M. D'Souza, J. Spencer. Explosive percolation in random networks. *Science* 323, 1453–1455 (2009).

[94] N. Metropolis, A. W. Rosenbluth, M. N. Rosenbluth, A. H. Teller, E. Teller. Equations of state calculations by fast computing machines. *J. Chem. Phys.* 21, 1087–1092 (1953).

[95] S. Kirkpatrick, C. D. Gelatt, M. P. Vecchi. Optimization by simulated annealing. *Science* 220, 671–680 (1983).

[96] R. M. Ziff. Explosive growth in biased dynamic percolation on two-dimensional regular lattice networks. *Phys. Rev. Lett.* 103, 045701 (2009).

[97] Y. S. Cho, J. S. Kim, J. Park, B. Kahng, D. Kim. Percolation transitions in scale-free networks under Achlioptas process. *Phys. Rev. Lett.* 103, 135702 (2009).

[98] F. Radicchi, S. Fortunato. Explosive percolation in scale-free networks, *Phys. Rev. Lett.* 103, 168701 (2009).

[99] E. J. Friedman, A. S. Landsberg, Construction and analysis of random networks with explosive percolation. *Phys. Rev. Lett.* 103, 255701 (2009).

[100] F. Radicchi, S. Fortunato. Explosive percolation: a numerical analysis. *Phys. Rev. E* 81, 036110 (2010).

[101] R. M. Ziff. Scaling behavior of explosive percolation on the square lattice. *Phys. Rev. E* 82, 051105 (2010).

[102] R. M. D'Souza, M. Mitzenmacher. Local cluster aggregation models of explosive percolation. *Phys. Rev. Lett.* 104, 195702 (2010).

[103] J. Nagler, A. Levina, M. Timme. Impact of single links in competitive percolation. *Nature Phys.* 7, 265-270 (2011).

[104] J. Spencer, N. Wormald. Birth control for giants. *Combinatorica* 27, 587–628 (2008).

[105] Y. S. Cho, B. Kahng, D. Kim. Cluster aggregation model for discontinuous percolation transition. *Phys. Rev. E* 81, 030103 (R) (2010).

[106] S. S. Manna, A. Chatterjee. A new route to explosive percolation. *Physica A* 390, 177–182 (2011).

[107] N. A. M. Araújo,J. S. Andrade Jr., R. M. Ziff, H. J. Herrmann. Tricritical point in explosive percolation. *Phys. Rev. Lett.* 106, 095703 (2011).

[108] N. A. M. Araújo, H. J. Herrmann, Explosive percolation via control of the largest cluster. *Phys. Rev. Lett.* 105, 035701 (2010).

[109] W. Chen, R. M. D'Souza, Explosive percolation with multiple giant components. *Phys. Rev. Lett.* 106, 115701 (2011)

[110] Y. S. Cho, S. W. Kim, J. D. Noh, B. Kahng, D. Kim. Finite-size scaling theory for explosive percolation transitions. *Phys. Rev. E* 82, 042102 (2010).

[111] O. Riordan, L Warnke. Achlioptas process phase transitions are continuous. *Science* 333, 322–324 (2011).

[112] P. Grassberger, C. Christensen, G. Bizhani, S.-W. Son, M Paczuski. Explosive Percolation is Continuous, but with Unusual Finite Size Behavior. *Phys. Rev. Lett.* 106, 225701 (2011).

[113] H. K. Lee, B. J. Kim, H. Park. Continuity of the explosive percolation transition. *Phys. Rev. E* 84, 020101(R) (2011).

[114] L. Tian, D-N Shi. The Nature of Explosive Percolation Phase Transition. *Phys. Lett. A* 376, 286–289 (2012.)

[115] H. Chae, S-H Yook, Y. Kim. Explosive percolation on the Bethe lattice *Phys. Rev. E* 85, 051118 (2012).

[116] S. Squires, K. Sytwu, D. Alcala, T. M. Antonsen, E. Ott, M. Girvan. Weakly explosive percolation in directed networks *Phys. Rev. E* 87, 052127 (2013).

[117] V. Privman. Finite-size scaling theory. In *Finite Size Scaling and Numerical Simulation of Statistical Systems*, ed. V. Privman. pp. 1-98. (Singapore, World Scientific, 1990).

[118] G. Ódor. Phase transition classes in triplet and quadruplet reaction-diffusion models. *Phys. Rev. E* 67, 056114 (2003).

[119] G. Ódor. Universality classes in nonequilibrium lattice systems. *Rev. Mod. Phys.* 76, 663–724 (2004).

[120] D. B. Johnson, D. A. Maltz. Dynamic source routing in ad hoc wireless networks. In *Mobile Computing*, 353, 153–181 (1996).

[121] E. M. Royer, C-K Toh. A review of current routing protocols for ad hoc mobile wireless networks. *IEEE Pers. Commun.* 6, 46–55 (1999).

[122] A. Rinaldo, I. Rodriguez-Iturbe, R. Rigon, R. L. Bras, E. Ijjasz-Vasquez, A. Marani. Minimum Energy and Fractal Structures of Drainage Network. *Water Resour. Res.* 28, 2183–2195 (1992).

[123] I. Rodrguez-Iturbe, A. Rinaldo, Fractal River Basins: Chance and Self-Organization. *Cambridge Univ. Press* (2001).

[124] J. P.M. Syvitski, A. J. Kettner, A. Correggiari, B. W. Nelson. Distributary channels and their impact on sediment dispersal. *Mar. Geol.* 222–223, 75–94 (2005).

[125] H. Seybold, J. S. Andrade, Jr., H. J. Herrmann. Modeling river delta formation. *Proc. Natl. Acad. Sci. USA* 104, 16804–16809 (2007).

[126] D. A. Edmonds, R. L. Slingerland. Stability of delta distributary networks and their bifurcations. *Water Resour. Res.* 44, W09426 (2008).

[127] M. Morisawa. Topologic properties of delta distributary networks. *in* W. J. Michael, ed., Models in Geomorphology. *Allen & Unwin* 239–268 (1985).

[128] C. Olariu. Terminal distributary channels and delta front architecture of river-dominated delta systems. *J. Sediment. Res.*76, 212–233 (2006).

[129] J. P.M. Syvitski, Y. Saito. Morphodynamics of deltas under the influence of humans. *Global Planet. Change* 57, 261–282 (2007).

[130] F. L. Forgerini. Interacting agents on complex networks and stochastic processes in them. Ph.D. thesis. University of Aveiro (2013).

[131] N. Crokidakis. Topologia e Dinâmica de Sistemas Complexos: Transições de Fase e Fenômenos Críticos. Ph.D. thesis. Universidade Federal Fluminense (2011).